# SEDIMENT TRANSPORT DYNAMICS IN DAM-BREAK MODELLING

**BY**

**Vincent PC Msadala**

**Dissertation presented for the degree of Doctor of Philosophy (Engineering) in the Faculty of Engineering at the University of Stellenbosch**

**Supervisor: Prof. GR Basson**

**Stellenbosch** **March** **2016**

# DECLARATION

I, the undersigned, hereby declare that the work contained in this dissertation is my own original work and that I have not previously in its entirety or in part submitted it at any university for a degree.

Date:

VP Msadala, March 2016

# SUMMARY

The prediction of breach characteristics during earth embankment dam-break modelling due to overtopping is dependent on the accurate modelling of the intrinsic breaching processes such as flow hydraulics, bed level changes, soil mechanics and sediment transport dynamics. Earth dams are characterised by steep embankment slopes (up to 1:2 (V:H), 50%). Commonly used sediment transport equations in dam-break modelling were based on slopes of up to 20%. The application of sediment transport equations that were derived from data on mild or moderately steep slopes is one of the sources of uncertainty in dam-break modelling. The general objective of this study was to develop new empirical sediment transport equations for steep slopes that can be applied in homogeneous earth embankment dam-break modelling and to assess the uncertainty that is associated with the input of sediment transport equations.

Physical experimental studies were conducted at the Hydraulic Laboratory of the University of Stellenbosch, South Africa. A 4.7 m long, 0.25 m wide and 0.3 m deep flume was used. Three preselected bed slope configurations of 25%, 33% and 40% were implemented. A total of 87 tests were carried out with median ($d_{50}$) sediment sizes of 0.2 mm, 1.0 mm and 2.4 mm.

New empirical sediment transport equations for steep slopes were developed based on the data from the experimental study. One of the two proposed sediment transport equations incorporated six parameters in its formulation, namely the particle sizes of the sample for which 30 % and 90% were finer ($d_{30}$ and $d_{90}$); shear velocity, average flow velocity, friction slope, dimensionless shear stress and critical dimensionless shear stress. The validity or statistical significance of the proposed sediment transport equations (Equations 5.2-5 and 5.2-6) was determined using statistical tests (F-Test and $r^2$). The predictive capability of the proposed sediment transport equations (Equations 5.2-5 and 5.2-6) was confirmed by the degree of correlation between measured and predicted sediment transport rates. There was a deviation of less than 22% between the measured and predicted sediment transport rates.

A comparative analysis was done between measured and predicted sediment transport rates using selected sediment transport equations from literature. The analytical comparison showed that the sediment transport predictions by one of the newly calibrated sediment transport equations (Equation 5.2-6) were within the same order of magnitude as those of the Meyer-Peter Müller (1948) and Camenen & Larson (2005) sediment transport equations, even though the Meyer-Peter Müller (1948) equation overestimated sediment transport rates at higher unit discharges.

The Smart and Jäeggi (1983) sediment transport equation predicted higher sediment transport rates than the measured sediment transport rates and those predicted by Equation 5.2-6.

The MIKE 21C two dimensional hydrodynamic model of the DHI Group was successfully applied to evaluate and compare the performance of the newly calibrated sediment transport equations in dam-break modelling using five dam-break case studies. The numerical simulation results using the newly calibrated sediment transport equations (Equations 5.2-5 and 5.2-6) were compared with the output results that were simulated by two selected sediment transport equations from literature, namely those of Camenen & Larson (2005) and Smart & Jäeggi (1983).

Specifically, Case studies 1 and 2 were applied to analyse the effect of sediment transport equations in the simulation of temporal bed level changes and the simulated breach shape respectively. Case studies 3 and 4 investigated the numerical modelling of dam-break outflow hydrographs on very steep slopes. Case Study 5 was used to analyse the effect of sediment transport equations on the simulated peak discharge and outflow volume and showed that the newly calibrated equations are applicable at prototype scale. The newly calibrated sediment transport equations performed better in Case studies 1 and 2 where the embankment slopes were within the equations' calibration range (25% - 40% slopes). Consistent and realistic predictions of numerical model output parameters were not possible when the sediment transport equations were applied to Case studies 3 and 4 where the embankment slopes were outside the calibration range of all four sediment transport equations (Equations 5.2-5 and 5.2-6, Camenen & Larson (2005) and Smart and Jäeggi (1983)).

The original contribution to knowledge of this dissertation is the development of sediment transport equations that are based on steep embankment slopes and are suitable for application in dam-break modelling. For dam-break studies, sensitivity analysis of model input parameters such as resistance and alternative sediment transport equations is recommended in order to evaluate a range of scenarios. The sensitivity analysis that was accomplished pertaining to Manning's resistance coefficient (n) showed that a lower Manning's resistance coefficient (n) in the numerical model resulted in a higher peak outflow discharge.

# OPSOMMING

Die voorspelling van breekkenmerke in die breekmodellering van gronddamme as gevolg van vloedwater wat oor die nie oorloopkruin van die dam spoel, berus op die akkurate modellering van die intrinsieke breekprosesse, soos vloeihidroulika, veranderinge in die bodemvlak, grondmeganika en sedimentvervoerdinamika. Gronddamme word gekenmerk deur steil wal hellings (tot 1:2 (V:H), 50%). Tog is die vergelykings wat meestal vir die berekening van sedimentvervoer gebruik word, gegrond op hellings van tot slegs 20%. Die toepassing van sedimentvervoervergelykings wat afgelei is van data vir matige hellings is dus een van die bronne van onsekerheid in dambreekmodellering. Daarom was die algemene oogmerk van hierdie studie om nuwe empiriese sedimentvervoervergelykings vir steil hellings te ontwikkel wat in homogene gronddambreekmodellering toegepas kan word, en om die onsekerheid te beoordeel wat met die inset van sedimentvervoervergelykings verband hou.

Fisiese modelstudies is in die Hidrouliese Laboratorium van die Universiteit Stellenbosch onderneem. ’n Kanaal met ’n lengte van 4.7 m, ’n breedte van 0.25 m en ’n diepte van 0.3 m is gebruik. Drie voorafgekose damhellings van 25%, 33% en 40% is toegepas. Altesaam 87 toetse is met gemiddelde ($d_{50}$) sedimentgroottes van 0.2 mm, 1.0 mm en 2.4 mm uitgevoer.

Nuwe empiriese sedimentvervoervergelykings vir steil hellings is op grond van die data uit die proefstudies ontwikkel. Die formulering van een van die twee voorgestelde sedimentvervoervergelykings het ses parameters ingesluit, naamlik die deeltjiegrootte van die monster, waarvan 30% en 90% fyner was ($d_{30}$ en $d_{90}$); sleursnelheid, gemiddelde vloeisnelheid, wrywingshelling, dimensielose skuifspanning en kritieke dimensielose skuifspanning. Die geldigheid of statistiese beduidendheid van die voorgestelde sedimentvervoervergelykings (vergelykings 5.2-5 en 5.2-6) is met behulp van statistiese toetse (F-toets en $r^2$) bepaal. Die voorspellingsvermoë van die vergelykings is bevestig deur die mate van korrelasie tussen die gemete en voorspelde sedimentvervoertempo’s, wat minder as 22% van mekaar verskil het.

’n Vergelykende ontleding van die gemete en voorspelde sedimentvervoertempo’s is met behulp van gekose sedimentvervoervergelykings uit die literatuur uitgevoer. Dít het getoon dat die sedimentvervoervoorspellings van die pas gekalibreerde vergelykings (vergelyking 5.2-6) in dieselfde grootteorde as dié van die vergelykings van Meyer-Peter Müller (1948) en Camenen & Larson (2005) val, hoewel Meyer-Peter Müller se vergelyking sedimentvervoertempo’s met hoër eenheidsdeurstromings oorskat het. Smart & Jäeggi se sedimentvervoervergelyking (1983) het hoër

vervoertempo's vergeleke met die gemete waardes sowel as die voorspelde tempo's van vergelyking 5.2-6 voorspel.

Hierna is die DHI Groep se tweedimensionele hidrodinamiese model MIKE 21C suksesvol toegepas om die akkuraatheid van die pas gekalibreerde sedimentvervoervergelykings in dambreekmodellering in vyf dambreekgevallestudies te beoordeel en te vergelyk. Die numeriese simulasieresultate van die pas gekalibreerde sedimentvervoervergelykings (vergelykings 5.2-5 en 5.2-6) is met die gesimuleerde uitsetresultate van twee gekose vergelykings uit die literatuur, naamlik dié van Camenen & Larson (2005) en Smart & Jäeggi (1983), vergelyk.

Meer bepaald is gevallestudie 1 en 2 toegepas om die uitwerking van die sedimentvervoervergelykings op gesimuleerde veranderinge in die bodemvlak oor tyd en die gesimuleerde breekvorm onderskeidelik te ontleed. Gevallestudies 3 en 4 het die numeriese modellering van uitvloeihidrograwe by dambreke met baie steil hellings ondersoek. Gevallestudie 5 is gebruik om die uitwerking van die sedimentvervoervergelykings op die gesimuleerde piek uitvloei deurstroming en uitvloeivolume te ontleed, en het getoon dat die pas gekalibreerde vergelykings op prototipeskaal toegepas kan word. Die prestasie van die pas gekalibreerde vergelykings was beter in gevallestudies 1 en 2, waar die damhellings binne die kalibreerbestek van die vergelykings geval het (25% - 40% helling). Konsekwente en realistiese voorspellings van numeriese modeluitsetparameters was onmoontlik toe die vergelykings op gevallestudie 3 en 4 toegepas is, omdat die damhellings buite die kalibreerbestek van ál vier vergelykings (vergelyking 5.2-5 en 5.2-6, Camenen & Larson (2005) en Smart & Jäeggi (1983)) geval het.

Hierdie verhandeling lewer 'n oorspronklike bydrae deur die ontwikkeling van sedimentvervoervergelykings vir steil damhellings wat in dambreekmodellering toegepas kan word. Sensitiwiteitsontleding van modelinsetparameters soos weerstand en alternatiewe sedimentvervoervergelykings word vir dambreekstudies aanbeveel sodat 'n verskeidenheid scenario's beoordeel kan word. Die sensitwiteitsontleding wat met betrekking tot Manning se ruheid (n) uitgevoer is, het getoon dat 'n laer (n) in die numeriese model tot 'n hoër piekuitvloei gelei het.

# ACKNOWLEDGEMENTS

I would like to acknowledge and express my gratitude to my study leader, **Professor GR Basson** (Head, Water Division, Department of Civil Engineering, University of Stellenbosch, South Africa) for his valuable help, assistance and guidance during the execution of this research and preparation of the dissertation.

I am grateful to the **University of Stellenbosch** (Department of Civil Engineering) for funding my studies during the first three years of my research.

I would like to thank **ANSTI/DAAD (German Academic Exchange Service)** for funding the final year of my research.

I would like to express my sincere appreciation to the **University of Malawi** for granting me the study leave and assisting me financially.

I wish to acknowledge colleagues in the postgraduate student office (**Ousmane Sawadogo, Jan Hoffmann and Placide Kanyabujinja**) and staff of the Department of Civil Engineering for their inspiration.

I would like to acknowledge the assistance that was given by staff in the **Hydraulics Laboratory** of the University of Stellenbosch during the physical experimental tests.

The **Danish Hydraulics Institute** (DHI Group) is gratefully acknowledged for making the software MIKE21C freely available for use in this study.

I salute all Malawians in Stellenbosch especially friends from **Malawi Society Stellenbosch University (MSSU)**. In particular, **Peter Mbewe** and **Rodwell Bakolo** – I appreciate so much.

Thanks to my wife **Chifundo** and our two sons; **Chipatso** and **Mlumbeni** for their love, support and inspiration.

# TABLE OF CONTENTS

**DECLARATION** ..... **I**

**SUMMARY** ..... **II**

**OPSOMMING** ..... **IV**

**ACKNOWLEDGEMENTS** ..... **VI**

**TABLE OF CONTENTS** ..... **VII**

**LIST OF FIGURES** ..... **XI**

**LIST OF TABLES** ..... **XIV**

**ABBREVIATIONS** ..... **XVI**

**LIST OF SYMBOLS** ..... **XVII**

**CHAPTER 1 INTRODUCTION** ..... **1**

1.1 BACKGROUND ..... 1
1.2 INTRODUCTION TO DAM-BREAK ANALYSIS ..... 3
1.3 PROBLEM STATEMENT AND MOTIVATION OF PRESENT RESEARCH ..... 4
1.4 OBJECTIVES OF THE RESEARCH ..... 6
1.5 STRUCTURE OF THE DISSERTATION ..... 7

**CHAPTER 2 LITERATURE STUDY ON DAM-BREAK ANALYSIS AND SEDIMENT TRANSPORT DYNAMICS** ..... **8**

2.1 OVERVIEW TO THIS CHAPTER ..... 8
2.2 FLOW HYDRAULICS AND SEDIMENT TRANSPORT ASPECTS OF THE BREACHING OF EARTH DAMS ..... 8
2.3 DAM SAFETY STRATEGIES ..... 12
2.4 PARAMETRIC (EMPIRICAL) DAM-BREAK MODELS ..... 13
2.5 SELECTED PHYSICALLY-BASED NUMERICAL DAM-BREAK MODELS ..... 16
*2.5.1 Cristofano Model - 1965* ..... *17*
*2.5.2 Harris and Wagner Model - 1967* ..... *17*
*2.5.3 BRDAM Model - 1981* ..... *17*
*2.5.4 Lou Dam-Break Model - 1981* ..... *17*
*2.5.5 BEED Model as Revised by Vijay P. Singh and Cesar A. Quiroga - 1987* ..... *17*
*2.5.6 NWS Breach Model - 1984* ..... *18*
*2.5.7 EDBREACH Model - 1998* ..... *18*
*2.5.8 DEICH-N1/N2 Models - 1998* ..... *18*

*2.5.9 BREADA Model - 2007* ..... *19*
*2.5.10 Junqiang Xia Dam-Break Model - 2010* ..... *20*
*2.5.11 Tingsanchali and Chinnarasri Dam-Break Model - 2001* ..... *20*
*2.5.12 Wang and Bowles Model - 2006* ..... *20*
*2.5.13 Roland Faeh Model (2dMb) - 2007* ..... *21*
*2.5.14 Zhang and Wu - 2011* ..... *22*
*2.5.15 Macchione's Dam-break Model - 2008* ..... *22*
*2.5.16 HR-BREACH - 2002* ..... *23*
*2.5.17 Simplified Dam-Break Analysis Model (SIMBA) - 2005* ..... *24*
*2.5.18 FIREBIRD - 2002* ..... *24*
*2.5.19 Wu et al. (2011) Model* ..... *24*
*2.5.20 Abderrezzak and Paquier Model - 2011* ..... *25*
*2.5.21 MIKE 11 Dam-Break Model (DHI, 2011)* ..... *25*
*2.5.22 AREBA (A Rapid Embankment Breach Assessment) – 2012* ..... *25*
*2.5.23 Summary* ..... *26*
2.6 SELECTED SEDIMENT TRANSPORT EQUATIONS BASED ON GENTLE SLOPES DATA (0 - 9%) ..... 26
*2.6.1 Engelund and Hansen (1967, 1972)* ..... *26*
*2.6.2 Wu and Long (1993)* ..... *27*
*2.6.3 Yang (1972, 1973, 1979, 1996)* ..... *28*
*2.6.4 Wu et al. (2000)* ..... *30*
*2.6.5 Van Rijn (1984a, 1984b)* ..... *32*
*2.6.6 Ackers and White (1973)* ..... *33*
*2.6.7 Molinas and Wu (2001)* ..... *34*
*2.6.8 Meyer-Peter Müller (1948)* ..... *34*
*2.6.9 Shu-Qing Yang Equation (2005)* ..... *35*
2.7 SEDIMENT TRANSPORT EQUATIONS BASED ON MODERATELY STEEP SLOPE DATA (10 – 20%) ..... 36
*2.7.1 Smart and Jäeggi equation (1983)* ..... *36*
*2.7.2 Rickenmann (1991)* ..... *37*
*2.7.3 Abrahams (2003)* ..... *38*
*2.7.4 Camenen and Larson (2005)* ..... *38*
2.8 SEDIMENT TRANSPORT EQUATION BASED ON GENTLY STEEP (8%) TO STEEP (50%) SLOPE DATA ..... 39
2.9 SUMMARY ..... 40

**CHAPTER 3 EXPERIMENTAL SETUP AND PROCEDURES ..... 42**

3.1 TESTING FLUME ..... 42
3.2 EXPERIMENTAL PROCEDURE – MEASUREMENT OF SEDIMENT TRANSPORT RATES ..... 42
*3.2.1 Significant considerations pertaining to sediment transport rate measurements on steep slopes* ..... *46*

3.3 EXPERIMENTAL PROCEDURE – DETERMINATION OF SEDIMENT DENSITY, MEDIAN ($D_{50}$) SEDIMENT SIZE AND SETTLING VELOCITY ..... 47
*3.3.1 Determination of densities* ..... *47*
*3.3.2 Determination of settling velocities* ..... *48*
*3.3.3 Determination of median sediment sizes* ..... *50*

**CHAPTER 4 EXPERIMENTAL RESULTS ..... 52**

4.1 ANALYSIS OF EXPERIMENTAL RESULTS ..... 52
4.2 SUMMARY ..... 58

**CHAPTER 5 THE DEVELOPMENT OF NEW EMPIRICAL SEDIMENT TRANSPORT EQUATIONS FOR STEEP SLOPES ..... 61**

5.1 BACKGROUND TO THE APPROACHES FOR THE DEVELOPMENT OF EMPIRICAL SEDIMENT TRANSPORT EQUATIONS ..... 61
5.2 CALIBRATION OF STEEP SLOPE SEDIMENT TRANSPORT EQUATIONS BASED ON THE DHI UNIVERSAL EMPIRICAL FORMULATION5.2.1 DHI (2011) UNIVERSAL EMPIRICAL FORMULATION ..... 62
5.3 CALIBRATION OF STEEP SLOPE SEDIMENT TRANSPORT EQUATIONS BASED ON KHORRAM AND ERGIL (2010) AND ZHANG ET AL. (2009) SEDIMENT TRANSPORT EQUATION FORMULATIONS ..... 70
*5.3.1 Khorram and Ergil (2010) equation formulation* ..... *70*
*5.3.2 Zhang et al. (2009) equation formulation* ..... *74*
*5.3.3 Summary of regression equations results* ..... *79*
5.4 COMPARATIVE ANALYSIS OF THE PERFORMANCE OF THE CALIBRATED EQUATION 5.2-6 BASED ON STEEP SLOPE DATA FROM THIS STUDY WITH SELECTED EMPIRICAL SEDIMENT TRANSPORT EQUATIONS ..... 80
*5.4.1 A comparative analysis of the predicted volumetric and mass sediment concentration at a specific discharge* ..... *81*
5.5 SUMMARY ..... 86

**CHAPTER 6 THE APPLICATION OF THE NEWLY CALIBRATED SEDIMENT TRANSPORT EQUATIONS IN DAM-BREAK MODELLING AND UNCERTAINTY ANALYSIS ..... 88**

6.1 SEDIMENT TRANSPORT EQUATIONS AND UNCERTAINTY ANALYSIS ..... 88
*6.1.1 Uncertainty analysis approach* ..... *88*
6.2 AN INTRODUCTION TO MIKE 21C ..... 90
6.3 DESCRIPTION OF THE MIKE 21C FLOW MODULE AND ITS SAND TRANSPORT MODULE ..... 90
6.4 MIKE 21C MODEL CAPABILITIES IN DAM-BREAK MODELLING ..... 91
6.5 BACKGROUND TO THE SELECTED CASE STUDIES ..... 91
6.6 CASE STUDY 1 ..... 92

*6.6.1 Analysis of numerical simulation results - Case Study 1 ..... 96*
6.7 CASE STUDY 2 ..... 100
*6.7.1 Analysis of numerical simulation results - Case Study 2 ..... 102*
*6.7.2 The sensitivity of the peak outflow to Manning's resistance coefficient (n) – Case Study 2 ..... 105*
6.8 CASE STUDY 3 ..... 108
*6.8.1 Analysis of numerical simulation results – Case Study 3 ..... 114*
*6.8.2 The sensitivity of the peak outflow to Manning's resistance coefficient (n) – Case Study 3 ..... 118*
6.9 CASE STUDY 4 ..... 120
*6.9.1 Numerical model setup and analysis of numerical simulation results - Case Study 4 ..... 126*
*6.9.2 The sensitivity of the peak discharge to Manning's resistance coefficient (n) – Case Study 4 ..... 132*
6.10 CASE STUDY 5 ..... 135
*6.10.1 Analysis of numerical simulation results – Case Study 5 ..... 137*
6.11 SUMMARY ..... 142

**CHAPTER 7 CONCLUSION AND DISCUSSION ..... 145**

**CHAPTER 8 RECOMMENDATIONS ..... 148**

**REFERENCES ..... 149**

**APPENDICES ..... 158**

# LIST OF FIGURES

Figure 2.2-1 Sketch of hydraulic control during overtopping (adapted from Powledge et al. (1989)) ..... 10
Figure 2.2-2 Discharge through breach in relation to breach development phases ..... 11
Figure 2.3-1 A conceptual framework of the relationship between dam safety and dam-break analysis ..... 12
Figure 2.5-1 Effects of sediment transport equations on discharge through breach (Faeh, 2007) ..... 22
Figure 2.8-1 Measured sediment transport capacity as a function of flow discharge for selected slopes using median ($d_{50}$) sediment size = 0.28 mm (Zhang et al., 2009) ..... 40
Figure 3.1-1 Schematic drawing of the experimental setup ..... 44
Figure 3.1-2 Photograph of the experimental setup ..... 45
Figure 3.2-1 Experimental flume - viewed from downstream ..... 45
Figure 3.2-2 Sediment feeding rate control gate (left), conveyor belt with sediment (middle) and sediment feeding into flume by conveyor (right) ..... 46
Figure 3.3-1 Cylindrical water column for settling velocity determination ..... 49
Figure 3.3-2 Sieve analysis results for median ($d_{50}$) sediment size = 0.2 mm ..... 50
Figure 3.3-3 Sieve analysis results for median ($d_{50}$) sediment size = 1 mm ..... 51
Figure 3.3-4 Sieve analysis results for median ($d_{50}$) sediment size = 2.4 mm ..... 51
Figure 4.1-1 Measured sediment transport rates for all slopes and median ($d_{50}$) sediment sizes = 1 mm and 2.4 mm ..... 59
Figure 4.1-2 Comparison of measured and predicted sediment transport rates ..... 60
Figure 5.2-1 An illustration of the critical value of F ..... 66
Figure 5.2-2 Predicted and measured sediment transport rates using Equation 5.2-5 ... 68
Figure 5.2-3 Predicted and measured sediment transport rates using Equation 5.2-6 ... 68
Figure 5.2-4 Predicted and measured sediment transport rates using Equation 5.2-5 – separate plots for different slopes ..... 69
Figure 5.2-5 Predicted and measured sediment transport rates using Equation 5.2-6 - separate plots for different slopes ..... 69
Figure 5.3-1 Measured and predicted sediment transport rates using Equation 5.3-7 for median ($d_{50}$) sediment size = 2.4 mm and 1 mm; bed slopes = 25%, 33% and 40% ..... 74
Figure 5.3-2 Predicted and measured sediment transport rates using Equation 5.3-9 ... 76
Figure 5.3-3 Predicted and measured sediment transport rates using Equation 5.3-10 . 77
Figure 5.3-4 Measured and predicted sediment transport rates using Equation 5.3-11 using median ($d_{50}$) sediment size = 2.4 mm and 1 mm and bed slopes = 25%, 33% and 40% ..... 79
Figure 5.4-1 Mass sediment discharge (kg/m/s) to mass flow discharge (kg/m/s) against gradient slope ..... 85

Figure 5.4-2 Sediment concentrations (mg/l) against gradient slope ..... 86
Figure 6.2-1 Empirical sediment transport theory specification: Smart and Jäeggi (1983) top and Equation 5.2-6 bottom ..... 89
Figure 6.6-1 Breach initiation with full reservoir on LHS ..... 93
Figure 6.6-2 Breach formation after 24 seconds ..... 94
Figure 6.6-3 Breach formation after 38 seconds ..... 94
Figure 6.6-4 Breach formation after 72 seconds ..... 95
Figure 6.6-5 Simulated temporal bed level changes after 24 Seconds ..... 96
Figure 6.6-6 Simulated temporal bed level changes after 38 Seconds ..... 97
Figure 6.6-7 Simulated temporal bed level changes after 72 Seconds ..... 97
Figure 6.6-8 Comparison of outflow hydrographs for Case Study 1 ..... 99
Figure 6.7-1 Embankment cross-section (Case Study 2) ..... 100
Figure 6.7-2 Photographs of the laboratory experiment (Radyn, 2010) ..... 101
Figure 6.7-3 Final observed and simulated breaching depths using different equations (Case Study 2) ..... 103
Figure 6.7-4 Observed inflow and simulated outflow hydrographs (Case Study 2) .... 105
Figure 6.7-5 Sensitivity analysis - comparison of measured inflow and simulated outflow hydrographs (Equation 5.2-5) – Case Study 2 ..... 106
Figure 6.7-6 Sensitivity analysis - comparison of measured inflow and simulated outflow hydrographs (Equation 5.2-6) - Case Study 2 ..... 107
Figure 6.7-7 Sensitivity analysis - comparison of measured inflow and simulated outflow hydrographs (Smart and Jäeggi, 1983) – Case Study 2 ..... 107
Figure 6.7-8 Sensitivity analysis - comparison of measured inflow and simulated hydrographs (Camenen and Larson, 2005) – Case Study 2 ..... 108
Figure 6.8-1 Embankment longitudinal section (Case Study 3) ..... 109
Figure 6.8-2 Observed water levels, inflow, and outflow hydrographs for Case Study 3 (Floodsite, 2011) ..... 109
Figure 6.8-3 Initial bathymetry - Case Study 3 ..... 112
Figure 6.8-4 Final bathymetry using Equation 5.2-5 - Case Study 3 ..... 112
Figure 6.8-5 Final bathymetry using Equation 5.2-6 – Case Study 3 ..... 112
Figure 6.8-6 Final bathymetry using Smart and Jäeggi (1983) - Case Study 3 ..... 113
Figure 6.8-7 Final bathymetry using Camenen and Larson (2005) - Case Study 3 ..... 113
Figure 6.8-8 Outflow hydrographs at breach opening (Case Study 3) ..... 115
Figure 6.8-9 Simulated bed profiles at breach opening on the central transverse cross-section using Equation 5.2-5, Equation 5.2-6, Smart and Jäeggi (1983) and Camenen and Larson (2005) sediment transport equations (Case Study 3) ..... 117
Figure 6.8-10 Sensitivity analysis: Smart and Jäeggi (1983) – Case Study 3 ..... 118
Figure 6.8-11 Sensitivity analysis: Equation 5.2-5 – Case Study 3 ..... 119
Figure 6.8-12 Sensitivity analysis: Equation 5.2-6 – Case Study 3 ..... 119

Figure 6.8-13 Sensitivity analysis: Camenen and Larson (2005) – Case Study 3 ..... 120
Figure 6.9-1 Embankment structure shape and design data for Impact Project Test 2 (adapted from Floodsite, 2011) ..... 122
Figure 6.9-2a Removing stop log from notch (Floodsite, 2011) ..... 123
Figure 6.9-2b Two step headcut development plus sediment fan (Floodsite, 2011) ..... 123
Figure 6.9-2c Breach formation (Floodsite, 2011) ..... 124
Figure 6.9-2d No signs of block affecting breach flow within 4 seconds of start of failure (Floodsite, 2011) ..... 124
Figure 6.9-2e Left side (facing downstream) block failure (Floodsite, 2011) ..... 125
Figure 6.9-2f Vertical sides of breach immediately after breach formation process (Floodsite, 2011) ..... 125
Figure 6.9-3 Initial Bathymetry (Case Study 4) ..... 127
Figure 6.9-4 Outflow hydrographs at breach opening (Case Study 4) ..... 128
Figure 6.9-5 Predicted outflow vs measured data for Case Study 4 of the Impact Project (Floodsite, 2011) ..... 131
Figure 6.9-6 Simulated final profiles using Equation 5.2-5, Equation 5.2-6, Smart & Jäeggi (1983) and Camenen & Larson (2005) sediment transport equations (Case Study 4) ..... 132
Figure 6.9-7 Sensitivity analysis: Equation 5.2-5 - Case Study 4 ..... 133
Figure 6.9-8 Sensitivity analysis: Equation 5.2-6 - Case Study 4 ..... 133
Figure 6.9-9 Sensitivity analysis: Camenen & Larson (2005) - Case Study 4 ..... 134
Figure 6.9-10 Sensitivity analysis: Smart and Jäeggi (1983) - Case Study 4 ..... 134
Figure 6.10-1 Longitudinal profile of the hypothetical long dam - Case Study 5 ..... 136
Figure 6.10-2 Initial bathymetry of the hypothetical long dam - Case Study 5 ..... 136
Figure 6.10-3 Simulated outflow hydrograph at the breach opening for a constant inflow of 100 $m^3/s$ – Case Study 5 ..... 138
Figure 6.10-5 Simulated final profiles using Equation 5.2-5, Equation 5.2-6, Smart & Jäeggi (1983) and Camenen & Larson (2005) sediment transport equations – Case Study 5 ..... 142

# LIST OF TABLES

Table 2.4-1 Selected parametric breach models: Sources (Wu (2011) and Zagonjolli (2007)) ..... 14
Table 2.5-1 The applicability of HR BREACH (Based on Wahl, 2009) ..... 23
Table 2.5-2 The applicability of SIMBA (Based on Wahl, 2009) ..... 24
Table 2.5-3 The applicability of FIREBIRD (Based on Wahl, 2009) ..... 24
Table 2.9-1 Summary of sediment transport equations and slope data ranges ..... 40
Table 3.3-1 Results of density determination by the pycnometer ..... 48
Table 4.1-1 Experimental results for all bed slopes and median ($d_{50}$) sediment size = 0.2 mm ..... 53
Table 4.1-2 Experimental results for all bed slopes and median ($d_{50}$) sediment size = 1 mm ..... 54
Table 4.1-3 Experimental results for all bed slopes and median ($d_{50}$) sediment size = 2.4 mm ..... 54
Table 4.1-4 Measured and predicted unit sediment transport rates for median ($d_{50}$) sediment size 2.4 mm ..... 56
Table 5.2-1 ANOVA table for Equation 5.2-5 using median ($d_{50}$) sediment size = 2.4 mm and 1 mm; bed slopes = 25%, 33% and 40% ..... 64
Table 5.2-2 ANOVA table for Equation 5.2-6 using median ($d_{50}$) sediment size = 2.4 mm and 1 mm; bed slopes = 25%, 33% and 40% ..... 65
Table 5.3-1 ANOVA table for Equation 5.3-7 using median ($d_{50}$) sediment size = 2.4 mm and 1 mm; bed slopes = 25%, 33% and 40% ..... 73
Table 5.3-2 ANOVA table for Equation 5.3-9 using median ($d_{50}$) sediment size = 1 mm and bed slopes = 25%, 33% and 40% ..... 75
Table 5.3-3 ANOVA table for Equation 5.3-10 using median ($d_{50}$) sediment size = 2.4 mm and bed slopes = 25%, 33% and 40% ..... 77
Table 5.3-4 ANOVA table for Equation 5.3-11 using median ($d_{50}$) sediment size = 2.4 mm and 1 mm; bed slopes = 25%, 33% and 40% ..... 78
Table 5.3-5 Summary of statistical test results ..... 80
Table 5.4-1 Flow conditions and applicable slopes ..... 82
Table 5.4-2 Flow and sediment properties ..... 82
Table 5.4-3 Sediment transport equations for comparative analyses ..... 82
Table 5.4-4 Predicted sediment transport rates in kg/m/s ..... 83
Table 5.4-5 Mass sediment discharge (kg/m/s) to mass flow discharge (kg/m/s) ..... 84
Table 5.4-6 Predicted sediment concentrations in mg/l ..... 84
Table 6.6-1 Calibrated model setup parameters – hydrodynamics (Case Study 1) ..... 95
Table 6.6-2 Calibrated model setup parameters – morphology (Case Study 1) ..... 95
Table 6.6-3 Simulated discharge at the flume outlet ..... 100
Table 6.7-1 Calibrated model setup parameters – hydrodynamics (Case Study 2) ..... 102
Table 6.7-2 Calibrated model setup parameters – morphology (Case Study 2) ..... 103

Table 6.8-1 Calibrated model setup parameters – hydrodynamics (Case Study 3).... 110
Table 6.8-2 Calibrated model setup parameters – morphology (Case Study 3)..... 111
Table 6.8-3 Measured data and output parameters for selected models (Adapted from Floodsite, 2011)..... 115
Table 6.9-1 Soil properties for Case Study 4..... 121
Table 6.9-2 Dam geometry..... 121
Table 6.9-3 Calibrated model setup parameters – hydrodynamics (Case Study 4).... 126
Table 6.9-4 Calibrated model setup parameters – morphology (Case Study 4)..... 126
Table 6.9-5 Peak discharges and times to peak as predicted by selected sediment transport equations (Case Study 4)..... 129
Table 6.9-6 Sensitivity of the peak discharge to sediment transport equations and Manning's resistance coefficient (n) (adapted from Floodsite, 2011) .... 129
Table 6.9-7 Sensitivity of the peak discharge to sediment transport equations (this study)..... 130
Table 6.10-1 Calibrated model setup parameters – hydrodynamics (Case Study 5).... 137
Table 6.10-2 Calibrated model setup parameters – morphology (Case Study 5)..... 137
Table 6.10-3 Predicted peak discharge at the breach opening by each of the four sediment transport equations..... 138
Table 6.10-4 Peak discharge estimation using empirical equations..... 139
Table 6.10-5 Predicted peak discharges by each of the four sediment transport equations at 1.85 km from the breach opening ..... 140
Table 6.11-1 Sensitivity analysis results ..... 143

# ABBREVIATIONS

| | |
|---|---|
| 1D | One Dimensional |
| 2D | Two Dimensional |
| ANOVA | Analysis of Variance |
| AREBA | A Rapid Embankment Breach Assessment |
| ARS | Agricultural Research Service |
| BEED | Breach Erosion of Earthfill Dams |
| BREADA | BReaching of EArthfill Dam |
| BRDAM | Brown and Rogers Dam-break Model |
| DEICH | Dam Erosion with Initial Breach Characteristics |
| DHI | Danish Hydraulic Institute |
| GUI | Graphical User Interface |
| HD | Hydrodynamic |
| LHS | Left Hand Side |
| MPM | Meyer-Peter Müller |
| NCCHE | National Centre of Computational and Hydrologic Engineering |
| NRCS | Natural Resources Conservation Service |
| NWS | National Weather Service |
| SANCOLD | South Africa National Commission on Large Dams |
| SIMBA | Simplified Dam-Break Analysis Model |
| USBR | United States Bureau of Reclamation |
| USDA | United States Department of Agriculture |
| SCS | Soil Conservation Service |
| S&J | Smart and Jäeggi (1983) |

# LIST OF SYMBOLS

## ROMAN

A Coefficient in Ackers and White (1973)

B Channel width, width of a rectangular laboratory flume and breach width (m)

$B_{avg}$ Average breach width (m)

C Coefficient in Ackers and White (1973), Chezy resistance coefficient resistance factor

$C_b$ Offset factor that varies as a function of reservoir volume

$Cr$ Courant number

$C_t$ Total sediment concentration by weight (ppm)

d Particle diameter (mm)

$d_{30}$ Sediment size for which 30% weight of a non-uniform sample is finer (mm)

$d_{50}$ Median diameter of bed material or median sediment size (50% finer) (mm)

$d_{90}$ Sediment size for which 90% weight of a non-uniform sample is finer (mm)

$d_i$ Median diameter for i-th size of bed material (mm)

DP Dimensionless parameter

$d_*$ Dimensionless particle diameter

$f$ Functional relationship symbol

$f^1$ Friction factor

F Statistic test value in the F distribution table

$F_{(k,n-p,\alpha)}$ An F value at the selected significance level ($\alpha$) for a calculated numerator (k or $df_1$) and denominator (n-p or $df_2$) degree of freedom

$F_{gr}$ Mobility number

$F_o$ F value in ANOVA table

$F_r$ Froude Number

g Acceleration due to gravity ($m/s^2$)

| | |
|---|---|
| h | Average depth of water; discharge head; water depth in channel; depth of flow; average depth of flow section (m) |
| $h_b$ | Height of breach (m) |
| $h_d$ | Dam wall height (m) |
| $h_w$ | Water depth in the reservoir initiating failure (m) |
| $k$ | Empirical calibration coefficient, numerator degree of freedom |
| K | Empirical parameter in Wu and Long (1993) |
| $k_o$ | A calibration coefficient that depends on the properties of the material and on the conditions in which erosion occurs $\left(\frac{m^5}{sN^{\frac{3}{2}}}\right)$ |
| $K_o$ | Factor = 1.4 for overtopping and 1.0 for piping |
| $k_s$ | Roughness coefficient |
| $m$ | Coefficient in Ackers and White (1973) |
| M | Empirical parameter in Wu and Long (1993), Manning's resistance number = (1/n) |
| $M_{SE}$ | Mean square on error |
| $m_{h20}$ | Mass of water (kg) |
| $m_s$ | Mass of sediment (kg) |
| $M_{SR}$ | Mean square on regression |
| $n$ | Manning's resistance coefficient $\left[\frac{s}{m^{\frac{1}{3}}}\right]$, porosity, coefficient in Ackers and White (1973), number of observation or sample size |
| $n'$ | Manning's roughness coefficient corresponding to grain roughness |
| n | Transition coefficient in Ackers and White (1973) |
| p | Degrees of freedom on the regression/numerator |
| $q$ | Total unit flow discharge per unit width ($m^3/s/m$) |
| Q | Flow discharge ($m^3/s$) |

$q_b$ Volumetric sediment transport rate of bed-load per unit width ($m^3/s/m$)

$q_{bi}$ Volumetric sediment transport rate of the i-th fraction of bed-load per unit width ($m^3/s/m$)

$q_{cr}$ The critical unit flow discharge at initiation of motion ($m^3/s/m$)

$Q_p$ Peak discharge ($m^3/s$)

$q_s$ Total volumetric sediment discharge per unit width, sediment flux ($m^3/s/m$)

$q_{si}$ Transport rate of the i-th fraction of suspended load per unit width ($m^3/s/m$)

$q_t$ Total mass sediment discharge per unit width (kg/m/s)

$Re_*$ Reynolds number

$R_h$ Hydraulic radius (m)

$r^2$ Coefficient of determination (r-square)

$s$ Relative unit weight of sediment or relative density of sediment

S Reservoir storage ($m^3$)

$S_f$ Water surface or friction slope (m/m) (%)

$S_o$ Bed slope (m/m) (%)

$S_{SE}$ Sum of squares on error

$S_{SR}$ Sum of squares on regression

$S_{yy}$ Total sum of squares

$t$ Time (s)

$T_c$ Total load sediment transport capacity ($kg/m^3$)

$t_P$ Time to peak (s)

$t_f$ Failure time (s), (min) and (hr)

$u$ Velocity in the x-direction (m/s)

$U_{max}$ Maximum velocity (m)

$U_*$ Shear velocity (m/s)

$U'_*$ Bed-shear velocity related to grains (m/s)

$U_{*c}$ Critical shear velocity (m/s)

v Velocity in the y-direction (m/s)

V Average flow velocity (m/s)

$V_{cr}$ Critical average water velocity at incipient motion (m/s)

$V_{er}$ Volume of embankment material eroded ($m^3$)

$V_{H2O}$ Volume of water ($m^3$)

$V_s$ Volume of solids or sediment ($m^3$)

$V_w$ Volume of water in the reservoir initiating failure, outflow volume ($m^3$)

$w_i$ Settling velocity of i-th fraction of sediment (m/s)

$w_m$ Settling velocity of suspended sediment in turbid water (m/s)

$w_s$ Settling or fall velocity of sediment particle (m/s)

$x$ Longitudinal distance (m)

$y$ Transverse distance (m)

Y Potential energy per unit weight of water (J/N)

z Breach side slope coefficient

$z_t$ Bed elevation (m)

**GREEK**

$\alpha$ Coefficient or exponent, statistical confidence level

$\beta$ Coefficient or exponent

$\gamma_m$ Specific weight of turbid water ($kN/m^3$)

$\gamma_s$ Specific weight of sediment particles ($kN/m^3$)

$\gamma_w$ Specific weight of water ($kN/m^3$)

$\varepsilon_o$ Grain packing density

$\varepsilon_r$ Erosion rate (m/s)

| | |
|---|---|
| $\theta$ | Dimensionless total bed shear stress parameter or Shields' parameter |
| $\theta_{cr}$ | Critical Shields' parameter or critical value of dimensionless total bed shear stress parameter |
| $v$ | Kinematic viscosity ($m^2/s$) |
| $\rho_s$ | Density of sediment or soil ($kg/m^3$) |
| $\rho_w$ | Density of water ($kg/m^3$) |
| $\tau$ | Mean shear stress ($N/m^2$) |
| $\tau_c$ | Critical bed shear stress ($N/m^2$) |
| $\tau_{ci}$ | Critical shear stress for the incipient motion of the i-th fraction of non-uniform sediment ($N/m^2$) |
| $\tau_o$ | Bed shear stress ($N/m^2$) |
| $\Psi$ | Universal stream power |
| $\emptyset$ | Non-dimensional sediment transport rate |
| $\emptyset_b$ | Non-dimensional bed-load sediment transport rate |
| $\emptyset_{bi}$ | Non-dimensional fractional bed-load sediment transport rate |
| $\emptyset_{si}$ | Non-dimensional fractional suspended load sediment transport rate |
| $p_{bi}$ | The gradation of the i-th fraction of bed material |
| $\nabla$ | Nabla / Vector, a differential operator |
| $\Delta t$ | Time step (s) |
| $\Delta x$ | Grid size (m) |

**SIGNS**

| | |
|---|---|
| = | Equivalent or equal |
| ± | Negative or positive/ plus or minus |

# CHAPTER 1 INTRODUCTION

## 1.1 Background

Earth dams are constructed to impound water in the absence of adequate naturally flowing stream water or natural reservoirs. This water is needed for irrigation, drinking and hydro power generation. Earth dams, dykes and levees can also be used to control flooding. Earth dams refer to embankment wall structures that are constructed using erodible materials. Though extremely rare, an unfortunate event of failure of an earth dam or dyke can have catastrophic consequences for the people or property downstream of the impoundment. This "potential catastrophic failure and the resultant downstream flood damage is a scenario that is of great concern" to dam safety personnel (Biscarini et al., 2010). Historical cases and incidents of dam failures bear testimony to the potential catastrophes that can be caused by dams or dykes in the event of breaching. Due to this concern, continuous efforts are being made by dam practitioners and hydraulic engineers to enhance the safety of earth dams.

Earth dams are sometimes provided with fuse plug levees or dykes with a crest lower than the top of the main dam. The fuse plugs are designed to wash out and provide emergency spillway capacity in the event of an overtopping flood. The safe operation of fuse plugs requires knowledge of the erosion rates and breach formation times in order to evaluate the impacts associated with the operation of the fuse plugs at various design floods.

Dam-break analysis contributes to dam safety by using tools for risk estimation and evaluation, risk computation and analysis, which are based on case histories, past incidents and/or process modelling. Process modelling involves the hydrologic and hydraulic analysis of dam, fuse plug levee, or dike breach flow and the resulting flood. It includes three primary tasks:- (1) predicting the breach characteristics (e.g., shape, depth, width, and formation time) and processes, (2) routing the upstream inflows through the breach opening, and (3) routing the breach outflow hydrograph through the downstream area (Wu, 2011). In order to assess the probability of failure and its impacts, dam-break analysis is needed for the estimation of the consequences of a probable failure. Dam-break analysis is achieved by using empirical (analytical or parametric) and physically-based models. Empirical models are based on fitting relationships between dominant parameters such as water depth behind the dam, reservoir volume and historic observations of breach dimensions during past incidents. Analytical and parametric models make use of past incidents to predict possible dam-break characteristics. The successful application of parametric and analytical models has been limited by the quality of data from previous dam incidents. In addition, any simplifications and assumptions that were made in the derivation of the parametric equations may also limit their predictive capability considering that they are event specific. Wu (2011) pointed out that detailed multidimensional physically-based models can provide better physical insight and knowledge on the complex earth dam breaching processes. It

is expected that physically-based models could offer more improved predictive capability as long as further attempts are made to accurately simulate the underlying physical processes.

Physically-based models simulate the dynamic interactions between the flowing water and the erosion of sediment in order to quantify the development of the breach. The rate of erosion is calculated based on a defined sediment transport equation.

The selected sediment transport equation from a number of optional equations within a numerical model, determines the rate and extent to which the embankment material is predicted to be eroded by the overtopping water. The two major erosion categories include head-cut erosion and surface erosion. The accurate representation of these physical processes is a huge challenge. According to the results of laboratory and field tests of earth dam failures that were conducted under the IMPACT project (Floodsite, 2011), multiple flow processes can occur at any given time during the breach formation process since the earth dam and breach geometry are rarely regular. This results in approach flow conditions that are not normally symmetrical and uniform and are characterized by high energy flows which typically remove soil blocks that fall into the breach within seconds. It was observed under the IMPACT project that the sediment erosion and removal is not uniform or steady (Floodsite, 2011). Apart from sediment erosion, there is also mass erosion and soil wasting, which occur under a very transient and dynamic environment and significantly influence the rate of breach growth and widening. The sediment erosion rarely occurs in typical instantaneous equilibrium conditions and this phenomenon requires special consideration during numerical modelling.

There is an inherent uncertainty in the predictive ability of the sediment transport capacity relationships that were developed under gentle slope conditions for earth dam breach flow as the actual sediment transport takes place under highly unsteady and non-uniform flow conditions. According to Zagonjolli (2007), during dam breaching, the flow might develop into unsteady, supercritical flow and if these conditions apply, the use of unsteady non–uniform sediment transport equations is more appropriate. However, due to the limited availability of equations that are based on steep slopes, sediment transport equations based on uniform and steady flow conditions data are commonly used. The uncertainty in the sediment transport equation could influence the accurate representation of sediment transport dynamics, which is key to the accurate simulation with physically-based numerical models. Even though the critical conditions for the entrainment of sediment on steep slopes have a significant influence on the results, most numerical models assume that erosion, sediment entrainment and transport can all be determined by the transportation capacity that is estimated by the selected sediment transport equation. To improve the predictions, there is need for better understanding of the sensitivity of the sediment transport equation that is applied in the numerical models.

There are dozens of available sediment transport equations in literature. The majority of these were based on data from slopes of natural rivers or laboratory flumes that were relatively gently sloping. This is contrary to typical earth dam slopes where bed slopes range from moderately

steep to steep. The predictive capabilities of physically-based dam-break numerical models are dependent on the improved understanding of the effects of steep slopes on the sediment transport rates and the uncertainty of the output results associated with the application of any given sediment transport equation. In this regard, the accurate estimation of sediment transport dynamics should result in the accurate simulation of the breach geometry development. The breach geometry development determines the temporal evolution of the outflow hydrograph. The knowledge of the estimated range of the outflow hydrograph peaks is significant for dam safety planning and the development of early warning systems, early preparedness and possible future evacuation procedures for the population at risk.

## 1.2 Introduction to dam-break analysis

Dam-break analysis must simulate two main activities, namely: the failure process analysis and the consequent downstream inundation extent and effects analysis. The failure process analysis looks at the mechanism, geometry, rate of formation and development of the breach. The downstream inundation extent and effect analysis mainly involves the determination of the behaviour and characteristics of the ensuing waves, outflow routing and consequences of the flood waves as they pass through downstream reaches of the channel. The downstream effects are directly dependent on the nature and physical behaviour of the outflow from the breach. The specific parameters that are required for the downstream inundation extent and effects analysis include the outflow hydrograph, peak discharge and the resultant depths and velocities of the flow at the relevant downstream spatial locations at any given point in time. An accurate prediction of these specific parameters depends on the accurate quantification of the breach characteristics obtained from the failure process analysis.

In South Africa, dam safety legislation requires that the hazard rating of a dam be considered in the classification of dams (SANCOLD, 1991). Hazard rating is partially based on a dam-break analysis study. Dam-break analysis provides results for the formulation of relevant interventions to limit or mitigate the risk of failure, the formulation of dam safety strategies and the delineation of the area that could likely be affected by flooding in the event of a dam failure. Some of the activities that deal with dam safety within the context of operation of dams such as surveillance, monitoring, assessment, evaluation and emergency preparedness are also based on dam-break analysis results.

Research work on dam-break analysis has been ongoing for over half a century, in order to improve the understanding of breach characteristics and the associated physical processes. The general objective was to develop improved understanding of dam-break floods, dam breach theories, modes of failure, breach mechanisms and geometry, characteristics of flow through the breach, flood routing and inundation characteristics. These studies have led to the development of much improved dam-break analysis methods for application in flood routing and inundation assessment, with the aim of improving the overall dam safety strategies. This research contributes to the improved understanding of the processes of sediment transport dynamics in dam-break analysis. Unlike typical river or alluvial sediment transport processes, dam-break

sediment transport processes take place on varying steep slope configurations. This contributes to the uncertainty in the results as the sediment transport equations were derived from physically-based models with mild steep slopes.

## 1.3 Problem statement and motivation of present research

Various methods for dam-break analysis have been developed (Fread, 1988; Broich, 1998; Zagonjolli, 2007; Wang and Bowles, 2006a; Wu et al., 2011). The successful application of these methods depends on the accuracy in which they simulate the breach formation processes. Empirical and parametric methods have uncertainties that are associated with the various components of the flood prediction process. There is interest among dam practitioners in learning from past experience and information on past incidents has helped with the derivation of mathematical relationships for breach development as well as downstream flood behaviour (Hydropower and Dams, 2014).

While specific events have provided good lessons for particular dam safety situations, there are still a number of limiting issues, particularly in the general applicability of empirical methods. Even the inclusion of erodibility effects in some of the empirical methods has failed to significantly improve their predictive capability. This was after it was realised that the governing processes of erodibility/erosion play a crucial role in breach development. As a result, the focus for some of the current research efforts on dam-break modelling has shifted towards physically-based models (Wahl, 2009).

Physically-based models appear to offer improved predictive capabilities. Physically-based models have the potential to solve some of the limitations that have been experienced when using parametric and empirical models. “Many physically-based dam-break analysis tools and techniques have been developed, owing to the technological advancement mainly in computational methods” (Zagonjolli, 2007). Computational methods have helped in the improved understanding of fluid flow and sediment transport through numerical simulations by employing computer software. However, the accurate simulation of the critical breach processes of hydrodynamics and sediment transport dynamics is still uncertain in physically-based models. According to Morris (2000) “uncertainties within the breach and sediment modelling processes probably offer the greatest contribution to uncertainty within the whole dam-break analysis process in comparison to hydrodynamic processes”. As such, the quality of results of a physically-based dam-break analysis depends directly on the quality of the prediction of the sediment transport rates during dam breach development.

The sediment transport dynamics involve sediment entrainment and transport rates or capacity. Sediment transport rate is defined as “the mass of sedimentary material, both particulate and dissolved, that passes across a given transverse cross section of a given flow in unit time” (MIT,

2010). “The selection of a sediment transport equation to be used in any mobile bed problem is difficult and is typically based on professional judgment, previous experience, or even personal preference” (Mohamed et al., 2002). Wang et al. (2006) pointed out that any efforts to improve the simulation of the hydrodynamics in breach modelling can be in vain if the mathematical computation of sediment transport processes is poorly performed. This shows the critical role in which the realistic mathematical computation and modelling of sediment transport have in dam-break analysis. It is one of the major obstacles that have restricted modellers’ ability to accurately predict the hydrodynamics and rate of development of a breach through an embankment to date. This can probably be attributed to lack of data and understanding of the breach processes (Hassan et al., 2010) as well as lack of limited verification and validation data for the physically-based models.

Physically-based computer models require more data, sophisticated mathematical modelling tools and significant user expertise in order to accurately simulate the details of the physical processes that are involved. The verification is concerned with ascertaining the accuracy or reliability of the simulation of the combined effects of the hydrodynamic and sediment transport processes during the breach occurrence. The validation is mainly to do with a comparison between the model output and the actual recorded or prototype dam failure events. Unfortunately, actual recorded data for validation is very limited and almost non-existent in some cases.

Mohamed et al. (2002) explained that the evidence from the documentation of actual failures shows that the failure of an earth dam progresses through general erosion of the earth dam material to mass failures caused by soil slope instability. Assuming there is an unlimited supply of sediment during dam-break from all possible sources and processes, the sediment transport capacity can be the main factor influencing dam breach development. The earth dam material is mainly eroded due to the transport capacity of the overtopping water (Faeh, 2007).

There have been cooperative efforts to develop physically-based computational dam breach models that can simulate both the erosion processes and the associated hydraulics in a detailed manner (Wahl, 2009). The results from the cooperative efforts have helped to improve the estimates of breach outflow discharges, breach evolution and width, outflow peak and flooding consequences. It is expected that further improved knowledge of the sediment transport processes on steep slopes can greatly improve the predictive capacity of the existing physically-based models.

Based on this background information to physically-based computational models, it can be concluded that the accurate representation of sediment transport is one of the major challenges, considering that the flow conditions during dam-break are mostly unsteady and supercritical. Wu (2011) pointed out that the modelling of dam-break/breaching flow and sediment transport over movable beds is mainly dependent on the way the models handle sediment entrainment at the bed for any type of modelling approach used, i.e. single phase, two phase or two layer flow

theories. The major challenge is the availability of methods that can be "sufficiently validated against experiment and real-life cases". Since field data on sediment transport under rapidly varying flow conditions is quite limited (Mohamed, 2002), additional data on sediment transport can best be achieved through basic physical laboratory research. There is need for sediment transport equations that have improved capability for simulating flow on steep slopes. According to the United States Department of Agriculture (USDA, 2013), "slopes of 2 to 9 percent are classified as gently sloping; slopes of 9 to 30 percent are considered moderately steep; slopes of 30 to 50 percent are considered to be steep slopes; and slopes greater than 50 percent are considered very steep". The percentage slope of an embankment dam is equal to one hundred (100) times the ratio of the vertical rise distance to the horizontal run distance over the ground surface.

Typical downstream embankment slope gradients for earth dams range from 20% to 40%. The accurate simulation of sediment transport capacity on steep slopes requires the application of sediment transport equations that are based on similar slope data. The use of sediment transport equations that were derived for slopes other than typical earth dams' slopes could result in uncertainties. The uncertainty and limitations of various numerical models with regard to sediment dynamics formulation on steep slopes dictate the need for a detailed understanding of the existing sediment transport theory in order to determine how best the existing knowledge on sediment transport can be adapted for dam-break analysis.

## 1.4 Objectives of the research

"It is difficult to identify a single best model or type of model that can be claimed to be appropriate to any or all dam-break flow conditions" (Morris, 2000). However, sensitivity and uncertainty analysis can be conducted for various aspects of model uncertainties in the existing models in order to compare different scenarios. The aim of this study was to conduct an evaluation of the accuracy of existing sediment transport equations on steep slopes and to develop new sediment transport equations for steep slopes considering typical embankment dam slopes, in order to improve the prediction and modelling of the rate of breach formation. The accurate modelling of the rate of breach formation due to overtopping of the non-overspill crest of the dam during a large flood, is expected to result in reasonable prediction of the peak discharge and volume of the outflow hydrograph. The general objective was to assess existing and develop empirical sediment transport equations for homogeneous earth dam-break analysis due to overtopping failure and to assess the uncertainty that is associated with sediment transport equations.

These were the specific objectives:

a) To derive new sediment transport equations for use in dam-break numerical modelling on steep slopes.
b) To conduct a comparative evaluation of the measured and predicted sediment transport rates on steep slopes by different sediment transport equations.

c) To compare the performance of sediment transport equations in dam-break numerical modelling in order to assess the uncertainty in the model results.

## 1.5 Structure of the dissertation

This dissertation has been organized into eight chapters that deal with the experimental study of sediment transport rates on steep slopes and the application of the results in dam-break modelling. The first chapter gives an introductory background to study the topic and the broad aspects and interrelationships between sediment transport dynamics and dam-break modelling. Chapter 1 also gives the general and specific objectives of this research.

A literature review of dam-break models of selected sediment transport equations for gentle slopes and sediment transport equations that were derived from data for moderately steep slopes is given in Chapter 2. Chapter 3 contains descriptions of the experimental setup and of procedures for the determination of sediment transport rates on steep slopes. Chapter 4 provides an analysis of the results, general remarks of the experimental study and a comparative evaluation of the measured and predicted sediment transport rates on steep slopes with different sediment transport equations.

Chapter 5 discusses the formulations that have been applied in the development of the new sediment transport equations. The predictive capability and adequacy of the proposed sediment transport equations are analysed using statistical tests and comparisons with existing sediment transport equations from literature. Chapter 6 demonstrates the application of the new proposed sediment transport equations in dam-break numerical modelling. The uncertainty in model output results due to the application of different sediment transport equations is also quantified in Chapter 6. A summary of discussions and conclusions is presented in Chapter 7. Chapter 8 gives recommendations for further studies and research. Other significant raw and processed data are provided in tables and graphs in the Appendices.

# CHAPTER 2 LITERATURE STUDY ON DAM-BREAK ANALYSIS AND SEDIMENT TRANSPORT DYNAMICS

## 2.1 Overview to this chapter

This chapter gives a review of dam-break analysis, flow hydraulics, dam-break models and sediment transport equations. Dam-break analysis involves breach formation and flow modelling. The ultimate goal of dam-break analysis is to develop dam safety strategies and emergency management plans. These emergency and dam safety plans need to be based on either past experience from dam failures or on an understanding of the underlying physical processes. The critical analysis of past dam incidents and accidents is significant in order to learn not only the breach characteristics but also any other contributions to dam failure by factors such as human behaviour, lack of proper communication procedures, training for dam operating personnel and the provision of adequate levels of redundancy for critical control equipment (Hydropower and Dams, 2014). A review of dam-break models (analytical, parametric and numerical) and relevant sediment transport equations is also presented.

## 2.2 Flow hydraulics and sediment transport aspects of the breaching of earth dams

An understanding of the flow hydraulics and sediment transport aspects of breaching of earth dams is a key requirement for the accurate prediction of the peak of the outflow hydrograph. The calculation of discharge downstream of the breached dam at any point in time is dependent on the development of the breach, which is in turn dependent on flow hydraulics and sediment transport. The discharge also depends on the reservoir water level and volume. Dam-break could result from overtopping, seepage and piping. In overtopping, the flow of water through the breach results in channel erosion over the crest and the downstream face due to shear forces. Overtopping is the cause of more than 50% of South African dam incidents (Oosthuizen, 2009).

Figure 2.2-1 shows a schematic drawing of flow hydraulics and sediment transport during overtopping. At breach development phase 1, the initial breach opening is initiated by the interaction of the overflowing flow and dam material after the reservoir water level has exceeded the embankment crest height. A minimal discharge head (h) at a certain water level in the reservoir is responsible for the initiation of the breaching process. According to Powledge et al. (1989) as cited by Broere (1999), erosion starts at the points of slope discontinuity such as at the crest of the dam or any other sloping part of the embankment between the toe and the crest. As erosion undercuts the slopes, the bed level changes continue to the upstream crest side, resulting in the hydraulic controls shown in Figure 2.2-1. The breach development phase 1 in Figure 2.2-1 refers to the initial crest notch that is made by the advancing erosion at the top of the embankment. When a larger portion of the crest is eroded, at breach development phase 2; the discharge increases rapidly and this phenomenon further exacerbates the erosion process. Different erosion rates take place on the dam embankment depending on the slope configuration. Upstream of the dam, the hydraulic flow regime is subcritical; while downstream, the hydraulic flow regime is supercritical before it goes to subcritical after a hydraulic jump in the downstream

tail water. The accurate modelling of the flow hydraulics and sediment transport in order to come up with the breach shape and outflow hydrograph are the major challenges in dam-break analysis. The breach outflow hydrograph is of crucial importance for the assessment of the flooding characteristics in the downstream areas (Zagonjolli, 2007).

The breach development needs to be accurately predicted both spatially and temporally. The breach development phases that have been illustrated in Figure 2.2-1 correspond to the discharges through the breach as shown in Figure 2.2-2. Figure 2.2-1 shows four time duration markers that indicate different stages of breach development. Each stage has some specific relevance.. The start of breach initiation and progression of breach initiation is characterized by slow breach flows that slowly increase due to increased upstream water level and / or progressive removal of material. Between stage 1 and 2, flow is typically small and its rate of change is slow or very slow. During stage 3, there is a transition to breach formation. This is a critical stage where steady (and relatively slow) erosion cuts through to the upstream face of the embankment initiating breach growth. There are visibly changing flow conditions and quickening erosion of the embankment through to the upstream face. This stage is followed by breach formation, where rapid vertical erosion of the embankment takes place. The extent and rate of vertical erosion depends on the volume of available flood water and design and condition of embankment. Rapid breach growth results in the continued widening of the breach after initial formation due to the turbulent and sediment laden flow. This stage is significant for predicting potential inundation downstream. Stage 4 is the peak discharge that is a function of available flood water and embankment design and condition. It is often used as a measure of worst case scenario but the peak discharge at the breach opening does not necessarily relate to worst flood conditions downstream of the dam.

Numerical models are sometimes preferred instead of analytical models due to their detailed representation, in space and time, of these critical processes of flow hydraulics and sediment transport. Wu (2007), as cited by Moges (2010), explains that “computational simulation (using numerical models) gives direct, real scale predictions without any scale distortion and is cost effective”. Erosion and sediment entrainment are modelled using sediment transport equations and the reliability of the computational simulation relies on the following (Moges, 2010):

a) How accurately the governing differential equations are discretized using numerical schemes;
b) How effectively the discretized algebraic equations are solved using direct or iterative solution methods;
c) Whether the numerical solution procedures are correctly coded and;
d) How well the physical processes are mathematically described through governing equations, boundary conditions, and empirical equations.

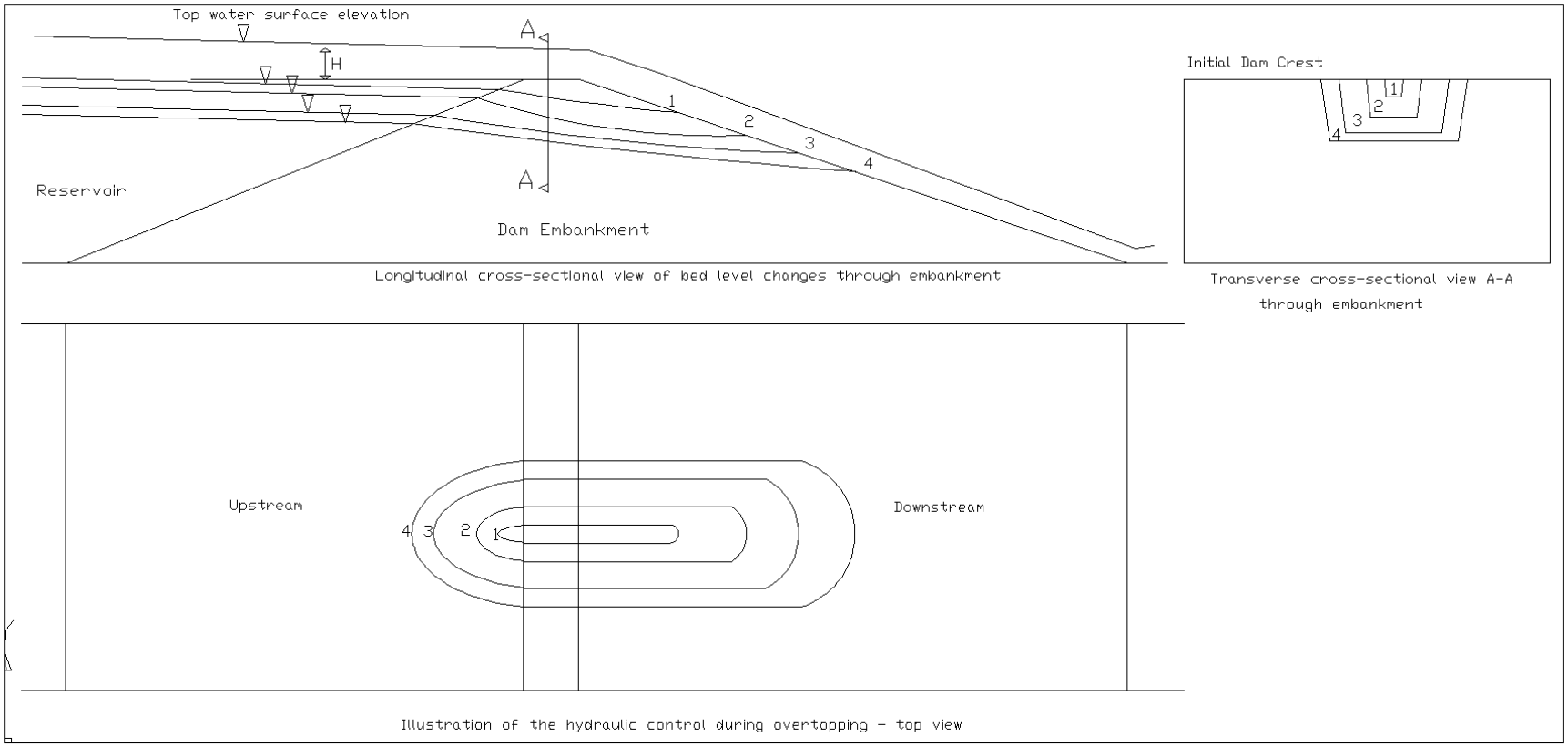


**Figure 2.2-1 Sketch of hydraulic control during overtopping (adapted from Powledge et al. (1989))**

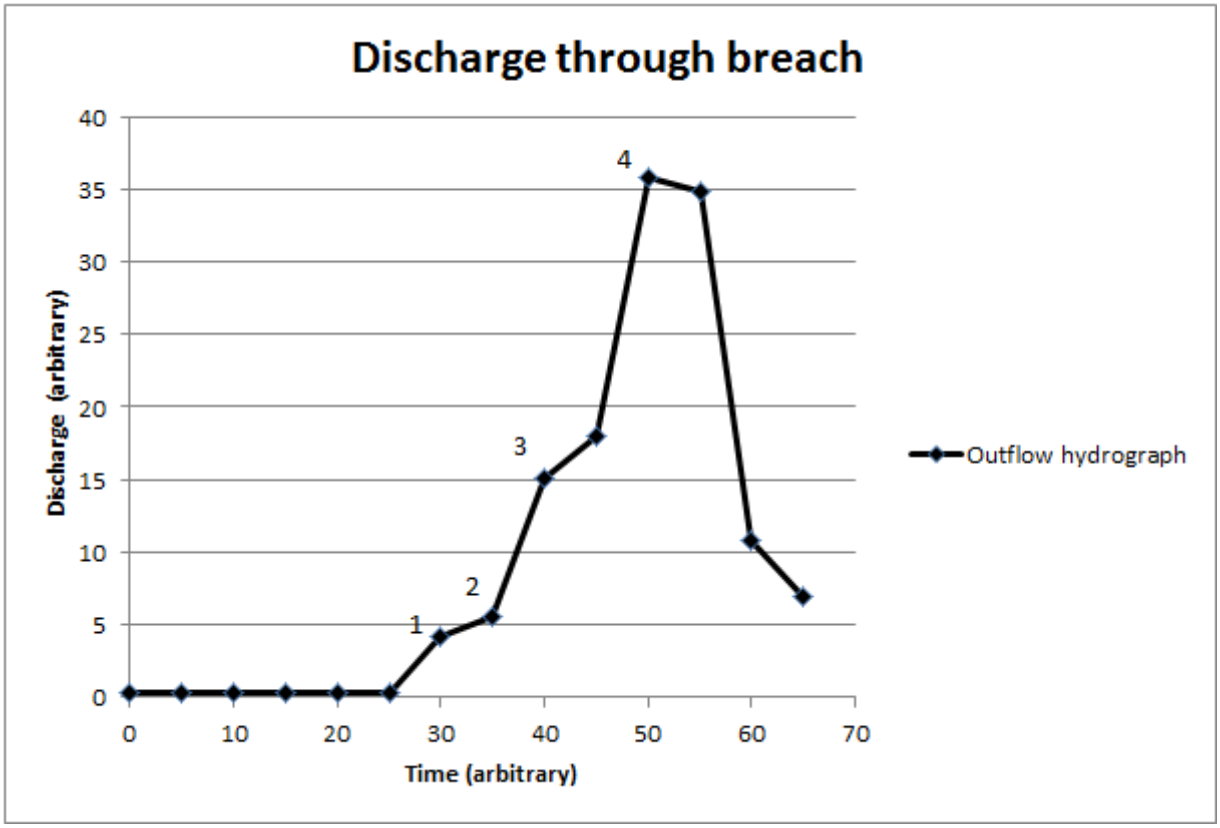


**Figure 2.2-2 Discharge through breach in relation to breach development phases**

## 2.3 Dam safety strategies

Dam-break analysis provides an improved understanding and management of dam safety risks and the formulation of appropriate dam safety strategies. Figure 2.3-1 below illustrates interrelatedness between dam-break analysis and dam safety.

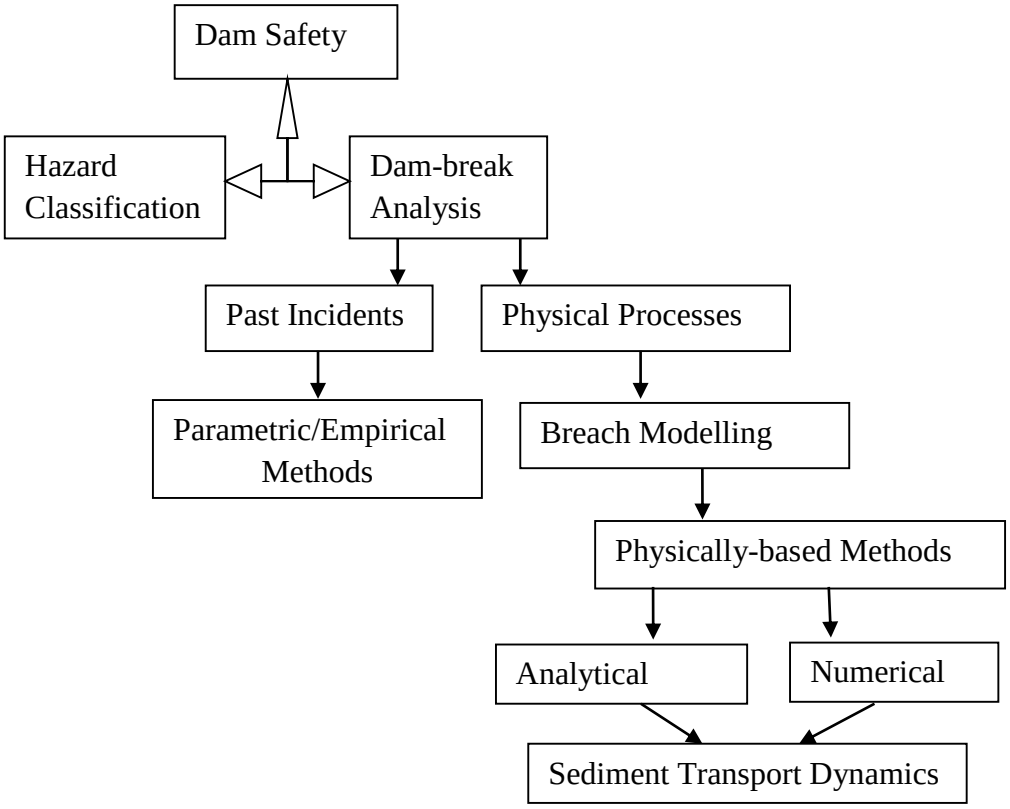


**Figure 2.3-1 A conceptual framework of the relationship between dam safety and dam-break analysis**

Figure 2.3-1 shows that dam-break analysis is required in order to estimate and evaluate the actual risk in the unfortunate event of a dam-break. The results from the estimation and evaluation are then used to compute the extent of risk to the vulnerable people, critical infrastructure and property downstream. Dam safety strategies are formulated to deal with this risk to public safety including the design of procedures for surveillance, monitoring, assessment, evaluation, planning and emergency action preparedness.

Sediment transport dynamics are some of the critical input parameters in the dam-break modelling of the physical processes apart from those dealing with flow hydraulics. The conceptual framework in Figure 2.3-1 shows that dam-break models can be classified as parametric, empirical or physically-based depending on the approach that is used in the prediction of the breach formation processes and characteristics.

## 2.4 Parametric (empirical) dam-break models

Even though this research was more concerned with physically-based dam-break models, a brief review of parametric models is provided for purposes of appreciating their limitations and to show the need to supplement their application with process based models in dam-break modelling. The empirical models directly predict the breach outflow using derived regression equations from a set of data on recorded past incidents of dam failures. Parametric models predict the breach outflow and other breach characteristics based on the user's input parameters such as dam type, dam height, storage volume, initial water height, etc. The predicted breach characteristics include peak discharge, breach width, shape, slope, failure time, etc.

Table 2.4-1 shows selected parametric breach models as cited by Wu (2011) and Zagonjolli (2007). The empirical equations that have been labelled with ID numbers 13 and 15 in Table 2.4-1 include the effect of erodibility in the equations. Erodibility is the relative ability or strength of earth material to withstand eroding forces. The fact that these researchers decided to include the effect of material erodibility as an independent variable in parametric models shows the significant role that erosion plays in the determination of breach characteristics. The effect of erodibility as an earth material property upon the rate of breach formation was confirmed by Morris et al. (2007). Morris et al. (2007) showed that even though it was higher in cohesive soils, it was still significant in non-cohesive soils. Macchione (2008) pointed out that the extent of the lateral erosion and shape of the breach sides depends on the "erodibility of the dam body" apart from "the shape of the reservoir, and the water volume stored".

**Table 2.4-1 Selected parametric breach models: Sources (Wu (2011) and Zagonjolli (2007))**

| ID | Reference | Relations Proposed | Number of case studies | Remarks |
|---|---|---|---|---|
| 1 | Kirkpatrick (1977) | $Q_P = 1.268(h_w + 0.3)^{2.5}$ | 16 (plus 5 hypothetical failures) | |
| 2 | SCS (1981) | $Q_P = 16.6(h_w)^{1.85}$ | 13 | |
| 3 | Hagen (1982) | $Q_P = 0.54(h_d S)^{0.5}$ | 6 | |
| 4 | Singh and Snorrason (1984) | Guidance for B, z, $t_f$ $Q_P = 1.776(S)^{0.47}$ $Q_P = 13.4(h_d)^{1.89}$ | 20 real failures and 8 simulated failures | $Q_p$ Relations on the basis of simulations |
| 5 | MacDonald and Langridge-Monopolis (1984) | $V_{er} = 0.0261(V_w h_w)^{0.769}$ (earth fill) $V_{er} = 0.00348(V_w h_w)^{0.852}$ (non-earth fills) $t_f = 0.0179(V_{er})^{0.5}$ $Q_P = 1.154(V_w h_w)^{0.41}$ | 42 | |
| 6 | Costa (1985) | $Q_P = 0.981(h_d S)^{0.42}$ | 31 constructed dams | |
| 7 | Evans (1986) | $Q_P = 0.72(V_w)^{0.53}$ | | |
| 8 | USBR (1988) | $B_{avg} = 3h_w$ $t_f = 0.011B_{avg}$ $Q_P = 19.1(h_w)^{1.85}$ (envelope equation) | 21 | |

| | | | | |
|---|---|---|---|---|
| 9 | Von Thun and Gillette (1990) | Guidance for z,<br>$B_{avg} = 2.5h_w + C_b$<br>$t_f = \frac{B_{avg}}{(4h_w)}$<br>Erosion-resistant,<br>$t_f = \frac{B_{avg}}{(4h_w+61)}$ highly erodible | 57 | Including erodibility |
| 10 | Molinaro and Maione (1991) | $Q_P = 0.116[\frac{V_w}{(h_d)^3}]^{0.221}(g)^{0.5}(h)^{2.5}$ | Not specified | |
| 11 | Froehlich (1995a) | $Q_P = 0.607(V_w)^{0.295}(h_w)^{1.24}$ | 22 | |
| 12 | Froehlich (1995b) | Guidance for z,<br>$B_{avg} = 0.1803K_0(V_w)^{0.32}(h_w)^{0.19}$<br>$t_f = 0.00254(V_w)^{0.53}(h_b)^{-0.9}$ | 63 | Including overtopping/piping in $K_o$ |
| 13 | Walder and O'Connor (1997) | $Q_P = f(V_w, relative\ erodibility)$ | Not specified | Including erodibility |
| 14 | Broich (1998) | $Q_P = 255.859(V_w h_w)^{0.449}$<br>$Q_P = 72.611(V_w h_w^4)^{0.256}$ | 39 | |
| 15 | Xu and Zhang (2009) | B, $Q_P$<br>$t_f = f(V_w, h_w, erodibility, etc.)$ | 75 | Considering overtopping and piping, low, medium and high erodibility |
| 16 | Pierce et al. (2010) | $Q_P = 0.0176(V_w h_w)^{0.606}$<br>$Q_P = 0.038V_w^{0.475}\ \ h_w^{1.09}$ | 87 | |

The variables in Table 2.4-1 include:

B Breach width
$B_{avg}$ Final average breach width
$C_b$ Offset factor that varies as a function of reservoir volume
g Acceleration due to gravity
h Depth of water behind dam
$h_b$ Height of breach
$h_d$ Dam height
$h_w$ Water depth in the reservoir initiating failure
$K_o$ 1.4 for overtopping and 1.0 for piping
$Q_p$ Peak discharge
S Reservoir storage
$t_f$ Failure time
$V_{er}$ Volume of embankment material eroded
$V_w$ Volume of water in the reservoir initiating failure
z Breach side slope coefficient

## 2.5 Selected physically-based numerical dam-break models

Physically-based numerical dam-break models "typically simulate the embankment failure mechanisms, trying to simulate the physical processes observed. These approaches entail detailed computations combining principles of hydraulics, sediment processes and soil mechanics. The advantage of this approach is that the model provides an estimation of the breach formation process and the consequently potential flood hydrograph" (Morris and Hassan, 2002).

Process based dam-break models involve computational simulations of the physical processes. Wu (2007) points out that the reliability of computational simulations is dependent on how well the physical processes are mathematically described through the governing equations, boundary conditions, and empirical equations. By extension, within the dam-break analysis considerations, one can add the fact that the reliability of the computational simulation depends on how well the empirical equations that deal with sediment transport represent actual breach conditions.

Physically-based models simulate in single or multidimensional space the detailed sediment transport processes, hydraulics, and breach mechanics over time with minimum simplifying assumptions in comparison with parametric models. According to Kahawita (2007) physically-based models can be divided into two groups. The first group of models subdivides the breaching process into phases in which different flow and erosion mechanics are predominant. The individual phases are modelled semi-empirically using equations for which coefficients, exponents and other parameters have been determined empirically from laboratory or real world data. The second group of models attempts to simulate hydraulic conditions and sediment transport processes with fundamental differential equations that are intended to accurately describe the interactions between flow hydraulics and sediment transport processes. The latter

simulates a much more detailed consideration of the physical processes with minimal use of empirical data. The sediment transport modelling through the breach is governed by the sediment mass balance equation over the depth of flow. Despite the detailed consideration of the physical processes, empirical equations are needed to describe the (equilibrium) concentration, total load and the bed load and suspended load transport capacities depending on the particular model's configuration or complexity. Some of the physically-based numerical dam-break models that are applicable on earth embankments are described below:

### *2.5.1 Cristofano Model - 1965*

Cristofano (1965), a sediment transport specialist with the US Bureau of Reclamation (USBR, 2014), developed a physically-based numerical dam-break model. According to Wahl (2010), it can be considered to be one of the first process based dam breach models. The sediment transport is based on an empirical equation/relation that describes the rate of erosion of the breach channel as a function of the rate of change of water flowing through the breach. The geometry of the breach was assumed to be trapezoidal with the side angle equal to the angle of repose of the compacted material.

### *2.5.2 Harris and Wagner Model - 1967*

Harris and Wagner (1967) used the modified bed load Schoklitsch sediment transport equation and the suspended load equation based on turbulence and fall velocity. The breach was assumed to commence its downward progression immediately upon overtopping and the erosion of the breach was assumed to progress to the bottom of the dam.

### *2.5.3 BRDAM Model - 1981*

Brown and Rogers (1981) developed the BRDAM model based on the modified bed load Scholitsch sediment transport equation. The BRDAM model simulates breach erosion for both piping and overtopping.

### *2.5.4 Lou Dam-Break Model - 1981*

Lou (1981) developed a numerical dam breach model that used the following sediment transport equations: Du Boys (1879) and Einstein (1942), Lou (1981) and Cristofano (1965). The breach geometry was taken as the most effective stable section (cosine curve shape).

### *2.5.5 BEED Model as Revised by Vijay P. Singh and Cesar A. Quiroga - 1987*

Another notable physically-based dam-break model was developed by Singh and Quiroga (1987). It was named Breach Erosion of Earthfill Dams (BEED). The BEED model computed the aspects of the evolution of the dam breach and the subsequent flood and sediment routing by assuming that the breach erosion rate and the subsequent breach section enlargement is either a linear or nonlinear function of the outflow mean water velocity or water flow. The breach geometry is assumed to be trapezoidal. Manning's n is applied to represent the flow resistance. A

small rivulet was assumed initially along the flow path that was widened and deepened by the continued flow and the subsequent erosion. The simulation of dam breach evolution is based on hydrologic, geometric and geotechnical considerations. The model uses the Einstein-Brown (Brown, 1950; Einstein, 1942) and Bagnold (1966) sediment transport equations for the computation of the rate of erosion in the breached section. Brown's (1950) modification to Einstein's (1942) equation is utilized to compute the rate of erosion because it does not require specification of such factors as critical shear stress that cannot be measured reliably. The sediment graph is routed based on a modified Muskingum method scheme.

### *2.5.6 NWS Breach Model - 1984*

BREACH is an erosion model for earth dam failure analysis (Fread, 1984). It is a physically-based mathematical model that predicts the breach characteristics (size, time of formation) and the discharge hydrograph emanating from a breached earth dam based on soil stability mechanics and sediment transport relationships. The sediment transport capacity of the unsteady uniform flow along an erosion formed breach channel is based on the Meyer-Peter-Müller equation as modified by Smart (1984) given information regarding the soil characteristics of the dam material, the inflow hydrograph, etc. Enlargement of the breach over time is computed by sediment transport equations, sudden collapse due to excess hydrostatic pressure and width expansion by slope stability.

In this regard, the growth of the breach channel is dependent on the dam's material properties (median ($d_{50}$) sediment size, unit weight, friction angle and cohesive strength). The erosion transport can be for either non-cohesive (granular) materials or cohesive (clay) materials. Erosion is assumed to occur equally along the bottom and sides of the breach channel except when the sides of the breach channel collapse. The BREACH model has the capability of simulating the removal of the collapsed material along the breach at the rate of the sediment transport capacity of the breach channel at the instant of collapse. Breach bottom and sides continue to erode upon completion of the removal of the collapsed material. The maximum discharge through the breach is dependent on the rate of breach enlargement via erosion and the rate at which the reservoir head decreases as a result of the increasing flow caused by the increased opening.

### *2.5.7 EDBREACH Model - 1998*

Loukola and Houkuna (1998) developed the EDBREACH model that uses the Meyer-Peter-Müller sediment transport equation and trapezoidal shaped breach geometry.

### *2.5.8 DEICH-N1/N2 Models - 1998*

Broich (1998) developed the numerical models DEICH N1 and N2 (1D and 2D). The models simulate flow and sediment transport using the shallow water equations and the Exner (1925) equation. The Exner (1925) equation is a statement of conservation of mass that is applied to

sediment in a fluvial system such as a river. The Exner (1925) equation is expressed by Equation 2.5-1:

$$\frac{\partial z_t}{\partial t} = -\frac{1}{\varepsilon_o}\nabla . q_s \qquad 2.5\text{-}1$$

Where

$z_t$ Bed elevation

$t$ Time

$\varepsilon_o$ Grain packing density

$\nabla$ Divergence (vector and differential operator) of the sediment flux, $q_s$

In two dimensional (2D) representation, $\nabla . q_s = \frac{dq_s}{dx} + \frac{dq_s}{dy}$ 2.5-2

The Exner (1925) equation describes conservation of mass between sediment in the bed of a channel and the sediment that is being transported. It states that the bed elevation increases (the bed aggrades) proportionally to the amount of sediment that drops out of transport and conversely decreases (the bed degrades) proportionally to the sediment that is being entrained by the flow. The Exner (1925) equation requires a sediment transport equation to determine the sediment flux or total volumetric sediment discharge per unit width $q_s$. Different numerical models have applied different sediment transport equations in conjunction with the Exner (1925) equation.

The geometrical representation of the DEICH model uses the diffusion approach for the hydraulics and sediment transport by applying the Saint-Venant and several classical sediment transport equations. The break and depletion period assumes that shallow water characteristics are dominant.

Broich (1998) recognized the fact that most sediment transport equations are derived for steady subcritical flow. Smart (1984) undertook experiments to check the quality of other sediment transport equations when applied to steep channel flow. The Smart (1984) sediment transport equation is an extension of Meyer-Peter Müller (MPM) (1948) that was validated for subcritical and supercritical flow conditions. Broich (1998) came up with different sediment transport equations and compared the results to Smart's (1984) measurements. Broich (1998) concluded that the equations by Smart (1984), Meyer-Peter Müller (1948) and Bagnold (1966) performed best and were finally adopted for use in the DEICH N1/N2 model simulations.

### *2.5.9 BREADA Model - 2007*

The BREADA model (Breach Model for Earthfill Dams) was developed by Zagonjolli (2007) for modelling the overtopping failure of earth dams. It is one of the recently developed models. It gives the user the choice between two breaching developments – trapezoidal or triangular. Once

the dam bottom is reached the model simulates breaching development in the lateral direction only. The model applies the reservoir routing principle of the flow through the breach. In the BREADA model (Zagonjolli, 2007), the sediment transport of the dam material is calculated using an empirical equation presented by Meyer-Peter Müller.

### *2.5.10 Junqiang Xia Dam-Break Model - 2010*

Xia et al. (2010) developed a 2D morphodynamic model for predicting dam-break flows over mobile beds. In this model, the common 2D shallow water equations were modified, so that the effects of sediment concentrations and bed evolution on the flood wave propagation can be considered. The sediment transport capacity is calculated using an equation that was proposed by Wu and Long (1993). This equation is used to compute the sediment transport capacity of the suspended load. Two empirical parameters that can be calibrated need to be applied in the sediment transport equation. As for the bed load transport capacity, an equation proposed by Dou et al. (1999) is used. The model has the ability to simulate the sorting of the different grain sizes for sediment transport capacity purposes. The bed load equation by Xia et al. (2010) is used to compute the transport capacity of sand or gravel bed-load with diameters ranging from 0.05 to 200 mm.

### *2.5.11 Tingsanchali and Chinnarasri Dam-Break Model - 2001*

Tingsanchali and Chinnarasri (2001) developed an erosion and force/moment equilibrium based three-dimensional dam breach model for the non-cohesive earth dam overtopping breach problem. The breach location can be anywhere along the dam. The model considers the topography of the entire dam site. Tingsanchali and Chinnarasri (2001) tested several methods for calculating soil transportation capacity and concluded that the method of Smart (1984), with some modifications, fitted their dam-break experiments better than other methods. Therefore they used Smart's (1984) method in the calculation of the soil transportation capacity, following the approach in the BREACH model (Fread, 1984). Other multiple sediment transport equations are available for the user to choose from. However, in the model, the soil transport capacity is not the condition used to determine equilibrium erosion of a breach. The equilibrium is limited by the resisting force and the driving force that is applied along the failure surface of each slice of failure mass.

### *2.5.12 Wang and Bowles Model - 2006*

Wang and Bowles (2006a, 2006b) developed a three dimensional non-cohesive earth dam model for overtopping breaches of a long dam. The development of the breach channel is checked using Bishop's simplified method (Hungr, 1987) before the dam is fully breached through, i.e. before the dam is eroded all the way down to the natural ground surface across an entire cross section of the dam. Three kinds of phenomena are modelled during the breaching process: a) vertical erosion of the dam faces or breach channel where the flow surface is above the eroded soil surface; b) undercutting of the breach channel sides where the flow surface is below the dam

face, followed by sudden collapse of the undercut soil; and c) possible sudden collapse of the sides of the breach channel entrance upon loss of local stability. The erosion rate ($\varepsilon_r$) is calculated by the method of Chen and Anderson (1987) using Equation 2.5-3.

$$\varepsilon_r = 0.0513[\tau - \tau_c]^{1.3} \qquad 2.5\text{-}3$$

Where

$\tau$ Mean shear stress

$\tau_c$ Critical shear stress

$\varepsilon_r$ Erosion rate

Chen and Anderson (1987) used Equation 2.5-3 to compute the erosion rate based on $d_{50}$ = 4 mm and suggested that it could be applied to non-cohesive embankments with $d_{50}$ < 8 mm which represents the median grain size. The transport of the eroded soil is limited to the transportation capacity estimated using the sediment transport equation of Smart (1984).

### *2.5.13 Roland Faeh Model (2dMb) - 2007*

Faeh (2007) developed a depth averaged two dimensional numerical model for breach erosion of earth dams based on the fact that the process of breach erosion depends on the interaction between flow, sediment transport, and the corresponding morphological changes. "The dam material is mainly eroded due to the transport capacity of the overtopping water. Both bed load and suspended load are of importance. For breach formation, the lateral erosion due to slope instabilities has a significant impact" (Faeh, 2007). The results of Faeh (2007) showed that the most sensitive parameter of an erosion-based dike-breach simulation is the breach side-slope angle which determines the lateral erosion. The model gives the user the choice to select the preferred equilibrium sediment transport capacity from different transport equations.

The model can also simulate multiple grain fractions using the approach of Hunziker and Jäeggi (2002). The sediment transport capacity is determined with a modified Meyer-Peter and Müller equation applied to each diameter of the different grain size classes. The bed load from lateral transport occurring on a transverse bed slope is determined according to the approach of Ikeda (1988). These equations apply two dominant variables namely shear stress and bed slope. Faeh (2007) studied the influence of the sediment transport module parameters on the output results and investigated the influence of different transport equations and the effect of suspended load transport on the outflow through the breach. Faeh (2007) observed deviations related to the peak discharge of up to 20% of the calibrated value when the bed load sediment transport equation was applied. However, the suspended load transport equation did not significantly change the outflow hydrograph as shown in Figure 2.5-1.

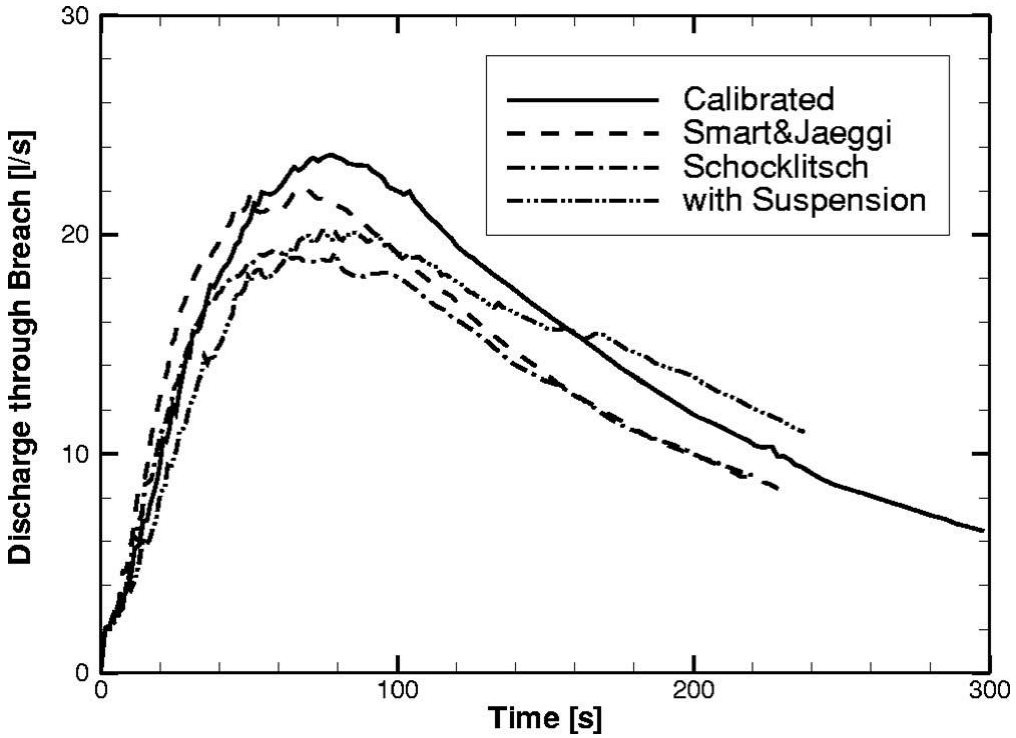


**Figure 2.5-1 Effects of sediment transport equations on discharge through breach (Faeh, 2007)**

### *2.5.14 Zhang and Wu - 2011*

Zhang and Wu (2011) developed a two dimensional hydrodynamic and sediment transport model for dam-break based on the finite volume method with quadtree. "The two dimensional shallow water equations are resolved based on the finite volume method with an unstructured quadtree mesh. The sediment transport and bed evolution modules are coupled with the hydrodynamic module to predict simultaneously the hydrodynamics, sediment concentrations and morphological changes" Zhang and Wu (2011). For the transport capacity equation of the bed-load induced during bed evolution, the equations by Bai et al. (2005) and Xia et al. (2010) are used while the sediment transport capacity for suspended load for single particles is defined by Wu (2008).

### *2.5.15 Macchione's Dam-break Model - 2008*

Macchione (2008) proposed a dam-break model which predicts, in a simple but physically-based manner, not only the peak discharge but also the whole outflow hydrograph and breach development. The equation of the volumetric sediment discharge per unit width ($q_s$) is similar to the formulation by Meyer-Peter Müller with the assumption that the critical shear stress is negligible in comparison with the mean shear stress, $\tau$ as seen Equation 2.5-4:

$$q_s = k_o \tau^{3/2} \qquad 2.5\text{-}4$$

The coefficient $k_o$ depends on the properties of the material and on the conditions in which the erosion occurs. It is determined through model calibration.

$$\tau = \gamma_w R_h S_f \qquad 2.5\text{-}5$$

$$S_f = \frac{V^2}{k_s^2 R_h^{4/3}} \qquad 2.5\text{-}6$$

Where;

$\gamma_w$ Specific weight of water

$R_h$ Hydraulic radius

$S_f$ Friction slope

$k_s$ Roughness coefficient

V Average flow velocity

### *2.5.16 HR-BREACH - 2002*

This model was developed at HR Wallingford, Great Britain. (Mohamed et al., 2002, Mohamed 2002). HR BREACH is one of the three physically-based models that have been found to have potential for further development into the next generation embankment breach modelling tool (Wahl, 2009). According to Gee (2010) HR-BREACH was developed and applied for direct application to dam safety, emergency management and flood risk management needs. The erosion mechanics simulated in HR-BREACH include shear, sliding and overturning failure of soil masses. All three of these process models make use of measured, or estimated, embankment soil characteristics such as grain size and erodibility. The use of these parameters in a hydraulic sediment transport model sets them apart from previous techniques for estimating embankment breach parameters from curve fitting to historic events (Gee, 2010; Mohamed et al., 2002; Mohamed, 2002). The sediment transport capacity is determined using various equations, for non-cohesive and cohesive sediment transport. Table 2.5-1 shows the applicability of HR BREACH.

**Table 2.5-1 The applicability of HR BREACH (Based on Wahl, 2009)**

| Embankment Types | Erosion Modes | Erosion Processes |
|---|---|---|
| Homogeneous cohesive, or simple composite embankments with non-cohesive zones, surface protection (grass or rock) and cohesive core | Overtopping, piping | Variety of sediment transport/erosion equations and multiple methods for application. Discrete breach growth using bending, shear, sliding and overturning failure of soil masses |

### *2.5.17 Simplified Dam-Break Analysis Model (SIMBA) - 2005*

Simplified Dam-Break Analysis Model (SIMBA) was developed at the United States Department of Agriculture-Agricultural Research Service (USDA-ARS) Hydraulic Engineering Research Unit, Stilwater, Oklahoma (Temple et al., 2005; Hanson et al., 2005). The model was originally developed to analyse laboratory dam breach experiments and is being incorporated into a larger suite of dam analysis tools targeted at application to the large inventory of Natural Resources Conservation Service (NRCS) dams. The SIMBA breach formation algorithm includes head-cut formation, deepening, lateral widening and upstream advancement (Gee, 2010). The sediment transport is based on parametric relations for headcut advance, bottom, and lateral erosion. Table 2.5-2 shows the applicability of SIMBA.

**Table 2.5-2 The applicability of SIMBA (Based on Wahl, 2009)**

| Embankment Types | Erosion Modes | Erosion Processes |
|---|---|---|
| Homogeneous cohesive | Overtopping | Headcut formation, deepening, and upstream advancement, lateral widening |

### *2.5.18 FIREBIRD - 2002*

This model was developed at Montreal Polytechnic (Wang and Kahawita, 2002; Wang et al., 2006). The FIREBIRD model was developed mostly as a research tool for studying the ability of different sediment transport models to simulate dam breach processes. Therefore it applies several sediment transport equations or erosion rate equations. Table 2.5-3 shows the applicability of FIREBIRD.

**Table 2.5-3 The applicability of FIREBIRD (Based on Wahl, 2009)**

| Embankment Types | Erosion Modes | Erosion Processes |
|---|---|---|
| Homogeneous cohesive or non-cohesive | Overtopping | Coupled equations for hydraulics and sediment transport |

### *2.5.19 Wu et al. (2011) Model*

Wu et al. (2011) developed a depth-averaged two dimensional model for the simulation of the unsteady flow and non-cohesive sediment transport due to earth embankment dam-break and overtopping breaching. The model adopts the generalized shallow water equations that consider the effects of sediment transport and bed change on the flow, thus leading to coupled calculations of these processes (Wu et al., 2011). The non-equilibrium total-load sediment transport capacity equation of Wu et al. (2000) is applied. The model has the ability to simulate the non-cohesive embankment slope avalanching. The sediment transport capacity of Wu et al. (2000) is applied with special modifications as suggested by Wu (2008) to consider the effect of gravity on sediment transport over steep slopes.

### *2.5.20 Abderrezzak and Paquier Model - 2011*

Abderrezzak and Paquier (2011) developed a 1D model based on the shallow-water equations, a bed update "Exner (1925)" equation, a space-lag equation for the non-equilibrium sediment transport and an empirical equation calculating the sediment transport capacity of the flow. The model was specifically set up to investigate the applicability of sediment transport equations to dam-break flows over movable beds. Abderrezzak and Paquier (2011) wanted to investigate the extent to which well-known sediment transport equations are applicable in one dimensional (1D) numerical modelling of dam-break waves over movable beds.

The model requires the user to choose from a variety of sediment transport equations proposed by Meyer-Peter and Müller (1948), Bagnold (1966), Engelund and Hansen (1967), Ackers and White (1973), Smart and Jäeggi (1983), van Rijn (1984a), Rickenmann (2001), Cheng (2002), Abrahams (2003) and Camenen, and Larson (2005). The performance of each equation was analysed by simulating four idealized laboratory cases of dam-break waves over sandy beds. It was found from the comparative analysis of the numerical results and measurements that for each case, better predictions are obtained using a particular equation. However, overall, the equations proposed by Meyer-Peter and Müller (1948) with the factor 8 being replaced by 12, Smart and Jäeggi (1983), Cheng (2002), Abrahams (2003), and Camenen and Larson (2005) rank as the best predictors for the entire range of conditions that were studied. In addition, they observed that in the cases where a bed step exists, implementing a mass failure mechanism in the numerical modelling played an important role in reproducing the bed and water profiles.

### *2.5.21 MIKE 11 Dam-Break Model (DHI, 2011)*

MIKE 11 is a one dimensional model that is based on the Saint-Venant equations for shallow water waves that was developed by the Danish Hydraulic Institute (DHI). The MIKE 11 numerical model is used for dam-break simulation and to estimate the flood peak downstream of a dam using an empirical breach shape. The MIKE 11 model can simulate both piping and overtopping failure. The dam-break development caused by overtopping is simulated using the National Water Service (NWS) approach (Fread, 1988) or an energy equation. The energy equation approach allows the breach to be erosion based and a sediment transport equation is applied. The dam-break model in MIKE 11 computes the water levels and the peak of the outflow hydrograph based on the modeller's description of the reservoir, dam geometry, the spillway structure and dam-break structure. The failure moment (time) and mode are specified based on empirical breach shape development when using the NWS approach. The mode of failure is defined by the dam breach level, the dam breach width and the dam breach slope that are specified for varying moments in time.

### *2.5.22 AREBA (A Rapid Embankment Breach Assessment) – 2012*

A Rapid Embankment Breach Assessment (AREBA) is a numerical model that was developed at HR Wallingford to simulate breach growth for different embankment failure mechanisms and

was specifically designed for use in flood risk analysis (Morris, 2011). AREBA simulates the process of breaching within embankments using an equation that requires a value for soil erodibility. It incorporates the effects of a grass cover on the flood hydrograph shape, and calculates a flood hydrograph for surface erosion, headcut erosion or piping failures. It was designed specifically for use in probabilistic flood risk analysis models that require the impact of multiple breach scenarios to be evaluated. According to van Damme et al. (2012), any error that is introduced in the prediction of breach formation translates to an error in predicting the risk of flooding of downstream areas.

### *2.5.23 Summary*

A critical analysis of the various models that were reviewed shows that the choice of the sediment transport equation to be applied in the various models was either based on the developer's preference or comparative results' accuracy when compared to other equations. The most critical aspect in all the models that have been discussed in this study is the use and application of sediment transport equations. It is observed that each model applies its own sediment transport equations based on the underlying assumptions and the simulation approach within the modelling system. It is worth noting in Section 2.5.20 that, three (i.e. Smart and Jäeggi (1983), Abrahams (2003), and Camenen and Larson (2005)) out of the five sediment transport equations (Meyer-Peter and Müller (1948), Smart and Jäeggi (1983), Cheng (2002), Abrahams (2003), and Camenen and Larson (2005)) that were shown to provide overall good results and were ranked as the best predictors for the entire range of conditions were derived from data on gentle and moderately steep slopes. Specific model limitations could be directly related to the derivation of the applicable sediment transport equation(s).

The next sections evaluate the equations that have been applied in the previously reviewed dam-break models, with particular emphasis on the slope range data from which they were derived.

## 2.6 Selected sediment transport equations based on gentle slopes data (0 - 9%)

This section provides details of sediment transport equations that are commonly applied in numerical models, some of which were applied in the selected models described in Section 2.5. The following sediment transport equations were derived from data that was predominantly from gentle slopes (0 – 9%):

### *2.6.1 Engelund and Hansen (1967, 1972)*

Engelund and Hansen (1967, 1972) developed equations for total load sediment transport capacity in which the sediment transport is related to the shear stress and the friction factor of the bed. The following steps illustrate the method of application of the modified Engelund and Hansen (1967, 1972) equations.

a) Compute the dimensionless total shear stress parameter $\theta$, with Equation 2.6-1.

$$\theta = \frac{\tau_o}{(\gamma_s - \gamma_w) d_{50}} \qquad 2.6\text{-}1$$

Where

$d_{50}$ Median diameter of bed particles

$\gamma_s$ Specific weight of sediment particles

$\gamma_w$ Specific weight of water

$\tau_o$ Bed shear stress

b) Compute $f^1$ the friction factor of the bed using Equation 2.6-2.

$$f^1 = \frac{2gS_f h}{V^2} \qquad 2.6\text{-}2$$

Where

$S_f$ Friction slope

h Depth of flow

$V$ Average flow velocity

$g$ Acceleration due to gravity

c) Obtain the total volumetric sediment discharge per unit width $q_s$ ($m^2/s$) from Equation 2.6-3

$$q_s = 0.1 \left[\gamma_s \left(\frac{\gamma_s - \gamma_w}{\gamma_w}\right) g d_{50}^3\right]^{\frac{1}{2}} \frac{\theta^{\frac{5}{2}}}{f^1} \qquad 2.6\text{-}3$$

$q_s$ Total volumetric sediment discharge per unit width ($m^2/s$)

According to Voogt et al. (1991), as cited by Abderrezzak and Paquier (2011), the Engelund and Hansen (1967) equation was based on bed slopes of less than 1.9%. The application of the Engelund and Hansen (1967) equation on steep slopes above 20% is therefore questionable.

### *2.6.2 Wu and Long (1993)*

Wu and Long (1993) developed a total load sediment transport capacity, $T_c$ ($kg/m^3$) equation which is given as:

$$T_c = K \left[\frac{\gamma_w}{\gamma_s - \gamma_w} \frac{V^3}{g h w_s}\right]^M \qquad 2.6\text{-}4$$

Where

K and M Empirical parameters (K = 0.452 kg/m$^3$ and M = 0.762)

$w_s$ Settling velocity of graded suspended sediments

$\gamma_s$ Specific weight of sediment particles

$\gamma_w$ Specific weight of water

$\tau_o$ Bed shear stress

h Water depth or depth of flow

$u$ Velocity in the x-direction

V Average flow velocity ($V = \sqrt{u^2 + v^2}$)

$v$ Velocity in the y-direction

$g$ Acceleration due to gravity

### *2.6.3 Yang (1972, 1973, 1979, 1996)*

The unit stream power ($S_f\vec{u}$) is defined as the rate of potential energy expenditure per unit weight of water (Yang, 1979) as given in Equation 2.6-5.

$$\frac{dY}{dt} = \frac{dY}{dx}\frac{dx}{dt} = S_f\vec{u} \qquad 2.6\text{-}5$$

Where

$S_f$ Friction or water surface slope

$\vec{u}$ Velocity in the x-direction

t Time

x Longitudinal distance

Y Potential energy per unit weight of water

Unit stream power, defined as the time rate of potential energy expenditure per unit weight of water, is shown to be the dominant factor in the determination of total sediment concentration. Yang developed the unit stream power equation for the transport of sediment in natural rivers (Yang, 1972). This equation provides good estimation of total sediment concentration of alluvial channels (Yang and Stall, 1974).

Yang's (1973) equation for total sand load concentration, $C_t$ is written:

$$logC_t = 5.435 - 0.286log\left(\frac{w_s d_{50}}{v}\right) - 0.457log\left(\frac{U_*}{w_s}\right) + \left[1.799 - 0.409log\left(\frac{w_s d_{50}}{v}\right) - 0.314log\left(\frac{U_*}{w_s}\right)\right] log\left[\frac{\gamma_m}{\gamma_s - \gamma_m}\frac{VS_f}{w_s}\right] \quad 2.6\text{-}6$$

Where

$C_t$ Concentration in parts per million (ppm)

$w_s$ Settling velocity of sediment in clear water

$v$ Kinematic viscosity

$d_{50}$ Median sediment size

$U_*$ Shear velocity

V Average flow velocity

$\gamma_s$ Specific weight of sediment particles

$\gamma_m$ Specific weight of turbid water

Yang (1979) also developed the unit stream power equation for total load. The dimensionless unit stream power equation for the computation and prediction of total sediment concentration was obtained with consideration of the criterion for incipient motion. The equation was derived from laboratory data with energy slopes that ranged from 0.4% to 2.79% as reported by Khorram and Ergil (2010).

Yang's (1979) equation for total sediment concentration ($C_t$) is given as:

$$logC_t = 5.435 - 0.286log\left(\frac{w_m d_{50}}{v}\right) - 0.457log\left(\frac{U_*}{w_m}\right) + \left[1.799 - 0.409log\left(\frac{w_m d_{50}}{v}\right) - 0.314log\left(\frac{U_*}{w_m}\right)\right] log\left[\frac{VS_f}{w_m} - \frac{V_{cr}S_f}{w_m}\right] \quad 2.6\text{-}7$$

Where

$V_{cr}$ Critical velocity of flow

The major difference between the two equations of Yang (1973) and Yang (1979) is that the former (Yang, 1973) does not consider the criterion for incipient motion in terms of taking into consideration the critical velocity of flow ($V_{cr}$) at the initiation of sediment transport. In contrast, Yang's (1979) equation is a dimensionless unit stream power equation for the prediction of the total sediment concentration ($C_t$) in parts per million by weight with a criterion for incipient motion.

Yang (1996) developed an equation for the concentration of sediment in sediment laden flow for rivers with highly- concentrated suspended materials:

$$logC_t = 5.165 - 0.153log\left(\frac{\omega_m d_{50}}{v}\right) - 0.297log\left(\frac{U_*}{\omega_m}\right) + \left[1.780 - 0.360log\left(\frac{\omega_m d_{50}}{v}\right) - 0.480log\left(\frac{U_*}{\omega_m}\right)\right] log\left[\frac{\gamma_m}{\gamma_s - \gamma_m}\frac{VS_f}{\omega_m}\right] \quad 2.6\text{-}8$$

Where

$C_t$ Concentration in parts per million (ppm)

$\omega_m$ Settling velocity of suspended sediment in turbid water

Mohamed et al. (2002) found in their review and comparison of sediment transport equations and assumptions that the Yang's (1979) equation for total sediment transport performed very well out of the eight sediment transport equations that were used especially when the flow was supercritical. Considering that the Yang (1973, 1979, and 1996) equations were developed for mild alluvial channel slopes, their applicability to dam-break conditions that are characterized by very steep slopes could be uncertain.

### *2.6.4 Wu et al. (2000)*

Wu et al. (2000) developed a non-uniform sediment transport equation for alluvial rivers. The sediment transport equation takes into consideration the hiding and exposure mechanism of non-uniform sediment transport. Wu et al. (2000) came up with the equation to calculate the critical shear stress of incipient motion and the fractional bed-load and suspended load transport rates of non-uniform sediment.

The relationship for the fractional transport rates of non-uniform bed-load is based on the non-dimensional fractional bed-load transport rate, $\emptyset_{bi}$ which is defined as in Equation 2.6-9:

$$\emptyset_{bi} = \frac{q_{bi}}{p_{bi}\sqrt{\frac{\gamma_s}{\gamma_w - 1}gd_i^3}} \quad 2.6\text{-}9$$

Where

$d_i$ Diameter of the i-th fraction of sediment

$q_{bi}$ Volumetric sediment transport rate of the i-th fraction of bed-load per unit width ($m^2/s$)

$p_{bi}$ The gradation of the i-th fraction of bed material

The bed shear stress ($\tau_o$) can be calculated using Equation 2.6-10:

$$\tau_o = \gamma_w R_h S_f \quad 2.6\text{-}10$$

Where

$R_h$ Hydraulic radius of channel bed

$S_f$ Friction slope

By least square curve fitting, the following Equation 2.6-11 for the fractional transport rate of non-uniform bed-load ($\emptyset_{bi}$) was obtained:

$$\emptyset_{bi} = 0.0053\left[\left[\frac{n'}{n}\right]^{3/2}\frac{\tau_o}{\tau_{ci}} - 1\right]^{2.2} \qquad 2.6\text{-}11$$

$\tau_{ci}$ Critical bed shear stress for the incipient motion of the i-th fraction of non-uniform sediment

$n$ Manning's resistance coefficient for channel bed

$n'$ Manning's resistance coefficient corresponding to grain roughness $\left\{d_{50}^{1/6}/20\right\}$

The suspended load transport rate is related to the rate of energy available to the alluvial system and the non-dimensional fractional suspended load transport rate ($\emptyset_{si}$) has the relationship shown in Equation 2.6-12:

$$\emptyset_{si} = f\left[\left(\frac{\tau_o}{\tau_{ci}} - 1\right)\frac{V}{\omega_i}\right] \qquad 2.6\text{-}12$$

Where

$$\emptyset_{si} = \frac{q_{si}}{p_{bi}\sqrt{\frac{\gamma_s}{\gamma_{w-1}}gd_i^3}} \qquad 2.6\text{-}13$$

Where

$f$ Functional relationship

V Average flow velocity

$q_{si}$ The transport rate of the i-th fraction of suspended load per unit width

$\omega_i$ Settling velocity of i-th fraction of sediment

The trend line for all the data points could be expressed using Equation 2.6-14:

$$\emptyset_{si} = 0.0000262\left[\left(\frac{\tau_o}{\tau_{ci}} - 1\right)\frac{V}{\omega_i}\right]^{1.74} \qquad 2.6\text{-}14$$

The summation of bed load ($q_{bi}$) and suspended load ($q_{si}$) fractional transport rates gives the total transport rate for non-uniform bed-material load ($q_b$). The bed load equations were derived from laboratory data and river data with energy slopes that ranged from 0.011% to 1.62%. The suspended load equations were derived from laboratory data and river data with energy slopes that ranged from 0.018% to 0.695%. Similar energy slopes on steep bed slopes should typically

transport more sediment. The application of this equation in Wu et al.'s (2011) dam-break model was achieved by modifying the equation to include the effect of gravity on steep slopes.

### *2.6.5 Van Rijn (1984a, 1984b)*

Van Rijn (1984a, 1984b) developed a numerical model, in which the sediment transport equation for the prediction of bed load sediment transport was given as Equation 2.6-15.

$$q_b = \emptyset_{bi}\left[p_{bi}\sqrt{\frac{\gamma_s}{\gamma_w - 1} g d_{50}^3}\right] \quad \text{2.6-15}$$

$$\emptyset_{bi} = \frac{0.053}{{d_*}^{0.3}}\left[\frac{\theta}{\theta_{cr}} - 1\right]^{2.1} \quad \text{2.6-16}$$

Where

$\emptyset_{bi}$ Non-dimensional bed-load transport rate for the i-th sediment fraction

$q_b$ Volumetric sediment transport rate of bed-load per unit width

$p_{bi}$ The gradation of the i-th fraction of bed material

$\theta$ Dimensionless bed shear stress

$\theta_{cr}$ Critical dimensionless bed shear stress

$$\theta = \frac{\tau_o}{\rho_w (s-1) g d_*} \quad \text{2.6-17}$$

Where

$\tau_o$ Bed shear stress

$g$ Acceleration due to gravity

$\rho_w$ Density of water

$d_*$ Dimensionless particle diameter

s Relative unit weight of sediment

$$d_* = d\left[\frac{s-1}{v^2}\right]^{1/3} \quad \text{2.6-18}$$

Where

$v$ Kinematic viscosity

d Particle diameter

The parameters for the calculation of the critical dimensionless bed shear stress ($\theta_{cr}$) are given by Van Rijn (1984a) as follows:

$$\theta_{cr} = \frac{\tau_o}{\rho_w (s-1) g d_{50}} \qquad 2.6\text{-}19$$

Where

$\tau_o$ Bed shear stress

$g$ Acceleration due to gravity

$\rho_w$ Density of water

$d_{50}$ Median sediment particle diameter

s Relative unit weight of sediment

### *2.6.6 Ackers and White (1973)*

Hassanzadeh et al. (2011) reported that Ackers and White (1973) used dimensional analysis based on the flow power concept, as explained by Bagnold (1966), in order to express sediment transport rate by several dimensionless parameters. The proposed equations were formulated as Equations 2.6-20 and 2.6-21:

$$C_t = Cs \frac{d_{50}}{h} \left(\frac{V}{U_*}\right) \left(\frac{F_{gr}}{A} - 1\right)^m \qquad 2.6\text{-}20$$

$$F_{gr} = \frac{U_*^n}{\sqrt{g d_{50} (s-1)}} \left[\frac{V}{\sqrt{32} \mathrm{Log} \frac{10h}{d_{50}}}\right]^{1-n} \qquad 2.6\text{-}21$$

Where

$C_t$ Concentration in parts per million (ppm)

$U_*$ Shear velocity

h Average depth of flow section

s Relative unit weight of sediment given by $\left(\frac{\gamma_w}{\gamma_s}\right)$

C, A, n and m Coefficients

n Transition exponent (depending on sediment size)

$d_{50}$ Sediment particle size

$F_{gr}$ Mobility number

Ackers' and White's (1973) equation was derived using 1000 laboratory data points for particle sizes larger than 0.04 mm, Froude numbers less than 0.8 and bed slopes of less than 3.7%.

### *2.6.7 Molinas and Wu (2001)*

Molinas and Wu (2001) developed a sediment transport equation based on universal stream power which can be applied in the prediction of bed-material concentrations in large sand-bed rivers. According to their analysis, they observed that the sediment transport relationships derived from flume experiments with shallow flows cannot be universally applied to large rivers with deep flows. This shows the significance of flow and sediment transport conditions in the application of sediment transport relationships.

Molinas' and Wu's (2001) universal stream power equation is given by Equations 2.6-22 and 2.6-23.

$$C_t = \frac{1430\left(0.86+\sqrt{\Psi}\right)\Psi^{1.5}}{0.016+\Psi} \qquad 2.6\text{-}22$$

$$\Psi = \frac{V^3}{g\left(\frac{\gamma_s-\gamma_w}{\gamma_s}\right)R_h w_s\left[log_{10}\left[\frac{R_h}{d_{50}}\right]\right]^2} \qquad 2.6\text{-}23$$

Where

$C_t$ Concentration in parts per million (ppm)

$w_s$ Settling velocity of sediment in clear water

$V$ Average flow velocity

$\gamma_w$ Specific weight of water

$\gamma_s$ Specific weight of sediment

$d_{50}$ Median sediment particle size

$R_h$ Hydraulic radius

### *2.6.8 Meyer-Peter Müller (1948)*

The Meyer-Peter Müller (1948) empirical equation for the bed-load discharge in natural streams was developed for bed-load transport prediction only. It is based on the wall shear stress formulation in which slope and bed roughness are some of the significant parameters. The sediment transport rate is based on the excess shear stress that is applied by the flowing water. It is one of the equations that is widely applied in bed evolution models as well as dam breach models. The Meyer-Peter Müller (1948) sediment transport equation is used to compute the volumetric sediment transport rate of bed-load material per unit width, $q_b$ ($m^3/m/s$) with respect to a dimensionless bed load transport rate ($\emptyset_b$), the relative density ($s = \frac{\rho_s}{\rho_w}$) and the median particle diameter ($d_{50}$).

$$\emptyset_b = 8[\theta - \theta_{cr}]^{1.5} \qquad 2.6\text{-}24$$

with

$$q_b = \emptyset_b[(s-1)g]^{\frac{1}{2}} d_{50}^{\frac{3}{2}} \qquad 2.6\text{-}25$$

Where

$\theta$ Dimensionless bed shear stress

$\theta_{cr}$ Critical dimensionless bed shear stress

$\rho_s$ Soil density

$\rho_w$ Water density

$d_{50}$ Median particle diameter

According to Abderrezzak and Paquier (2011), the equation was derived from data with bed slopes ranging from 0.04% to 2%.

### *2.6.9 Shu-Qing Yang Equation (2005)*

Yang (2005) developed an equation for the relationship between flow conditions and sediment discharge. The total volumetric sediment transport rate of sediment per unit width, $q_s$ ($m^3/m/s$) is based on the equation of Yang and Lim (2003). The following is the procedure for calculating the total volumetric sediment transport rate of sediment per unit width in steady, uniform and fully developed turbulent channels according to Yang (2005):

a) Determine the critical bed shear velocity ($U_{*c}$) from the Shields curve based on the median sediment particle size ($d_{50}$) or using the empirical equation proposed by Guo (1997).

b) Calculate the bed-shear velocity related to grains ($U'_*$) using Equation 2.6-26.

$$U'_* = \frac{V}{2.5ln\frac{11R_h}{2d_{50}}} \qquad 2.6\text{-}26$$

Where

$V$ Average flow velocity

$R_h$ Hydraulic radius

c) Calculate the mean bed shear stress using $\tau_o = \gamma_w R_h S_f$

Where

$\gamma_w$ Specific weight of water

$S_f$ Friction slope

d) Calculate the sediment settling velocity ($w_s$) based on the median sediment particle size ($d_{50}$) using van Rijn (1989) equation:

$$w_s = 1.1\left(\sqrt{\left(\frac{\gamma_s-\gamma_w}{\gamma_w}\right)d_{50}}\right) \quad \text{2.6-27}$$

Where

$\gamma_s$ Specific weight of sediment

e) Calculate the total volumetric sediment discharge per unit width, $q_s$ using Equation 2.6-28:

$$q_s = k\left(\frac{\gamma_s}{\gamma_s-\gamma_w}\right)\tau_o\left(\frac{U_*'^2-U_{*c}^2}{w_s}\right) \quad \text{2.6-28}$$

Where

$\tau_o$ Bed shear stress

k Empirical calibration coefficient

## 2.7 Sediment transport equations based on moderately steep slope data (10 – 20%)

In this section, a number of sediment transport equations that were developed from data for moderately steep slopes (10 – 20%) are presented.

### *2.7.1 Smart and Jäeggi equation (1983)*

Smart and Jäeggi (1983) noted that a major drawback of the Meyer-Peter Müller (1948) equation was that it seriously underestimated sediment transport rates on steep slopes. What prompted their research was the fact that all equations for predicting sediment transport capacity at the time were only applicable to low values of channel slope. Smart and Jäeggi (1983) conducted experimental studies at a laboratory in Zurich and did computer analyses to derive an equation suitable for alluvial sediment studies with median grain diameter larger than 0.4 mm on slopes up to 20%. The equation was applicable to the prediction of sediment transport capacity of steeper channels with uniform and non-uniform natural sediment beds at slopes from 3 to 20%. They used more natural river-rounded sands and gravels with median grain diameters between 4.3 and 10.5 mm. The discharges were varied between 5 and 301/s and the measured sediment transport rates ranged between 0.07 and 16.24 kg/s.

Smart and Jäeggi (1983) studies resulted in sediment transport Equation 2.7-1:

$$\emptyset_b = 4\left(\frac{d_{90}}{d_{30}}\right)^{0.2} CS_o^{0.6}\theta^{0.5}(\theta-\theta_{cr}) \quad \text{2.7-1}$$

Where

$\emptyset_b$ Dimensionless bed-load sediment transport rate = $\frac{q_b}{[g(s-1)d_{50}^3]^{0.5}}$

$d_{90}, d_{30}$ Grain diameters for which 90% or 30% weight of a non-uniform sample are finer (m), respectively

$q_b$ Volumetric sediment transport rate of bed-load material per unit width

$S_o$ Stream bed slope

g Acceleration due to gravity

$\theta$ Dimensionless bed shear stress

$\theta_{cr}$ Critical dimensionless bed shear stress

s Relative unit weight of sediment

$d_{50}$ Median sediment grain diameter

The resistance factor C is the ratio of mean flow velocity (V) to bed shear velocity ($U_*$). Smart and Jäeggi (1983) showed that this new equation not only gave satisfactory results on steeper slopes but also gave better estimates of sediment transport capacity than the Meyer-Peter and Müller (1948) equation for the flatter slope data from which the Meyer-Peter and Müller (1948) equation was derived (Smart and Jäeggi, 1983).

### *2.7.2 Rickenmann (1991)*

According to Nitsche et al. (2011), Rickenmann (1991) proposed a shear-stress-based equation to compute bed-load transport. The equation was based on 252 laboratory experiments conducted by Meyer-Peter and Müller (1948), Smart and Jäeggi (1983), and Rickenmann (1991) for a slope range of 0.04 to 20%. The equation is given in Equation 2.7-2:

$$\emptyset_b = \frac{3.1\left[\left(\frac{d_{90}}{d_{30}}\right)^{0.2}\sqrt{\theta}(\theta-\theta_{cr})F_r^{1.1}\right]}{\sqrt{s-1}} \qquad 2.7\text{-}2$$

Where

$\emptyset_b$ Dimensionless bed-load sediment transport rate = $\frac{q_b}{[g(s-1)d_{50}^3]^{0.5}}$

$q_b$ Volumetric sediment transport rate of bed-load material per unit width

$d_{90}, d_{30}$ Grain diameter for which 90% or 30% weight of a non-uniform sample is finer (m) respectively

$\theta$ Dimensionless bed shear stress

$\theta_{cr}$ Critical dimensionless bed shear stress

B Width

$F_r$ Froude Number

s Relative unit weight of sediment

$d_{50}$ Median sediment grain diameter

Another equation was developed using regression analysis and it was valid for the slope ranges from 5% to 20%. It was based on data of clay-suspension experiments and was analysed together with the Smart and Jäeggi (1983) tests' data. It reads:

$$q_b = \frac{12.6}{(s-1)^{1.6}} \left(\frac{d_{90}}{d_{30}}\right)^{0.2} (q - q_{cr}) S_f^2 \qquad 2.7\text{-}3$$

Where

q Unit flow discharge

$q_{cr}$ Critical flow discharge at the initiation of motion

$S_f$ Friction slope

### *2.7.3 Abrahams (2003)*

Abrahams (2003) developed equations for predicting the bed-load transport rate, $q_b$ ($m^3/m/s$) in sheet flow. The general equation is written in this form (assuming the critical dimensionless shear stress is negligible):

$$\emptyset_b = \theta^{1.5} \frac{V}{U_*} \qquad 2.7\text{-}4$$

$\emptyset_b$ Dimensionless bed-load sediment transport rate = $\frac{q_b}{[g(s-1)d_{50}^3]^{0.5}}$

$V$ Average flow velocity

$U_*$ Shear velocity

$\theta$ Dimensionless bed shear stress

s Relative unit weight of sediment

g Acceleration due to gravity

$d_{50}$ Median grain diameter

The equation was based on bottom slopes ranging from 3% to 21% and flow depths ranging from 3 mm to 10.5 mm.

### *2.7.4 Camenen and Larson (2005)*

Camenen and Larson (2005) developed a bed load equation for non-cohesive sediment based on the bed-shear concept of Meyer-Peter Müller (1948). It was validated for steady flows, oscillatory flows, and combined steady and oscillatory flows. It was derived from data on experimental and field measurements for a wide range of flows and sediment conditions, as occurring in river, coastal, and marine environments with slopes ranging from 3% to 20%.

The general form of the equation is written as:

$$\emptyset_{\mathrm{b}} = 12\theta^{1.5}\mathrm{e}^{-4.5\frac{\theta_{cr}}{\theta}} \qquad 2.7\text{-}5$$

$\emptyset_b$ Dimensionless bed-load sediment transport rate = $\frac{q_b}{[g(s-1)d_{50}^3]^{0.5}}$

s Relative unit weight of sediment or specific gravity

$g$ Acceleration due to gravity

$\theta$ Dimensionless bed shear stress

$e$ Approximately = 2.718

$\theta_{cr}$ Critical dimensionless bed shear stress

## 2.8 Sediment transport equation based on gently steep (8%) to steep (50%) slope data

Zhang et al. (2009) developed a sediment transport equation for the estimation of sediment transport capacity on steep slopes which applicable in physically-based erosion models. This is one of the few available equations that was derived from data on steep slopes with gradient slopes ranging from 8.8 to 46.6%. In addition, the study also investigated the effects of unit flow discharge (q), bed slope gradient ($S_o$), and average flow velocity (V) on sediment transport capacity or rates in shallow flows. The relationship between the sediment transport capacity and shear stress, stream power, and unit stream power on steep slopes was also analysed. The unit discharges were very small and ranged from $0.625 \times 10^{-3}$ to $5 \times 10^{-3}$ $m^2/s$. The median diameter of the test riverbed sediment was 280µm. Zhang et al. (2009) showed that sediment transport capacity increased as a power function with discharge and slope gradient. Overall, stream power seemed to be the preferred predictor for estimating sediment transport capacity for steep slopes. Multivariate, nonlinear regression analyses between sediment transport capacity, unit flow discharge, and slope gradient produced the relationship in Equation 2.8-1 (Zhang et al., 2009).

$$q_t = 19831q^{1.237}S_o^{1.227} \qquad 2.8\text{-}1$$

Where

$q_t$ Transport capacity (kg/m/s)

$q$ Unit flow discharge ($m^2/s$)

$S_o$ Bed slope gradient (m/m)

Figure 2.8-1 shows the measured sediment transport capacity as a function of flow discharge for the data that was used to derive Equation 2.8-1.

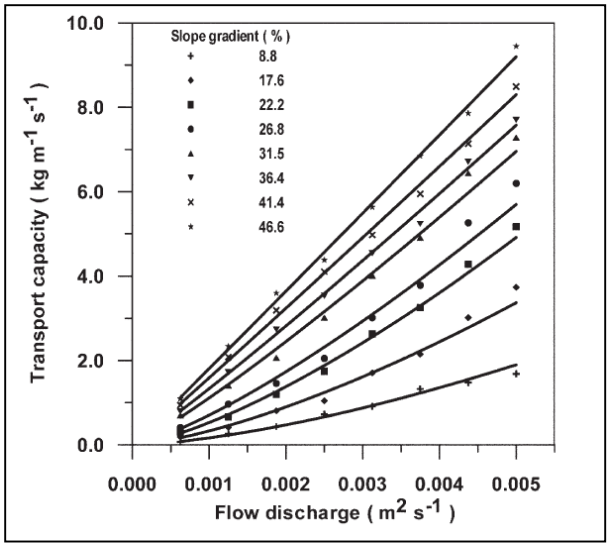


**Figure 2.8-1 Measured sediment transport capacity as a function of flow discharge for selected slopes using median ($d_{50}$) sediment size = 0.28 mm (Zhang et al., 2009)**

## 2.9 Summary

The significant aspects of flow hydraulics and sediment transport in dam breach have been reviewed. Commonly used numerical models have been analysed with respect to the applied sediment transport equations and their derivation slope data. All the applicable sediment transport equations are based on slopes of less than 21% slope. The results are summarized in Table 2.9-1.

**Table 2.9-1 Summary of sediment transport equations and slope data ranges**

| ID | Sediment Transport Equation | Breach Models | Bed Slope (%) |
|---|---|---|---|
| 1 | Meyer-Peter Müller (1948) | NWS BREACH (Fread, 1991), EDBREACH (Loukola and Huokuna, 1998), DEICH N1/N2 (Broich, 1998), BREADA (Zagonjolli, 2007), Macchione (2008) and Abderrezzak and Paquier (2011). | 0.04% to 2 |
| 2 | Abrahams (2003) | Abderrezzak and Paquier (2011). | 3 to 21 |
| 3 | Camenen and Larson (2005) | Abderrezzak and | 3 to 20 |

| | | | |
|---|---|---|---|
| | | Paquier (2011). | |
| 4 | Smart and Jäeggi (1983 | NWS BREACH (Fread, 1991), DEICH N1/N2 (Broich, 1998), Tingsanchali and Chinnarasri (2001) and, Wang and Bowles (2006a, 2006b) and Abderrezzak and Paquier (2011). | 3 to 20 |
| 5 | Zhang et.al. (2009) | N/A | 8.8 to 46.6 |

Most earth dams have slopes of more than 20%, however the equations in Table 2.9-1 have been applied because there are no equations for steep slopes. There are many significant factors and variables that could affect the accurate simulation of dam breaching processes such as soil properties, erodibility, unsteady and non-uniform flow conditions, the extent of head cutting and side channel or vertical erosion, side slope collapse, mass failure, breach widening, shear and sliding and overturning failure of soil masses. All these need to be carefully considered through the inclusion of appropriate algorithms in numerical models for the accurate simulation of breaching processes and tracking of the progression of the hydraulic control. As much as it is difficult to precisely consider each and every significant aspect and variable in the breaching processes, the specific sediment transport equation used plays a significant role in the breach formation/development processes since it directly affects the timing and magnitude of potential dam breach flooding. From the review of the equations that have been applied in physically-based numerical models, it was shown that all of these equations were derived from data on slopes of up to 20% even though most earth dams have slopes up to 40%. Lack of appropriate sediment transport equations that were derived from data on slopes above 20% justifies the need to derive new sediment transport equations for use in dam-break numerical modelling on steep slopes.

# CHAPTER 3 EXPERIMENTAL SETUP AND PROCEDURES

## 3.1 Testing flume

The physical laboratory model tests were conducted in a flume measuring 4.7 m long and 0.25 m wide; with 0.3 m high side walls. The physical model was installed in the Hydraulic Laboratory of the University of Stellenbosch. The floor and the walls of the main flume channel were made of Perspex glass to allow for visual observation of the behaviour of the flow and sediment. A pump was used to deliver water to the flume at preselected flow rates through the adjustment of a control valve.

The selected approach for the analysis of sediment transport rates for steep slopes was by means of sets of laboratory experiments using three different ranges of mean sediment grain sizes – namely, 0.2 mm, 1 mm and 2.4 mm. Earth embankments are characterised by cohesive materials, gravel and rocks. The sediment that was used during the experimental study did not have similar characteristics. Cohesive sediment particles are generally more resistant to soil erosion. Lack of cohesiveness accelerates the erosion process and has an effect on the peak discharge, time to peak and final breach size. Sediment transport equations that are derived from non-cohesive sediment data are still applicable in earth embankments because they simulate scenarios that assume very little cohesive strength and therefore provide conservative estimates of output parameters. Non-cohesive sediment transport equations might not be truly representative of actual dam conditions but still offer practical alternatives in the absence of appropriate cohesive sediment transport equations.

The water from the pump was fed through the inlet at the upstream end of the flume at the preselected inflow rates. The schematic drawing of the model setup is shown in Figure 3.1-1 and a photograph of the experimental setup in the laboratory is shown in Figure 3.1-2. A digital flow meter was used to determine the flow rate to be set to preselected values for each set of experiments. The digital flow meter (SAFMAG Flowmetrix) was attached to the inlet pipe into the flume before the control valve. Three point gauges were mounted over guide rails above the flume and were used for water level measurements.

## 3.2 Experimental procedure – measurement of sediment transport rates

The flume gradients (bed slope) were set at three preselected slopes of 25%, 33% and 40% for each of the three ranges of sediment grain sizes that were tested during the experiments. The percentage slope is expressed as the vertical distance “y” divided by the horizontal distance “x” multiplied by 100. The “y” and “x” reference projections are shown in Figure 3.1-1. The 25% to 40% gradient range of the downstream slope is typical for most earth dams. A horizontal wooden flume was placed upstream of the fixed percentage slope inclined Perspex glass flume. Sediment was supplied into the inclined Perspex glass flume, at a fixed position that was 0.5 m from the starting point of the inclined flume as shown in Figure 3.1-2, while water was flowing through it. For each experimental run, the flume was set at one of the three preselected slopes and the discharge flow rate was set at the specified rate. Flow depth measurements (flow without

sediment) were then recorded using water level gauges. The sediment was fed through a conveyor belt that was drawing the sediment from a trough (Refer to Figure 3.2-1).

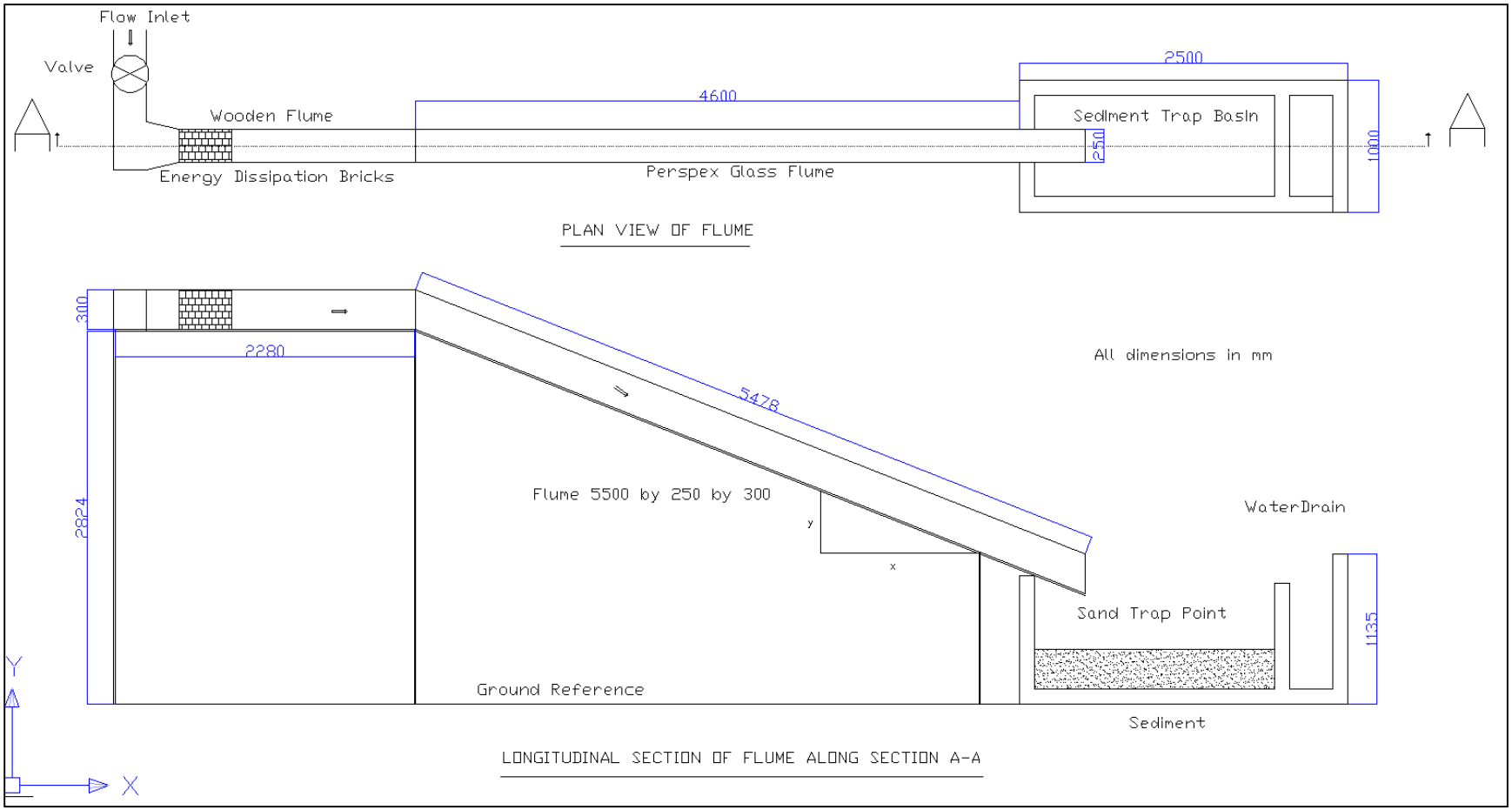


**Figure 3.1-1 Schematic drawing of the experimental setup**

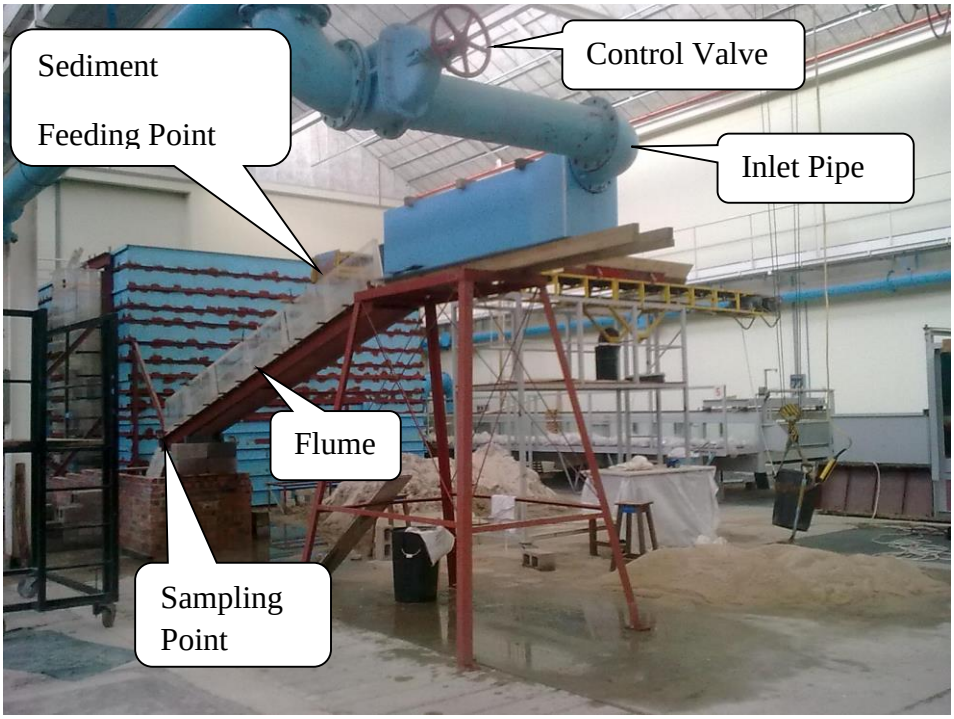


**Figure 3.1-2 Photograph of the experimental setup**

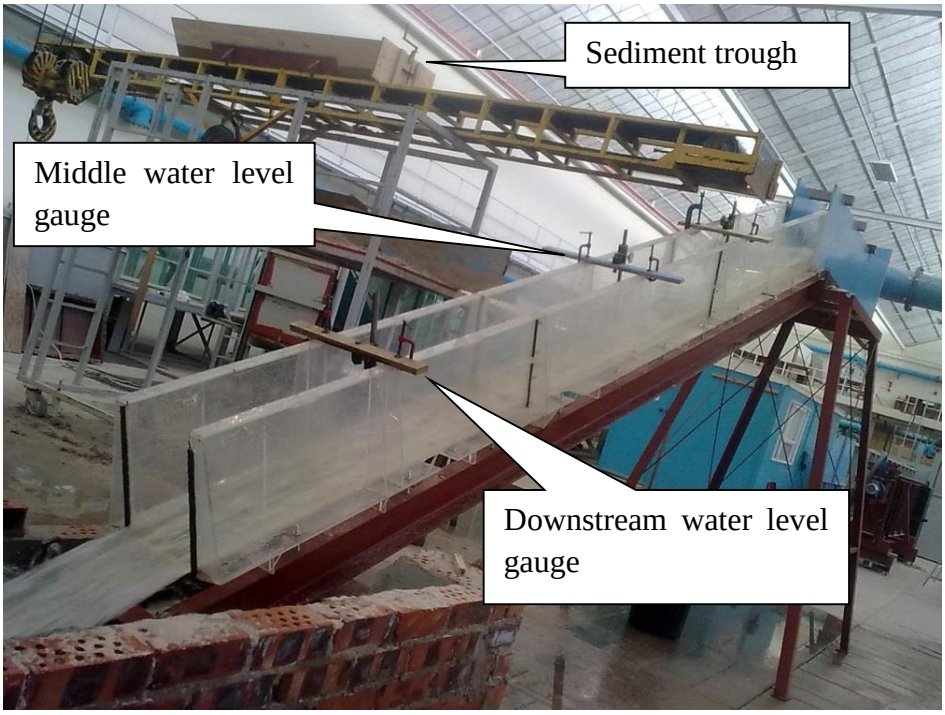


**Figure 3.2-1 Experimental flume - viewed from downstream**

The sediment was supplied from the trough at a fixed rate through a preselected gate opening size at the exit point of the conveyor belt. Sediment was introduced through the conveyor belt until a point in time was reached where the sediment was observed to be depositing on the flume bed at 1.5 m from the feeding position. At the feeding position, sediment was dropped directly onto the flume bed. This made it difficult to observe deposition, since sediment appeared on the flume floor due to the dropping effect and not to the actual flow conditions. At 1.5 m from the feeding position, it was determined that any deposition was due to the prevailing flow and sediment conditions. The estimation of the feeding rate at which deposition could be observed was done through trial and error adjustment of the feeding control gate opening size. The feeding control gate was adjusted to supply more or less sediment as the speed of the conveyor belt remained constant. By changing the gate opening, the amount of sediment being supplied could be increased or decreased. At the downstream end of the flume, the sediment inflow from the flume was trapped using a bag and the sampling time recorded. The rest of the sediment was collected in the sediment trap and reused during the next set of tests.

Figure 3.2-2 shows the control gate opening mechanism (left) that was used to control the sediment feeding rate, the view of the conveyor belt with sediment from the sediment trough (middle) and the sediment feeding into the Perspex flume (right).

**Figure 3.2-2 Sediment feeding rate control gate (left), conveyor belt with sediment (middle) and sediment feeding into flume by conveyor (right)**

### *3.2.1 Significant considerations pertaining to sediment transport rate measurements on steep slopes*

By visually observing the sediment deposition onto the flume bed during feeding, the hypothetical equilibrium conditions could be estimated. At this hypothetical equilibrium point, the sediment transport rate was assumed to be close to the sediment transport capacity of the flow on the understanding that the flow could not entrain any more sediment. In this case the

total sediment load (comprising both suspended and bed load) was measured in order to determine the total sediment transport rates in kg/m width per second.

A sediment transport rate per slope configuration and flow rate was obtained from an average of three separate sediment sampling attempts. The first median ($d_{50}$) sediment size to be tested was 0.2 mm. Secondly, the median ($d_{50}$) sediment size of 2.4 mm was tested. For both median ($d_{50}$) sediment sizes 0.2 mm and 2.4 mm, the discharges ranged from 16 l/s to 45 l/s. The third set of tests was for 1 mm median ($d_{50}$) sediment size and six discharges were applied for each of the three slope configurations. The discharges for the median ($d_{50}$) sediment size of 1 mm ranged from 8 l/s to 15 l/s. A V-notch was used to measure discharges that ranged from 8 l/s to 15 l/s. The choice of the discharge ranges was guided by the need to ensure two dimensional (2D) flow conditions; whereby the ratio of the flume width (B) over flume depth (h) was supposed to always be higher than 3.5 according to Song et al. (1995). Flow hydraulics and sediment transport data were recorded for all the datasets. The final computed unit sediment transport rates were based on the weight of oven dried sediment samples.

The following parameters were applied to compute the sediment transport rates

$$q_t = \frac{m_s}{Bt} \qquad 3.2\text{-}1$$

Where

$q_t$ Total mass sediment discharge per unit width (kg/m/s)

$m_s$ Mass of oven dried sediment sample (kg)

$t$ Sampling time (s)

B Width of flume (m)

Since from a hydraulic engineering point of view, the total volumetric sediment transport rate, $q_t$ ($m^3$/m/s) is the one which is significant, the developed equation was for total sediment load or rate without differentiating between bed or suspended load.

## 3.3 Experimental procedure – determination of sediment density, median ($d_{50}$) sediment size and settling velocity

The data on the median ($d_{50}$) sediment sizes and sediment density was needed for the derivation of sediment transport equations. Sieve analysis was conducted to determine the median ($d_{50}$) sediment sizes. The density of sediment $\rho_s$ was obtained from density experiments using a pycnometer.

### *3.3.1 Determination of densities*

The density of homogeneous particulate sedimentary matter is defined as the ratio of its mass $m_s$ to its volume, $v_s$.

$$\rho_s = \frac{m_s}{V_s} \qquad 3.3\text{-}1$$

Since sediment does not dissolve in water, the pycnometer method is very accurate using the procedure outlined below:

a) The mass of the pycnometer container was measured
b) The mass of the pycnometer container and water was measured
c) The mass of the pycnometer container and sediment was measured – after emptying the water and drying the sediment and the pycnometer container.

Table 3.3-1 shows the values that were obtained.

**Table 3.3-1 Results of density determination by the pycnometer**

| ID | Explanation | Median ($d_{50}$) sediment = 0.2 mm | Median ($d_{50}$) sediment = 1 mm | Median ($d_{50}$) sediment = 2.4 mm |
|---|---|---|---|---|
| 1 | Mass of the pycnometer container (g) | 584 | 580 | 580 |
| 2 | Mass of the pycnometer container and water (g) | 1653 | 1653 | 1653 |
| 3 | Mass of the pycnometer container and sediment (g) | 890 | 990 | 1021 |
| 4 | Mass of the pycnometer container, sediment and water (g) | 1843 | 1902 | 1920 |
| 5 | Density of water at 20°C (g/cm$^3$) | 0.998 | 0.998 | 0.998 |
| 6 | Volume of the pycnometer container (cm$^3$) | 1069 | 1073 | 1073 |
| 7 | Volume of water in sediment mixture (cm$^3$) | 955 | 914 | 901 |
| 8 | Volume taken by sediment in pycnometer container (cm$^3$) | 119 | 160 | 173 |
| 9 | Mass of sediment (g) | 306 | 410 | 441 |
| 10 | Density of sediment (g/cm$^3$) | 2.565 | 2.560 | 2.550 |
| 11 | Density of sediment (kg/m$^3$) | 2565 | 2560 | 2550 |

### *3.3.2 Determination of settling velocities*

The settling velocity of the larger sized sediment of 2.4 mm was obtained from the average of the settling or fall velocities of individual sediment grains in a settling column. Figure 3.3-2 shows the cylindrical column that was used for settling velocity determination. A 1m deep clear water vertical glass pipe column and a stop watch were used. Fifty four (54) sediment particles were

individually dropped into the pipe. The time taken for each sediment particle or grain to reach the bottom of the cylinder was recorded.

**Figure 3.3-1 Cylindrical water column for settling velocity determination**

With the travel distance through the pipe known, the settling velocity was calculated as the average of the fall distance divided by the corresponding times taken for each individual sediment particle. The final average settling velocity was calculated as 0.184 m/s for the sediment with median size, $d_{50}$ = 2.4 mm.

Due to their tiny sediment grain sizes, it was extremely difficult to experimentally determine the settling velocities of the sediment with median ($d_{50}$) size of 0.2 mm and 1 mm using the cylindrical column. Therefore, the settling velocity was calculated using an empirical equation that was proposed by Van Rijn (1989) as cited by Cheng (1997). This empirical equation is shown as Equation 3.3-1:

$$w_s = 1.1\left(\sqrt{\left(\frac{\gamma_s - \gamma_w}{\gamma_w}\right) d_{50}}\right) \qquad 3.3\text{-}1$$

Where

$\gamma_w$ Specific weight of water

$\gamma_s$ Specific weight of sediment

$d_{50}$ Median sediment size

The median ($d_{50}$) sediment size was obtained from the sieve analysis procedure that is explained in Section 3.3.3. The calculated settling velocities were 0.019 m/s and 0.04 m/s for median ($d_{50}$) sediment sizes of 0.2 mm and 1 mm respectively. The unit weight was based on the actual computed sediment density.

### *3.3.3 Determination of median sediment sizes*

Figures 3.3-2, 3.3-3, and 3.3-4 show the sieve analysis results for median ($d_{50}$) sediment sizes of 0.2 mm, 1 mm and 2.4 mm. The grading curves from the sieve analysis show that medium sand to very fine gravel was used during the experimental study.

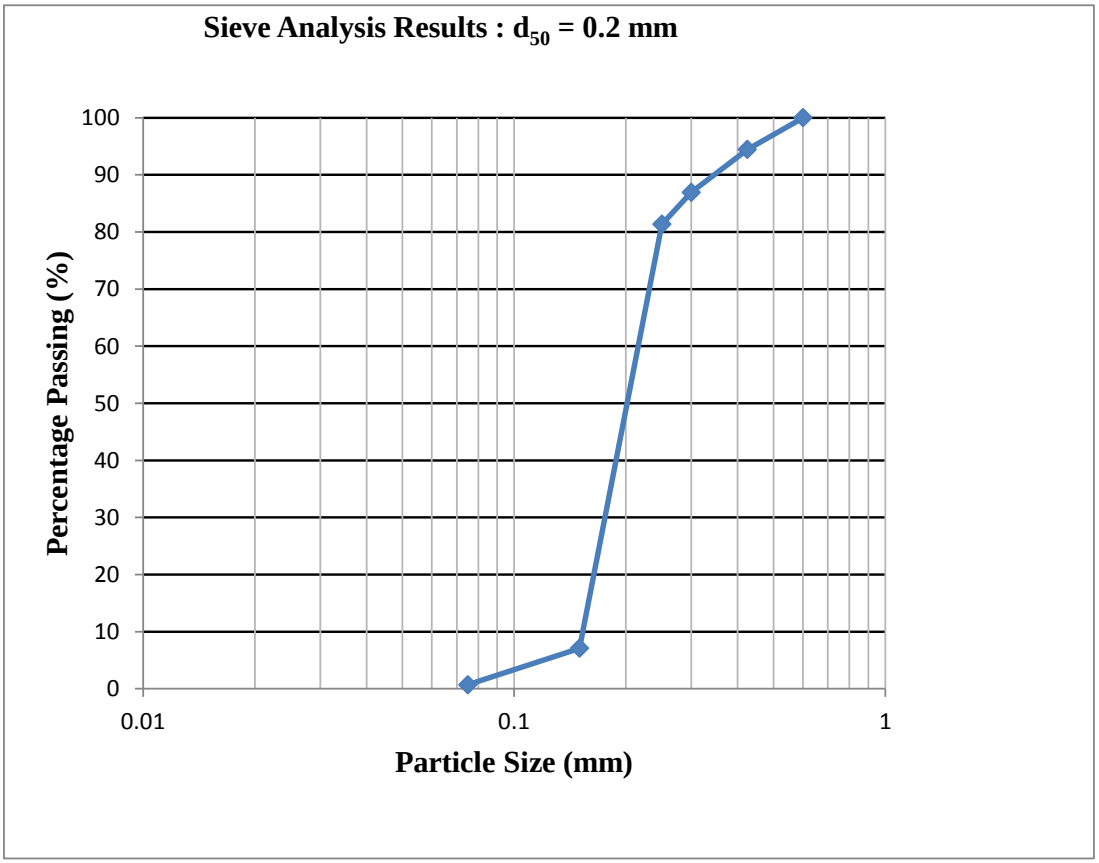


**Figure 3.3-2 Sieve analysis results for median ($d_{50}$) sediment size = 0.2 mm**

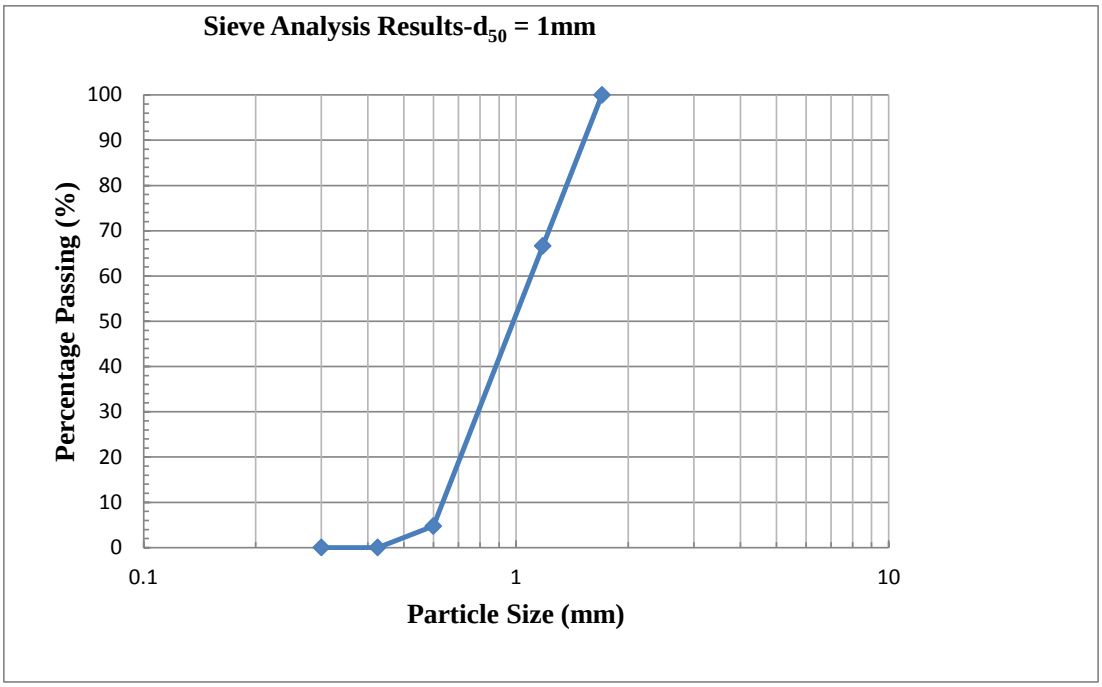


**Figure 3.3-3 Sieve analysis results for median ($d_{50}$) sediment size = 1 mm**

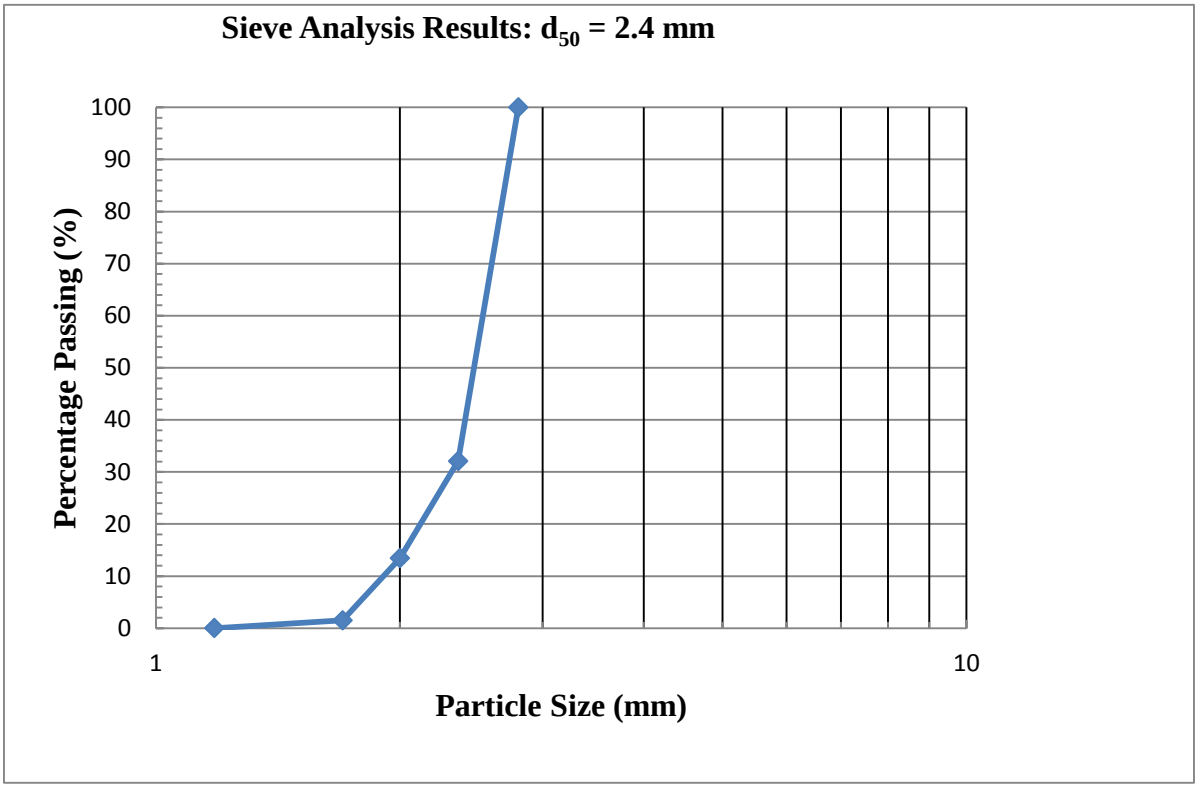


**Figure 3.3-4 Sieve analysis results for median ($d_{50}$) sediment size = 2.4 mm**

# CHAPTER 4 EXPERIMENTAL RESULTS

## 4.1 Analysis of experimental results

Tables 4.1-1, 4.1-2 and 4.1-3 show the measured flow rates, bed and friction slopes, water surface slopes and sediment transport rates data for median ($d_{50}$) sediment sizes of 0.2 mm, 1 mm and 2.4 mm respectively.

Some of the measured sediment transport rates in Tables 4.1-1, 4.1-2 and 4.1-3 show high sediment transport rates at comparatively lower flow rates. For example, the measured unit sediment transport rate for ID4 is lower than ID3 in Table 4.1-1, even though it was taken at a slightly higher flow rate. Typically a higher flow rate at the same slope configuration is supposed to transport more sediment. The observed phenomena could be attributed to the complex nature of sediment and the inability to measure sediment transport rates with high precision even in controlled laboratory settings. The recorded sediment transport rates were based on the average of three experimental runs. The averaging of four or more experimental runs did not significantly improve the accuracy of the results in terms of the tendency to predict higher sediment transport rates at comparatively low flows. The use of the term "sediment transport rates" and not "sediment transport capacity" was adopted in recognition of the fact that any particular flow could possibly transport more sediment than not what was actually recorded. Overall, the discrepancies were not considered to be so significant as to render the results invalid as is evident from the graphical plots in Figure 4.1-1.

The measured unit sediment transport rates, using median ($d_{50}$) sediment size = 2.4 mm, were compared with the results obtained using selected equations from literature. The equations were: Smart and Jäeggi (1983) and Meyer-Peter Müller (1948). The comparisons with predicted results using these selected equations from literature are shown in Table 4.1-4. The comparative analysis in Table 4.1-4 was based on median ($d_{50}$) sediment size = 2.4 mm only because the lowest median ($d_{50}$) sediment size that was used in the calibration of Smart and Jäeggi (1983) was closer to 2.4 mm. The measured sediment transport rates from this study compare very well with predicted results from the Meyer-Peter Müller (1948) equation, even though the Meyer-Peter Müller (1948) equation overestimated sediment transport rates at higher unit discharges as shown in Figure 4.1-2.

**Table 4.1-1 Experimental results for all bed slopes and median ($d_{50}$) sediment size = 0.2 mm**

| ID | Bed Slope (%) | Flow Rate ($m^3/s$) | Unit Discharge ($m^2/s$) | Friction Slope (%) | Water Surface Slope (%) | Measured Unit Sediment Transport Rate (kg/m/s) |
|---|---|---|---|---|---|---|
| 1 | 25 | 0.019 | 0.074 | 24.2 | 25.6 | 10.742 |
| 2 | 25 | 0.020 | 0.081 | 24.2 | 25.6 | 11.093 |
| 3 | 25 | 0.022 | 0.089 | 24.5 | 25.6 | 16.061 |
| 4 | 25 | 0.026 | 0.102 | 24.5 | 25.5 | 15.844 |
| 5 | 25 | 0.028 | 0.111 | 24.7 | 25.5 | 20.469 |
| 6 | 25 | 0.030 | 0.121 | 24.9 | 25.5 | 14.986 |
| 7 | 25 | 0.033 | 0.132 | 24.3 | 25.7 | 14.333 |
| 8 | 25 | 0.035 | 0.141 | 24.7 | 25.5 | 16.880 |
| 9 | 25 | 0.038 | 0.152 | 24.9 | 25.5 | 21.775 |
| 10 | 25 | 0.040 | 0.160 | 24.5 | 25.6 | 27.678 |
| 11 | 25 | 0.043 | 0.171 | 24.3 | 25.9 | 26.916 |
| 12 | 25 | 0.045 | 0.180 | 24.3 | 25.8 | 24.233 |
| 13 | 33 | 0.018 | 0.073 | 30.6 | 32.9 | 8.045 |
| 14 | 33 | 0.020 | 0.081 | 32.8 | 32.7 | 7.102 |
| 15 | 33 | 0.023 | 0.091 | 32.8 | 32.7 | 9.103 |
| 16 | 33 | 0.026 | 0.104 | 32.8 | 32.7 | 11.330 |
| 17 | 33 | 0.028 | 0.114 | 32.5 | 32.8 | 12.853 |
| 18 | 33 | 0.031 | 0.123 | 32.5 | 32.8 | 12.552 |
| 19 | 33 | 0.033 | 0.132 | 32.6 | 32.8 | 17.444 |
| 20 | 33 | 0.035 | 0.141 | 31.9 | 32.9 | 17.960 |
| 21 | 33 | 0.038 | 0.152 | 31.5 | 33.0 | 19.395 |
| 22 | 33 | 0.040 | 0.160 | 32.2 | 32.9 | 22.059 |
| 23 | 33 | 0.043 | 0.171 | 32.2 | 32.9 | 20.046 |
| 24 | 33 | 0.046 | 0.182 | 30.0 | 33.3 | 24.010 |
| 25 | 40 | 0.017 | 0.068 | 38.2 | 40.1 | 5.296 |
| 26 | 40 | 0.020 | 0.081 | 38.2 | 40.1 | 6.684 |
| 27 | 40 | 0.022 | 0.088 | 38.4 | 40.1 | 8.004 |
| 28 | 40 | 0.026 | 0.102 | 36.7 | 40.2 | 9.998 |
| 29 | 40 | 0.035 | 0.141 | 35.4 | 40.1 | 11.996 |
| 30 | 40 | 0.038 | 0.152 | 36.4 | 40.1 | 12.935 |
| 31 | 40 | 0.040 | 0.160 | 35.7 | 40.1 | 15.087 |
| 32 | 40 | 0.043 | 0.171 | 35.9 | 40.1 | 15.329 |
| 33 | 40 | 0.046 | 0.183 | 35.0 | 40.1 | 14.438 |

**Table 4.1-2 Experimental results for all bed slopes and median ($d_{50}$) sediment size = 1 mm**

| ID | Bed Slope (%) | Flow Rate ($m^3/s$) | Unit Discharge ($m^2/s$) | Friction Slope (%) | Water Surface Slope (%) | Measured Unit Sediment Transport Rate (kg/m/s) |
|---|---|---|---|---|---|---|
| 1 | 25 | 0.008 | 0.032 | 24.1 | 25.3 | 19.885 |
| 2 | 25 | 0.009 | 0.036 | 23.8 | 25.3 | 23.424 |
| 3 | 25 | 0.010 | 0.041 | 23.0 | 25.3 | 26.098 |
| 4 | 25 | 0.011 | 0.045 | 23.4 | 25.3 | 27.364 |
| 5 | 25 | 0.012 | 0.048 | 23.6 | 25.3 | 29.791 |
| 6 | 25 | 0.014 | 0.058 | 23.2 | 25.3 | 34.539 |
| 7 | 33 | 0.008 | 0.032 | 30.8 | 32.7 | 25.397 |
| 8 | 33 | 0.009 | 0.036 | 30.1 | 32.7 | 25.942 |
| 9 | 33 | 0.010 | 0.041 | 30.1 | 32.7 | 28.077 |
| 10 | 33 | 0.011 | 0.045 | 29.3 | 32.7 | 30.918 |
| 11 | 33 | 0.012 | 0.048 | 30.4 | 32.7 | 34.420 |
| 12 | 33 | 0.014 | 0.058 | 28.9 | 32.7 | 41.467 |
| 13 | 40 | 0.008 | 0.032 | 35.1 | 40.1 | 27.577 |
| 14 | 40 | 0.009 | 0.036 | 36.1 | 40.1 | 33.521 |
| 15 | 40 | 0.010 | 0.041 | 36.8 | 40.1 | 36.932 |
| 16 | 40 | 0.011 | 0.045 | 36.0 | 40.1 | 40.506 |
| 17 | 40 | 0.012 | 0.048 | 36.3 | 40.1 | 41.013 |
| 18 | 40 | 0.014 | 0.058 | 34.5 | 40.1 | 44.173 |

**Table 4.1-3 Experimental results for all bed slopes and median ($d_{50}$) sediment size = 2.4 mm**

| ID | Bed Slope (%) | Flow Rate ($m^3/s$) | Unit Discharge ($m^2/s$) | Friction Slope (%) | Water Surface Slope (%) | Measured Unit Sediment Transport Rate (kg/m/s) |
|---|---|---|---|---|---|---|
| 1 | 25 | 0.020 | 0.082 | 24.2 | 25.6 | 21.760 |
| 2 | 25 | 0.023 | 0.091 | 24.5 | 25.6 | 21.508 |
| 3 | 25 | 0.025 | 0.101 | 24.5 | 25.5 | 24.693 |
| 4 | 25 | 0.026 | 0.102 | 24.5 | 25.6 | 26.550 |
| 5 | 25 | 0.027 | 0.110 | 24.7 | 25.5 | 25.961 |
| 6 | 25 | 0.030 | 0.120 | 24.9 | 25.5 | 28.986 |
| 7 | 25 | 0.033 | 0.133 | 24.3 | 25.7 | 31.211 |

| | | | | | | |
|---|---|---|---|---|---|---|
| 8 | 25 | 0.035 | 0.141 | 24.7 | 25.5 | 30.275 |
| 9 | 25 | 0.038 | 0.152 | 24.9 | 25.5 | 36.990 |
| 10 | 25 | 0.041 | 0.164 | 24.5 | 25.6 | 37.081 |
| 11 | 25 | 0.042 | 0.170 | 24.3 | 25.9 | 32.832 |
| 12 | 25 | 0.046 | 0.183 | 24.3 | 25.8 | 32.346 |
| 13 | 33 | 0.020 | 0.081 | 30.6 | 32.9 | 25.377 |
| 14 | 33 | 0.022 | 0.087 | 32.8 | 32.7 | 25.552 |
| 15 | 33 | 0.025 | 0.101 | 31.6 | 32.9 | 28.444 |
| 16 | 33 | 0.028 | 0.114 | 32.9 | 32.7 | 32.674 |
| 17 | 33 | 0.030 | 0.121 | 32.5 | 32.8 | 34.424 |
| 18 | 33 | 0.033 | 0.133 | 32.6 | 32.8 | 33.500 |
| 19 | 33 | 0.035 | 0.141 | 31.9 | 32.9 | 38.275 |
| 20 | 33 | 0.036 | 0.143 | 31.5 | 33.0 | 36.465 |
| 21 | 33 | 0.039 | 0.156 | 31.5 | 33.0 | 40.699 |
| 22 | 33 | 0.040 | 0.161 | 32.2 | 32.9 | 40.251 |
| 23 | 33 | 0.046 | 0.183 | 31.1 | 33.1 | 47.055 |
| 24 | 33 | 0.046 | 0.183 | 30.0 | 33.3 | 45.349 |
| 25 | 40 | 0.020 | 0.081 | 38.2 | 40.1 | 34.235 |
| 26 | 40 | 0.020 | 0.082 | 38.2 | 40.1 | 31.984 |
| 27 | 40 | 0.023 | 0.091 | 38.4 | 40.1 | 35.556 |
| 28 | 40 | 0.026 | 0.102 | 36.7 | 40.2 | 39.669 |
| 29 | 40 | 0.028 | 0.111 | 35.8 | 40.3 | 38.287 |
| 30 | 40 | 0.030 | 0.120 | 35.8 | 40.3 | 44.522 |
| 31 | 40 | 0.033 | 0.132 | 35.5 | 40.3 | 41.947 |
| 32 | 40 | 0.035 | 0.139 | 35.4 | 40.1 | 46.133 |
| 33 | 40 | 0.038 | 0.151 | 36.4 | 40.1 | 49.915 |
| 34 | 40 | 0.040 | 0.160 | 35.7 | 40.1 | 53.521 |
| 35 | 40 | 0.044 | 0.175 | 35.9 | 40.1 | 53.229 |
| 36 | 40 | 0.045 | 0.180 | 35.0 | 40.1 | 67.737 |

The discrepancy percentage was computed using Equation 4.1-1:

$$Discrepancy\ Percentage = \left[\frac{Observed - Predicted}{Observed}\right] \times 100 \qquad 4.1\text{-}1$$

The average discrepancy percentage in Table 4.1-4 using the Meyer-Peter Müller (MPM) (1948) sediment transport equation is 17% and it was concluded that the equation closely predicted the measured sediment transport rates. The results predicted by the Smart and Jäeggi (1983) sediment transport equation were approximately three times higher, with an average discrepancy of 282% more than the measured sediment transport rates at the same unit discharges. The discrepancy percentages by Smart and Jäeggi (1983) sediment transport equation ranged from 157% to 562% as indicated in Table 4.1.4. The applicable slope gradient range is from 0.04% to 20% for the Smart and Jäeggi (1983) sediment transport equation. Apart from the median sediment size, the slope gradient range which was outside its derivation data range could

probably be the main reason why Smart and Jäeggi (1983) sediment transport equation overestimated the sediment transport rates.

**Table 4.1-4 Measured and predicted unit sediment transport rates for median ($d_{50}$) sediment size 2.4 mm**

| Bed Slope (%) | Unit Discharge ($m^2/s$) | Measured Unit Sediment Transport Rates - (kg/m/s) | Meyer-Peter Müller (1948) Equation Predicted Unit Sediment Transport Rates – (kg/m/s) | Smart and Jäeggi (1983) Equation Predicted Unit Sediment Transport Rates - (kg/m/s) | Meyer-Peter Müller (1948) Equation - Discrepancy Percentage | Smart and Jäeggi (1983) Equation-Discrepancy Percentage |
|---|---|---|---|---|---|---|
| 25 | 0.082 | 21.840 | 18.272 | 56.233 | 16.337 | -157.477 |
| 25 | 0.091 | 21.680 | 21.044 | 62.595 | 2.934 | -188.722 |
| 25 | 0.101 | 24.690 | 25.439 | 69.918 | -3.034 | -183.183 |
| 25 | 0.102 | 25.960 | 26.965 | 70.865 | -3.871 | -172.978 |
| 25 | 0.110 | 28.980 | 27.739 | 76.235 | 4.282 | -163.061 |
| 25 | 0.120 | 25.599 | 29.308 | 83.410 | -14.489 | -225.833 |
| 25 | 0.133 | 31.211 | 30.906 | 92.366 | 0.977 | -195.941 |
| 25 | 0.141 | 30.275 | 40.185 | 98.093 | -32.733 | -224.007 |
| 25 | 0.152 | 36.990 | 43.755 | 106.243 | -18.289 | -187.221 |
| 25 | 0.164 | 37.081 | 46.498 | 114.370 | -25.396 | -208.433 |
| 25 | 0.170 | 32.832 | 51.192 | 118.980 | -55.921 | -262.390 |
| 25 | 0.183 | 32.346 | 53.112 | 127.981 | -64.200 | -295.663 |
| 33 | 0.081 | 25.555 | 22.131 | 86.699 | 13.399 | -239.264 |
| 33 | 0.087 | 32.674 | 24.062 | 93.738 | 26.357 | -186.889 |
| 33 | 0.101 | 34.420 | 31.229 | 109.421 | 9.271 | -217.899 |
| 33 | 0.114 | 33.500 | 38.994 | 123.696 | -16.400 | -269.242 |
| 33 | 0.121 | 36.465 | 42.494 | 132.197 | -16.534 | -262.531 |
| 33 | 0.133 | 40.690 | 46.093 | 144.877 | -13.278 | -256.051 |
| 33 | 0.141 | 40.250 | 51.040 | 153.433 | -26.807 | -281.200 |
| 33 | 0.143 | 47.280 | 51.040 | 156.223 | -7.953 | -230.421 |
| 33 | 0.156 | 25.722 | 58.769 | 170.448 | -128.478 | -562.655 |
| 33 | 0.161 | 28.379 | 61.425 | 176.123 | -116.445 | -520.610 |
| 33 | 0.183 | 38.180 | 65.482 | 200.017 | -71.509 | -423.879 |
| 33 | 0.183 | 45.763 | 65.482 | 200.017 | -43.089 | -337.071 |
| 40 | 0.081 | 31.984 | 27.274 | 118.430 | 14.726 | -270.279 |
| 40 | 0.082 | 35.556 | 27.274 | 120.307 | 23.293 | -238.359 |
| 40 | 0.091 | 39.669 | 32.369 | 134.805 | 18.402 | -239.825 |
| 40 | 0.102 | 38.287 | 36.377 | 151.106 | 4.989 | -294.667 |

| | | | | | | |
|---|---|---|---|---|---|---|
| 40 | 0.111 | 49.915 | 39.134 | 164.505 | 21.599 | -229.570 |
| 40 | 0.120 | 53.229 | 44.846 | 178.082 | 15.749 | -234.558 |
| 40 | 0.132 | 41.947 | 49.297 | 195.398 | -17.522 | -365.821 |
| 40 | 0.139 | 46.133 | 52.341 | 206.896 | -13.457 | -348.477 |
| 40 | 0.151 | 34.248 | 55.446 | 224.570 | -61.896 | -555.717 |
| 40 | 0.160 | 44.619 | 57.020 | 237.501 | -27.793 | -432.287 |
| 40 | 0.175 | 52.506 | 60.213 | 260.487 | -14.678 | -396.109 |
| 40 | 0.180 | 67.570 | 63.463 | 268.220 | 6.078 | -296.951 |

The results in Tables 4.1-2 and 4.1-3 are plotted in Figure 4.1-1 for various bed slopes and median ($d_{50}$) sediment sizes 1 mm and 2.4 mm. The results for median ($d_{50}$) sediment size 0.2 mm were excluded from the results in Figure 4.1-1 for the following reasons:

- A comparative analysis of the trend lines for median ($d_{50}$) sediment sizes 0.2 mm showed that the sediment transport capacity did not increase as a linear function with discharge or bed slope ($S_o$).
- The trend lines for median ($d_{50}$) sediment sizes 0.2 mm showed that the measured sediment transport rates were higher at the bed slope of 25% and lower at bed slope of 40% (Refer to Appendix A1).

Normally a steeper bed slope is expected to transport more sediment than a less steep slope. This is the case when sediment is transported as bed load based on the understanding that the bed slope influences movement of the sediment when the bed load mode of sediment transport is predominant. Another possible explanation was that flow and sediment transport conditions for $d_{50}$ = 0.2 mm had not yet reached equilibrium due to its mode of transport which was suspected to be suspended transport using the criteria of motion. The suspended mode of transport typically has a longer adaptation length than bed load and it is possible that full equilibrium conditions had not yet been reached within the available flume length. In view of the observed characteristics, the data for median ($d_{50}$) sediment size 0.2 mm was not used during the final derivations of the sediment transport equations.

Figure 4.1-2 shows the comparison between the measured sediment and predicted sediment transport rates by Meyer-Peter Müller (1948) equation for median ($d_{50}$) sediment size 1 mm and 2.4 mm. Meyer-Peter Müller (1948) equation overestimates sediment transport rates at higher unit discharges. The overestimation could be attributed to the influence of high flow depths at high flow rates that resulted in high hydraulic radii values within the shear stress formulation in Meyer-Peter Müller (1948) sediment transport equation. In addition, the overestimation could be due to the application of the Meyer-Peter Müller (1948) sediment transport equation outside its range of 0 to 2% slopes. The detailed results for all sediment sizes and graphical data plots have been included in Appendix A1.

## 4.2 Summary

The experimental data was collected and analysed for its use in developing sediment transport equations for steep slopes. As mentioned above, the Meyer-Peter Müller (1948) sediment transport equation provides reasonable predictions of the experimental results particularly for smaller unit discharges although there are clearly some anomalies. The development of alternative empirical sediment transport equations for steep slopes using the experimental data is presented in Chapter 5.

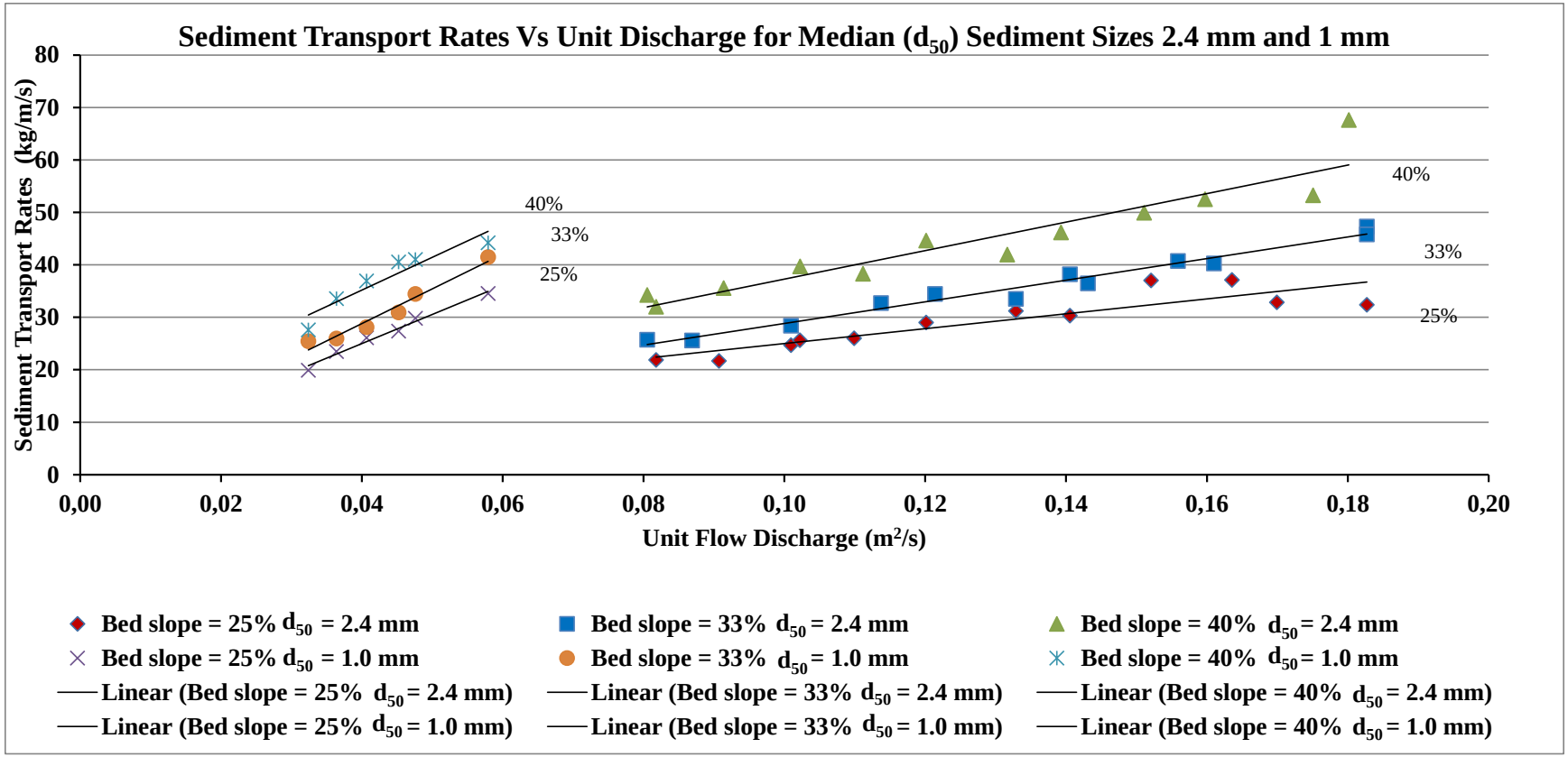


**Figure 4.1-1 Measured sediment transport rates for all slopes and median ($d_{50}$) sediment sizes = 1 mm and 2.4 mm**

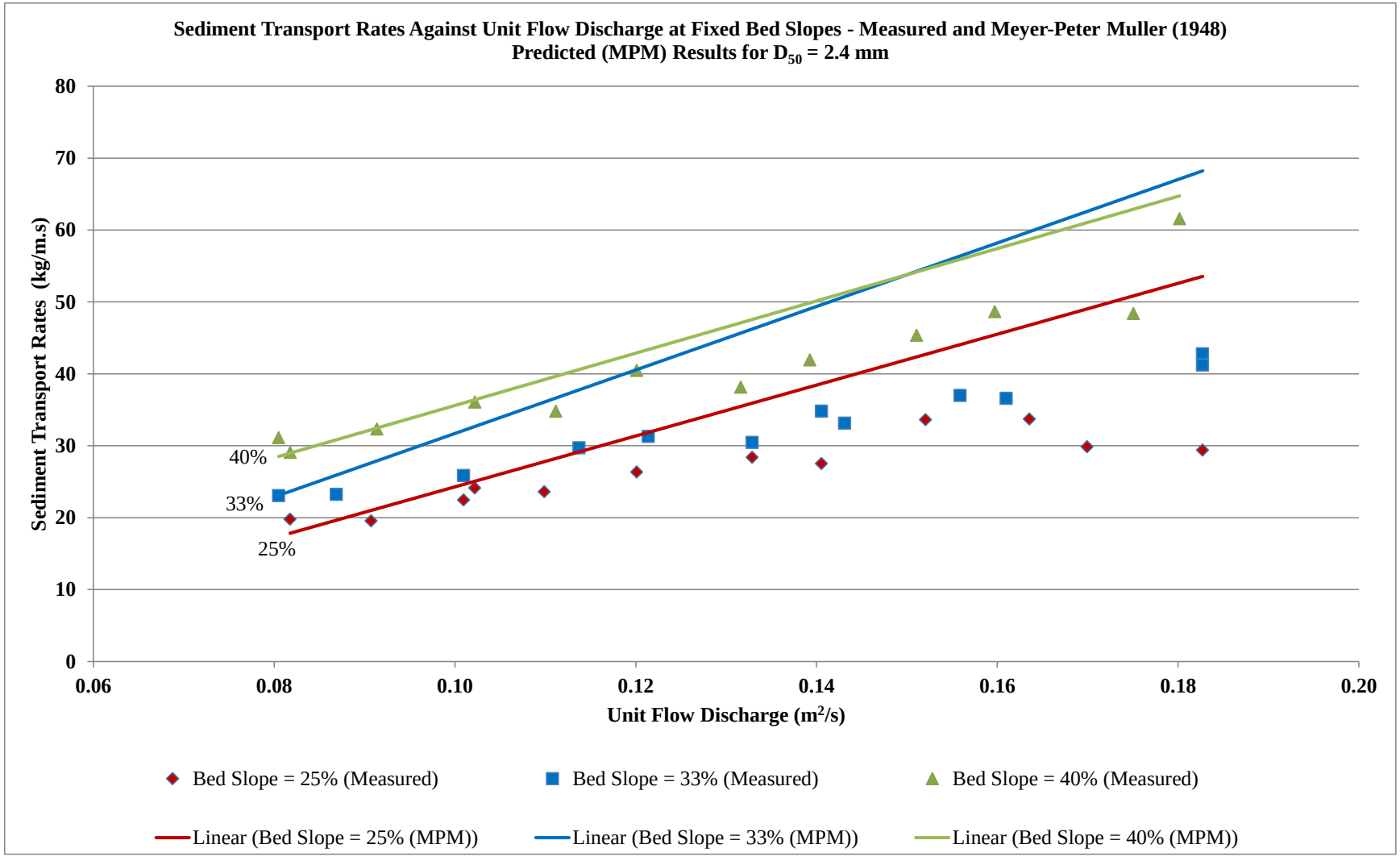


**Figure 4.1-2 Comparison of measured and predicted sediment transport rates**

# CHAPTER 5 THE DEVELOPMENT OF NEW EMPIRICAL SEDIMENT TRANSPORT EQUATIONS FOR STEEP SLOPES

## 5.1 Background to the approaches for the development of empirical sediment transport equations

Sediment transport is a complex phenomenon and no single hydraulic parameter can describe the sediment transport rate under all conditions (Sinnakaudan et al., 2010). The basic assumption in one of the approaches that are used in the derivation of sediment transport equations, namely the deterministic approach, is that there is a one-to-one relationship between selected independent and dependent variables (USBR, 2014). The choice of predictor variables is subjective and depends on the modeller's requirements and needs.

According to Yang (1996), the basic form of most sediment transport equations adopts one or more of the following variables corresponding to concentration or sediment discharge per unit width of channel: water discharge, average flow velocity, energy or water surface slope, shear stress, total stream power per unit bed area and unit stream power. Even though these variables are interrelated within many individual equations, the dominant variable within the equation determines the general accuracy of the equation within the context in which it is to be applied. It is believed that the lack of a well-defined strong correlation between sediment load or concentration and a dominant variable that is selected for the development of a sediment transport equation may be the fundamental reason for the discrepancies between computed and measured results (of sediment transport rates), under different flow and sediment conditions (Yang, 1996). It was found by Yang (1996), that the use of stream power as a dominant variable in sediment transport greatly improves the predictive capability of the total sediment discharge or concentration in channels. Yang's (1996) power approach is just one of the many power approaches for sediment transport equation derivation. Other power derived sediment transport equations include stream power (Bagnold, 1966), unit stream power (Yang, 1972, 1973, 1979) and gravitational power (Velikanov, 1954). Selected equations that are based on these concepts have already been reviewed in Chapter 2.

Several authors (Rooseboom, 1992; Basson, 1999) have confirmed the predictive capability of the unit stream power type equations. The concept of minimum stream power states that the stream or channel will begin to entrain particles when the power required to suspend the particles becomes less than the power required to maintain the particles in a stationary position. Rooseboom (1992) described the power balance in a one-dimensional open channel flow as the power deficit per unit volume. The power approach is explained further by Rooseboom (1992) in terms of the velocity variations from laminar flow and fully developed turbulent flow as well as the transition from laminar to turbulent flow and the critical Reynolds Number ($Re_*$).

The practical aspects of the interaction between the flowing fluid and transportable material can also be generally explained with regard to the applied stream power approach. Basson (1999)

developed a new sediment transport equation based on applied stream power. The equation was developed from fundamental mathematical principles of hydraulics and was calibrated and further verified against river and canal data. Rooseboom (1992) stated that the law of conservation of power provides a much clearer picture of sediment transporting processes including: parameters for erosion initiation for both cohesive and non-cohesive materials, suspended sediment transport with so-called bed load a special case, channel deformation processes and the interrelationship between flow resistance and sediment transport.

The above analysis of the various power approaches shows that the slope (whether friction or water surface) is a very important parameter since it is embedded in the applied, total or unit stream power terms. This indicates that the best sediment transport equations for dam-break models should be those in which both the water surface or energy slope and bed slope are within the ranges of typical slopes on earth dams in order to improve the predictive capability.

Only three different formulations were considered in the derivation and calibration of new empirical sediment transport equations based on the deterministic approach in this study. These were the DHI universal empirical relationship (DHI, 2011), Khorram and Ergil (2010) and the Zhang et al. (2009) formulations. These three formulations were applied as a guide for the choice of optimum hydraulic parameters or predictor variables for multiple regression analysis. Ultimately, the choice of the final proposed empirical sediment transport equation(s) was to be based on the equation that showed better predictive capabilities.

## 5.2 Calibration of steep slope sediment transport equations based on the DHI universal empirical formulation5.2.1 DHI (2011) universal empirical formulation

A regression approach was applied in the derivation of new sediment transport equations based on the DHI (2011) universal empirical formulation using specifically recommended predictors or variables. The general empirical equation can be specified by eight coefficients and exponents as shown in Equation 5.2-1.

$$\emptyset = a_1 \left[ \left( \frac{d_{90}}{d_{30}} \right)^{a_2} S_f^{a_3} C^{a_4} \theta^{a_5} [a_6 \theta^{a_7} - \theta_{cr}]^{a_8} \right] \qquad 5.2\text{-}1$$

Where

$\emptyset$ Dimensionless sediment transport rate

$d_{30}$ Grain diameter for which 30% weight of a non-uniform sample is finer

$d_{90}$ Grain diameter for which 90% weight of a non-uniform sample is finer

$S_f$ Energy or friction slope (could be replaced by bed slope under uniform flow conditions, $S_o$)

$\theta, \theta_{cr}$ Dimensionless shear stress and critical dimensionless shear stress respectively

C The resistance factor, a ratio of the average flow velocity to bed shear velocity

$\alpha_{1,2\ldots n}$ Coefficients or exponents

In order to derive a calibrated empirical sediment transport equation for steep slopes based on the DHI (2011) formulation, the laboratory data obtained in this study were used to compute the applicable predictor variables or hydraulic parameters in the subsequent multiple regression analysis. The dimensionless sediment transport rate (∅) was included as the dependent variable. The independent variables for multiple regression analysis were: $\left(\frac{d_{90}}{d_{30}}\right)$, $S_f$, C and $(\theta - \theta_{cr})$. The water surface or friction slope ($S_f$) was computed from the measured flow depth and velocity data. The friction slope was computed from the difference of the sum of water depths and velocity head at selected cross-sections based on Bernoulli's theorem. The grain diameters for which 90% and 30% weight of a non-uniform sample were finer ($d_{90}$ and $d_{30}$) respectively, were obtained from sieve analysis graphical data. The dimensionless shear stress and critical dimensionless shear stress ($\theta$ and $\theta_{cr}$) respectively were computed from water surface slope, average flow depth and density data. The dimensionless sediment transport rate was calculated from the measured mass sediment transport rate per unit channel width in kg/m/s ($q_t$), sediment density in kg/m$^3$ ($\rho_s$) and volumetric sediment discharge per unit channel width in m$^3$/m/s ($q_s$).

Where

$$\emptyset = \frac{q_s}{[g(s-1)d_{50}^3]^{0.5}} \qquad 5.2\text{-}2$$

$$q_t = q_s \rho_s \qquad 5.2\text{-}3$$

Where

s Relative unit weight of sediment

g Acceleration due to gravity

$d_{50}$ Median sediment grain diameter

The multiple regression analysis was based on this relationship;

$$\emptyset = f\left(\frac{d_{90}}{d_{30}}, S_f, C, \theta - \theta_{cr}\right) \qquad 5.2\text{-}4$$

According to Rooseboom (1992), sediment transport is a hydrological process and it is a function of the same parameters that influence all hydrological processes. It was observed that while hydrological data are usually strongly skewed, the logarithms of the data have a near symmetrical distribution (Hazen, 1914). In this regard, the dependent variable of the dimensionless sediment transport rate and the rest of the independent predictor variables were logarithmically transformed in order to achieve a better multiple regression fit. A Microsoft

Excel spreadsheet was prepared with a column of the dimensionless sediment transport rate as a dependent variable and four columns comprising the predictor variables that are shown on the right hand side of Equation 5.2-4 (Appendix A2 shows the values of the predictor variables and their logarithmic transformations). Multiple regression analysis was performed in Microsoft Excel using Data Analysis Regression tools. A forward selection approach of step regression analysis was conducted. This involved testing the addition of a selected predictor variable in Equation 5.2-4 and checking the improvement in the regression model results using the r-square comparison criterion. Two empirical sediment transport equations were determined based on the DHI (2011) formulation as given in Equations 5.2-5 and 5.2-6:

$$\emptyset = 0.54\left[\left(\frac{d_{90}}{d_{30}}\right)^{1.6} C^{1.05}[\theta - \theta_{cr}]^{1.2}\right] \qquad 5.2\text{-}5$$

$$\emptyset_b = 0.34\left[\left(\frac{d_{90}}{d_{30}}\right)^{1.57} S_f^{0.14} C^{1.05}[\theta - \theta_{cr}]^{1.16}\right] \qquad 5.2\text{-}6$$

*5.2.1.1 Determination of the predictive capability for Equations 5.2-5 and 5.2-6*

Prediction models have varying acceptable levels of correlation or degrees of accuracy. An acceptable degree of correlation or accuracy of an equation depends on the objective of the model. In sediment transport, equations are mostly developed to make rough estimates due to the complexity of sediment behaviour when in transport. This is because sediment transport equations do not entirely explain the total variation of the dependent variable against the selected independent variables. This simplistic representation of the variables means that the neglected variables might explain part of the variation in a regression model. The model's accuracy refers to the predictive capability of an individual equation. The degree of correlation determines the accuracy of a selected formula in comparison with other formulae. Statistical methods were applied to measure the degree of correlation, statistical reliability and significance of Equations 5.2-5 and 5.2-6.

*5.2.1.1 Introduction to the application of ANOVA table of results in testing an equation's statistical significance*

The ANOVA results are used to test the hypothesis claiming that the amount of variation explained by the regression model is more than the variation explained by the average (Hair et al., 1995). The best regression model can be selected based on the F ratio test and $r^2$. The results in Tables 5.2-1 and 5.2-2 were generated by Microsoft Excel after performing multiple regression analysis. The results in Tables 5.2-1 and 5.2-2 can also be calculated manually for a given regression model.

**Table 5.2-1 ANOVA table for Equation 5.2-5 using median ($d_{50}$) sediment size = 2.4 mm and 1 mm; bed slopes = 25%, 33% and 40%**

| Source of variation | Sum of squares | Degree of freedom | Mean square | $F_o$ |
|---|---|---|---|---|
| Regression | $SS_R$ = 3.6 | k = 3 | $SS_R/k = M_{SR}$ = 1.2 | $M_{SR}/ M_{SE}$ = 1500 |
| Error | $SS_E$ = 0.041 | n-p = 49 | $SS_E/(n-p) = M_{SE}$ = 0.0008 | |
| Total | $SS_{yy}$ = 3.641 | n-1 = 52 | r-square | 0.99 |

**Table 5.2-2 ANOVA table for Equation 5.2-6 using median ($d_{50}$) sediment size = 2.4 mm and 1 mm; bed slopes = 25%, 33% and 40%**

| Source of variation | Sum of squares | Degree of freedom | Mean square | $F_o$ |
|---|---|---|---|---|
| Regression | $SS_R$ = 3.6 | k = 4 | $SS_R/k = M_{SR}$ = 0.9 | $M_{SR}/ M_{SE}$ = 1171 |
| Error | $SS_E$ = 0.040 | n-p = 48 | $SS_E/(n-p) = M_{SE}$ = 0.0008 | |
| Total | $SS_{yy}$ = 3.640 | n-1 = 52 | r-square | 0.99 |

The sum of squares on the regression ($SS_R$) is calculated from the variance of each sample within groups of predictor variables. The sum of squares on error ($SS_E$) is calculated from the variance between groups of predictor variables. The addition of the sum of squares on the regression ($SS_R$) and sum of squares on error ($SS_E$) gives the total sum of squares ($SS_{yy}$). For example in Equation 5.2-6, the total number of predictor variables ($p$) was five. These were: the dimensionless sediment transport rate ($\emptyset$) as the dependent variable and independent variables$\left(\frac{d_{90}}{d_{30}}\right)$, $S_f$, C and $(\theta - \theta_{cr})$. The degree of freedom on the regression (k = p-1) is the total number of independent predictor variables. The total number of observations is denoted as $n$.

The degree of freedom on the error (n-p) is the total number of observations (n) less the total number of predictor variables ($p$). The mean square on the regression ($M_{SR}$) is obtained from dividing the sum of squares on the regression ($SS_R$) by degree of freedom on the regression/numerator (k). The mean square on the error ($M_{SE}$) is obtained from dividing the sum of squares on error ($SS_E$) by degree of freedom on the error/denominator (n-p). The F ratio ($F_o$) value is calculated from the mean square on the regression ($M_{SR}$) and mean square on the error ($M_{SE}$). The final analysis involves the determination of the critical value of F, from an F distribution table, that is needed to be compared with $F_o$ in order to assess the validity of the

regression model. A sample of the F distribution table is given in Appendix A3. An F distribution table contains information that is illustrated in Figure 5.2-1. The critical value of F gives a score that is needed in order to reject the null hypothesis or ascertain the validity of the regression model.

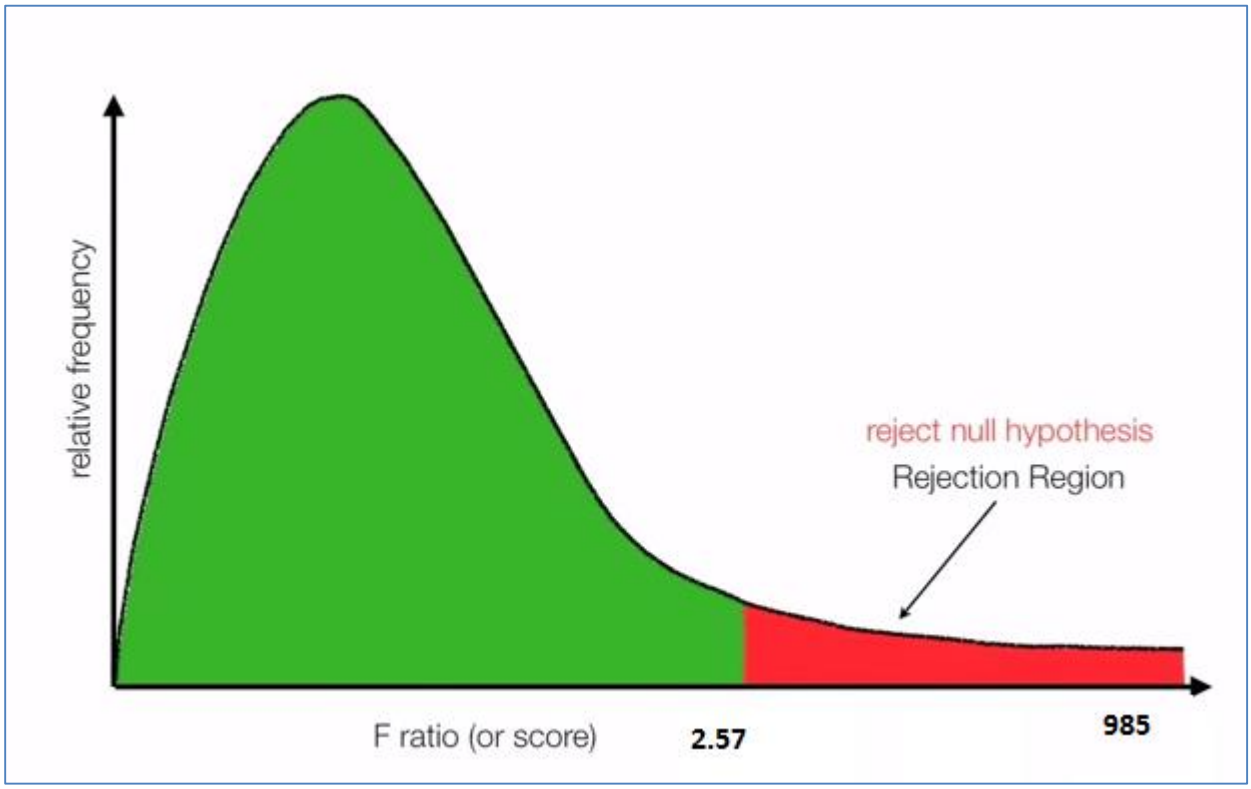


**Figure 5.2-1 An illustration of the critical value of F**

An F distribution table gives $F_{(k,n-p,\alpha)}$, the critical value of F for the selected level of significance ($\alpha$) and the degree of freedom on the regression/numerator ($k$) and degree of freedom on the error/denominator ($n-p$). The applicable significance level ($\alpha$) determines the level of significance that is expected to be attached to the prediction. An $\alpha$ value of 0.05 corresponds to 95% confidence interval. The null hypothesis is rejected if $F_O > F_{(k,n-p,\alpha)}$. From the F distribution table in Appendix A3, a critical F value corresponding to the degree of freedom on the regression/numerator (k, it is given as $df_1$ in the F distribution table in Appendix A3) and degree of freedom on the error/denominator (n-p), it is given as $df_2$ in the F distribution table in Appendix A3) can be obtained.

From the ANOVA results in Table 5.2-1, the number of independent variables, k = (3+1-1) = 3, n-p = (53-4) = 49 and total variance (n-1) = 52. The critical value of F at the level of significance $\alpha$ = 0.05, $F_o$ from the ANOVA table is 1500. From the Standard F distribution table in Appendix A3, $F_{3,49,0.05}$ = 2.79 (after interpolation). Since $F_{(k,n-p,\alpha)} < F_O$, the null hypothesis is rejected and the regression model is accepted as being adequate or valid in terms of the set model

objectives. By rejecting the null hypothesis, one is satisfied that at 5% significance level, there is a direct relationship between the dependent and independent predictor variables for that particular data set. By the same criterion and using an $F_o$ of 1171 in Table 5.2-2, it was shown that the regression model for Equation 5.2-6 was also adequate and valid.

The coefficient of determination is a statistical test that measures the discrepancy between measured and predicted model results. The coefficient of determination is sometimes referred to as the r-square ($r^2$). The coefficient of determination is the estimation of the combined dispersion against the single dispersion of the observed and predicted series. The r-square ranges between 0 and 1.0. It is a measure of the amount of the observed dispersion that is explained by the prediction. A value of zero signifies lack of correlation whereas a value of 1 shows that the dispersion of the prediction is equal to that of the observation. Consideration of an acceptable r-square value depends on several factors such the nature of the variable being predicted, the size of the sample and results of statistical tests on regression and correlation.

The coefficient of determination (r-square ($r^2$)) was 0.99 and an adjusted r-square was 0.99 for both Equations 5.2-5 and 5.2-6. It should be noted that the r-squares of the regression models for Equations 5.2-5 and 5.2-6 in the ANOVA tables 5.2-1 and 5.2-2 are related to the dimensionless sediment transport rate as the dependent variable. While the r-squares in Figures 5.2-2 and 5.2-3 are related to the equation for the prediction of sediment transport rates in kg/m/s, after converting from the dimensionless sediment transport rate using Equations 5.2-2 and 5.2-3. Based on the three criteria of the F test, r-square and adjusted r-square, the prediction models were accepted as significant/valid and statistically reliable. Therefore, Equations 5.2-5 and 5.2-6 were further checked using the discrepancy error criteria. The graphs of the predicted sediment transport rates against the measured sediment transport rates are given in Figure 5.2-2 and 5.2-3.

The discrepancy error of the predicted values using Equations 5.2-5 and 5.2-6 ranged from -21.49% to 8.7% and -12.2% to 19.63% respectively as indicated in Appendix A4. The measured and predicted sediment transport rates were plotted together for all slopes (Figures 5.2-2 and 5.2-3) and separately for each slope (Figures 5.2-4 and 5.2-5). An assessment of the graphical plots in Figures 5.2-2, 5.2-3, 5.2-4 and 5.2-5 as well as an analysis of the range of discrepancy errors showed that the regression prediction model Equations (5.2-5 and 5.2-6) had tolerable accuracy and are valid for application within the prescribed range of steep slopes.

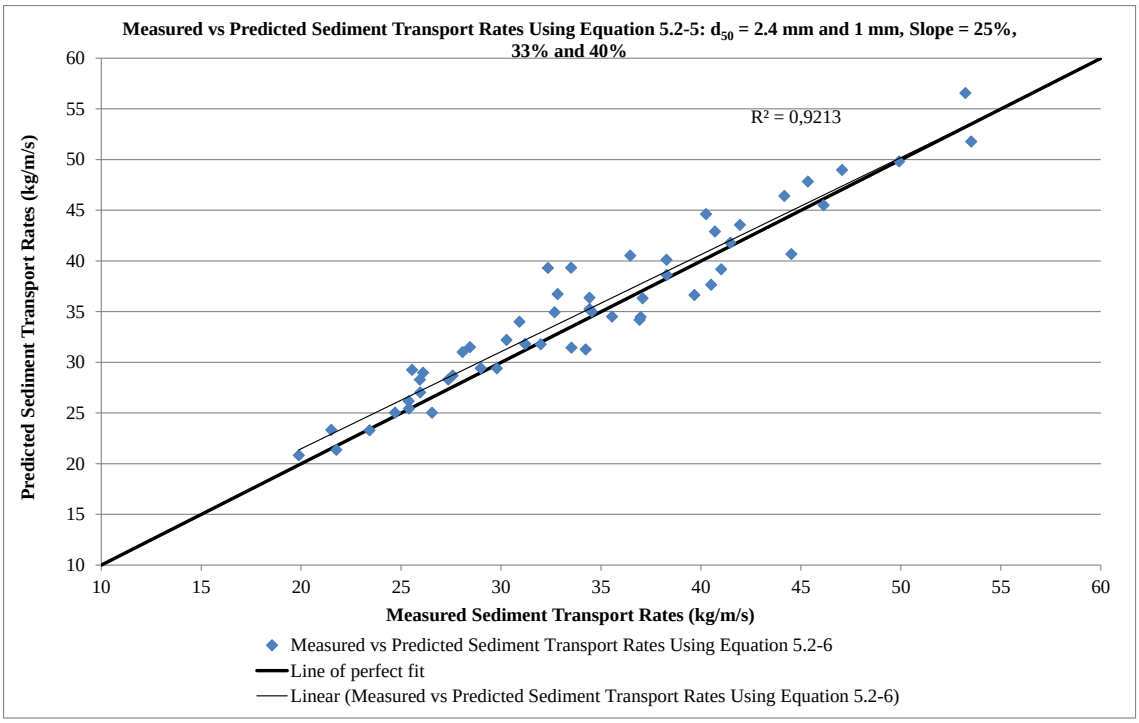


**Figure 5.2-2 Predicted and measured sediment transport rates using Equation 5.2-5**

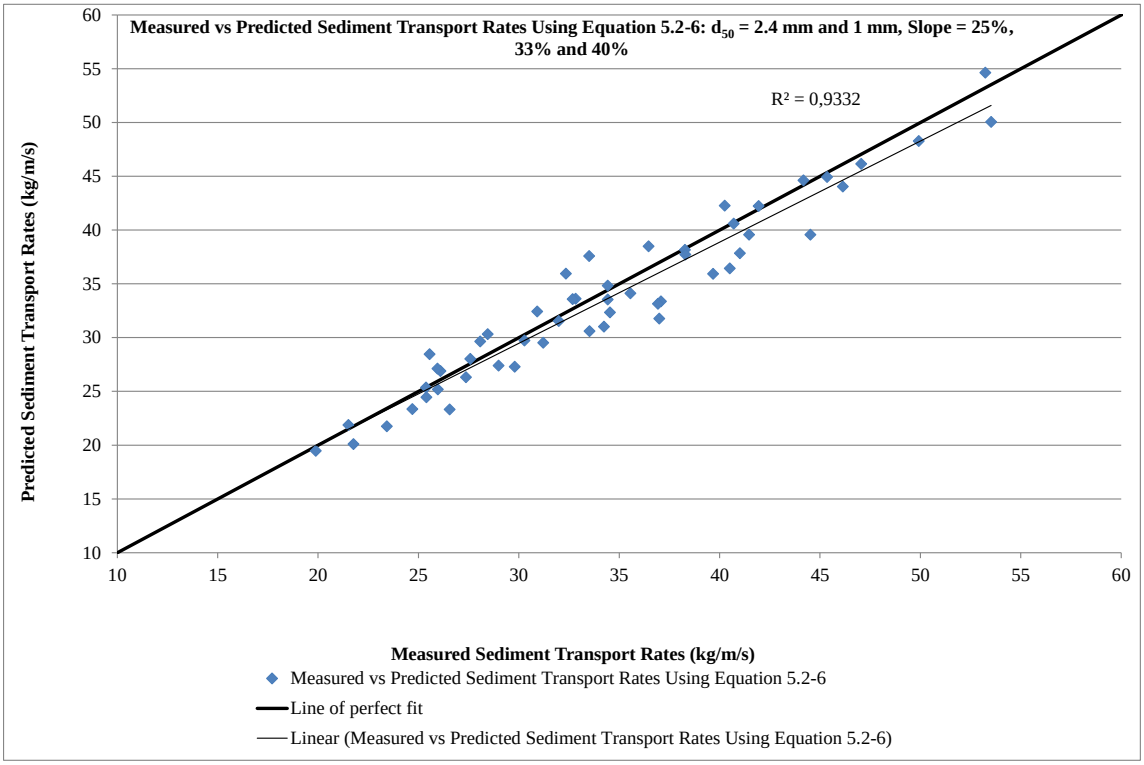


**Figure 5.2-3 Predicted and measured sediment transport rates using Equation 5.2-6**

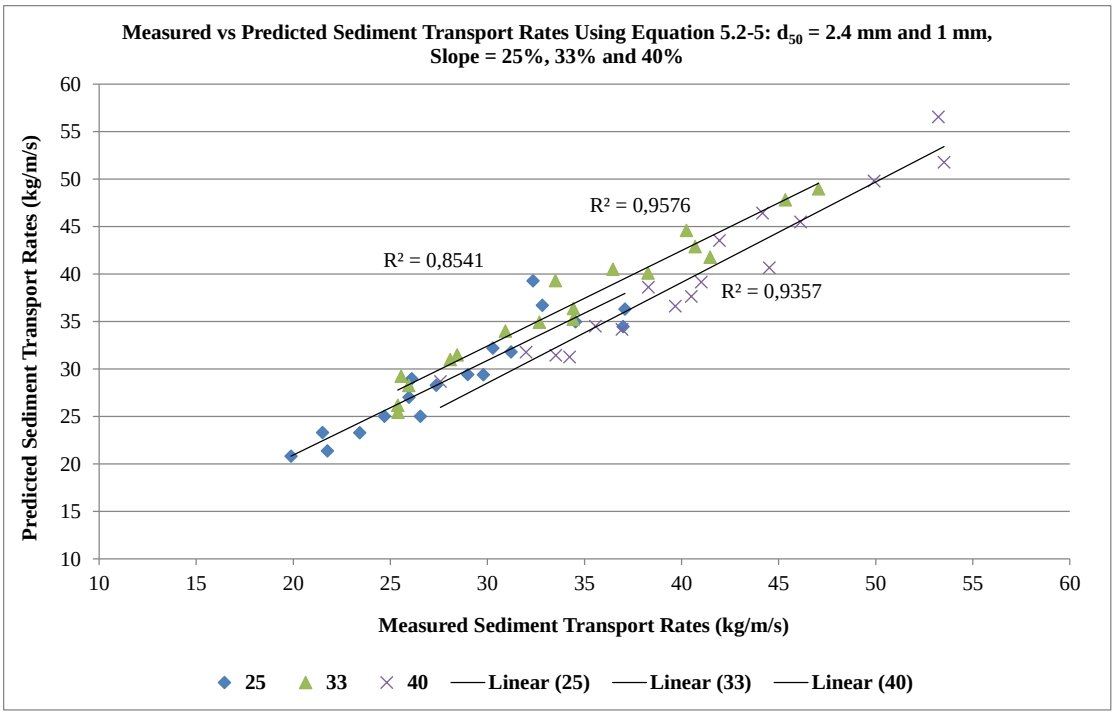


**Figure 5.2-4 Predicted and measured sediment transport rates using Equation 5.2-5 – separate plots for different slopes**

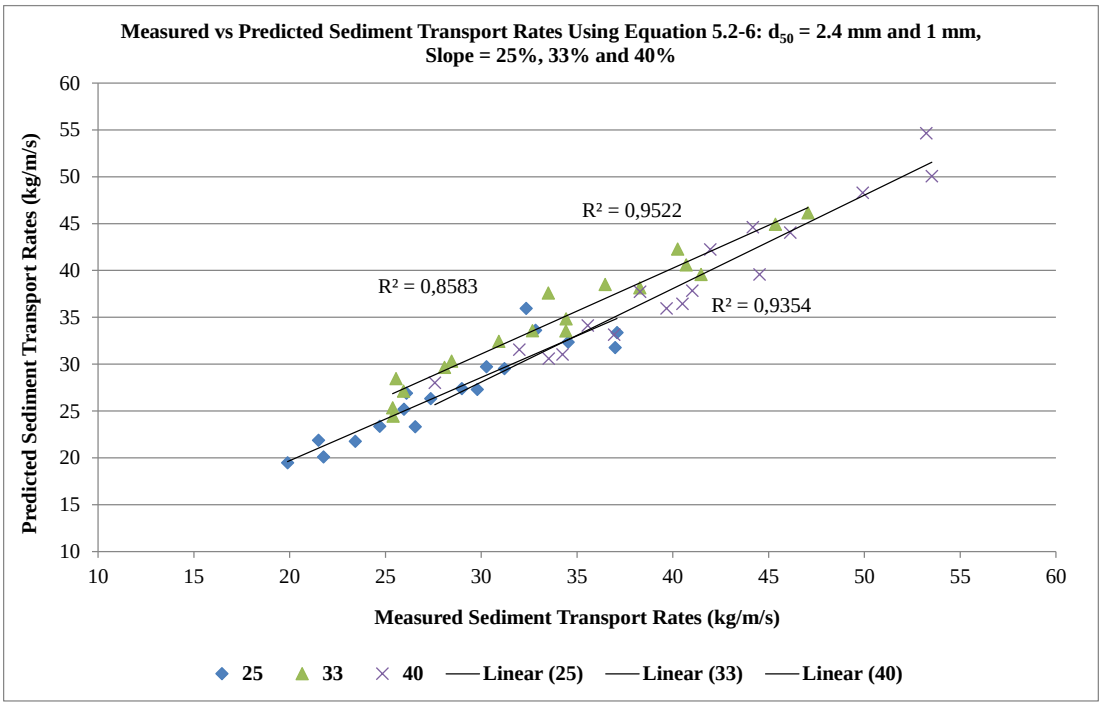


**Figure 5.2-5 Predicted and measured sediment transport rates using Equation 5.2-6 - separate plots for different slopes**

## 5.3 Calibration of steep slope sediment transport equations based on Khorram and Ergil (2010) and Zhang et al. (2009) sediment transport equation formulations

Two other deterministic approaches were investigated. These were Khorram and Ergil (2010) and Zhang et al. (2009) sediment transport equation formulations. The reason for investigating two other empirical formulations was to determine if a better predictive capability could be achieved using different formulations.

### *5.3.1 Khorram and Ergil (2010) equation formulation*

Khorram and Ergil (2010) also observed that the lack of a well-defined, strong correlation between sediment transport load and the dominant variable selected for the development of a sediment transport equation is one of the fundamental reasons for discrepancies between computed and measured results under different flow and sediment transport conditions. From their (Khorram and Ergil, 2010) analysis of twenty-three total-load equations for non-cohesive particles and by studying the relative strengths, weaknesses and limitations of the relevant parameters, they came up with recommended dimensionless parameters (DP). The recommended parameters were determined from an investigation of 300 individual parameters/ hydraulic variables used in 52 frequently applied existing sediment transport equations using detailed sensitivity analysis through a multilinear regression method.

According to Khorram and Ergil (2010), the findings of that research can guide researchers in the development of new sediment transport equations. Khorram and Ergil (2010) found that, the most influential parameter for sediment transport equations in alluvial rivers for sand particles is the gravitational power due to the Shields' parameter with an energy slope ($\frac{V^3}{(s-1)gd_{50}w_s}\frac{S_f(\theta)}{log\left(1/d_{50}\right)}$). For the gravel particles, the most influential parameter is the universal stream power due to critical Shields' parameter with an energy slope ($\frac{(s-1)VS_f(\theta)}{w_s}$) (Khorram and Ergil, 2010). The five most influential primary parameters based on their ranking criteria for sand particles were average flow velocity ($V$), median ($d_{50}$) sediment size, settling velocity ($w_s$), shear velocity ($U_*$) and friction slope ($S_f$).

The rest of the most influential proposed dimensionless parameters (DP) based on the Khorram and Ergil (2010) ranking criteria for sand particles were as follows: the gravitational power due to Shields' parameter with an energy slope ($\frac{V^3}{(s-1)gd_{50}w_s}\frac{S_f(\theta)}{log\left(1/d_{50}\right)}$), the Shields' parameter with an energy slope ($S_f(\theta)$), the critical unit stream power with Shields' parameter ($\frac{V_{cr}S_f\theta}{w_s}$), the critical Shields' parameter with an energy slope ($S_f\theta_{cr}$), and the universal gravitational power due to Shields' parameter with an energy slope ($\frac{VU_*'^2}{gd_{50}w_s)}\frac{S_f(\theta)}{S-1}$). For their flume dataset, the most influential proposed parameters were the gravitational power due to Shields' parameter with an

energy slope ($\frac{V^3}{(s-1)gd_{50}w_s}\frac{S_f(\theta)}{log\left(1/d_{50}\right)}$), the universal stream power due to Shields' parameter with an energy slope ($\frac{(s-1)VS_f(\theta)}{w_s}$), the critical Shields' parameter with an energy slope ($S_f\theta_{cr}$), the critical unit stream power ($V_{cr}S_f$), and the Shields' parameter ratio ($\frac{\theta}{\theta_{cr}}$).

In summary, Khorram and Ergil (2010) said that "due to the complexity of the flow and sediment conditions, engineers must select equations that are appropriate for the specific flow and sediment conditions, as each equation contains a number of parameters and has many constraints.

Khorram and Ergil (2010) recommended different dimensionless parameters or hydraulic variables on which new sediment transport equations should be based. The general functional relationships for sand (5.3-1) and gravel (5.3-2) were formulated as follows:

$$q_t = f\left(\frac{V^3-V_{cr}^3}{(s-1)gd_mw_s}\frac{S_f(\theta-\theta_{cr})}{log\left(1/d_m\right)}, S_f\theta, \frac{V_{cr}S_f\theta}{w_s}, S_f\theta_{cr}, \frac{(s-1)VS_f(\theta-\theta_{cr})}{w_s}\right) \quad 5.3\text{-}1$$

$$q_t = f\left(\frac{V^3-V_{cr}^3}{(s-1)gd_mw_s}\frac{S_f(\theta-\theta_{cr})}{log\left(1/d_m\right)}, \frac{VU_*'^2S_f\theta}{(s-1)gd_mw_s}, S_f\theta, \frac{V_{cr}S_f\theta}{w_s}, \frac{\theta}{\theta_{cr}}\right) \quad 5.3\text{-}2$$

In this study, only four dimensionless parameters were applied after modifying the dimensionless parameters that are given in Equations 5.3-1 and 5.3-2. The modified dimensionless parameters were determined after excluding the critical parameter terms. It is common for equations that are applied in sediment transport modelling to assume that the critical parameters are negligible in comparison with the mean parameter values, i.e. critical shear stress being negligible in comparison to mean shear stress. For instance, Abrahams (2003) and Engelund and Hansen (1967) sediment transport equations ignored the concept of a threshold for the onset of sediment transport as reported by Abderrezzak and Paquier (2011). The four modified dimensionless parameters (DP) were the universal stream power due to Shields' parameter with an energy slope (DP1), Shields' parameter with an energy slope (DP2), the gravitational power due to Shields' parameter with an energy slope (DP3) and the universal gravitational power due to Shields' parameter with an energy slope (DP4).

Khorram and Ergil (2010) provided a guide to those parameters that proved to have a significant influence on sediment transport phenomena by coming up with dimensionless parameters that were based on the physical quantities that are involved in sediment transport. The individual dimensionless parameters were based on dimensional analysis of 300 individual parameters/ hydraulic variables used in 52 frequently applied existing sediment transport equations. In dimensional analysis, one first predicts the physical quantities or parameters that will influence the flow and sediment, and grouping these 300 parameters in dimensionless combinations to better describe the flow and sediment phenomena.

$$q_t = \alpha_1 \left[\frac{(s-1)VS_f(\theta)}{w_s}\right]^{\beta_1} \quad \text{(DP1)} \quad 5.3\text{-}3$$

$$q_t = \alpha_2 \left[S_f\theta\right]^{\beta_2} \quad \text{(DP2)} \quad 5.3\text{-}4$$

$$q_t = \alpha_3 \left[\frac{V^3}{(s-1)gd_{50}w_s}\frac{S_f(\theta)}{log\left({}^1/_{d_{50}}\right)}\right]^{\beta_3} \quad \text{(DP3)} \quad 5.3\text{-}5$$

$$q_t = \alpha_4 \left[\frac{VU_*'^2}{gd_{50}w_s)}\frac{S_f(\theta)}{s-1}\right]^{\beta_4} \quad \text{(DP4)} \quad 5.3\text{-}6$$

Where

$q_t$ Unit discharge of sediment (kg/m/s)

$s$ Specific density of sediment

$V$ Average flow velocity

$S_f$, Friction or water surface slope

$\theta$ Dimensionless bed shear stress or Shields' parameter

$w_s$ Sediment settling velocity

$d_{50}$ Median sediment grain size

$g$ Acceleration due to gravity

$\alpha_1, \alpha_2, \alpha_3$ and $\alpha_4$ Linear coefficients

$\beta_1, \beta_2, \beta_3$, and $\beta_4$ Power coefficients

Sediment transport equations can be derived from the relationship between sediment transport rates and one or more dimensionless parameters (from Equations 5.3-3 to 5.3-6). This study sought to derive new sediment transport equations for steep slopes using the functional relationships recommended by Khorram and Ergil (2010). In order to determine whether one or more dimensionless parameters could be used in an equation, stepwise regression was done.

The dependent and independent predictor variables (based on the dimensionless parameters) were computed from the laboratory data of this study. A stepwise regression analysis was carried out which involved entering and removing the given dimensionless parameter predictors in a stepwise manner. Possible combinations of less than four dimensionless parameters were tried but they did not yield any significantly improved goodness of fit. The final formulation of four dimensionless parameters was the best possible combination based on r-square and ANOVA

results in Table 5.3-1. The predictor variables were logarithmically transformed prior to multiple regression analysis using the general procedure explained in Section 5.1.1 in order to derive the calibrated Equation 5.3-7. Equation 5.3-7 includes all four dimensionless parameters from Equations 5.3-3 to 5.3-6. A combination of less than four dimensionless in the final equation could also have sufficed if it produced a better goodness of fit after stepwise regression analysis.

$$q_t = 0.55\left[\frac{V^3}{(S-1)gd_{50}w_s}\frac{S_f(\theta)}{log\left({}^1/_{d_{50}}\right)}\right]^{1.124} \times \left[S_f\theta\right]^{0.5} \times \left[\frac{(s-1)VS_f(\theta)}{w_s}\right]^{-0.59}\left[\frac{VU_*'^2S_f(\theta)}{(s-1)gd_{50}w_s)}\right]^{-0.68} \quad 5.3\text{-}7$$

**Table 5.3-1 ANOVA table for Equation 5.3-7 using median ($d_{50}$) sediment size = 2.4 mm and 1 mm; bed slopes = 25%, 33% and 40%**

| Source of variation | Sum of squares | Degree of freedom | Mean square | $F_o$ |
|---|---|---|---|---|
| Regression | $SS_R$ = 0.6 | K =4 | $SS_R$/k = $M_{SR}$ = 0.147 | $M_{SR}$/ = $M_{SE}$ = 144 |
| Error | $SS_E$ = 0.05 | n-p = 49 | $SS_E$/(n-p) = $M_{SE}$ = 0.001 | |
| Total | $SS_{yy}$ = 0.64 | n-1 = 52 | r-square | 0.921 |

Figure 5.3-1 shows the measured and the predicted sediment transport rates using Equation 5.3-7.

From the ANOVA results in Table 5.3-1, the number of independent variables, k = (4+1-1) = 4, n-p = (53-5) = 49 and total variance (n-1) = 53. The critical value of F at the level of significance $\alpha$ = 0.05, $F_o$ from the ANOVA table is 144. From the Standard F distribution table in Appendix A3, $F_{4,49,0.05}$ = 2.57 (after interpolation). Since $F_{\alpha,k,n-p} < F_O$, the regression model (Equation 5.3-7) is a statistically valid. Figure 5.3-1 shows the measured and the predicted sediment transport rates using Equation 5.3-7. Similarly, the r-square of the regression model for Equations 5.3-7 in the ANOVA table 5.3-1 is related to the dimensionless sediment transport rate as the dependent variable and the r-square in Figure 5.3-1 is related to the equation for the prediction of sediment transport rates in kg/m/s.

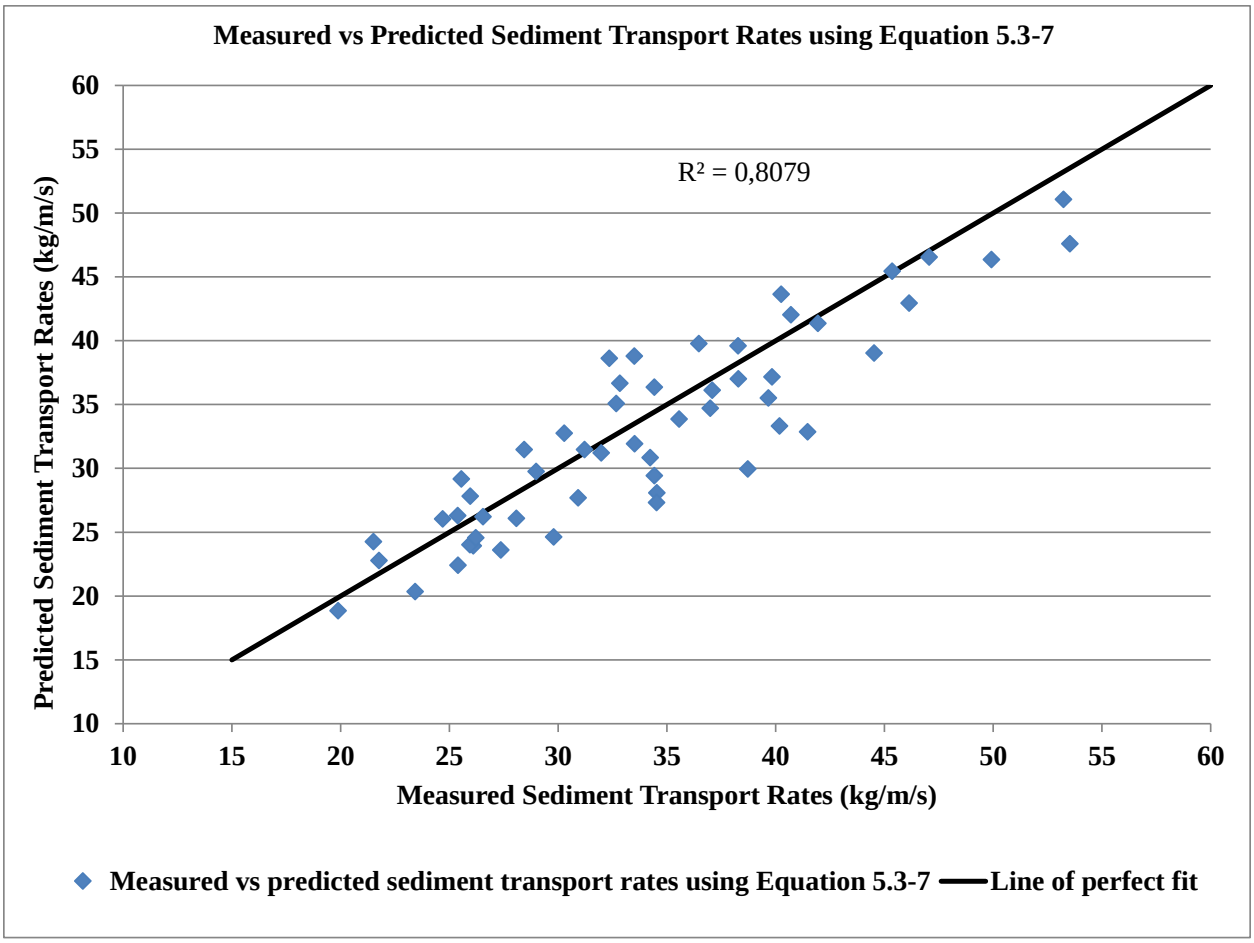


**Figure 5.3-1 Measured and predicted sediment transport rates using Equation 5.3-7 for median ($d_{50}$) sediment size = 2.4 mm and 1 mm; bed slopes = 25%, 33% and 40%**

### *5.3.2 Zhang et al. (2009) equation formulation*

The Zhang et al. (2009) sediment transport equation formulation is a simple relationship for sediment transport capacity that is widely used in hill slopes and fluvial geomorphology. It is given as:

$$q_t = \frac{\alpha_5 S_o^{\beta^5} q^{\beta 6}}{d_{50}} \qquad 5.3\text{-}8$$

Where

$q_t$ Unit discharge of sediment in kg/m/s
$q$ Unit flow discharge ($m^2\ s^{-1}$)
$\alpha_7$ Linear coefficient

$\beta_8$ and $\beta_9$ Power coefficients.

Zhang et al. (2009) observed that sediment transport rates are strongly affected by sediment size. Zhang et al. (2009) plotted sediment transport rates as a function of flow discharge and bed slope for separate median ($d_{50}$) sediment sizes and also for all median ($d_{50}$) sediment sizes combined together. The same procedure was adopted in this study in the calibration of empirical sediment transport equations based on the Zhang et al. (2009) formulation.

Multiple linear regression analyses between measured sediment transport rates for sediment median grain size ($d_{50}$ = 1 mm), flow discharge and water surface slopes resulted in Equation 5.3-9. The ANOVA data for Equation 5.3-9 is shown in Table 5.3-2. Figure 5.3-2 shows the measured and the predicted sediment transport rates using Equation 5.3-9.

$$q_t = 38.77 q^{0.91} S_f^{0.78} \qquad 5.3\text{-}9$$

**Table 5.3-2 ANOVA table for Equation 5.3-9 using median ($d_{50}$) sediment size = 1 mm and bed slopes = 25%, 33% and 40%**

| **Source of variation** | **Sum of squares** | **Degree of freedom** | **Mean square** | **$F_o$** |
|---|---|---|---|---|
| Regression | $SS_R$ = 0.151 | K = 1 | $SS_R/k = M_{SR}$ = 0.08 | $M_{SR}/ = M_{SE}$ = 192 |
| Error | $SS_E$ = 0.006 | n-p = 16 | $SS_E/(n-p) = M_{SE}$ = 0.0004 | |
| Total | $SS_{yy}$ = 0.157 | n-1 = 17 | r-square | 0.96 |

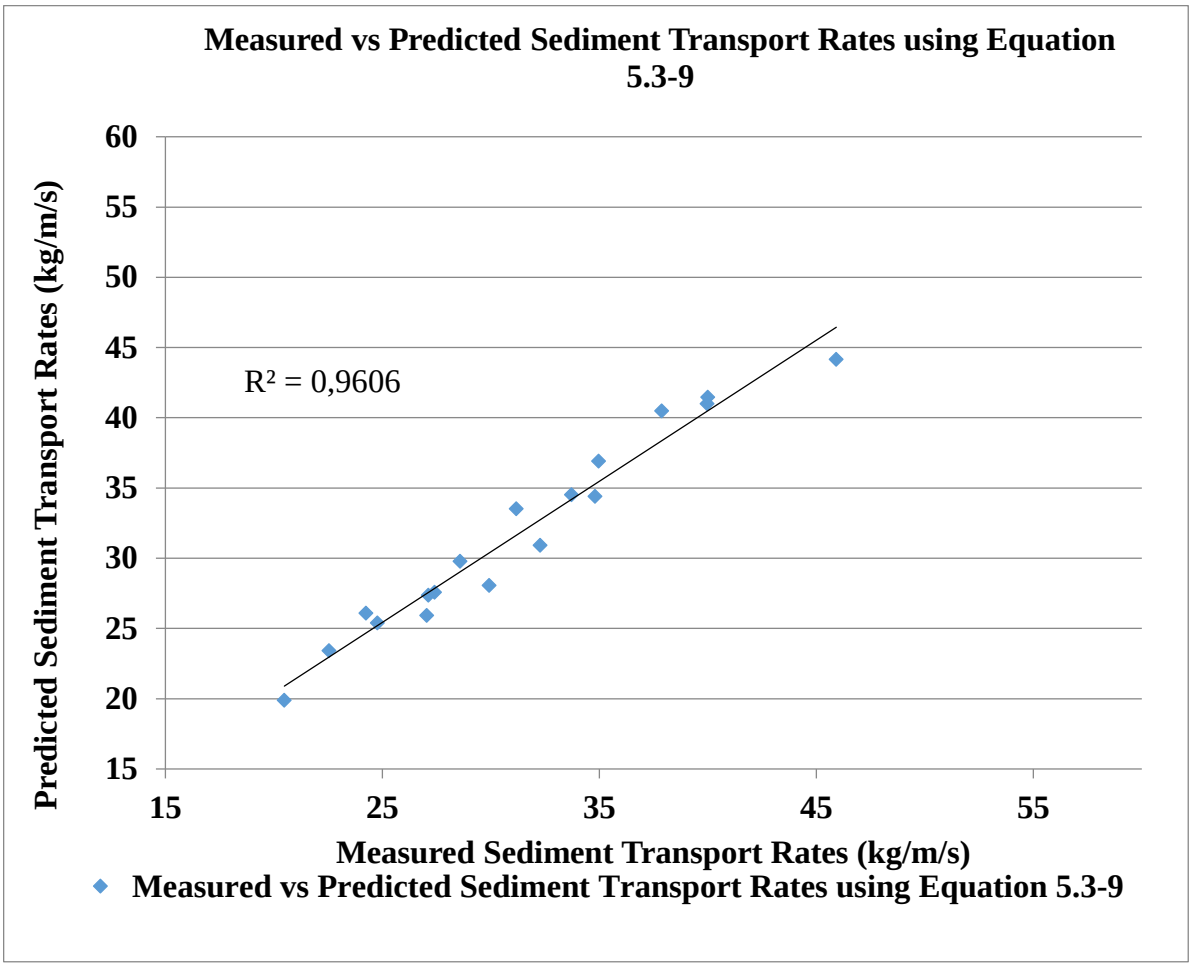


**Figure 5.3-2 Predicted and measured sediment transport rates using Equation 5.3-9**

The prediction model for the median ($d_{50}$) sediment size = 2.4 mm was determined as given in Equation 5.3-10. The ANOVA table of results for Equation 5.3-10 is shown in Table 5.3-3. Figure 5.3-3 shows the measured and the predicted sediment transport rates using Equation 5.3-10.

$$q_t = 4.9q^{0.74}S_f^{1.02} \qquad 5.3\text{-}10$$

**Table 5.3-3 ANOVA table for Equation 5.3-10 using median ($d_{50}$) sediment size = 2.4 mm and bed slopes = 25%, 33% and 40%**

| Source of variation | Sum of squares | Degree of freedom | Mean square | $F_o$ |
|---|---|---|---|---|
| Regression | $SS_R = 0.4$ | K = 1 | $SS_R/k = M_{SR} = 0.2$ | $M_{SR}/ = M_{SE} = 150$ |
| Error | $SS_E = 0.044$ | n-p = 34 | $SS_E/(n-p) = M_{SE} = 0.001$ | |
| Total | $SS_{yy} = 0.454$ | n-1 = 35 | r-square | 0.90 |

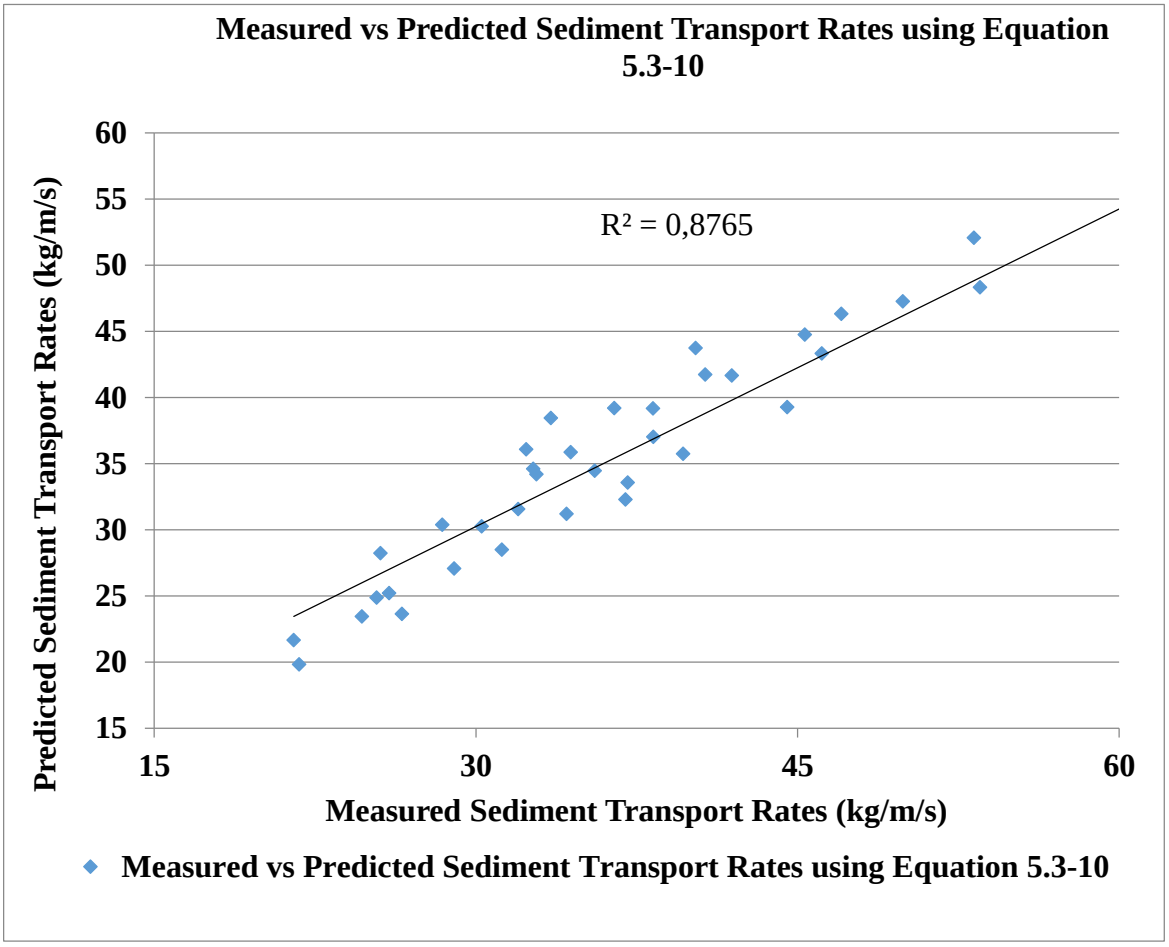


**Figure 5.3-3 Predicted and measured sediment transport rates using Equation 5.3-10**

From the ANOVA results in Tables 5.3-2 and 5.3-3, $F_o$ values are 192 and 150, respectively. From the Standard F distribution table in Appendix A3, $F_{1,16,0.05}$ and $F_{1,34,0.05}$= 4.49 and 4.08 respectively. Since $F_{\alpha,k,n-p} < F_O$ for both equations, the regression models (Equation 5.3-9 and 5.3-10) are statistically valid.

The regression equation for the sediment transport rate ($q_t$) as a function of unit flow discharge ($q$), water surface slope ($S_f$) and all median sediment sizes ($d_{50}$ =1 mm and 2.4 mm) is given by Equation 5.3-11. The ANOVA results for Equation 5.3-11 are shown in Table 5.3-4.

$$q_t = \frac{4.8q^{0.49}S_f^{1.16}}{d_{50}^{1.179}} \qquad 5.3\text{-}11$$

**Table 5.3-4 ANOVA table for Equation 5.3-11 using median ($d_{50}$) sediment size = 2.4 mm and 1 mm; bed slopes = 25%, 33% and 40%**

| Source of variation | Sum of squares | Degree of freedom | Mean square | $F_o$ |
|---|---|---|---|---|
| Regression | $SS_R$ = 0.99 | K = 3 | $SS_R/k = M_{SR}$ = 0.33 | $M_{SR}/ = M_{SE}$ = 97 |
| Error | $SS_E$ = 0.169 | n-p = 49 | $SS_E/(n-p) = M_{SE}$ = 0.003 | |
| Total | $SS_{yy}$ = 1.15 | n-1 = 52 | r-square | 0.85 |

From the ANOVA results in Table 5.3-4, the critical value of F at the level of significance $\alpha$ = 0.05, is 97. From the Standard F distribution table in Appendix A3, $F_{3,49,0.05}$ = 2.805. Since $F_{\alpha,k,n-p} < F_O$, the regression model (Equation 5.3-11) is statistically valid. Figure 5.3-4 shows the measured and predicted sediment transport rates using Equation 5.3-11.

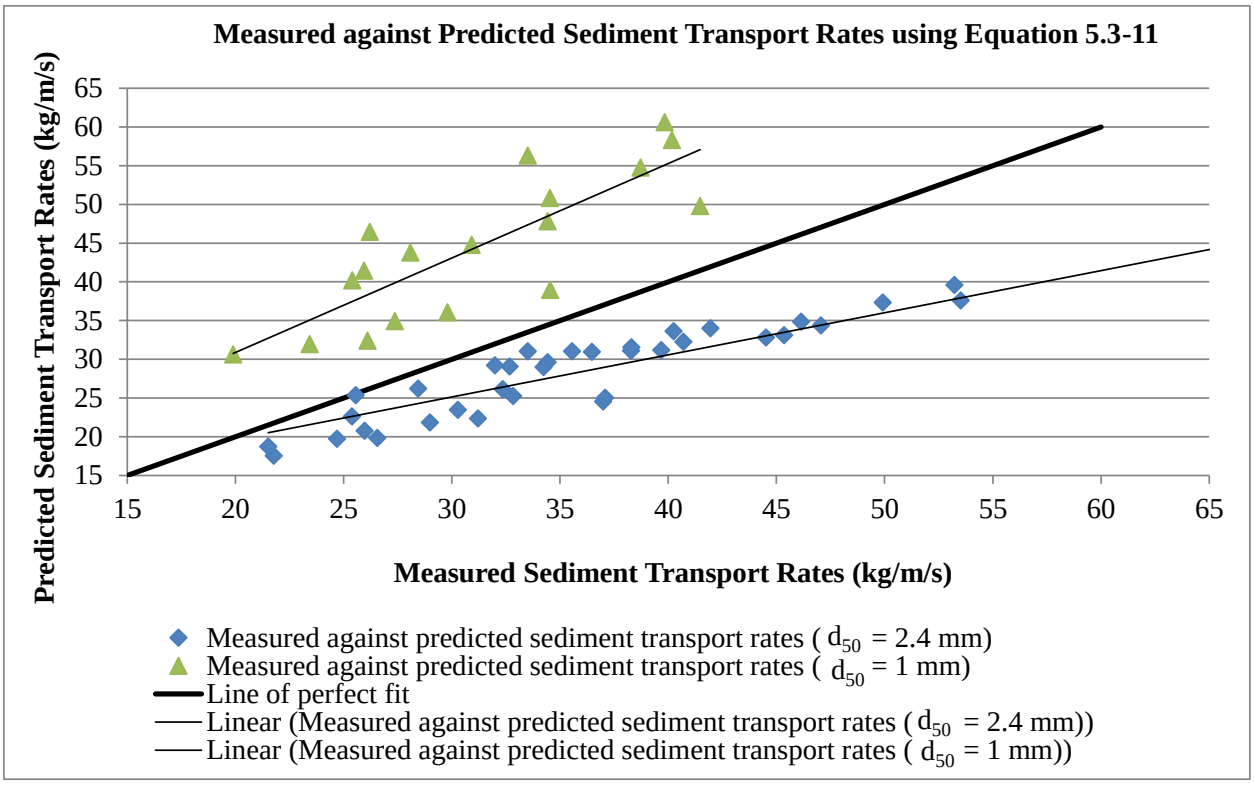


**Figure 5.3-4 Measured and predicted sediment transport rates using Equation 5.3-11 using median ($d_{50}$) sediment size = 2.4 mm and 1 mm and bed slopes = 25%, 33% and 40%**

Figure 5.3-4 shows that sediment transport rates are inversely related to the median ($d_{50}$) sediment size. The plot of measured and predicted sediment transport rates in Figure 5.3-4 shows a significantly high scatter. The results in Figure 5.3-4 indicate that when Equation 5.3-11 is divided by a smaller sediment size, higher sediment rates are predicted and lower sediment rates are predicted by the larger sediment size. The results confirm the fact that the accuracy of empirical equations are limited within the sediment sizes that were used in their derivation.

### *5.3.3 Summary of regression equations results*

Table 5.3-5 shows the summary of statistical test results for the derivation of empirical sediment transport equations on steep slopes. The summarised results in Table 5.3-5 show that the derived sediment transport equations have varying degrees of correlation (r-square) even though they were all statistically valid (using the F test).

**Table 5.3-5 Summary of statistical test results**

| Equation No | Sample Size, n | Predictors | Median ($d_{50}$) Sediment Size | Slopes, $S_o$ | r- square ($r^2$) |
|---|---|---|---|---|---|
| 5.2-5 | 53 | $\frac{d_{90}}{d_{30}}, S_f, C, \theta - \theta_{cr}$ | 2.4 mm and 1 mm | 25%, 33% and 40% | 0.99 |
| 5.2-6 | 53 | $\frac{d_{90}}{d_{30}}, C, \theta - \theta_{cr}$ | 2.4 mm and 1 mm | 25%, 33% and 40% | 0.99 |
| 5.3-7 | 53 | DP1, DP2, DP3 and DP4 | 2.4 mm and 1 mm | 25%, 33% and 40% | 0.921 |
| 5.3-9 | 18 | $S_o$ and q | 1 mm | 25%, 33% and 40% | 0.96 |
| 5.3-10 | 36 | $S_o$ and q | 2.4 mm | 25%, 33% and 40% | 0.90 |
| 5.3-11 | 53 | $S_o$, q and $d_{50}$ | 2.4 mm and 1 mm | 25%, 33% and 40% | 0.85 |

A significantly high scatter along the line of best fit was exhibited by Equation 5.3-11 as evidenced by the lowest r-square. This means that its (Equation 5.3-11) predictive capability is limited. The graphical plots (Figures 5.2-2, 5.2-3, 5.3-1, 5.3-2, 5.3-3 and 5.3-4) were intended to show the general goodness of fit and the quantitative agreement between dependent and independent predictor variables. Based on the r-squares, ANOVA table results above and the respective graphical plots, Equations 5.2-5 and 5.2-6 are the best predictors from this study.

## 5.4 Comparative analysis of the performance of the calibrated Equation 5.2-6 based on steep slope data from this study with selected empirical sediment transport equations

From the literature study, four sediment transport equations were found to be commonly applied in most of the numerical models that were reviewed (Refer to Table 2.9-1). These empirical sediment transport equations (Smart and Jäeggi (1983), Camenen and Larson (2005), Abrahams (2003) and Meyer-Peter Müller (1948)) were compared with Equation 5.2-6 in terms of their predictive capability of the measured laboratory sediment transport rates on steep slopes. Equation 5.2-6 was chosen from Table 5.3-5 because it had a higher r-square for the plot of measured and predicted sediment transport rates in Figure 5.2-3 in comparison to Equation 5.2-5 (Figure 5.2-2) even though both had the same r-square for the regression model. Equation 5.2-6 was used for comparative purposes instead of Equation 5.2-5 because it had the slope parameter in its formulation. Theoretically, the predictive capabilities of Equations 5.2-5 and 5.2-6 were similar based on the statistical test results and graphical plots data. Considering that this study was for steep slopes, a sediment transport equation with slope in its formulation should be more representative and appropriate for application purposes.

It should be pointed out that the comparative analysis is not completely consistent because these sediment transport equations were originally developed from different sets of slope data. The comparative analysis is not strictly fair, because the applicable laboratory slope data is outside the range of application recommended by the authors of the sediment transport equations. The comparison was mainly motivated by the need to demonstrate the relevance of applying sediment transport equations on similar slope data ranges within which they were derived.

Theoretically, the general practice involves the comparison of the actual computed sediment transport rates using a selected equation against the measured sediment transport rates from flume or field tests. The sediment transport equation that gives the best agreement with the measured data or experimental data is taken as the best predictor. However, in this comparative analysis, the objective was to directly compare probable maximum volumetric or mass sediment concentration for a specific discharge. This type of comparative analysis is unique and relevant because it provides the indicative sediment concentration in the discharge against practically accepted values. By analysing the minimum and maximum threshold concentrations as predicted by the individual equation at the specified fixed discharge, the equation's performance can be judged based on the expected deviation from typical equilibrium concentration values that are observed in practical conditions. This criterion provides a direct quantitative analysis of how different prediction models' results compare with results of other sediment transport equations.

### *5.4.1 A comparative analysis of the predicted volumetric and mass sediment concentration at a specific discharge*

The transported sediment is taken as the concentration to represent the amount of sediment per unit discharge of fluid. The concentration can be taken as a volumetric concentration ($v_s$/ $v_{h2o}$, dimensionless) or mass concentration ($m_s/m_{h20}$, dimensionless). $v_s$ and $v_{h2o}$ represent the volume of sediment and water respectively ($m^3$). $m_s$ and $m_{h20}$ represent the mass of sediment and water respectively (kg). Flow and sediment properties were obtained from a randomly selected flow configuration from the experimental data. An analysis of the data involved detailed calculations of the predicted mass and volumetric sediment concentrations by each sediment transport equation.

The specific flow and sediment properties that were used are shown in Tables 5.4-1 and 5.4-2, respectively. There was no specific reason for choosing median ($d_{50}$) sediment size = 2.4 mm (that is shown in Table 5.4-2), apart from the fact that it was part of the data from the randomly selected sediment and flow configuration from the laboratory experiment. The hydraulic radius was considered to be equal to the average flow depth under the selected flow conditions ($R_h$= h). Table 5.4-3 shows the list of equations that were used in the quantitative analysis.

**Table 5.4-1 Flow conditions and applicable slopes**

| | | | |
|---|---|---|---|
| Bed slope (%) | 25 | 33 | 40 |
| Friction slope (%) | 24.2 | 30.6 | 38.2 |
| Discharge ($m^3/s$) | 0.0201 | 0.0201 | 0.0201 |
| Unit discharge ($m^2/s$) | 0.0805 | 0.0805 | 0.0805 |
| Average flow depth (mm) | 21 | 18 | 17 |
| Average velocity (m/s) | 3.893 | 4.472 | 4.735 |

**Table 5.4-2 Flow and sediment properties**

| | |
|---|---|
| Flow width (m) | 0.25 |
| Acceleration due to gravity (kg/m/s) | 9.81 |
| Sediment density ($kg/m^3$) | 2550 |
| Water density ($kg/m^3$) | 1000 |
| Median ($d_{50}$) sediment size (mm) | 2.4 |
| Settling velocity (m/s) | 0.18 |

**Table 5.4-3 Sediment transport equations for comparative analyses**

| ID | Formulation | Author/Source |
|---|---|---|
| 1 | $\emptyset_b = 0.34\left[\left(\frac{d_{90}}{d_{30}}\right)^{1.57} S_f^{0.14} C^{1.05}[\theta - \theta_{cr}]^{1.16}\right]$ | Equation 5.2-6 (DHI (2011) equation calibrated in this study (Section 5.1.1)) |
| 2 | $\emptyset_b = 8[\theta - \theta_{cr}]^{1.5}$ with $q_b = \emptyset_b[(s-1)g]^{\frac{1}{2}} d_{50}^{\frac{3}{2}}$ | Equation 2.6-24 (Meyer-Peter Müller, 1948) |
| 3 | $\emptyset_b = 4\left(\frac{d_{90}}{d_{30}}\right)^{0.2} CS_o^{0.6}\theta^{0.5}(\theta - \theta_{cr})$ with $\emptyset_b = \frac{q_b}{[g(s-1)d_{50}^3]^{0.5}}$ | Equation 2.7-1 (Smart and Jäeggi, 1983) |
| 4 | $\emptyset_b = \theta^{1.5}\frac{V}{U_*}$ with $\emptyset_b = \frac{q_b}{[g(s-1)d_{50}^3]^{0.5}}$ | Equation 2.7-4 (Abrahams, 2003) |
| 5 | $\emptyset_b = 12\theta^{1.5}\exp\left[-4.5\frac{\theta_{cr}}{\theta}\right]$ with $\emptyset_b = \frac{q_b}{[g(s-1)d_{50}^3]^{0.5}}$ | Equation 2.7-5 (Camenen and Larson, 2005) |

The literature review in Chapter 2 contains detailed information on these equations and their specific variables. The five equations in Table 5.4-3 were used to predict the sediment transport rates in kg/m/s from the data given in Table 5.4-1 and 5.4-2. The predicted sediment transport rates are shown in Table 5.4-4. The results show that the sediment transport rates vary significantly depending on the selected sediment transport equation. For example, in Table 5.4-4, Equation 5.2-6 predicted a sediment transport rate of 20 kg/m/s while the Smart and Jäeggi (1983) equation predicted a sediment transport rate of 56 kg/m/s at 25% bed slope using the same flow conditions and sediment properties. The analytical results in Table 5.4-4 highlight how predicted sediment transport rates on steep slopes depend on the selected empirical sediment transport equation. For the same flow conditions at 25% bed slope, the Meyer-Peter Müller (1948) and the Camenen and Larson (2005) sediment transport equations predicted sediment transport rates of 18 kg/m/s and 26 kg/m/s respectively. These two values are significantly closer to the observed laboratory data values (22 kg/m/s). This is despite Meyer-Peter Müller (1948) and Camenen and Larson (2005) sediment transport equations having been based on slope data ranges of 0.04 to 2% and 2 to 20%, respectively. It is worth mentioning that the predicted sediment transport rates can be different for different sediment transport equations not only because of varying slope range conditions but also the flow and sediment data from which they were calibrated. Moreover, Meyer-Peter Müller (1948) and Camenen and Larson (2005) sediment transport equations do not have a slope variable in any of their deterministic predictors. This could explain why their effect on the steep slope data is not as marked as that of Smart and Jäeggi (1983).

**Table 5.4-4 Predicted sediment transport rates in kg/m/s**

| | **Bed Slope (25%)** | **Bed Slope (33%)** | **Bed Slope (40%)** |
|---|---|---|---|
| **Measured** | 21.76 | 25.38 | 34.29 |
| Equation 5.2-6 | 20.086 | 25.348 | 31.025 |
| Meyer-Peter Müller (1948) | 18.384 | 22.262 | 27.429 |
| Smart and Jäeggi (1983) | 56.576 | 112.922 | 154.230 |
| Abrahams (2003) | 41.546 | 53.995 | 65.449 |
| Camenen and Larson (2005) | 24.897 | 30.506 | 38.017 |

The unit mass sediment discharges were divided by the unit mass flow discharge, to obtain mass concentration ratio values for each of the sediment transport equations. Table 5.4-5 shows the mass concentration ratio values that were computed. The applicable unit flow discharge (q) was 80 kg/m/s.

**Table 5.4-5 Mass sediment discharge (kg/m/s) to mass flow discharge (kg/m/s)**

| | Bed Slope (25%) | Bed Slope (33%) | Bed Slope (40%) |
|---|---|---|---|
| **Measured** | 0.272 | 0.317 | 0.43 |
| **Equation 5.2-6** | 0.25 | 0.316 | 0.387 |
| **Meyer-Peter Müller (MPM) (1948)** | 0.230 | 0.278 | 0.343 |
| **Smart and Jäeggi (S&J) (1983)** | 0.707 | 1.412 | 1.928 |
| **Abrahams (2003)** | 0.519 | 0.675 | 0.818 |
| **Camenen and Larson (2005)** | 0.311 | 0.381 | 0.475 |

The concentration ratio values that are given in Table 5.4-5 can be converted to sediment concentration in mg/l as shown in Table 5.4-6. Figure 5.4-1 shows the graphs of mass sediment discharge (kg/m/s) against mass flow discharge (kg/m/s) for the specific unit flow discharge (q = 80 l/s/m). Figure 5.4-1 also indicates the line at which the mass of sediment is equal to the mass of water ($m_s = m_{h20}$). Above this line, it theoretically means that the water transports more sediment in comparison to its own mass. The computed sediment concentrations are given in Figure 5.4-2. Sediment concentrations at very high transport rates were reported to reach as high as 1600000 mg/l in 40 rivers that were measured in China (Ying, 1996). The annual average concentration was 600000 mg/l. It can be concluded that even though concentrations above 1000000mg/l are possible, they could be unrealistic for certain (especially non-cohesive) grain sizes.

**Table 5.4-6 Predicted sediment concentrations in mg/l**

| | Bed Slope = 25% – Concentration ( mg/l) | Bed Slope = 25% – Concentration ( mg/l) | Bed Slope = 25% – Concentration ( mg/l) |
|---|---|---|---|
| **Equation 5.2-6** | 250 000 | 316 000 | 387 000 |
| **Meyer-Peter Müller (1948)** | 229 800 | 278 275 | 342 863 |
| **Smart and Jäeggi (1983)** | 707 200 | 1 411 525 | 1 927 875 |
| **Abrahams (2003)** | 519 325 | 674 938 | 818 113 |
| **Camenen and Larson (2005)** | 311 213 | 381 325 | 475 213 |

Figure 5.4-2 shows the volumetric concentration of sediment in mg/l in comparison with an arbitrary probable maximum concentration. The results in Figures 5.4-1 and 5.4-2 show that the predicted sediment concentrations can even be twice as high as those predicted by other sediment transport equations. Such varying predictions have implications for numerical simulation of bed evolution on steep slopes due to the direct relationship between bed evolution and sediment transport rates. This phenomenon justifies the need and relevance of having slope appropriate sediment transport equations.

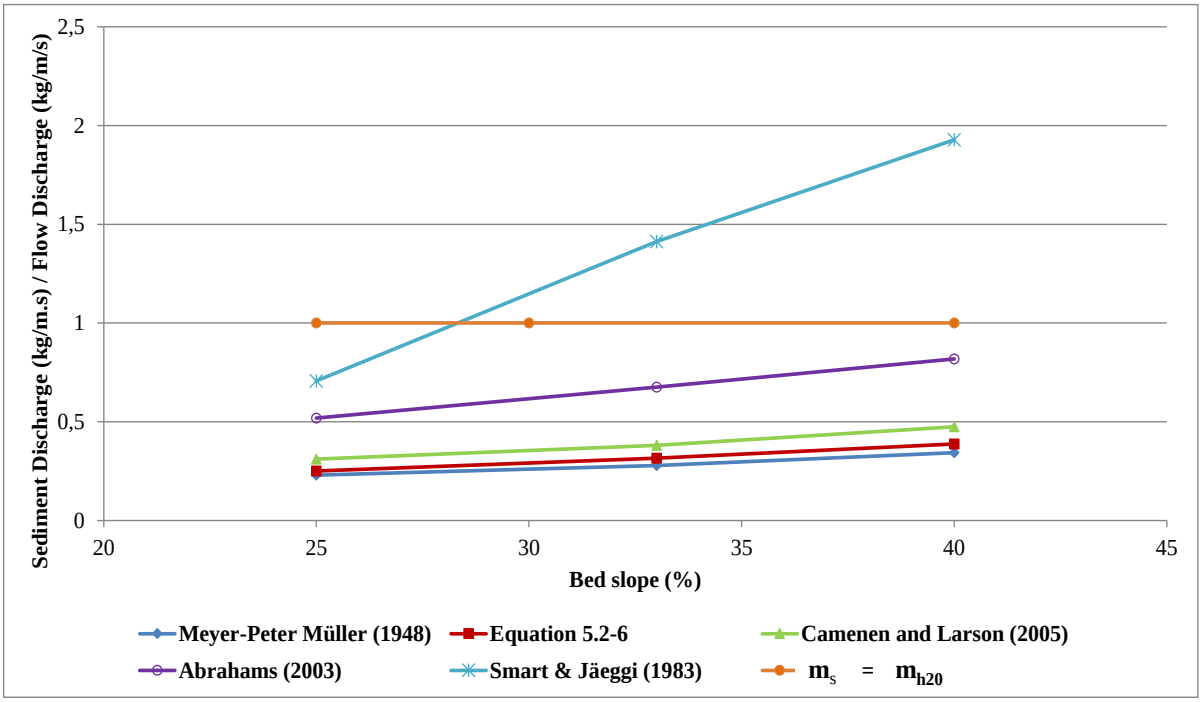


**Figure 5.4-1 Mass sediment discharge (kg/m/s) to mass flow discharge (kg/m/s) against gradient slope**

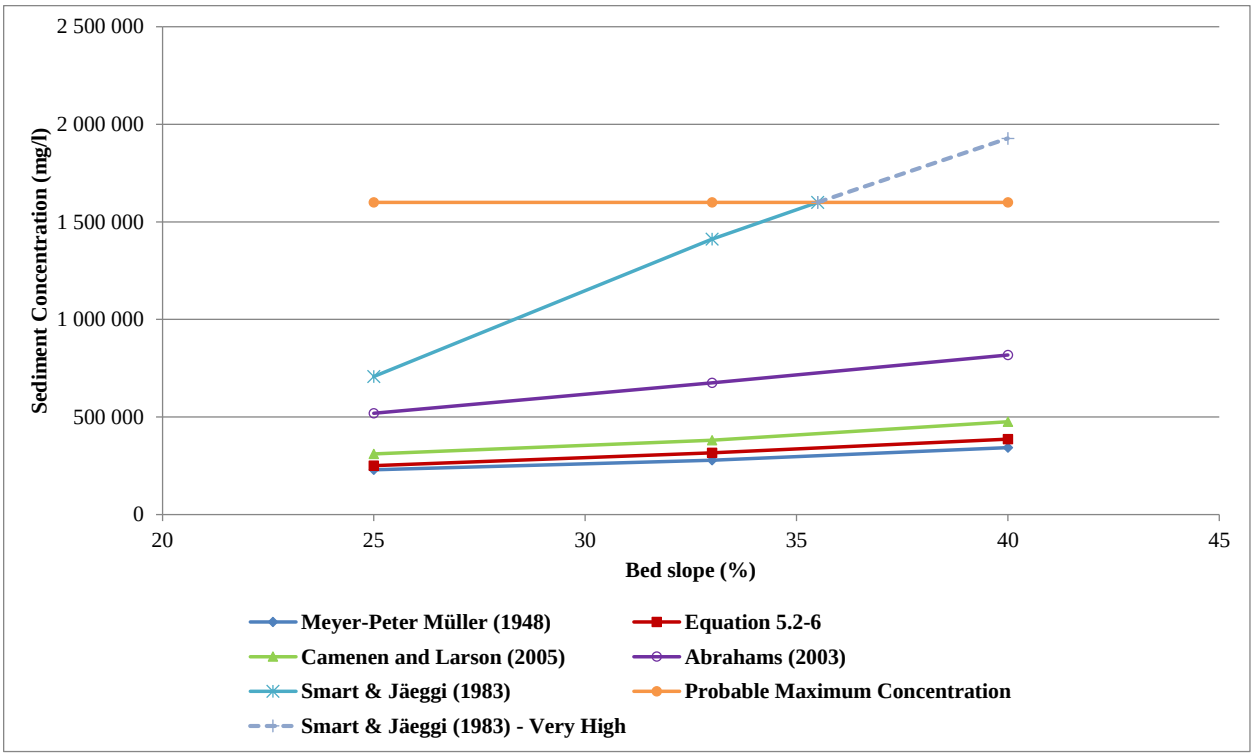


**Figure 5.4-2 Sediment concentrations (mg/l) against gradient slope**

## 5.5 Summary

Equations for the prediction of sediment transport rates on steep slopes have been calibrated based on the laboratory data from this study in terms of the DHI (2011), Khorram and Ergil (2010) and Zhang et al. (2009) empirical sediment transport formulations. The best regression predictor models were selected based on the computed coefficient of determination (r-square) and the F test. The overall accuracy of the proposed equation was checked using the percentage discrepancy (the ratio of calculated values to measured values multiplied by 100). There was a deviation of less than 22% between the measured and predicted sediment transport rates.

In comparison with selected existing widely used sediment transport equations derived for steep rivers (not dams), it was shown that different equations predict different sediment transport rates and concentrations when applied todata for steep slopes. The highest variance was recorded between Smart and Jäeggi (1983) and the newly developed sediment transport Equation (5.2-6). The recorded discrepancy percentages are not uncommon, considering that estimated sediment transport rates for different equations vary over several orders of magnitude (Gomez and Church, 1989). Meyer-Peter Müller (1948) predicted sediment transport rates that were in close agreement with Equation 5.2-6 even though it overestimated sediment transport rates at higher unit discharges.

The analytical results have shown that the accuracy of sediment transport equations is limited to the slope conditions and sediment characteristics from which they were derived. The newly

developed sediment transport equations did not include the effect of sediment shape and grading in their derivation. The sediment was from crushed quarry stone similar to what would typically be used in dam construction. It was not from river sand, which is normally rounded or smooth edged. The sediment shape has an effect on the settling velocity and sediment transport rates and it is normally recommended to include the effect of shape in the derivation of sediment transport equations. It is recommended that shape factor or effect of grading be considered in future research.

The results further indicate that the various sediment transport equations produce different rates of total sediment transport for the same slope and flow. In engineering applications, this means that for the same unit flow discharge through a breach opening, it is possible that one equation could predict excessively higher sediment concentrations while another equation could predict lower sediment concentrations resulting in different simulated temporal bed level changes in numerical modelling. Therefore, utilisation of these sediment transport equations in a numerical model would provide different results, such as bed level changes and outflow hydrographs.

Based on the expected direct relationship between sediment transport rates and the extent of bed level changes in numerical modelling, the different sediment transport equations would provide different results for both overtopping breach formation and outflow hydrograph shape over time. For the same flow discharge through a dam breach, the variation between the predicted sediment transport rates due to the discharge could vary by a factor of up to 3 or more depending on the selected sediment transport equation as indicated by the analytical results on mass sediment concentration. Normally, the equation that predicts higher sediment transport rates should predict more rapid bed level changes and consequently shorter times to peak discharge. The detailed practical implications and relevance of the findings in this Chapter have been further demonstrated in the next section on numerical modelling of dam-break flows.

# CHAPTER 6 THE APPLICATION OF THE NEWLY CALIBRATED SEDIMENT TRANSPORT EQUATIONS IN DAM-BREAK MODELLING AND UNCERTAINTY ANALYSIS

## 6.1 Sediment transport equations and uncertainty analysis

The aim of this chapter is to demonstrate the application of the calibrated sediment transport Equations 5.2-5 and 5.2-6 in dam-break modelling and to assess the level of uncertainty due to sediment transport equations. For practical applications, uncertainty analysis of any selected sediment transport equation is a crucial aspect of numerical modelling. In this study, model uncertainty to the input of sediment transport equations was assessed through sensitivity analysis. Further sensitivity analysis to the input of Manning's resistance coefficient (n) values was conducted with specific emphasis on the sensitivity of the peak discharge.

Uncertainty analysis for input parameters that have a defined range of probable values in numerical models is not as challenging as that for sediment transport equations. Well-defined parameters such as Manning's resistance coefficient (n) can be easily varied within typical ranges in order to test their influence on the model output results. For instance, by increasing or decreasing the Manning's resistance coefficient (n), it is possible to predict the probable ranges of the percentage increase or decrease in the peak discharge. However, on account of the sensitivity of numerical model results for the sediment transport equations, it is more challenging to predict the percentage increase or decrease in the peak discharge if one equation is selected instead of another. Sediment transport equations give the highest degree of variability in the model output results in comparison to other input parameters as reported by Floodsite (2011). It is generally recommended in dam-break modelling to apply two or more equations, in order to analyse the sensitivity in the model output results (Floodsite, 2011). The probable band of uncertainty in output results is significant for the determination of low, medium and worst case scenarios in dam-break risk analysis and emergency planning.

### *6.1.1 Uncertainty analysis approach*

The new Equation 5.2-5 was applied in the base simulation. The base simulation was the numerical model that best reproduced the measured or observed data. The reproduction of measured conditions was achieved through calibration of hydrodynamic and morphological parameters (mainly the hydraulic roughness). Base simulation results for Equation 5.2-5 were compared with the results for Equation 5.2-6, the Smart and Jäeggi (1983) and the Camenen and Larson (2005) sediment transport equations, without changing the rest of the numerical model input parameters and simulation conditions. The decision to apply Equation 5.2-5 in the base simulation was taken in order to assess its applicability in numerical modelling and to determine the variability in the output results when other sediment transport equations were applied. Smart

and Jäeggi (1983) and Camenen and Larson (2005) sediment transport equations were chosen for comparison purposes because they were calibrated on slopes of up to 20%.

The two dimensional hydrodynamic model Mike 21C of the DHI Group was selected to carry out the simulations as part of the sensitivity analysis. The sensitivity analysis was aimed at providing a quick estimation of the potential uncertainty between the four sediment transport equations. This 2D model was selected because of its capability in simulating breaching conditions for both field and laboratory conditions as confirmed by Beck (2005). Beck (2005) showed that the MIKE 21C computational model could accurately simulate breaching processes. The MIKE 21C model was applied by Beck (2005) on a laboratory breaching test that was conducted at the Hydraulic Laboratory of the University of Stellenbosch, South Africa, and a field breaching case study of an estuary mouth. This model is fully hydrodynamic and sediment transport and hydrodynamics are coupled in each time step. Secondary currents at the breach are also simulated with a quasi-3D approach in the model. Secondly, the model was chosen because of potential users' ability to apply Equation 5.2-5 without the need to modify its existing computational algorithm or adding any user defined functions to its code. Other models such as DEICH N2 (Broich, 1998), whose code could be easily modified were considered, but had limited modelling capabilities and application requirements. MIKE 21C was selected because it simulates a coupled numerical solution for sediment and hydrodynamics. Breach morphological changes and flow including associated secondary currents are simulated in a two dimensional manner. Even though three dimensional numerical models have improved accuracy, they could not be selected because they are still in early stages of development (Wu, 2011).

The application of empirical sediment transport equations is achieved by varying the values of the exponents and coefficients in the MIKE 21C Graphical User Interface (GUI) to suit the formulation of a particular equation as illustrated in Figure 6.2-1 for the Smart and Jäeggi (1983) sediment transport equation and Equation 5.2-6.

Transport Theory Smart & Jaeggi (1983)

| | Bed load | Formula | a1 | a2 | a3 | a4 | a5 | a6 | a7 | a8 |
|---|---|---|---|---|---|---|---|---|---|---|
| Fraction 1 | ☒ | Empirical formula (S | 4.000000 | 0.200000 | 0.600000 | 1.000000 | 0.500000 | 1.000000 | 1.000000 | 1.000000 |
| Fraction 2 | ☒ | Empirical formula (S | 4.000000 | 0.200000 | 0.600000 | 1.000000 | 0.500000 | 1.000000 | 1.000000 | 1.000000 |
| Fraction 3 | ☒ | Empirical formula (S | 4.000000 | 0.200000 | 0.600000 | 1.000000 | 0.500000 | 1.000000 | 1.000000 | 1.000000 |

Transport Theory Equation 5.2-6

| | Bed load | Formula | a1 | a2 | a3 | a4 | a5 | a6 | a7 | a8 |
|---|---|---|---|---|---|---|---|---|---|---|
| Fraction 1 | ☒ | Empirical formula (S | 0.340000 | 1.570000 | 0.140000 | 1.050000 | 0.000000 | 1.000000 | 1.000000 | 1.160000 |
| Fraction 2 | ☒ | Empirical formula (S | 0.340000 | 1.570000 | 0.140000 | 1.050000 | 0.000000 | 1.000000 | 1.000000 | 1.160000 |
| Fraction 3 | ☒ | Empirical formula (S | 0.340000 | 1.570000 | 0.140000 | 1.050000 | 0.000000 | 1.000000 | 1.000000 | 1.160000 |

**Figure 6.2-1 Empirical sediment transport theory specification: Smart and Jäeggi (1983) top and Equation 5.2-6 bottom**

## 6.2 An introduction to MIKE 21C

MIKE 21C is one of the modelling software systems that was developed by DHI Division of Water and Environment for applications in oceanographic, coastal and estuarine environments. It is a curvilinear flow model that is applied in flow and sand transport modelling and analysis as well as in studies of overland flooding. It is a preferred system in overland flooding because of its ability to handle relevant depths of flooding and drying shocks for rapidly varying unsteady flows. In order to deal with the rapidly varying unsteady flows, sufficient flooding and drying depths need to be specified in the model. The model has special numerical procedures that help to handle wet-dry conditions in order to correctly compute the propagation of the wave front.

According to DHI (2011), flooding and drying depths are basic model parameters for MIKE 21C Curvilinear Model simulation that are applied to handle hydraulic conditions with varying water stages. Flooding and drying depths are required if initially dry regions of the model become inundated, or if initially wet regions become dry. The drying depth is the minimum water depth allowed in a point before it is removed from calculations. When the local depth becomes less than the specified value, the point is land. The flooding depth is the water depth at which the point will be re-entered into the calculation. When the local water depth becomes greater than this, the point is wet.

The MIKE 21C modelling system is based on the numerical solution of the two dimensional Reynolds averaged Navier-Stokes equations on the presumption of Boussineq and hydrostatic pressure formulation. This formulation assumes that vertical accelerations are negligible, water surface variations are small and pressure distribution is hydrostatic.

According to Zolghadr et al. (2011), the two dimensional shallow water equation assumptions are not completely satisfied, especially near the breach point and in the first stages of breaking which could sometimes limit the accuracy of dam-break modelling results. Sediment transport is modelled by a dedicated Sand Transport module within the modelling system that can be optionally evoked/activated, depending on the users' requirements.

## 6.3 Description of the MIKE 21C Flow Module and its Sand Transport Module

The relevant input parameters for MIKE 21C are the bathymetry, curvilinear grid, boundary specifications and other hydraulic and morphological parameters such as eddy viscosity and bed roughness. Two files are initially used to define the curvilinear grid, namely: a 2D grid describing the coordinates of the four corner points in each computational grid cell and a 2D grid describing the depths at the centre of each computational grid cell. The bathymetry represents the actual topography of the applicable area and it can be based on a digital elevation model (DEM) or on any other topographical data that adequately describes the land surface. In dam-break modelling, the embankment shape is automatically formed from the actual specified bathymetry data. The grid defines the relative locations of the elevation data points. Boundaries in MIKE 21C have a significant bearing on the output results. The version that was used in this study, can

apply a rating curve at the outlet boundary. This is an advantage compared to previous models which needed temporal or constant discharge and water level data as boundary conditions.

The MIKE 21C Sand Transport (ST) Module is the module for the calculation of sediment transport capacity and any related initial rates of bed level changes for non-cohesive sediment transport due to currents or combined waves-currents. The ST Module calculates sand transport rates on a flexible (unstructured grid) mesh covering the area of interest on the basis of the hydrodynamic data obtained from a simulation with the HydroDynamic (HD) module. The computations are based on the characteristics of the bed material such as sediment grain size and gradation, porosity and angle of repose that are provided by the user.

The simulation is performed on the basis of the hydrodynamic conditions that correspond to a given bathymetry. The morphological evolutions at each time step are recorded in order to simulate breach formation through the embankment. The ST Module can be applied to quantify sand transport capacity due to non-cohesive sediment movement by taking advantage of the river morphology application capability of MIKE 21C. The sediment transport rates are based on the local depth, mean horizontal velocity component, the properties of the bed material and the applicable sediment theory (sediment transport equation).

## 6.4 MIKE 21C model capabilities in dam-break modelling

Two main features of MIKE 21C make the model ideal for dam breach analysis:

(a) The first and most important factor are that the sediment transport module and hydrodynamics are coupled in each time step, and therefore the rapid changes in bed level is fed back to the hydrodynamic model for update at every time step.

(b) Secondary flow patterns are simulated with a quasi-3D formulation of the movement of coarse sediment at the bed which is important in the breach formation as flow converges from the reservoir, through the hydraulic control into the breach.

This study modelled bed level changes, breach dimensions, the potential peak discharge through a breach, outflow volume and the shape of the hydrograph.

## 6.5 Background to the selected case studies

Three laboratory case studies, one practical field case study and an idealized prototype dam case study were simulated to illustrate the sensitivity of model output parameters to sediment transport equations. In these five case studies, the evaluation of the application potential and relevance of Equations 5.2-5 and 5.2-6 was limited to the ability to predict bed level changes and the discharge at the flume outlet (Case Study 1), breach dimension and outflow hydrograph (Case Study 2), peak discharge (Case Study 3), shape of hydrograph and peak discharge (Case Study 4), and peak discharge and outflow volume (Case Study 5).

The physical laboratory tests for Case Studies 1 and 2 were conducted at the Hydraulics Laboratory of the University of Stellenbosch (South Africa) by the author of this dissertation and Radyn (2010), respectively. The experimental study for Case Study 2 was conducted in partial fulfilment of an undergraduate degree at University of Stellenbosch by Radyn (2010). Specifically, Radyn (2010) used the laboratory data to analyse the ability by the National Centre of Computational and Hydrologic Engineering (NCCHE) dam-break model to simulate the measured breach shape, peak discharge and outflow shape. This study utilised the laboratory data from Radyn (2010) to analyse dam-break output results when different sediment transport equations are applied using MIKE 21C. The third laboratory case study was conducted at HR Wallingford in the United Kingdom (Floodsite, 2011; Morris et al., 2002). The practical field test for Case Study 4 was undertaken in Norway under the Impact Project (Morris et al., 2002) and it comprised a 5 m high earth dam and reservoir. Case Study 5 is a hypothetical dam and reservoir with typical characteristics of a large earth embankment dam.

## 6.6 Case Study 1

The laboratory test setup for Case Study 1 comprised a 250 mm high embankment dam with an upstream and downstream slope (V: H) of 1:3. It was built in a 5 m long and 0.15 m wide laboratory flume. The median ($d_{50}$) sediment (sand) diameter was 1.5 mm. Figure 6.6-1 shows a photograph of the setup prior to breaching with full reservoir on the left hand side (LHS). The dam crest's longitudinal top width was 300 mm long. A constant flow of 1.0 l/s was supplied from a constant head tank. The water levels were measured using fixed measuring tapes that were mounted on the glass flume. The time durations at which the eroded bed levels reached breach depths of 0.05 m, 0.1 m and 0.15 m were recorded. Figures 6.6-2, 6.6-3 and 6.6-4 show photographs of the observed temporal breach development and the recorded times at which the bed levels at the centre of the embankment reached depths of 0.05 m, 0.1 m and 0.15 m respectively. This case study was conducted to simulate the measured breach depths from the laboratory experiment using the calibrated sediment transport Equation 5.2-5 and to compare with the output results as simulated by Equation 5.2-6 and; Smart and Jäeggi (1983) and Camenen and Larson (2005) sediment transport equations.

The MIKE 21C numerical model setup comprised of a rectangular grid with six hundred (600) grid cells in the longitudinal direction of flow and fifteen (15) grid cells along the transverse direction of flow. The grid size was 0.01 m by 0.01 m each. A constant inflow of 1.0 l/s was applied in the numerical simulation near the flume entrance as a source point. In order to achieve a uniform flow depth across the flume width before overtopping, a wooden block was held at the embankment crest across the flume width until there was an even distribution of flow with at least 2 cm water depth. The measured temporal water and bed levels were used for calibration purposes. The input parameter that was varied and appeared to have a significant effect on the numerical model results was the Manning's resistance coefficient (n). Manning's resistance coefficient (n) was calibrated against the observed water levels to be 0.040. In some numerical models, the Manning's resistance coefficient can also be selected based on the sediment size or

grain roughness. However, in this study the Manning number was calibrated against the observed water levels. In general, it was found that the effect of hydraulic roughness was much more than the particle roughness alone, possibly due to bedforms such as dunes forming on the bed during breaching.

The model time step was guided by the following relationship:

$$Cr = \frac{U_{max}\Delta t}{\Delta x} \qquad 6.6\text{-}1$$

Where

$Cr$ Courant Number

$U_{max}$ Maximum velocity (m)

$\Delta t$ Time step (s)

$\Delta x$ Grid size (m)

The calibrated model setup parameters for hydrodynamics and morphology are given in Tables 6.6-1 and 6.6-2.

**Figure 6.6-1 Breach initiation with full reservoir on LHS**

**Figure 6.6-2 Breach formation after 24 seconds**

**Figure 6.6-3 Breach formation after 38 seconds**

**Figure 6.6-4 Breach formation after 72 seconds**

**Table 6.6-1 Calibrated model setup parameters – hydrodynamics (Case Study 1)**

| Hydrodynamic Parameter | Default Values | Value Applied |
|---|---|---|
| Hydrodynamic time step (s) | - | 0.01 |
| Morphological time step (s) | - | 0.02 |
| Flooding depth (m) | - | 0.0009 |
| Drying depth (m) | - | 0.0008 |
| Manning's resistance coefficient (n) | 0.015 – 0.1 | 0.040 |

**Table 6.6-2 Calibrated model setup parameters – morphology (Case Study 1)**

| Morphological Parameter | Default Values | Applied Value |
|---|---|---|
| Median ($d_{50}$) grain diameter (mm) | - | 1.5 |
| Eddy viscosity ($m^2/s$) | - | Smagorinsky Formula – Velocity Based Constant – 0.5 |
| Mass density of sediment ($kg/m^3$) | 2000 - 2700 | 2650 |
| Porosity (Ratio) | 0.3 – 0.7 | 0.33 |
| Critical shield's' parameter | 0.030 – 0.056 | 0.047 |
| Transverse slope coefficient | 0 - 3 | 0.6 |

| | | |
|---|---|---|
| Transverse slope power | 0.5 - 1 | 0.5 |
| Longitudinal slope coefficient | 1 - 10 | 1 |

### *6.6.1 Analysis of numerical simulation results - Case Study 1*

Equation 5.2-5 in the base simulation was replaced by three equations, namely; Equation 5.2-6, Smart and Jäeggi (1983) and Camenen and Larson (2005) sediment transport equations. The primary performance criterion for the evaluation of the capability of the proposed equation in laboratory Case Study 1 was the degree to which Equation 5.2-5 reproduced the calibrated and measured breach depths. The simulated progression of the breaching process by Equation 5.2-5 was compared with simulations by Equation 5.2-6 and; Smart and Jäeggi (1983) and Camenen and Larson (2005) sediment transport equations without any calibration of hydrodynamic and morphological parameters. The measured and simulated temporal bed profiles along the longitudinal centreline using the four sediment transport equations are shown in Figures 6.6-5, 6.6-6 and 6.6-7.

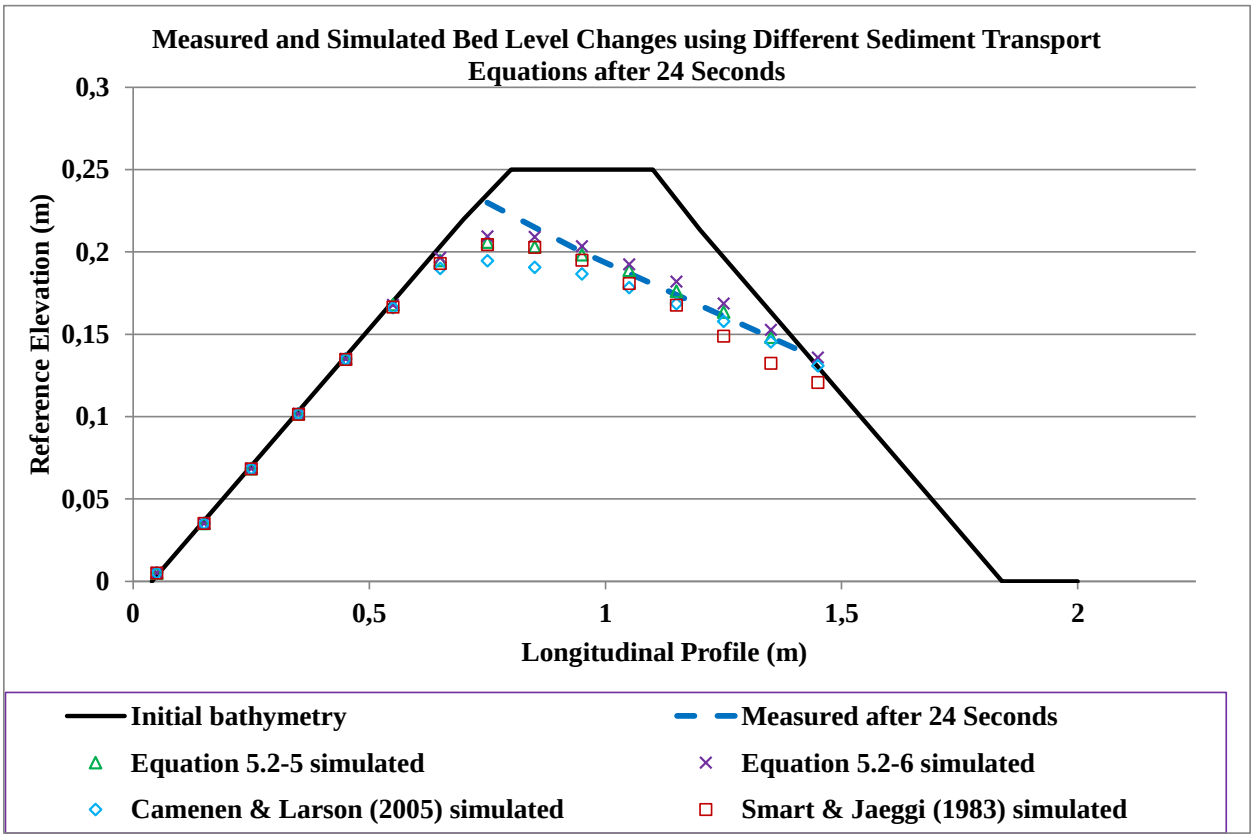


**Figure 6.6-5 Simulated temporal bed level changes after 24 Seconds**

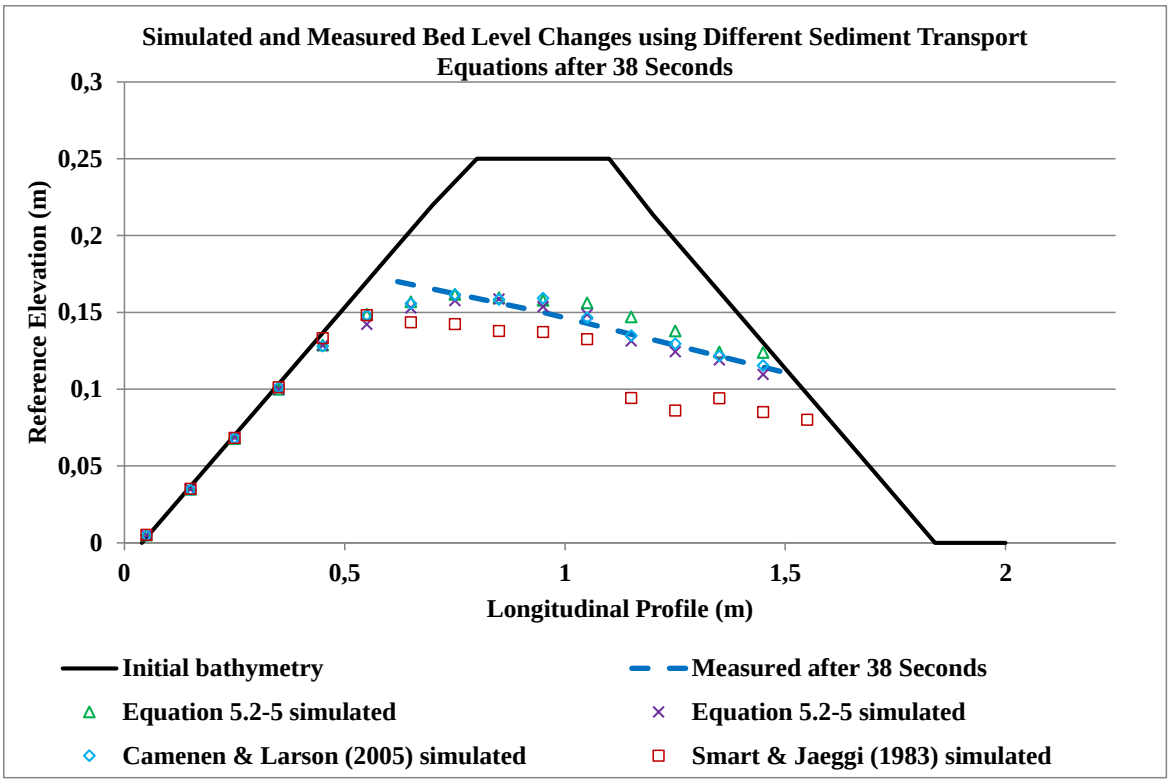


**Figure 6.6-6 Simulated temporal bed level changes after 38 Seconds**

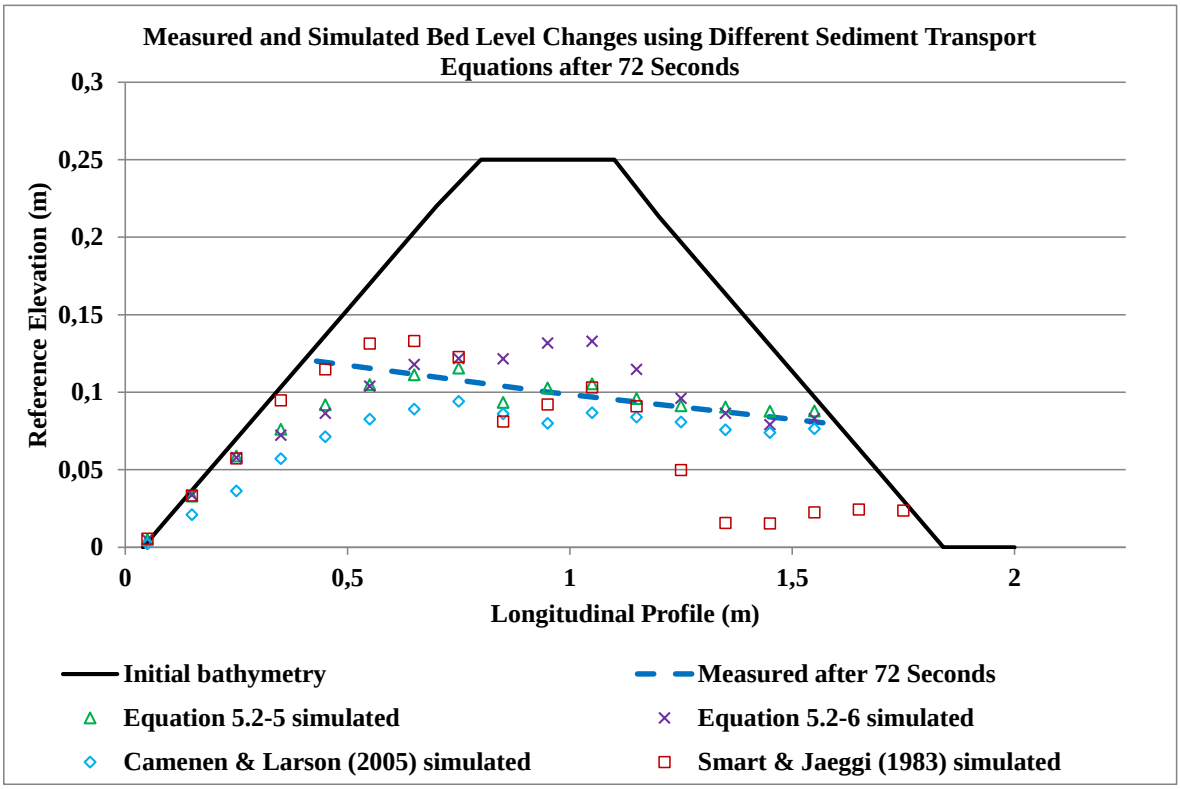


**Figure 6.6-7 Simulated temporal bed level changes after 72 Seconds**

As shown in Figure 6.6-5, the agreement between the measured and simulated bed profiles was found to be good for all the equations after 24 seconds. After 38 seconds, Smart and Jäeggi (1983) overestimated the sediment transport rates as evidenced by the deeper scouring of the embankment in comparison with the rest of the equations. In Figure 6.6-7, the overestimation of the sediment transport rates appear to be more pronounced with the toe of the embankment scoured away due to overestimation of erosion.

Different temporal bed profiles are bound to be predicted by each of the selected sediment transport equation due to the actual calculated sediment transport rates. The Smart and Jäeggi (1983) sediment transport equation predicted higher sediment transport rates in comparison with the other selected sediment transport equations in Section 5.4. This could result in the overestimation of erosion in numerical simulations as can be observed in Figures 6.6-6 and 6.6-7. Tingsanchali and Chinnarasri (2001) also reported similar observations, when it was found that Smart and Jäeggi (1983) overestimated the erosion process in the numerical modelling of dam failure due to overtopping. Equations 5.2-5 and 5.2-6, and Camenen and Larson (2005) sediment transport equation generally predicted well the temporal bed profiles in Figures 6.6-5, 6.6-6 and 6.6-7 even though they did not exactly match the observed longitudinal profile. In Figure 6.6-7, Equation 5.2-6 underestimates sediment transport rates after 72 seconds. This could be attributed to the effect of the gradient slope variable after 72 seconds, when the bed slope starts to flatten.

The local erosion and sediment transport as simulated at the embankment breach opening has a significant effect on the simulated outflow at the flume outlet or any other selected transverse section downstream of the breach opening. Predicted outflow discharges by the four sediment transport equations were compared. Figure 6.6-8 shows the outflow hydrographs for the four breach scenarios that were simulated by each of the four different sediment transport equations using identical input data.

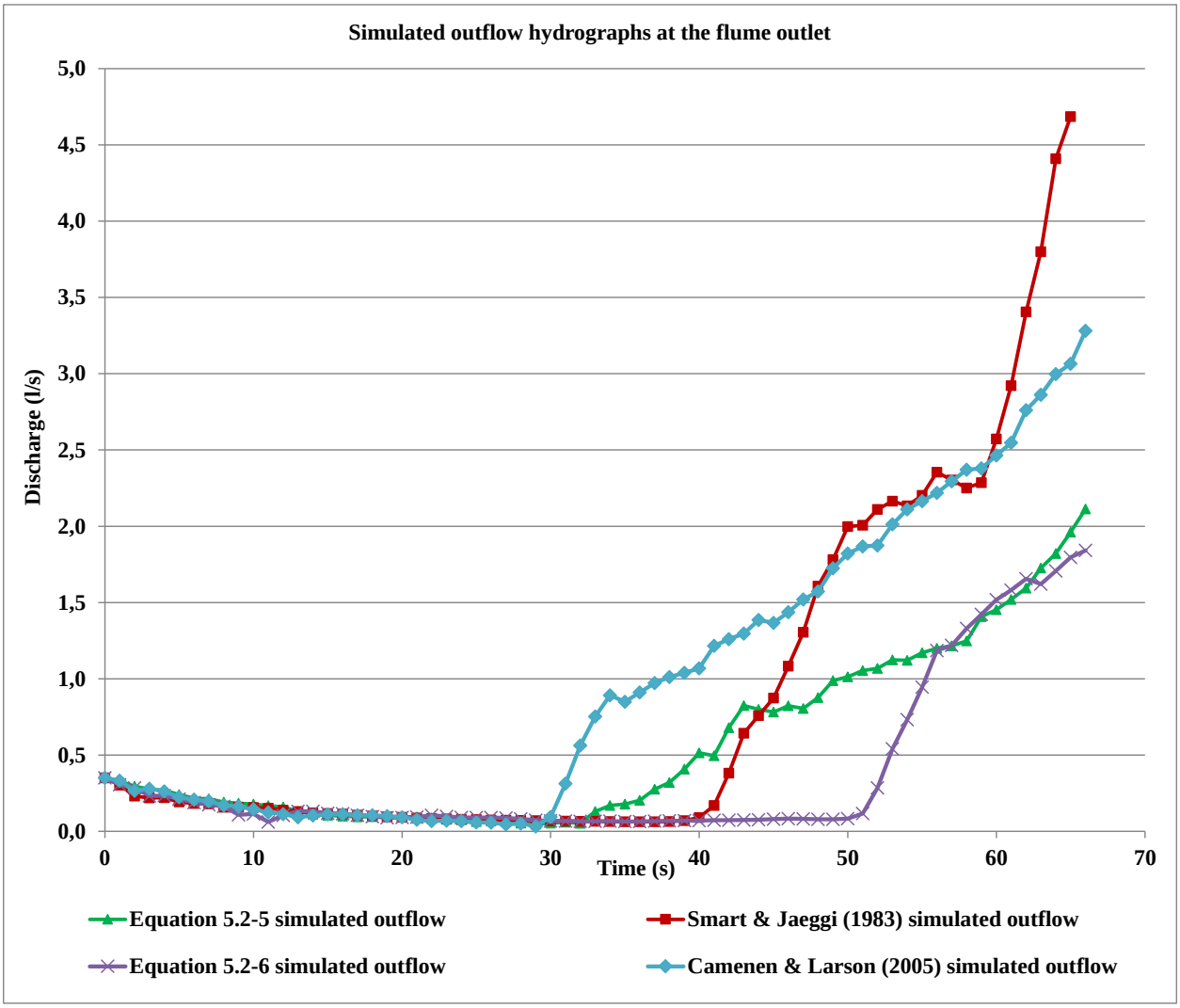


**Figure 6.6-8 Comparison of outflow hydrographs for Case Study 1**

High sediment transport rates result in rapid bed scour and higher simulated discharge at the outlet after the same time period. The results in Figure 6.6-8 show the influence of the sediment transport equation on the breach outflow discharge. Accurate prediction of the bed profiles is important for the prediction of realistic breach outflow characteristics. Any local uncertainty in the prediction of the temporal bed profiles can affect the peak discharge and outflow hydrograph shape as indicated in Table 6.6-3.

**Table 6.6-3 Simulated discharge at the flume outlet**

| Sediment Transport Equation | Final Discharge at Flume Outlet (l/s) |
|---|---|
| **Equation 5.2-5** | 2.1 |
| **Equation 5.2-6** | 1.8 |
| **Smart & Jäeggi (1983)** | 4.6 |
| **Camenen & Larson (2005)** | 3.2 |

## 6.7 Case Study 2

Case Study 2 was a laboratory setup of a 260 mm high earth dam with an upstream and downstream slope (V: H) of 1:3. The embankment was built in a 15 m long by 2 m wide flume. Figure 6.7-1 shows the embankment cross-section. Figure 6.7-2 shows photographs of the breaching experiment.

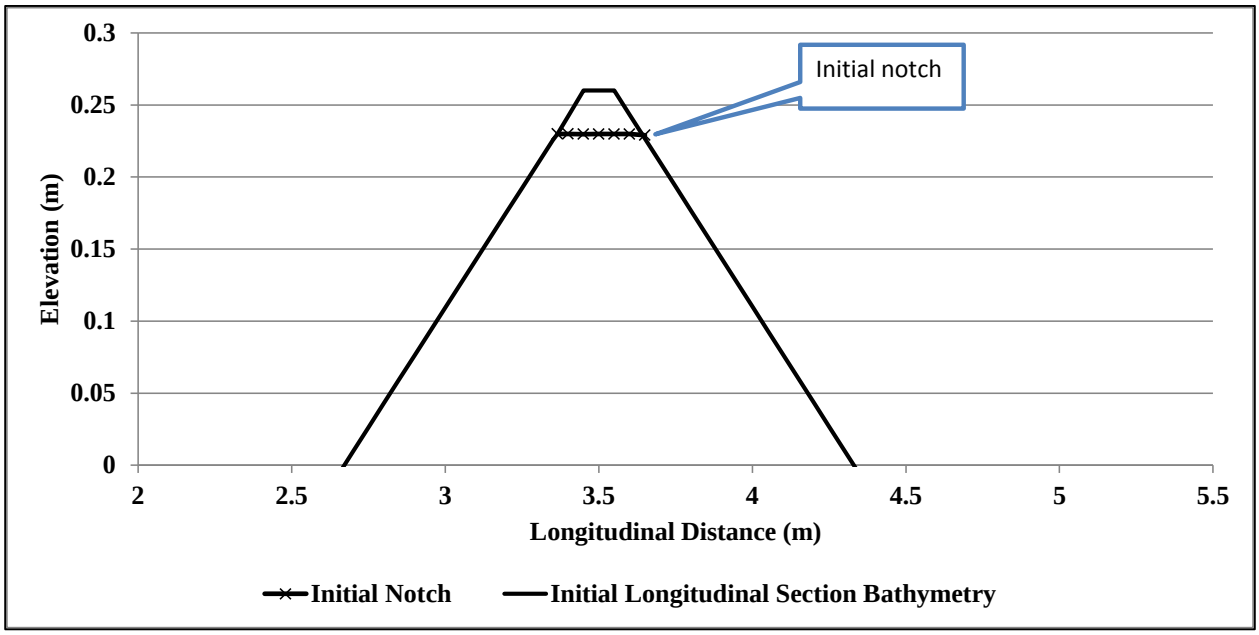


**Figure 6.7-1 Embankment cross-section (Case Study 2)**

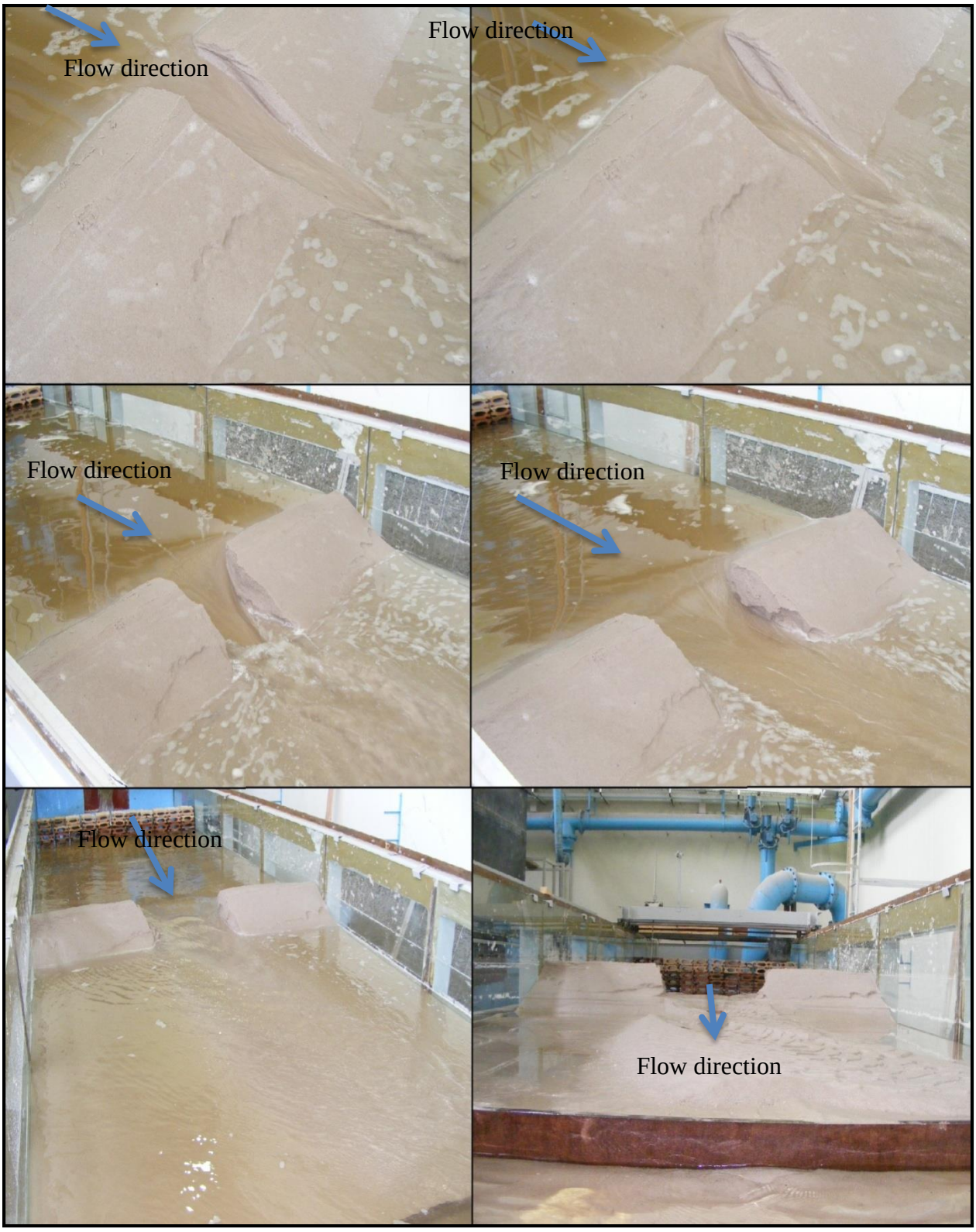


**Figure 6.7-2 Photographs of the laboratory experiment (Radyn, 2010)**

A variable inflow was supplied from a pump to try and maintain a constant water level upstream of the dam and was measured using a V-notch weir. The water levels were measured manually using gauges. The embankment was built with sediment of median ($d_{50}$) diameter = 0.3 mm. The embankment spanned across the total 2 m flume width. An initial notch 200 mm wide and 30 mm deep was provided at the centre of the embankment.

The MIKE 21C numerical model setup for Case Study 2 base simulation comprised a rectangular grid with 300 hundred (300) grid cells in the direction of flow and forty (40) grid cells across the flow direction that were sized 0.05 m by 0.05 m each. A considerably longer distance from the embankment to the outlet boundary was provided to minimize boundary effects on the embankment. The measured inflow was used as a boundary inflow at the flume inlet. A discharge rating curve was applied at the outlet boundary. The model was calibrated by closely matching the final breach opening shape with the laboratory measured final bed profile. Equation 5.2-5 was applied in the base simulation. The main input parameter that was varied and appeared to have a significant effect on the numerical model results was the Manning's resistance coefficient (n).

### *6.7.1 Analysis of numerical simulation results - Case Study 2*

The primary performance criterion for the evaluation of the application of the calibrated sediment transport equations in Case Study 2 was the measure of the extent to which Equations 5.2-5 and 5.2-6 predicted the breach dimension when applied in a numerical model. The calibrated model setup parameters for hydrodynamics and morphology are given in Tables 6.7-1 and 6.7-2, respectively.

**Table 6.7-1 Calibrated model setup parameters – hydrodynamics (Case Study 2)**

| Hydrodynamic Parameter | Default Values | Applied Value |
|---|---:|---:|
| Hydrodynamic time step (s) | - | 0.02 |
| Morphological time step (s) | - | 0.04 |
| Flooding depth (m) | - | 0.004 |
| Drying depth (m) | - | 0.003 |
| Manning's resistance coefficient (n) | 0.015 – 0.1 | 0.040 |

**Table 6.7-2 Calibrated model setup parameters – morphology (Case Study 2)**

| Morphological Parameter | Default Values | Applied Value |
|---|---|---|
| Median ($d_{50}$) grain diameter (mm) | - | 0.3 |
| Eddy viscosity ($m^2/s$) | - | 0.06 |
| Mass density of sediment ($kg/m^3$) | 2000 - 2700 | 2650 |
| Porosity (Ratio) | 0.3 – 0.7 | 0.33 |
| Critical shields' parameter | 0.030 – 0.056 | 0.047 |
| Transverse slope coefficient | 0 - 3 | 0.6 |
| Transverse slope power | 0.5 - 1 | 0.5 |
| Longitudinal slope coefficient | 1 - 10 | 1 |

Equation 5.2-5 was replaced by Equation 5.2-6 and the Smart and Jäeggi (1983) and Camenen and Larson (2005) sediment transport equations were also utilised in the base simulation with no other changes to the rest of the input parameters and simulation conditions. The final simulated breach dimensions using Equation 5.2-5, Equation 5.2-6, and Smart and Jäeggi (1983) and Camenen and Larson (2005) sediment transport equations are given in Figure 6.7-3.

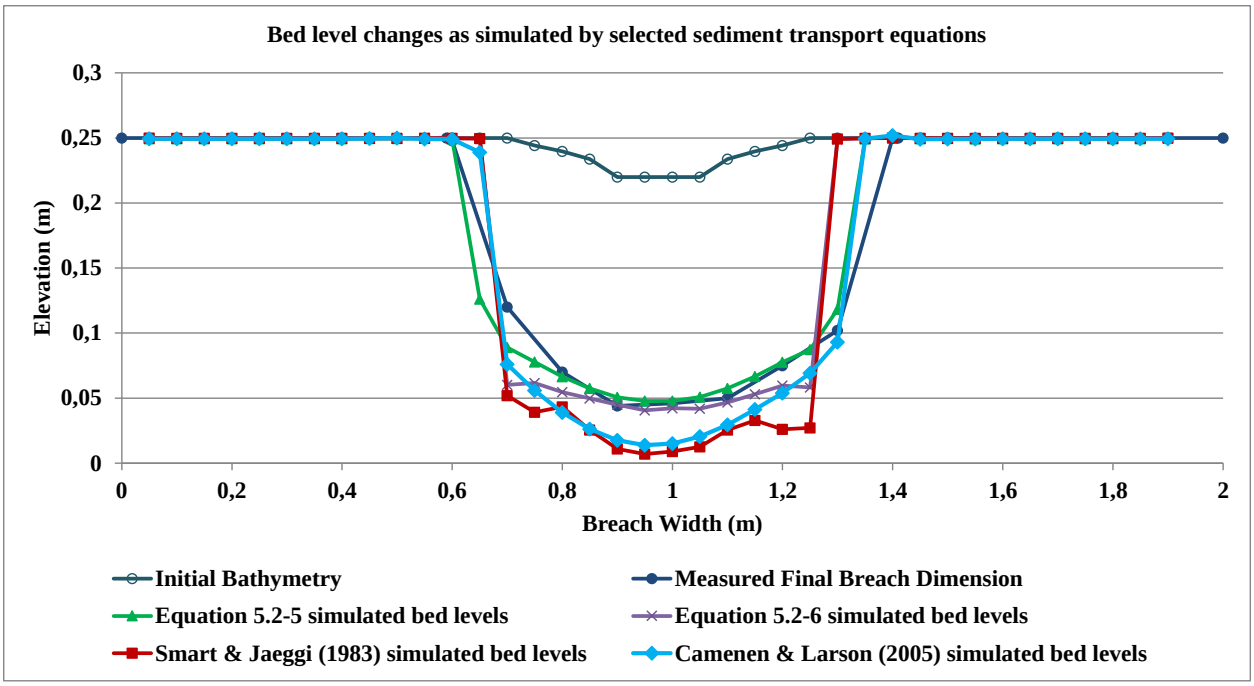


**Figure 6.7-3 Final observed and simulated breaching depths using different equations (Case Study 2)**

The Smart and Jäeggi (1983) and Camenen and Larson (2005) simulated final bed profiles were narrower and deeper than the final simulated bed profiles by Equations 5.2-5 and 5.2-6 as shown in Figure 6.7-3. According to Floodsite (2011), very few of the existing models consistently predict breach dimensions well despite predicting discharge reasonably well. Floodsite (2011) concluded that errors in breach dimensions are implicit within all models, but are normally compensated by other factors. The possible explanation for the narrow and deeper bed profile when Smart and Jäeggi (1983) was applied could be the overestimation of erosion or bed transport rates from the embankment. As a result, the pool drops rapidly and prevents inflow from overtopping parts of the total crest length that were initially dry. While the slower erosion process that is simulated by Equation 5.2-5 results in a comparatively slow pool drop. The slow pool drop encourages inflow to spread further on the sides away from the initial notch location where it erodes more crest length and produces a widened breach opening. The numerical modelling results are summarized in Table 6.7-3. No experimental measured data on the peak outflow and time to peak was available. In the numerical model, different peak outflows and times to peak were simulated by each of the four different sediment transport equations.

**Table 6.7-3 Numerical modelling results for Case Study 2**

| **Measured and simulated model results** | **Peak outflow (l/s)** | **Time to peak (s)** | **Final breach depth (m)** | **Final breach width (m)** |
|---|---|---|---|---|
| **Measured** | - | - | 0.209 | 0.6 |
| **Equation 5.2-5 (Base Simulation)** | 16.7 | 780 | 0.202 | 0.7 |
| **Equation 5.2-6 Simulation** | 15.2 | 660 | 0.209 | 0.6 |
| **Camenen and Larson (2005)** | 22.5 | 540 | 0.236 | 0.6 |
| **Smart and Jäeggi (1983)** | 15.1 | 720 | 0.240 | 0.6 |

In practical flood conditions, the determination of the outflow hydrograph through the breach opening is of utmost importance. The outflow through the breach opening was simulated using Equation 5.2-5, Equation 5.2-6, Smart and Jäeggi (1983) and Camenen and Larson (2005) sediment transport equations as shown in Figure 6.7-4. The results in Figure 6.7-4 show that the simulated outflow hydrograph is sensitive to the selection of a sediment transport equation. The simulated peak discharge by Smart and Jäeggi (1983) sediment transport equation is higher than the one simulated by Equation 5.2-5. Of worthy noting is that Camenen and Larson (2005)

simulated peak discharge is higher than that of Smart and Jäeggi (1983) sediment transport equation despite having the same final breach invert level at the middle of the embankment. The individual final depths and widths for the rest of the transverse bed profiles on the breach opening could be responsible for the differences in the peak discharge for Camenen and Larson (2005) sediment transport equation in comparison with Smart and Jäeggi (1983) sediment transport equation since Figure 6.7-3 only gives the middle transverse section.

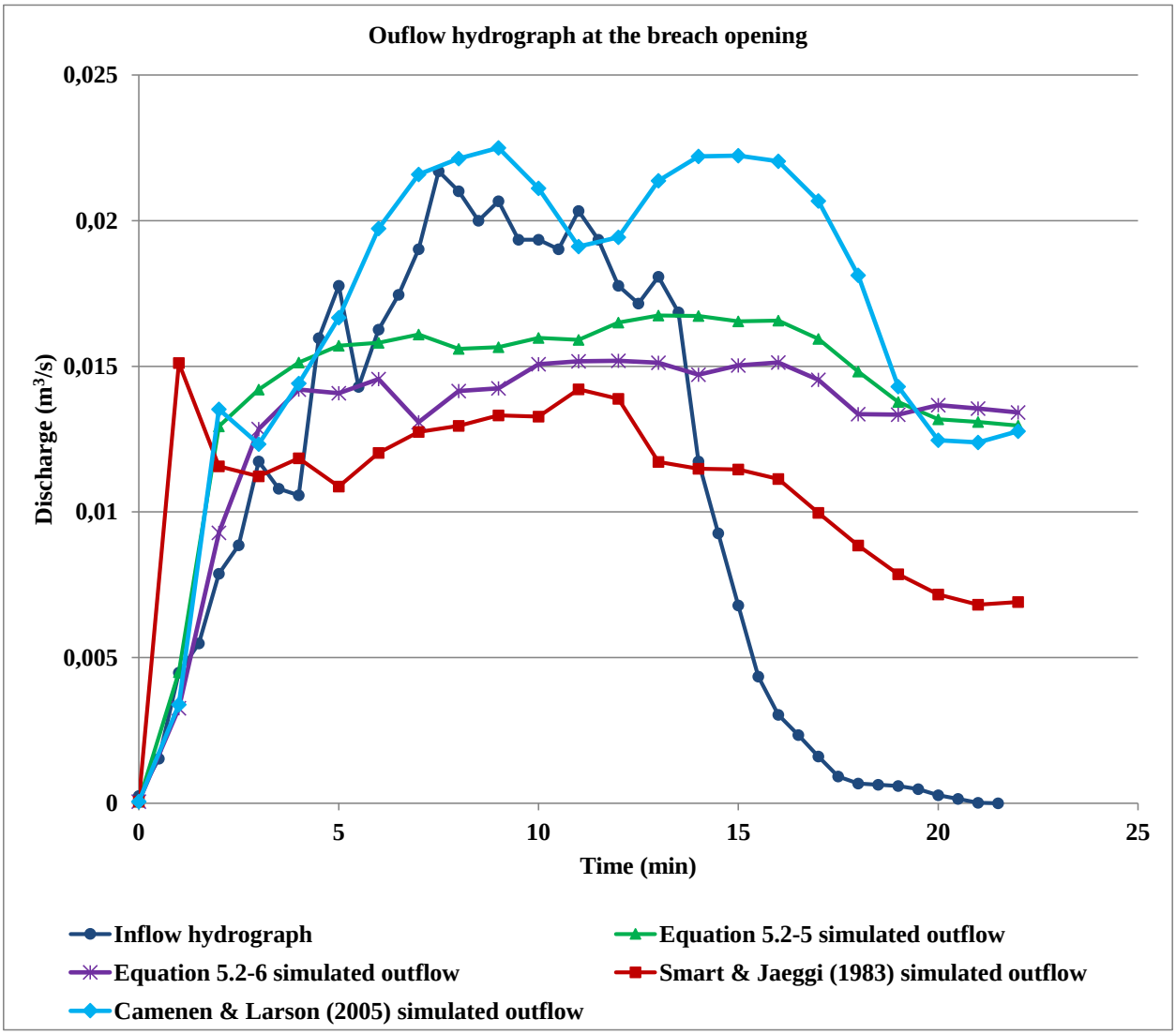


**Figure 6.7-4 Observed inflow and simulated outflow hydrographs (Case Study 2)**

### *6.7.2 The sensitivity of the peak outflow to Manning's resistance coefficient (n) – Case Study 2*

The sensitivity to Manning's resistance coefficient (n) of the four sediment transport equations was examined using three Manning's resistance coefficient (n) values. These were: n = 0.030, 0.040 (applied in the base simulation) and 0.050. The results in Figures 6.7-5, 6.7-6, 6.7-7 and

6.7-8 show that the Manning's resistance coefficient (n) has an effect on both the peak discharge and hydrograph shape. The most significant effect on the peak discharge of the Manning's resistance coefficient (n) is exhibited by the simulated outflow for the Camenen and Larson (2005) sediment transport equation. Specifically in Figure 6.7-8, it is shown that at low resistance (n = 0.030), the peak discharge is higher than at high resistance (n = 0.050). When resistance to flow is low, there is high flow velocity. For the same cross-sectional area, high velocity flow produces a higher peak discharge than slower moving flow. High velocity flow has more eroding effect resulting in quick bed level changes and quick time to peak. The peak discharge decreases for increasing resistance from 0.030 to 0.050. The results show that even though the selected sediment transport equation affects the peak discharge and hydrograph shape, Manning's resistance coefficient (n) also has an additional effect on the numerical model results. The additional uncertainty due to resistance increases the overall uncertainty in the output parameters. However, the analysis of the sensitivity due to resistance is easier to undertake since the input can be estimated within defined parameter value ranges unlike sediment transport equations that are not a defined input quantity but have a significant effect on the hydrograph shape.

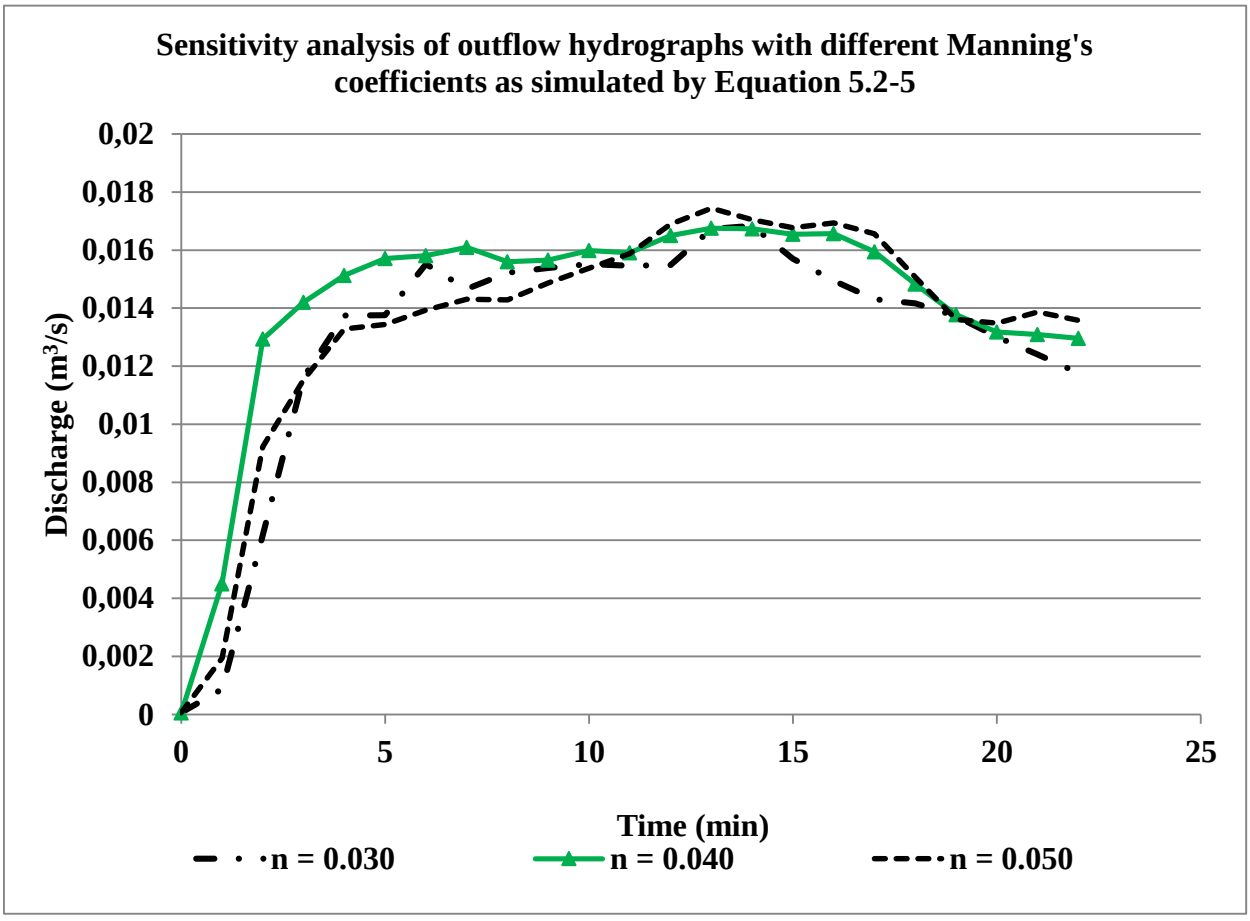


**Figure 6.7-5 Sensitivity analysis - comparison of measured inflow and simulated outflow hydrographs (Equation 5.2-5) – Case Study 2**

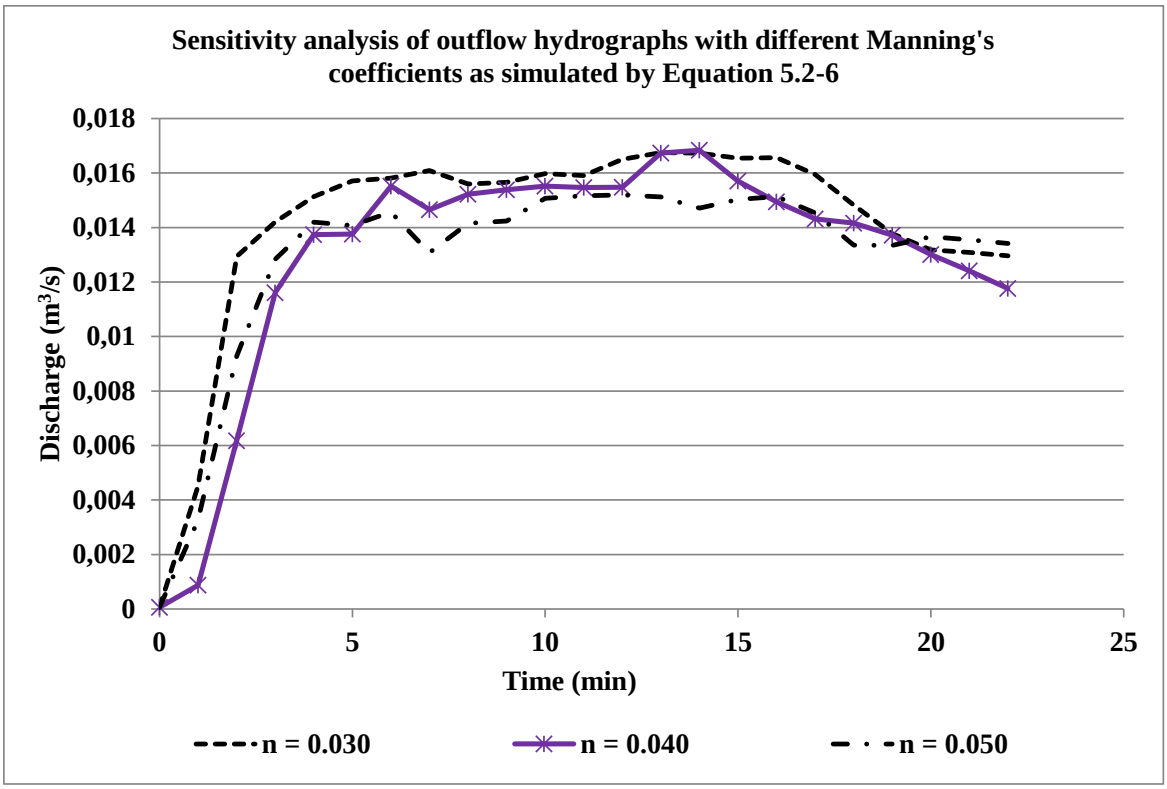


**Figure 6.7-6 Sensitivity analysis - comparison of measured inflow and simulated outflow hydrographs (Equation 5.2-6) - Case Study 2**

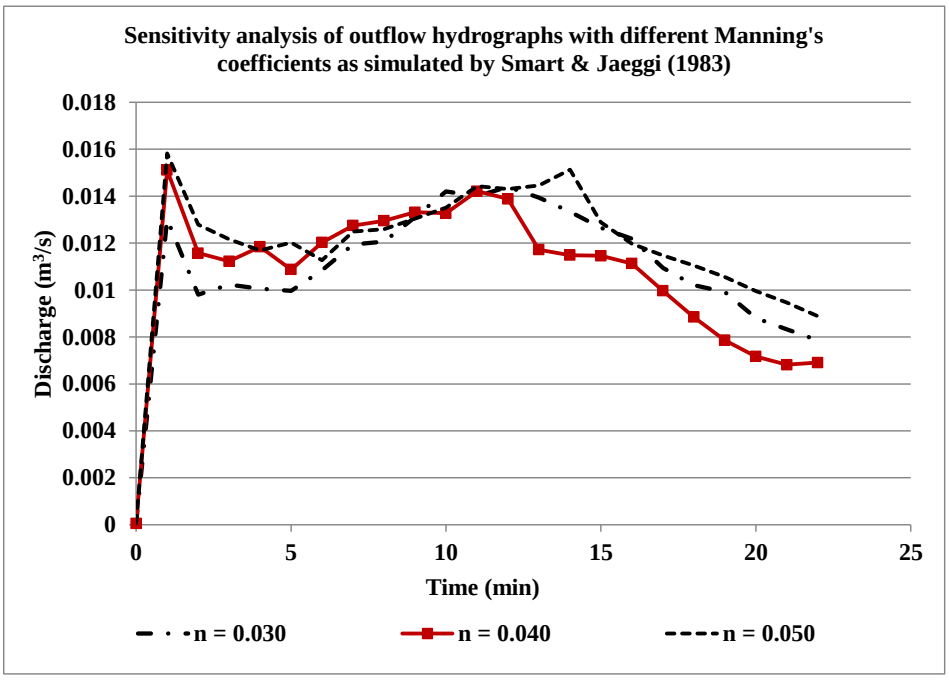


**Figure 6.7-7 Sensitivity analysis - comparison of measured inflow and simulated outflow hydrographs (Smart and Jäeggi, 1983) – Case Study 2**

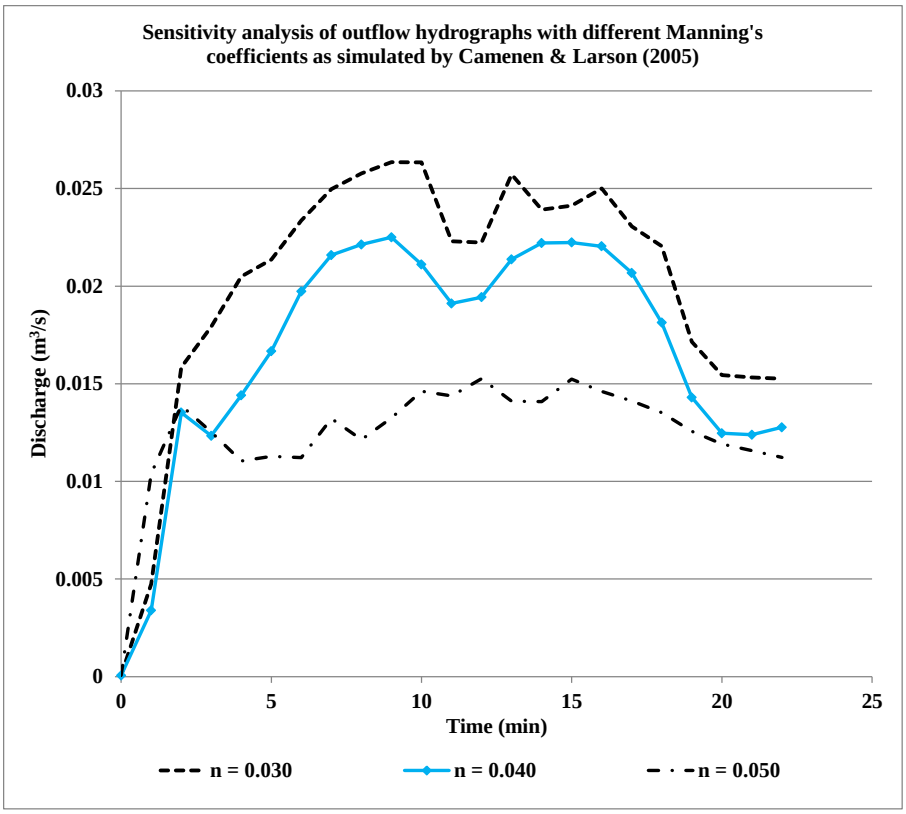


**Figure 6.7-8 Sensitivity analysis - comparison of measured inflow and simulated hydrographs (Camenen and Larson, 2005) – Case Study 2**

## 6.8 Case Study 3

Case Study 3 was based on an experimental laboratory dam-break study that was undertaken under the IMPACT Project (Floodsite, 2011). The IMPACT Project was a 3-year programme of research during which breach formation processes and modelling was conducted by a team of researchers from the United Kingdom, the United States, Germany, Belgium and Norway. The Research included an integrated programme of field and laboratory tests to observe breach initiation and formation processes (Hassan and Morris, 2008). Extensive and reliable datasets were collated and are available online. Researchers and modellers are free to obtain the data and apply it in their own numerical model analysis, verification and validation work.

The laboratory setup included a 0.5 m high homogeneous non-cohesive earth dam with an upstream slope (V: H) of 1:1.9 and downstream slope (V: H) of 1:1.7. It was built in a 50 m long by 10 m wide flume. The embankment was built with sediment (sand) of median ($d_{50}$) diameter = 0.25 mm. Figure 6.8-1 shows the embankment cross-section. The observed data with regard to water level, inflow and outflow hydrographs for Case Study 3 are given in Figure 6.8-2 (Floodsite, 2011).

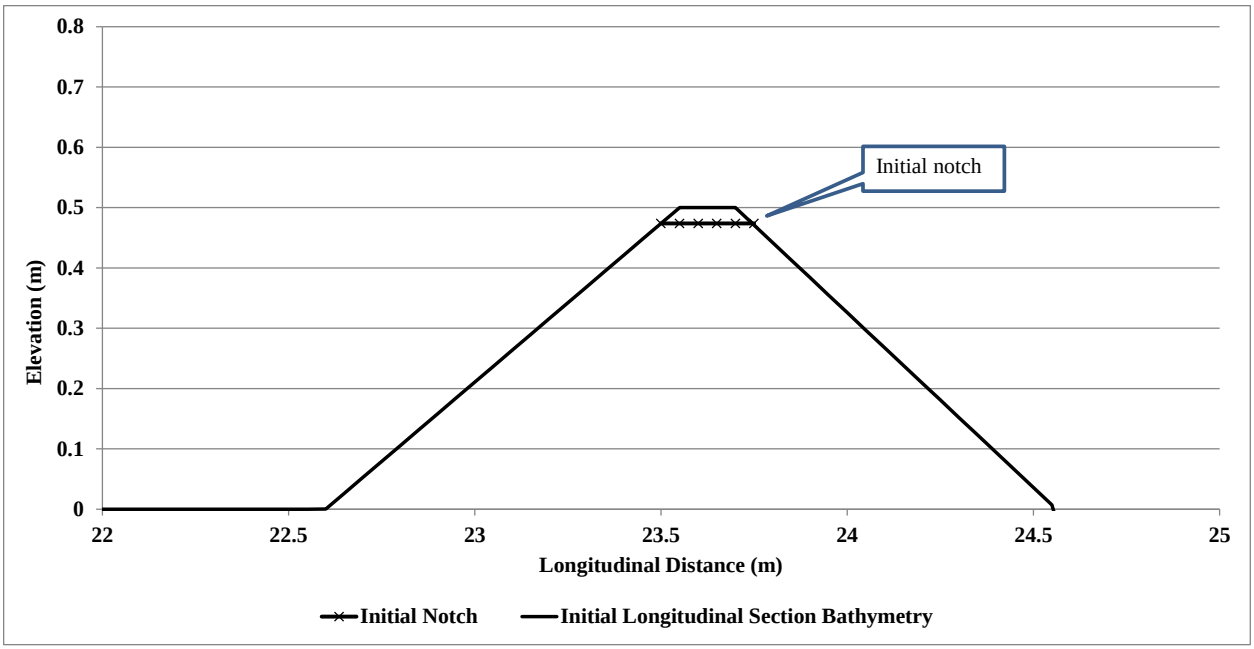


**Figure 6.8-1 Embankment longitudinal section (Case Study 3)**

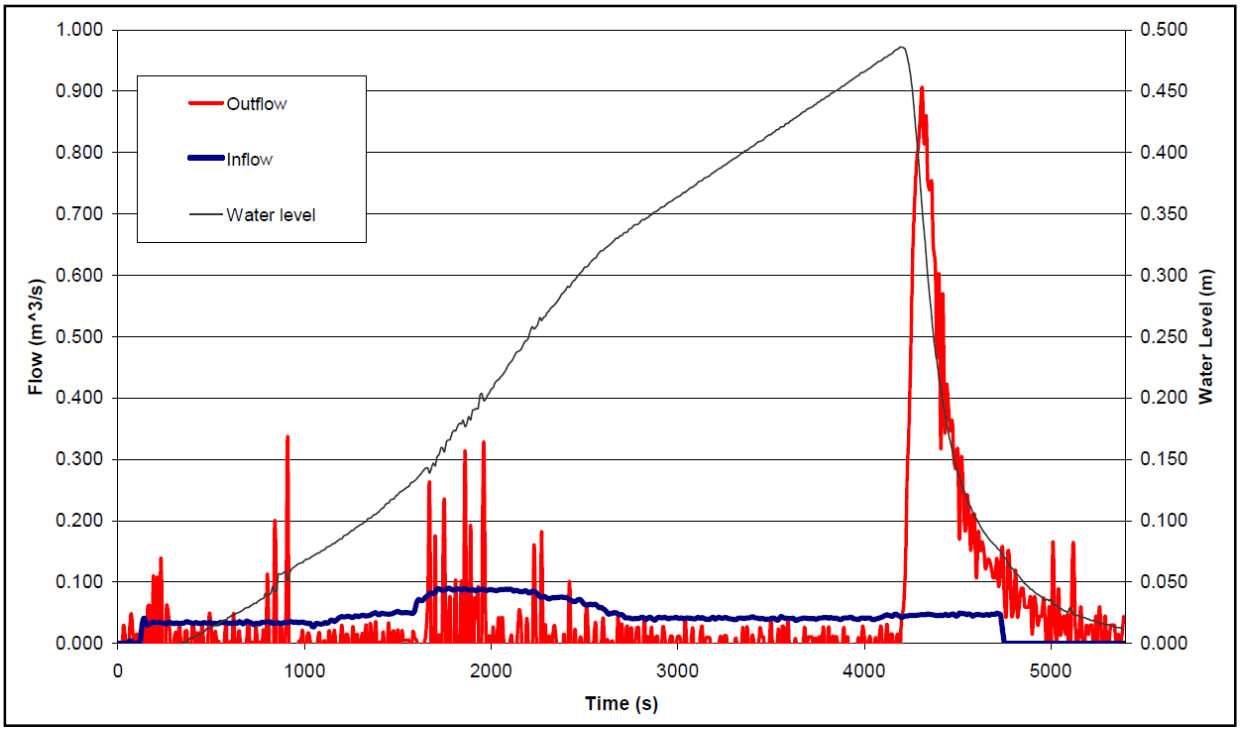


**Figure 6.8-2 Observed water levels, inflow, and outflow hydrographs for Case Study 3 (Floodsite, 2011)**

For the numerical model (base simulation) in Case Study 3, a rectangular grid with one thousand (1000) grid cells in the direction of flow and one hundred (100) grid cells across was set up. The grid sizes were 0.05 m by 0.05 m each. The bathymetry was set up with a central notch (1 m

wide and 0.026 m deep) for the initiation of overtopping. In order to limit water from overtopping the whole crest width, the crest of the embankment was made slightly higher towards the sides and sloped gently from the high sides towards the low lying notch.

Initial water levels were specified based on the measured final water levels at full supply level. This was done to reduce the computation time that was required to simulate the model from empty reservoir condition to full supply level condition prior to the initiation of breaching based on the water levels in Figure 6.8-2. For the upstream boundary, an approximately constant inflow (0.03 $m^3/s$) based on the estimated constant inflow was provided. The constant inflow was specified as a source point upstream of the embankment close to the flume inlet. For the downstream boundary, a rating curve (Q-h) was specified for the automatic computation of flow discharge based on the temporal water levels.

Equation 5.2-5 was applied in the base simulation (the numerical simulation model that was run to reproduce the measured or observed data in Figure 6.8-2). The measured breach hydrograph shape and peak discharge were used as reference parameters for calibration purposes. Manning's resistance coefficient (n) was calibrated based on the observed peak discharge in Figure 6.8-2 to a value of approximately 0.044. The rest of the calibration parameters for hydrodynamic and morphological modelling are shown in Tables 6.8-1 and 6.8-2. Figure 6.8-3 shows the initial bathymetry in the numerical model simulation. The final bathymetries using Equation 5.2-5, Equation 5.2-6, and Smart and Jäeggi (1983) and Camenen and Larson (2005) sediment transport equations are given in Figures 6.8-4, 6.8-5, 6.8-6 and 6.8-7 respectively. The source point had a marked effect on the simulated bed levels of the final bathymetries as shown in Figures 6.8-3 and 6.8-4 at a location where the source point was specified. Equation 5.2-6 simulated final bathymetry in Figure 6.8-5 showed antidunes on the bed surface that were not simulated by the other sediment transport equations. The cause could be implicit within the formula due to its formulation. The Camenen and Larson (2005) sediment transport equation predicted a conspicuous scour hole as seen on the final bathymetry in Figure 6.8-7.

**Table 6.8-1 Calibrated model setup parameters – hydrodynamics (Case Study 3)**

| Hydrodynamic Parameter | Default Values | Applied Value |
|---|---|---|
| Hydrodynamic time step (s) | - | 0.0275 |
| Morphological time step (s) | - | 0.055 |
| Flooding depth (m) | - | 0.004 |
| Drying depth (m) | - | 0.003 |
| Manning's resistance coefficient (n) | 0.015 – 0.1 | 0.044 |

**Table 6.8-2 Calibrated model setup parameters – morphology (Case Study 3)**

| Morphological Parameter | Default Values | Applied Value |
|---|---|---|
| Median ($d_{50}$) grain diameter (mm) | - | 0.25 |
| Eddy viscosity ($m^2/s$) | - | Smagorinsky Formula – Velocity Based Constant – 0.5 |
| Mass density of sediment ($kg/m^3$) | 2000 - 2700 | 2650 |
| Porosity (Ratio) | 0.3 – 0.7 | 0.33 |
| Critical shields' parameter | 0.030 – 0.056 | 0.047 |
| Transverse slope coefficient | 0 - 3 | 0.6 |
| Transverse slope power | 0.5 - 1 | 0.5 |
| Longitudinal slope coefficient | 1 - 10 | 1 |

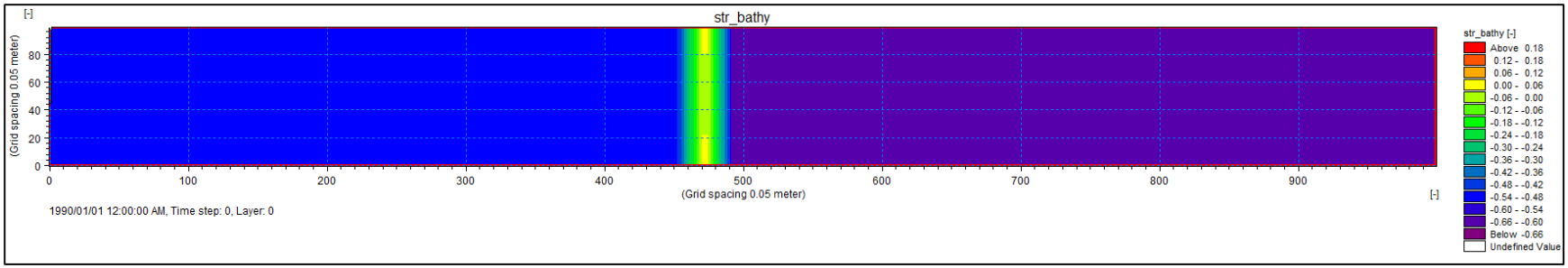


**Figure 6.8-3 Initial bathymetry - Case Study 3**

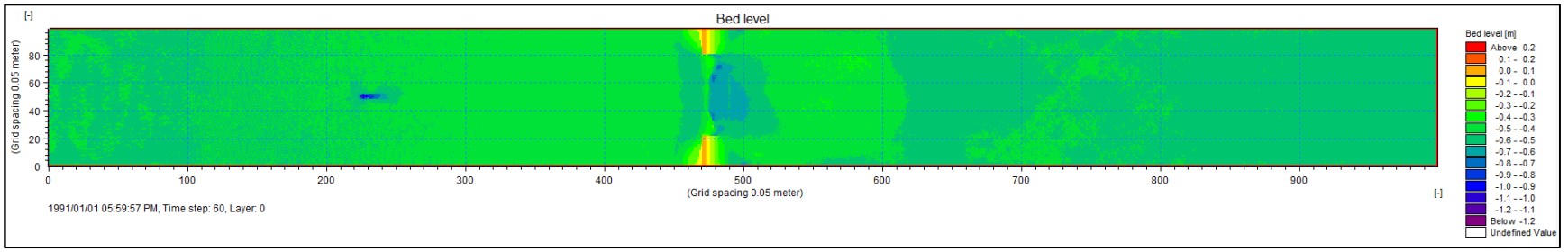


**Figure 6.8-4 Final bathymetry using Equation 5.2-5 - Case Study 3**

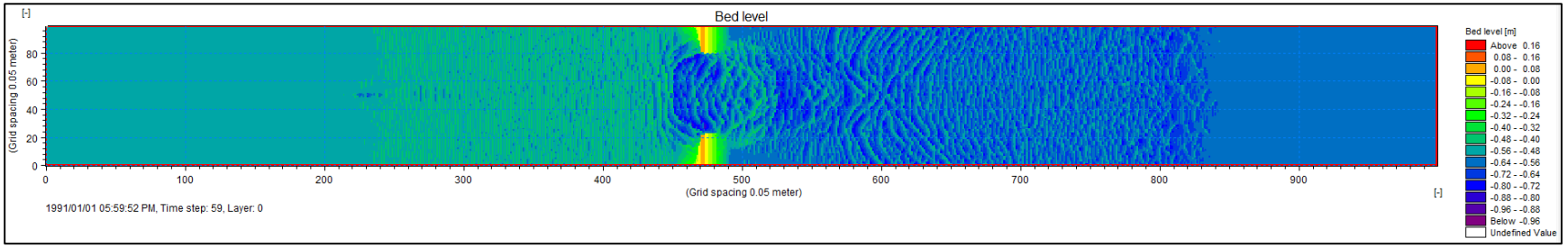


**Figure 6.8-5 Final bathymetry using Equation 5.2-6 – Case Study 3**

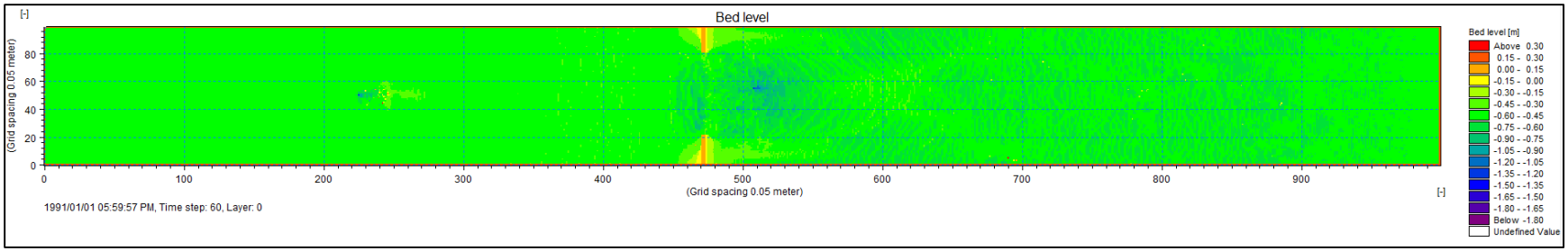


**Figure 6.8-6 Final bathymetry using Smart and Jäeggi (1983) - Case Study 3**

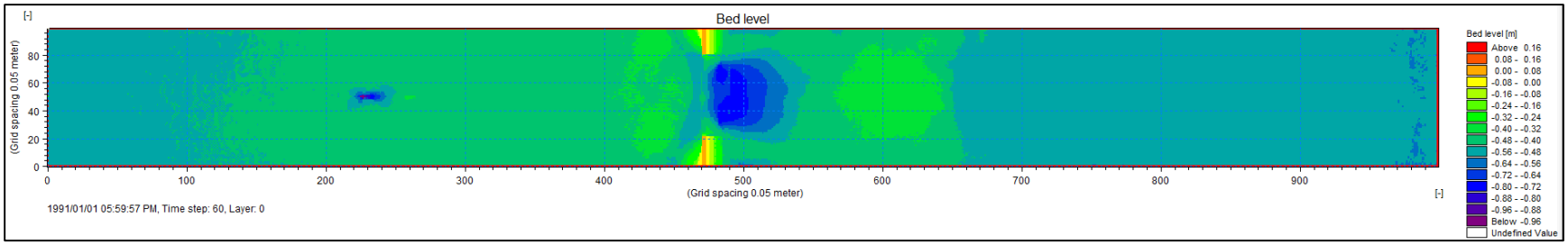


**Figure 6.8-7 Final bathymetry using Camenen and Larson (2005) - Case Study 3**

### *6.8.1 Analysis of numerical simulation results – Case Study 3*

It should be noted that the percentage slope (at 60%; V: H of 1:1.7) for Case Study 3 was outside the calibration range of all four sediment transport equations. The main aim of the numerical simulation for Case Study 3 was to analyse the predicted discharges through the breach opening as simulated by the selected equations (Equation 5.2-5, Equation 5.2-6, and the Smart and Jäeggi (1983) and the Camenen and Larson (2005) sediment transport equations). The objective of the numerical simulation during the IMPACT project was to assess the sensitivity of model results to the variation of input parameters such as breach shape, initial notch location, crest width, slope and sediment grading (Floodsite, 2011). Output parameter data from the base simulations of different dam-break models is shown in Table 6.8-3. As observed in Table 6.8-3, the models simulated different output values for the specified parameters. The modellers were provided with the experimental results and were aware of the expected output. The results in Table 6.8-3 werebased on the modellers best calibrated run. Apart from Cemagref and NWS BREACH, all models that were analysed under the Impact Project (Floodsite, 2011) predicted peak discharge to within 70% percent of the measured peak discharge at the breach opening. Cemagref is an organisation that was part of the Impact Project. The researchers from Cemagref applied a simple model in the numerical modelling programme of the selected field and laboratory case studies. Very little is reported in literature about the simple model that was applied by researchers from Cemagref. This is why it is not included in literature review. However, the researchers contributed output results from their numerical modelling of Case Study 3 that appear in Table 6.8-3.

In terms of this study, when Equation 5.2-5 was replaced by Equation 5.2-6 in the MIKE 21C numerical model, the predicted peak discharge increased from 0.93 to 0.99 $m^3/s$, which was 9% higher than the value predicted by Equation 5.2-5 (Figure 6.8-8).

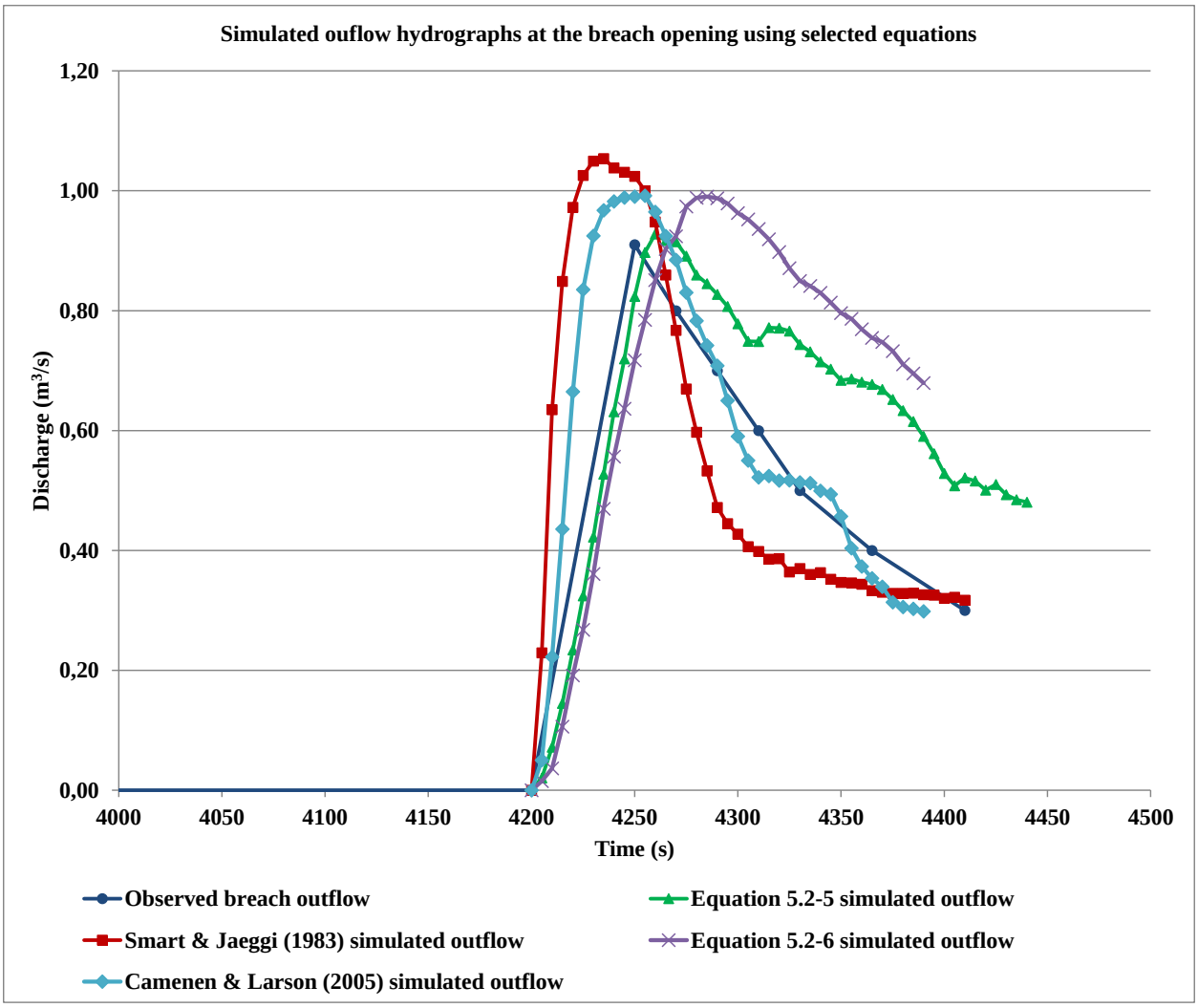


**Figure 6.8-8 Outflow hydrographs at breach opening (Case Study 3)**

**Table 6.8-3 Measured data and output parameters for selected models (Adapted from Floodsite, 2011)**

| *Parameter/* **Model** | *Peak outflow ($m^3/s$)* | *Time to peak (h)* | *Water level at peak - upstream of breach opening (m)* | *Peak water level - upstream of breach opening (m)* | *Final breach invert (m)* | *Breach invert at peak (m)* | *Final breach width (m)* | *Breach width at peak (m)* |
|---|---|---|---|---|---|---|---|---|
| **Measured Data** | 0.91 | 1.18 | 0.35 | 0.49 | 0 | - | 2.75 | 2.75 |
| **Cemagref** | *0.57* | *1.19* | *0.37* | *0.5* | *0* | *0* | *3.87* | *1.55* |

| | | | | | | | | |
|---|---|---|---|---|---|---|---|---|
| **DEICH** | *0.79* | *1.18* | *0.4* | *0.49* | *0* | *0* | *3.85* | *1.79* |
| **SOBEK** | *0.79* | *1.13* | *0.38* | *0.48* | *0.02* | *0.02* | *3.11* | *1.98* |
| **NWS BREACH** | *0.06* | *1.29* | *0.49* | *0.49* | *0* | *0* | *0.03* | *0.03* |
| **HR BREACH** | *0.96* | *1.22* | *0.41* | *0.48* | *0* | *0* | *5.18* | *3.14* |
| **MIKE 21C - Equation 5.2-5** | 0.93 | 1.18 | 0.41 | 0.49 | 0 | - | 2.95 | 2.95 |
| **MIKE 21C - Equation 5.2-6** | 0.99 | 1.19 | 0.49 | 0.49 | 0 | - | 2.95 | 2.95 |
| **MIKE 21C - Smart &** Jäeggi **(1983)** | 1.05 | 1.18 | 0.49 | 0.49 | -0.08 | - | 2.95 | 2.95 |
| **MIKE 21C - Camenen & Larson (2005)** | 0.99 | 1.18 | 0.49 | 0.49 | -0.04 | - | 2.95 | 2.95 |

A similar peak discharge of 0.99 $m^3/s$ was simulated by Camenen and Larson (2005) sediment transport equation albeit with a slightly longer time to peak in comparison with Equation 5.2-5. Smart and Jäeggi (1983) predicted a peak discharge that was 15% higher than the measured peak discharge. Floodsite (2011) suggested that an accuracy of peak discharge in the order of ±30% is acceptable. Based on this criterion, the four sediment transport equations' predictive capability performance against the measured laboratory peak discharge for Case Study 3 was considered to be generally fair according to ±30% acceptability criteria. Of worth noting was the fact that all four sediment transport equations predicted peak discharges that were greater than the laboratory observed peak discharges. It should be pointed out that the simulations were conducted to analyse the sensitivity of the sediment transport equations on the numerical model results considering that the slope of the embankment was outside the applicable ranges for all the four sediment transport equations. The aim was to analyse the uncertainty due to the application of sediment transport equations outside their calibration data range. The results showed that it was

difficult to accurately reproduce the measured peak discharge using the four sediment transport equations.

The effect of each of the four sediment transport equations on the final bed profile along the central transverse cross-section of the breach opening is shown in Figure 6.8-9. Camenen and Larson (2005) sediment transport equation had the most significant effect on the final bed profile as evidenced by the bed oscillations that could be attributed to the instabilities in the numerical model computations, when it was applied on very steep slopes (1V: 1.7H). Overall, the final breach invert was lower for the Camenen and Larson (2005) and Smart and Jäeggi (1983) sediment transport equations in comparison with Equations 5.2-5 and 5.2-6. The results highlight the limited capability of sediment transport equations when applied outside their empirical slope data calibration range.

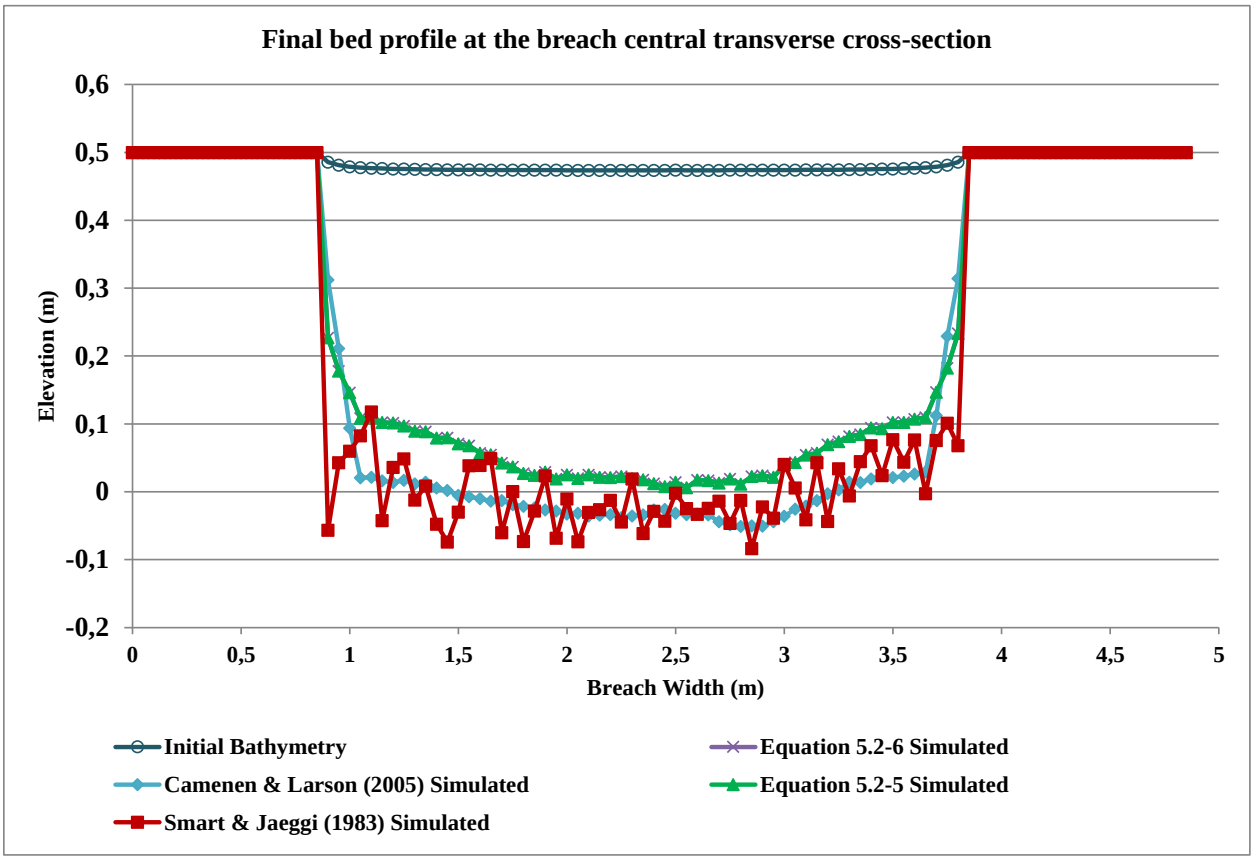


**Figure 6.8-9 Simulated bed profiles at breach opening on the central transverse cross-section using Equation 5.2-5, Equation 5.2-6, Smart and Jäeggi (1983) and Camenen and Larson (2005) sediment transport equations (Case Study 3)**

### *6.8.2 The sensitivity of the peak outflow to Manning's resistance coefficient (n) – Case Study 3*

The sensitivity to Manning's resistance coefficient (n) of the four sediment transport equations in the numerical simulations of Case Study 3 was examined using three selected Manning's resistance coefficient (n) values (Figures 6.8-10, 6.8-11, 6.8-12 and 6.8-13). The Manning's resistance coefficients were n = 0.040, 0.044 (base simulation) and 0.050. The most significant effects are for Equations 5.2-5 and 5.2-6, and the Camenen and Larson (2005) sediment transport equation as shown in Figures 6.8-11 to 6.8-13 respectively. The effect of Manning's resistance coefficient (n) is less for the Smart and Jäeggi (1983) sediment transport equation simulated peak discharge in comparison to the other sediment transport formulations. The results indicate that the combined effect of the selected sediment transport equation and Manning's resistance coefficient (n) varies from one sediment transport equation to the other. It has also been shown from the results that it is challenging to reproduce the observed dam-break output results in numerical modelling when sediment transport equations that were derived from specific slope ranges are applied outside their calibration range.

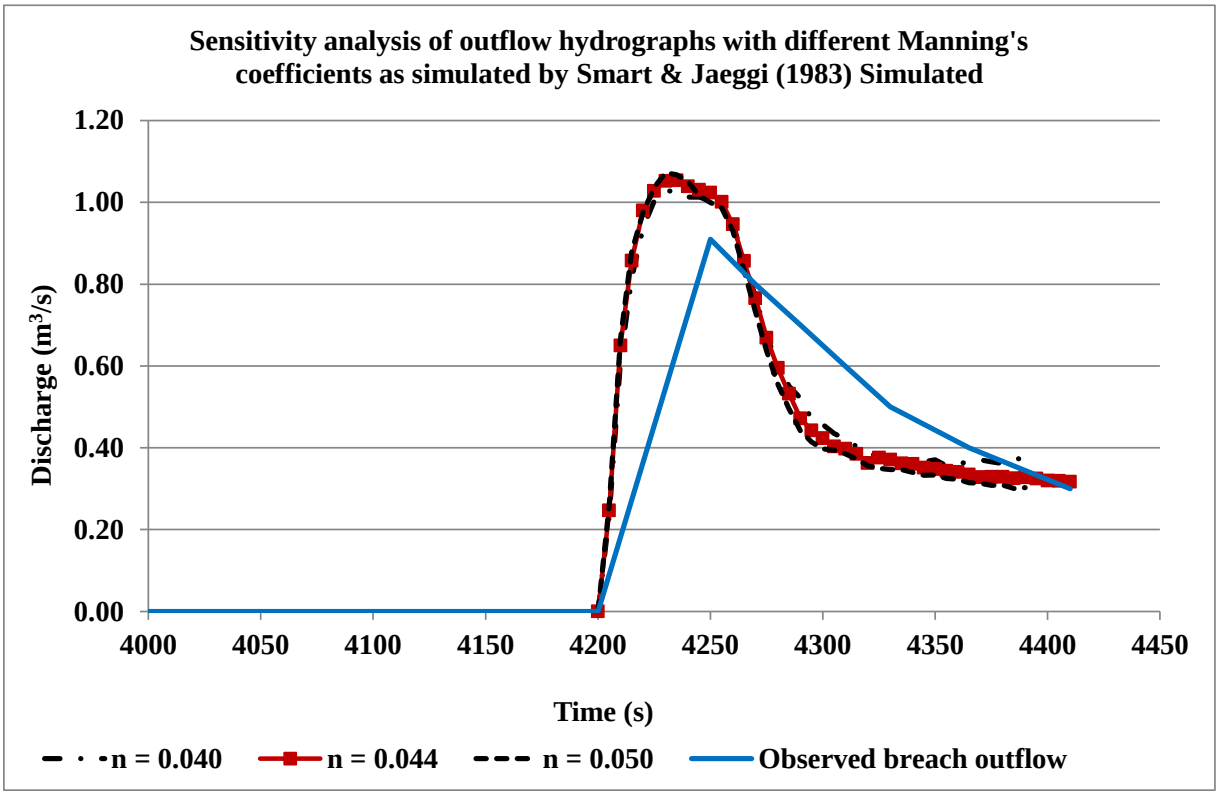


**Figure 6.8-10 Sensitivity analysis: Smart and Jäeggi (1983) – Case Study 3**

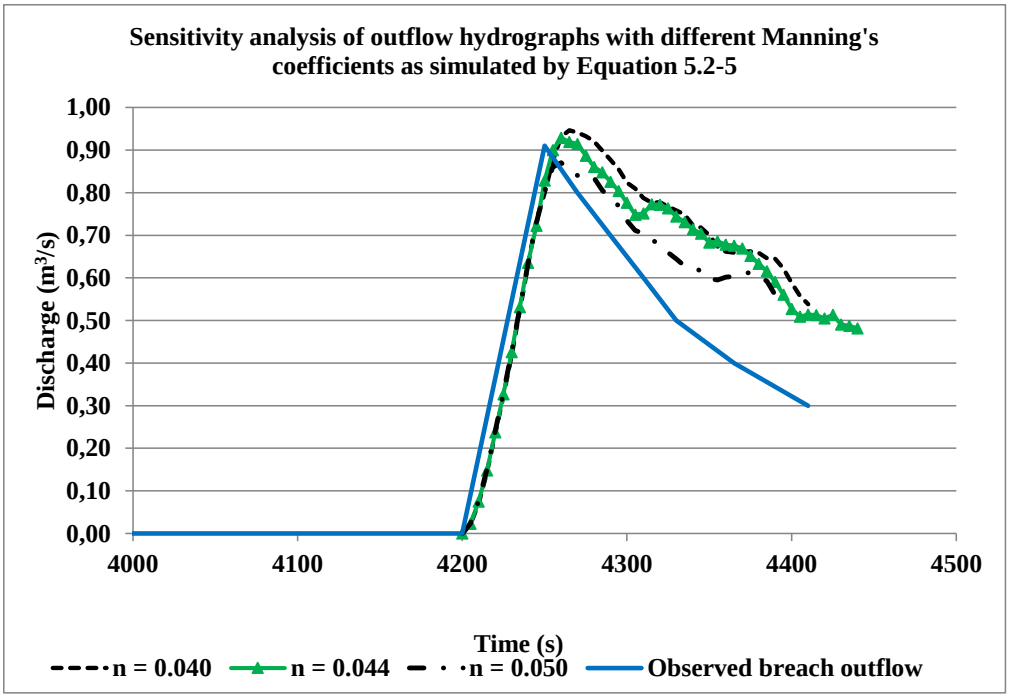


**Figure 6.8-11 Sensitivity analysis: Equation 5.2-5 – Case Study 3**

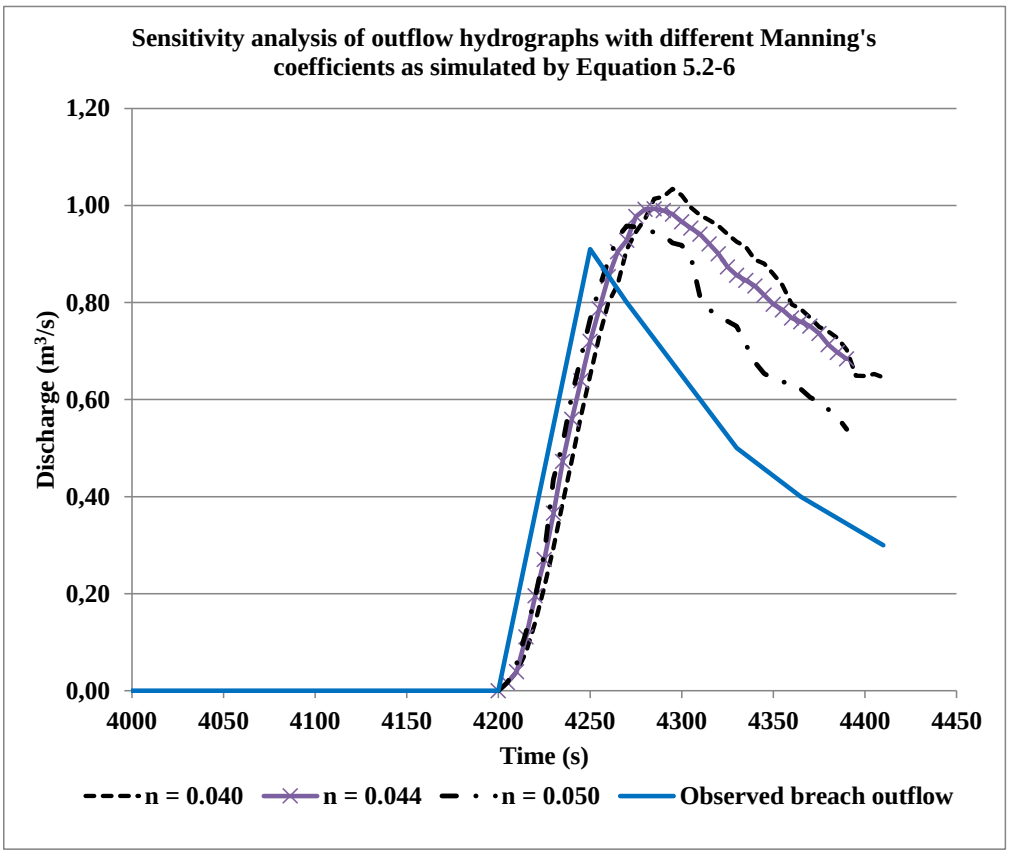


**Figure 6.8-12 Sensitivity analysis: Equation 5.2-6 – Case Study 3**

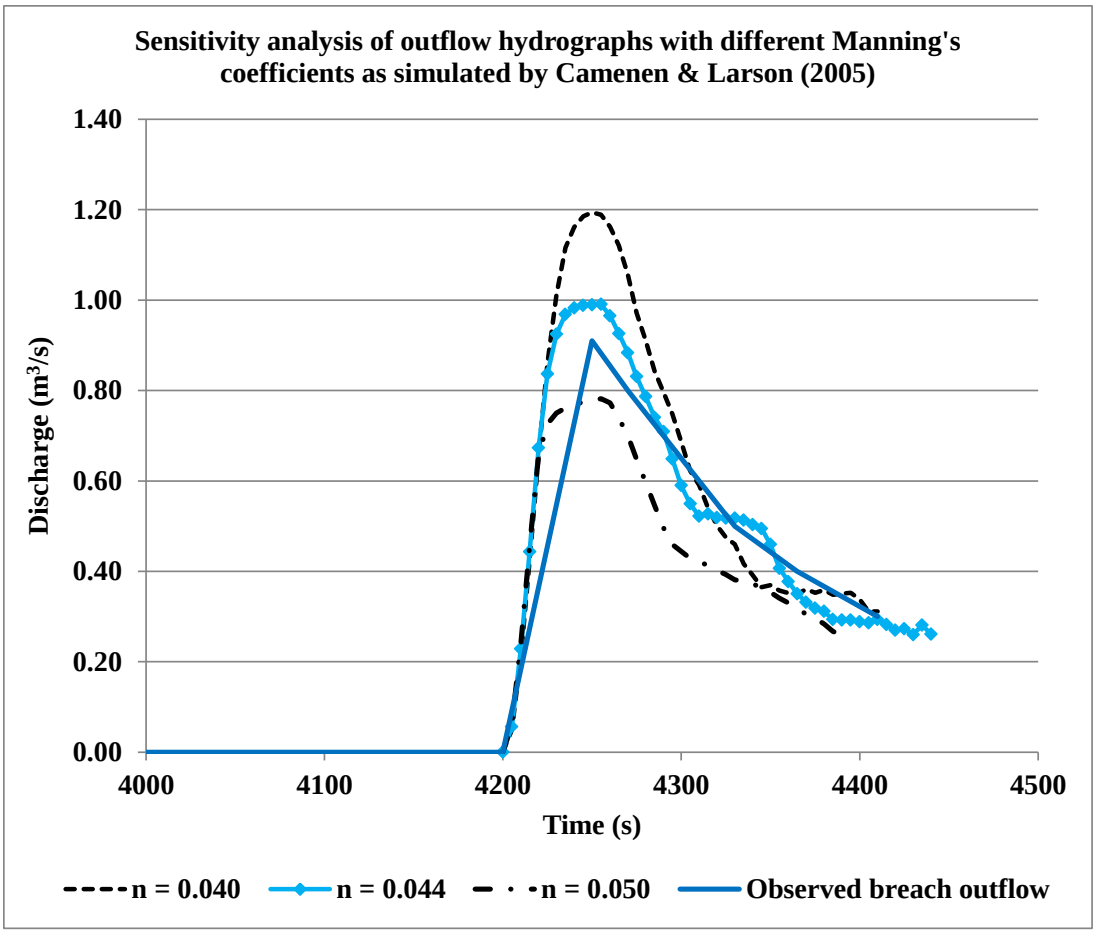


**Figure 6.8-13 Sensitivity analysis: Camenen and Larson (2005) – Case Study 3**

## 6.9 Case Study 4

Case Study 4 was based on an experimental dam-break field test that was undertaken under the IMPACT Project (Floodsite, 2011). The field test setup was made up of a 5 m high homogeneous non-cohesive earth dam with an upstream slope (V: H) of 1:1.9 and downstream slope (V: H) of 1:1.7. Data on soil parameters such as grading, cohesion, water content and density was recorded. Table 6.9-1 shows soil properties for Case Study 4. The field test analysed dam-break data for a non-cohesive embankment with median ($d_{50}$) sediment size of 4.65 mm. Table 6.9-2 gives the information on the dam geometry.

**Table 6.9-1 Soil properties for Case Study 4**

| Soil Properties | Value |
|---|---|
| Moisture content (%) | 7 |
| Median ($d_{50}$) sediment size (mm) | 4.65 |
| Porosity (Ratio) | 0.22 |
| Specific Weight (kN/m$^3$) | 21.2 |
| Angle of friction (degrees) | 42 |
| Cohesion (kN/m$^2$) | 0.9 |

**Table 6.9-2 Dam geometry**

| Dam Geometry | Value |
|---|---|
| Dam Height (m) | 5 |
| Upstream shoulder slope (V:H) | 1: 1.9 |
| Downstream shoulder slope (V:H) | 1: 1.7 |
| Initial breach depth (m) | 0.12 |
| Initial breach width (m) | 2 |

According to IMPACT (Floodsite, 2011), the purpose of this test was to better understand breach formation and to identify the different failure mechanisms in homogeneous non-cohesive embankments. In addition, the field test was done to assess and inspect the effect of seepage on the breach formation processes and to conduct a sensitivity analysis of the effect of various input parameters including sediment transport equations. Figure 6.9-1 shows the geometry of the embankment. A flow conveyance notch was cut at the top of the embankment in order to initiate the overtopping breach flow.

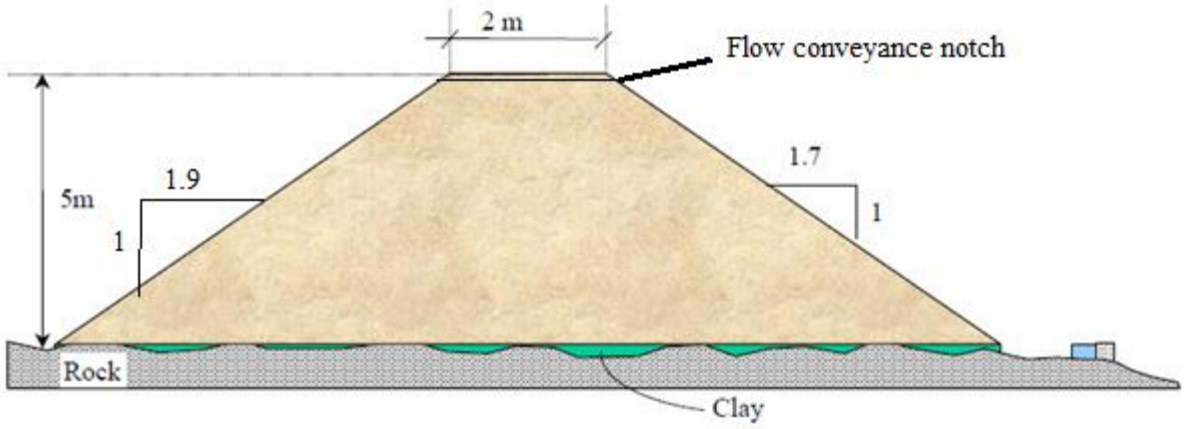


**Figure 6.9-1 Embankment structure shape and design data for Impact Project Test 2 (adapted from Floodsite, 2011)**

According to Floodsite (2011), the test started with a water level higher than the base of the initiation notch. A log or plank was inserted on the initiation notch. Due to the period in which the test was done, ice formed on the upstream reservoir and some of the surface of the gravel material had become frozen to an extent that the subsequent growth of the breach through the embankment might have been affected by the frozen material as the exact depth to which freezing occurred was unclear. Prior to testing, defrosting was done. Upon sufficient defrosting, the plank and sand bags that were used to block the initial notch were removed in order to start the test as shown on Figure 6.9-2a. The "headcut eroded back in a single step with vertical back and side faces, remaining exactly equal to the width of the initiation notch" Floodsite (2011). Figures 6.9-2b and 6.9-2c show the headcut development and the start of the breach formation. Figure 6.9-2d shows the breach formation before the time of failure. The breaking of the upstream face resulted in a gush of water through the breach. The mechanism of the breach development was through geotechnical block failure that was accompanied by the instantaneous falling of the upstream face. The time that was taken from initial crack in the embankment to the development of normal unobstructed flow through the breach was 3 minutes. A sample of the sizes of the blocks that were being cut is given in Figure 6.9-2e. Due to the falling of the embankment into the breach, it was not possible during the test to determine the final depth of the breach. However, the final measured breach width was 20 m with near vertical eroding faces. Figure 6.9-2f shows the nearly vertical sides of the breach immediately after the breach formation process. The breach sides were increased through erosion undercutting processes of the soil that resulted in soil blocks falling at the toe of the embankment.


**Figure 6.9-2a Removing stop log from notch (Floodsite, 2011)**


**Figure 6.9-2b Two step headcut development plus sediment fan (Floodsite, 2011)**


**Figure 6.9-2c Breach formation (Floodsite, 2011)**


**Figure 6.9-2d No signs of block affecting breach flow within 4 seconds of start of failure (Floodsite, 2011)**


**Figure 6.9-2e Left side (facing downstream) block failure (Floodsite, 2011)**


**Figure 6.9-2f Vertical sides of breach immediately after breach formation process (Floodsite, 2011)**

### *6.9.1 Numerical model setup and analysis of numerical simulation results - Case Study 4*

For the numerical model (base simulation) of Case Study 4, a rectangular grid with one thousand (1000) grid cells in the direction of flow and one hundred (100) grid cells across was set up. The grid sizes were 0.5 m by 0.5 m each. The bathymetry was set up with a central notch of 2 m width and 0.2 m depth. The notch was slightly deeper and sloped gently from the centre of the crest towards the sides where it was deeper in order to provide adequate flow depth for initiation of breaching in the numerical model. For the upstream boundary, water levels were specified based on the Impact Project's measured water levels. For the downstream boundary, a rating curve (Q-h) was specified for automatic computation of flow discharge based on the temporal water levels. A simulated hotstart file was used for the rest of the model runs. The calibration of the breach hydrograph was carried out by adjusting the the Manning's resistance coefficient (n). The observed breach hydrograph shape and peak discharge were used as reference parameters for calibration purposes. However, it was not possible to match the shape of the falling limb of the observed outflow hydrograph as seen in Figure 6.9-4. As such, the main consideration in the calibration was the peak discharge value only. The failure to reproduce the observed results was consistent with the findings in Section 6.8.2 where it was also challenging to reproduce the observed dam-break output results probably because the sediment transport equations were applied outside their calibration range. The calibrated model setup parameters for hydrodynamics and morphology are given in Tables 6.9-3 and 6.9-4 respectively. Figure 6.9-3 shows the initial bathymetry for Case Study 4.

**Table 6.9-3 Calibrated model setup parameters – hydrodynamics (Case Study 4)**

| Hydrodynamic Parameter | Default Values | Applied Value |
|---|---|---|
| Hydrodynamic time step (s) | - | 0.0275 |
| Morphological time step (s) | - | 0.055 |
| Flooding depth (m) | - | 0.05 |
| Drying depth (m) | - | 0.04 |
| Manning's resistance coefficient (n) | 0.015 – 0.1 | 0.050 |

**Table 6.9-4 Calibrated model setup parameters – morphology (Case Study 4)**

| Morphological Parameter | Default Values | Applied Value |
|---|---|---|
| Median ($d_{50}$) grain diameter (mm) | - | 4.65 |
| Eddy viscosity ($m^2/s$) | - | 0.06 |
| Mass density of sediment ($kg/m^3$) | 2000 - 2700 | 2161 |
| Porosity (Ratio) | 0.3 – 0.7 | 0.22 |

| | | |
|---|---|---|
| Critical Shields' parameter | 0.030 – 0.056 | 0.047 |
| Transverse slope coefficient | 0 - 3 | 0.6 |
| Transverse slope power | 0.5 - 1 | 0.5 |
| Longitudinal slope coefficient | 1 - 10 | 1 |

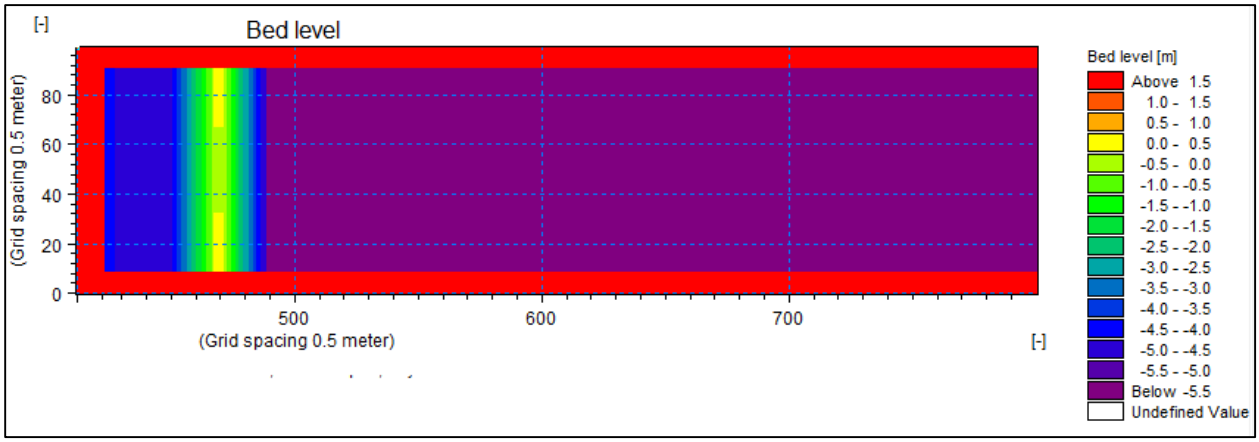


**Figure 6.9-3 Initial Bathymetry (Case Study 4)**

Equation 5.2-5 for the base simulation run was replaced by Equation 5.2-6, and also by the Smart and Jäeggi (1983) and Camenen and Larson (2005) sediment transport equations. Using the same data input, three separate model runs were simulated using the three selected sediment transport equations. The outflow hydrographs that were simulated by all the four sediment transport equations are plotted in Figure 6.9-4.

Figure 6.9-4 shows different peak discharges and times to peak that were predicted by each of the four different sediment transport equations that were investigated as part of this study. The peak discharges and times to peak are shown in Table 6.9-5. The results show a great variability not only in the peak discharges but also the times to peak. These differences (Figure 6.9-4) are not uncommon.

The Impact Project (Floodsite, 2011) analysed the results for 44 model runs in order to assess the sensitivity of the numerical models to the sediment transport equations and Manning's resistance coefficient (n). The Impact Project results are given in Table 6.9-6. According to the results in Table 6.9-6, the minimum predicted peak discharge for the field test in Case Study 4 was 50 $m^3/s$ and the maximum was 236 $m^3/s$ against a measured peak discharge of 117 $m^3/s$.

Table 6.9-7 shows the sensitivity of the peak discharge to the input of the sediment transport equations that were investigated as part of this study. The maximum predicted peak discharge during this study (Table 6.9-6) was lower than the maximum peak discharge during the Impact Project. This means that the band of uncertainty can be considerably reduced if slope appropriate sediment transport equations are applied. The results in this study showed that all the sediment

transport equations did not give good results. This meant that the four sediment transport equations have limited applicability when applied outside their empirical slope data calibration range.

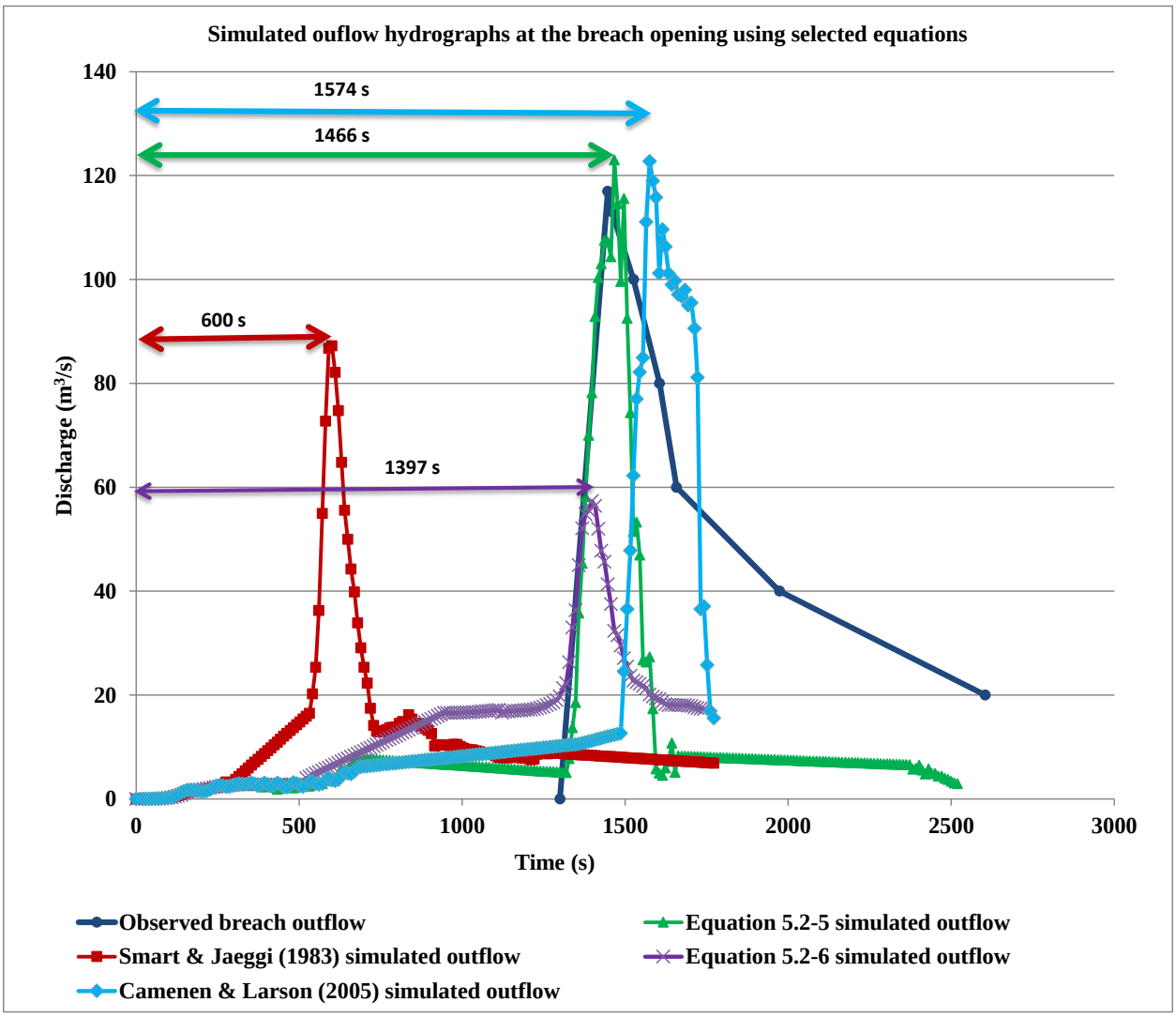


**Figure 6.9-4 Outflow hydrographs at breach opening (Case Study 4)**

**Table 6.9-5 Peak discharges and times to peak as predicted by selected sediment transport equations (Case Study 4)**

| *Parameter/* **Model** | *Peak outflow ($m^3/s$)* | *Reference time to peak (s)* |
|---|---|---|
| **Measured outflow at breach opening** | 117 | 1446 |
| **MIKE 21C - Equation 5.2-5** | 123 | 1466 |
| **MIKE 21C - Equation 5.2-6** | 57 | 1397 |
| **MIKE 21C - Smart &** Jäeggi **(1983)** | 87 | 600 |
| **MIKE 21C - Camenen & Larson (2005)** | 123 | 1574 |

**Table 6.9-6 Sensitivity of the peak discharge to sediment transport equations and Manning's resistance coefficient (n) (adapted from Floodsite, 2011)**

| **Input Parameter** | **Input Parameter Range** | | | | | **% Variation from the Mean** | | |
|---|---|---|---|---|---|---|---|---|
| | | **Min** | **Max** | **Mean** | **Base** | **Min** | **Max** | **Range** |
| Sediment transport equation | - | 50 | 236 | 118 | 131 | -57.4 | 100.4 | 157.7 |
| Manning's resistance coefficient (n) | 0.020 – 0.045 | 115 | 146 | 132 | 131 | -12.7 | 10.1 | 22.7 |

**Table 6.9-7 Sensitivity of the peak discharge to sediment transport equations (this study)**

| Input Parameter | Input Parameter Range | | | | % Variation from the Mean | | |
|---|---|---|---|---|---|---|---|
| | | Min | Max | Mean | Min | Max | Range |
| Sediment transport equation | - | 57 | 123 | 118 | -52 | 4 | 56 |

For the current study, Equation 5.2-6 computed the breach outflow hydrograph to have a peak equal to 0.49 times the observed peak discharge. This means that Equation 5.2-6 and the Smart and Jäeggi (1983) sediment transport equation's ability to predict the breach outflow hydrograph for the given slope data is quite limited. Equation 5.2-6 was based on slopes between 25% and 40% whereas the Smart and Jäeggi (1983) sediment transport equation was derived from slope data up to 20%. The results highlight the influence of the selected sediment transport equation and the applicable bed slope or water surface slope on the computed peak discharge. Equations 5.2-5 and 5.2-6 were developed outside the applicable range of slope for this Case Study 4 and Table 6.9-7 is only aimed at checking if the application of sediment transport equations for steep slopes can reduce the percentage variation from the mean.

It is also common for different numerical models to predict varying times to peak and peak discharges as shown in Figure 6.9-5. Apart from the same numerical model simulating different peak discharges and times to peak when different equations are applied, different numerical models can also simulate different peak discharges and times to peak for an identical input dataset as can be observed in Figure 6.9-5. Figure 6.9-5 compares the outflow hydrographs that were simulated by different numerical models with the data from the field test of Case Study 4.

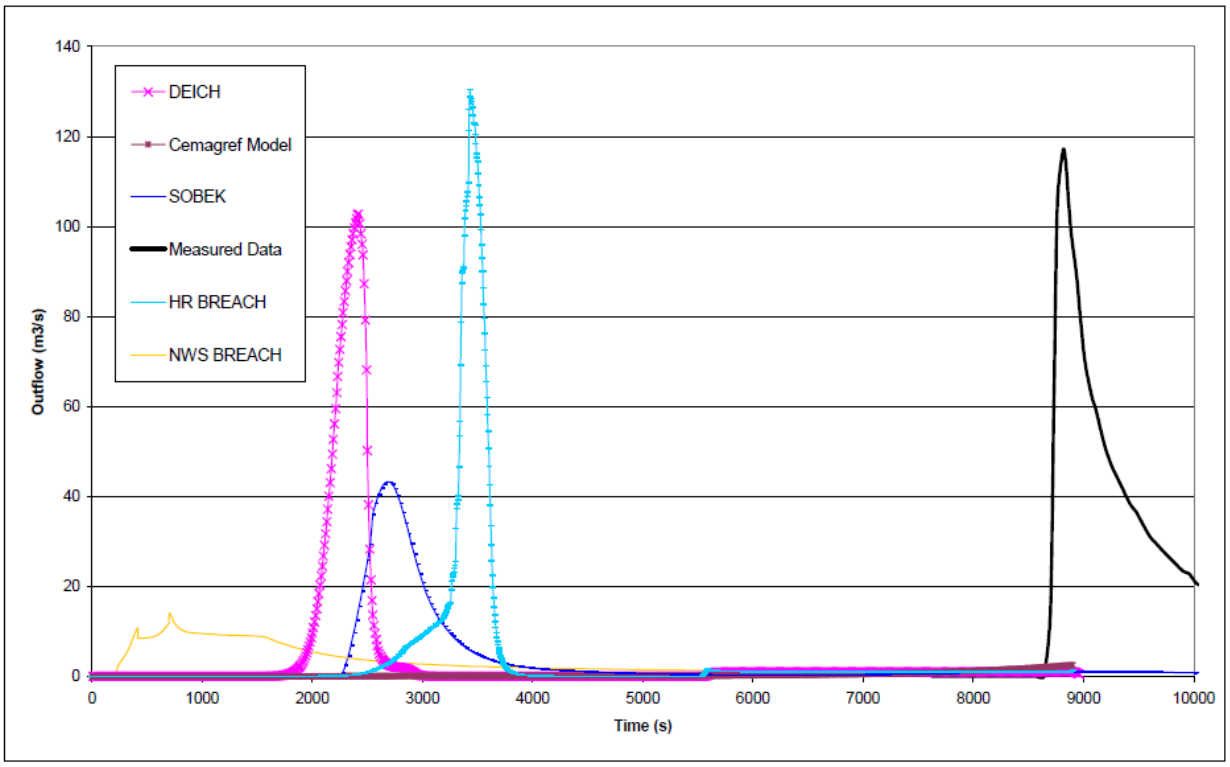


**Figure 6.9-5 Predicted outflow vs measured data for Case Study 4 of the Impact Project (Floodsite, 2011)**

The Impact Project study (Floodsite, 2011) pointed out that the accuracy of predicting the time to peak for different numerical models was found to be considerably worse than the prediction of peak discharge. This could explain why the Impact Study decided to consider only the peak discharge in the sensitivity analysis of the effects of Manning's resistance coefficient (n) and sediment transport equations.

The effects of the sediment transport equations for the current study on the final bed profile are shown in Figure 6.9-6. The Camenen & Larson (2005) sediment transport equation had the deepest final bed profile. The Smart & Jäeggi (1983) scoured a wavy final bed profile that is a typical characteristic of antidunes formation. The Equation 5.2-5 simulated final bed profile was located between the Equation 5.2-6 and Camenen & Larson (2005) sediment transport equation simulated bed profiles. The numerical model results show that the sediment transport equation does not only affect the peak discharge and time to peak but also the simulated final bed profile.

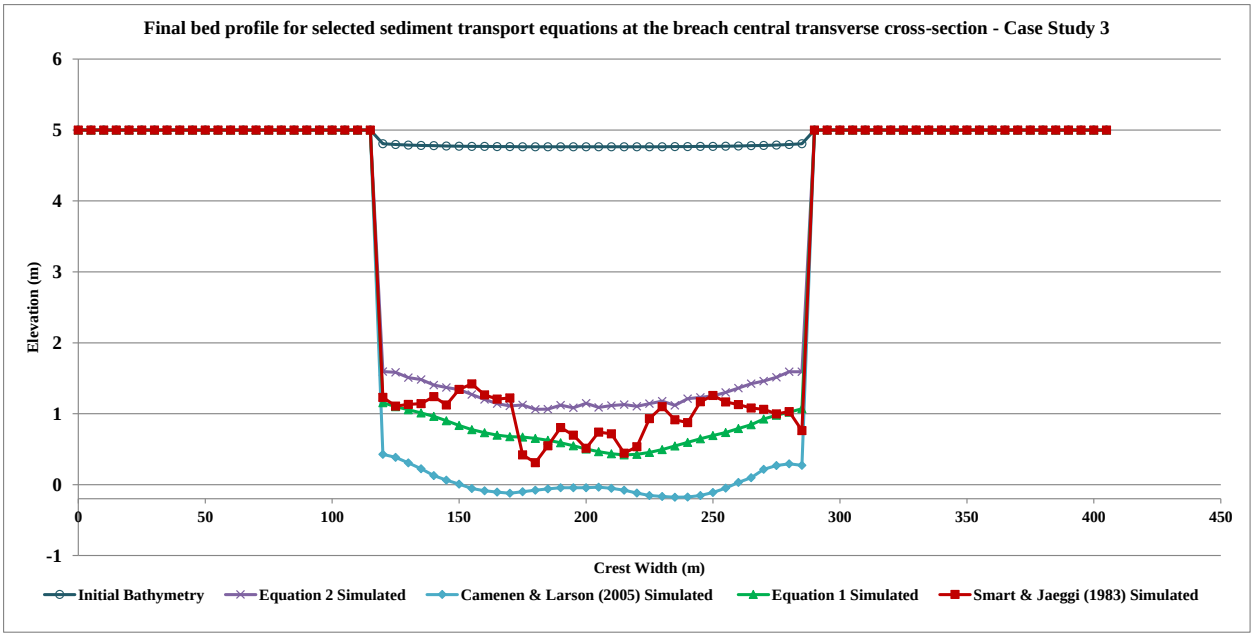


**Figure 6.9-6 Simulated final profiles using Equation 5.2-5, Equation 5.2-6, Smart & Jäeggi (1983) and Camenen & Larson (2005) sediment transport equations (Case Study 4)**

### *6.9.2 The sensitivity of the peak discharge to Manning's resistance coefficient (n) – Case Study 4*

The sensitivity to Manning's resistance coefficient (n) of the four sediment transport equations for Case Study 4 was examined using three selected Manning's resistance coefficient (n) values (Figures 6.9-7 to 6.9-10).

The Manning's resistance coefficient (n) in the base simulation was decreased by 12% (from 0.05 to 0.044) and increased by 10% (from 0.05 to 0.055). The most significant effect can be observed in Figure 6.9-9. When the resistance was decreased from 0.05 to 0.044, the peak discharged predicted by Camenen & Larson (2005) increased from 123 to 132 $m^3/s$ (representing a 7% increase in peak discharge). The numerical model results show that the peak discharge and time to peak are sensitive to both the specified sediment transport equation and the resistance values.

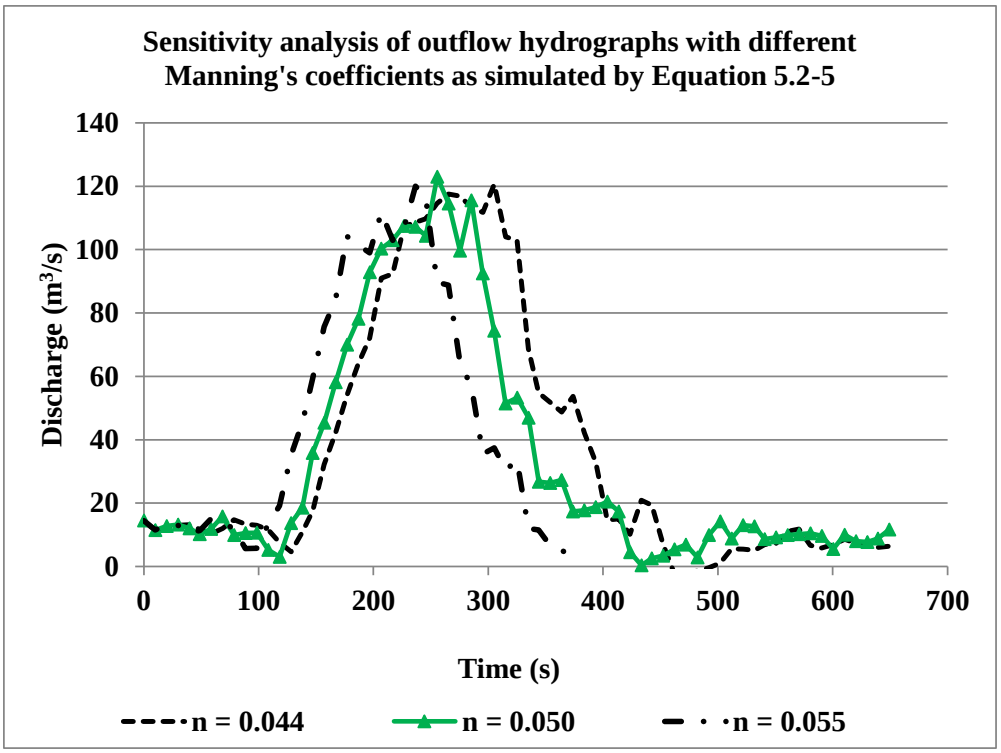


**Figure 6.9-7 Sensitivity analysis: Equation 5.2-5 - Case Study 4**

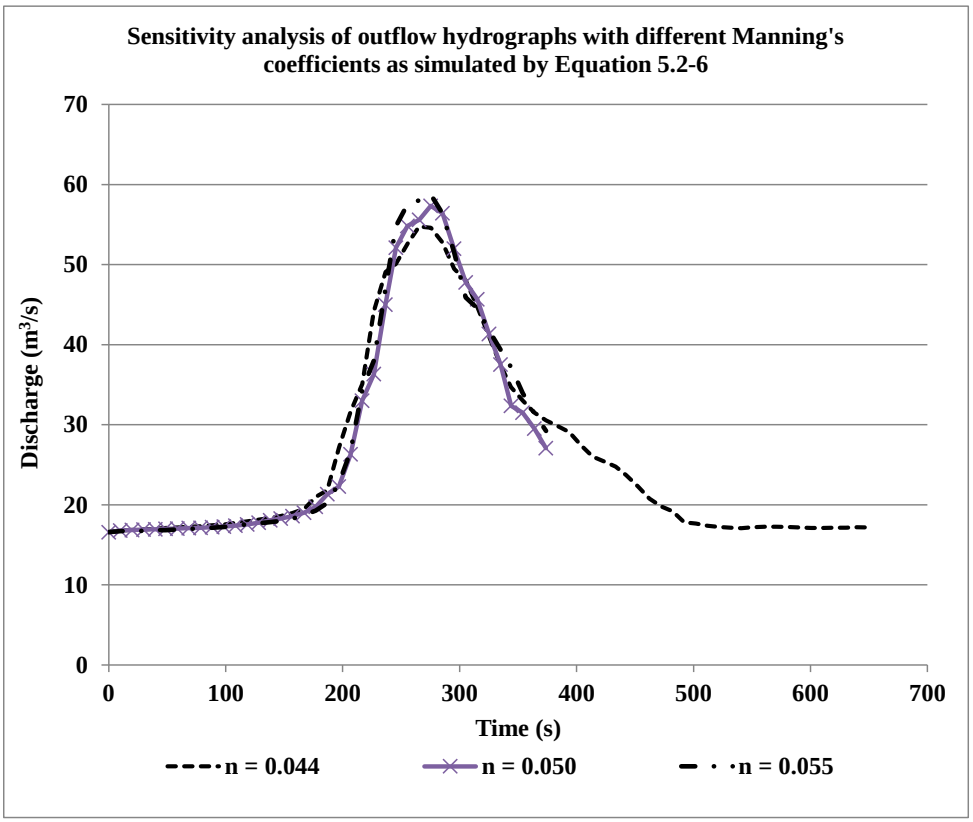


**Figure 6.9-8 Sensitivity analysis: Equation 5.2-6 - Case Study 4**

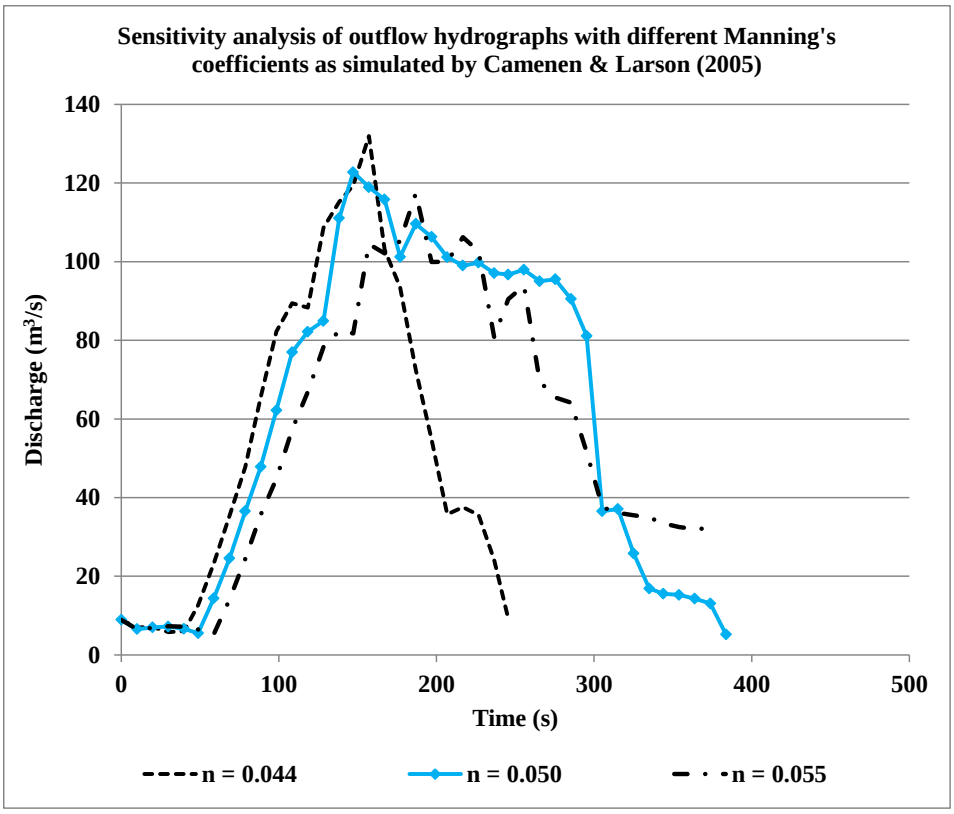


**Figure 6.9-9 Sensitivity analysis: Camenen & Larson (2005) - Case Study 4**

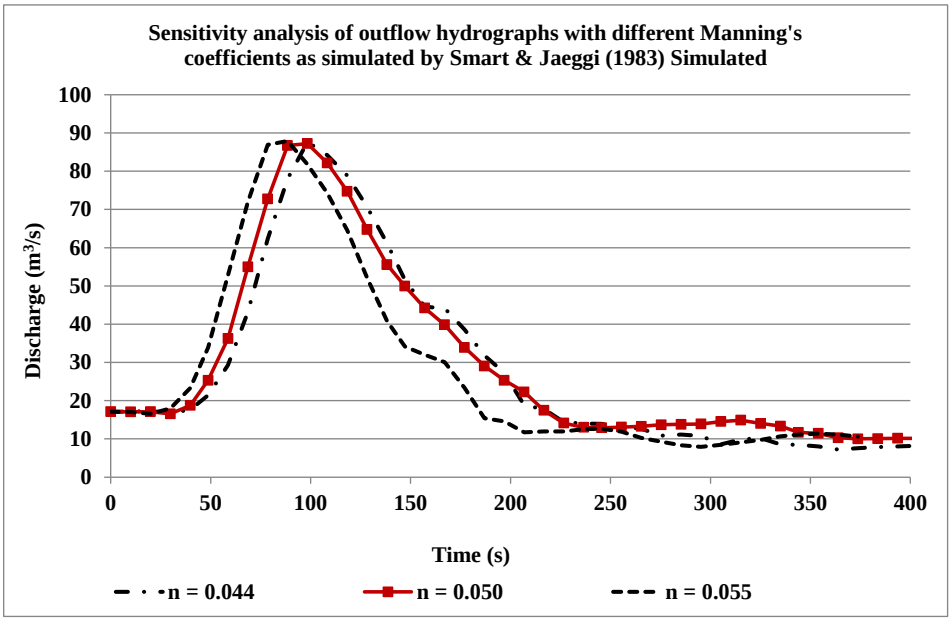


**Figure 6.9-10 Sensitivity analysis: Smart and Jäeggi (1983) - Case Study 4**

## 6.10 Case Study 5

As there is very limited observed prototype data from large historical dam-break case studies, a hypothetical large dam and its reservoir were simulated to assess the sensitivity of breach modelling to the selection of sediment transport equations and hydraulic roughness. The dam was assumed to have a height of 50 m, a crest length of 475 m and a top crest width of 4 m. The reservoir volume at full supply level was assumed to be $5.2\times10^6$ $m^3$. The downstream valley that was taken as part of the floodplain computational area was assumed to be 2 km long and 475 m wide (rectangular) with a 50 m wide and 5 m deep main channel in the middle. The slopes of the upstream and downstream embankment faces were both assumed to be 1:3 (V:H). Figure 6.10-1 shows the longitudinal profile of the hypothetical large dam and its floodplain. The embankment was assumed to be constructed of non-cohesive sediment (sand) of median ($d_{50}$) diameter of 2 mm.

The aim of this hypothetical study was to assess the predictions of Equations 5.2-5 and 5.2-6 and to conduct a comparison with the results for the Smart & Jäeggi (1983) and Camenen & Larson (2005) sediment transport equations at two selected locations (i.e. at the breach opening and 1.85 km from the breach opening).

For the numerical simulation, a rectangular grid with one thousand three hundred (1300) grid cells in the direction of flow and one hundred (100) grid cells across was set up. The grid sizes were 2 m in the longitudinal direction and 5 m in the transverse cross-section direction (2 m by 5 m each). Initial overtopping was assumed to occur at the middle 150 m of the crest of the dam. The upstream boundary was specified as a source point of a constant inflow discharge of a hundred (100) $m^3/s$. For the downstream boundary, a rating curve (Q-h boundary) was specified based on normal depth for automatic computation of flow depth. Figure 6.10-2 shows the initial bathymetry of the hypothetical long dam and its floodplain.

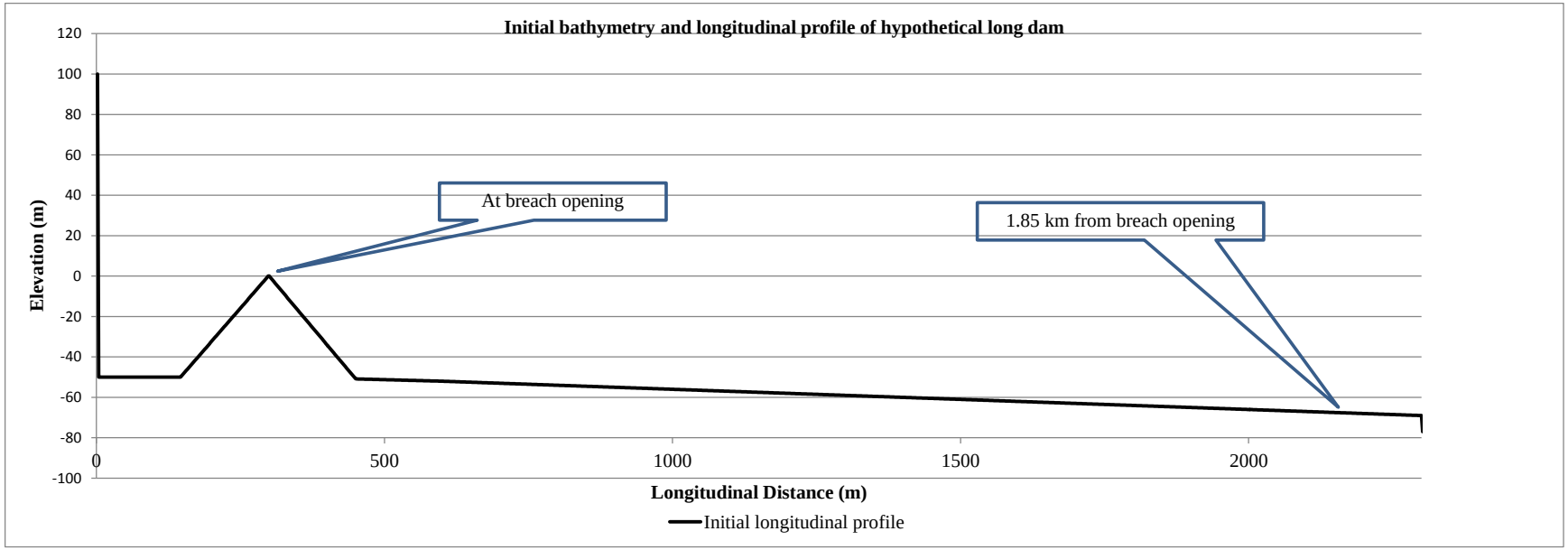


**Figure 6.10-1 Longitudinal profile of the hypothetical long dam - Case Study 5**

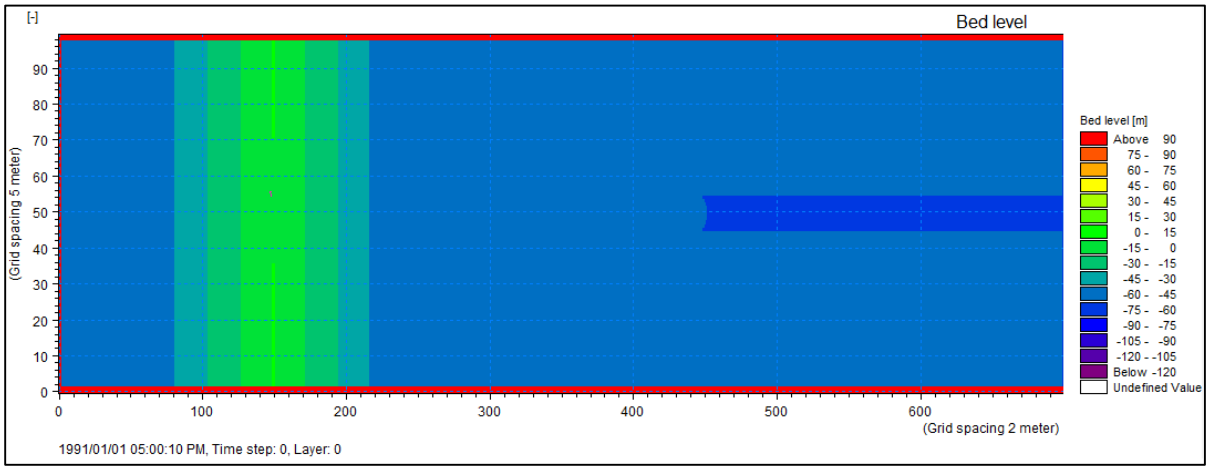


**Figure 6.10-2 Initial bathymetry of the hypothetical long dam - Case Study 5**

Since there is no comparative observed or measured data for calibration, hydrodynamic and morphological parameters given in Table 6.10-1 and 6.10-2 respectively were applied based on typical values from previous case studies in this report apart from the flooding and drying depths that were obtained from worked examples in literature (DHI, 2011).

**Table 6.10-1 Calibrated model setup parameters – hydrodynamics (Case Study 5)**

| Hydrodynamic Parameter | Value |
|---|---|
| Hydrodynamic time step (s) | 0.01 |
| Morphological time step (s) | 0.02 |
| Flooding depth (m) | 0.03 |
| Drying depth (m) | 0.02 |
| Manning's resistance coefficient (n) | 0.045 |

**Table 6.10-2 Calibrated model setup parameters – morphology (Case Study 5)**

| Morphological Parameter | Value |
|---|---|
| Median ($d_{50}$) grain diameter (mm) | 2 |
| Eddy viscosity ($m^2/s$) | Smagorinsky Formula – Velocity Based Constant – 0.5 |
| Mass density of sediment ($kg/m^3$) | 2650 |
| Porosity (Ratio) | 0.33 |
| Critical shields' parameter | 0.047 |
| Transverse slope coefficient | 0.6 |
| Transverse slope power | 0.5 |
| Longitudinal slope coefficient | 1 |

### *6.10.1 Analysis of numerical simulation results – Case Study 5*

The analysis of the numerical simulation results was limited to the peak discharge and outflow volume. The results in Figure 6.10-3 illustrate the effect of the sediment transport equation on the shape and peak of the outflow hydrograph. The simulated peak discharges and outflow volumes from the breach opening for each of the four sediment transport equations is given in Table 6.10-3. The results in Table 6.10-3 show good agreement between the predicted peak discharges by Equation 5.2-6 and Smart and Jäeggi (1983) sediment transport equation. This is contrary to the observed trends for Case Studies 1 and 2 that showed significant disparities between the two equations. This could be due to the possibility that at a large prototype scale, the effects of the sediment transport equations become compensated.

**Table 6.10-3 Predicted peak discharge at the breach opening by each of the four sediment transport equations**

| Sediment Transport Equation | Peak discharge ($m^3/s$) | Outflow volume ($10^6\ m^3$) |
|---|---|---|
| Equation 5.2-5 | 8130 | 2.271 |
| Equation 5.2-6 | 7618 | 1.893 |
| Smart & Jäeggi (1983) | 7543 | 2.250 |
| Camenen & Larson (2005) | 3832 | 2.225 |

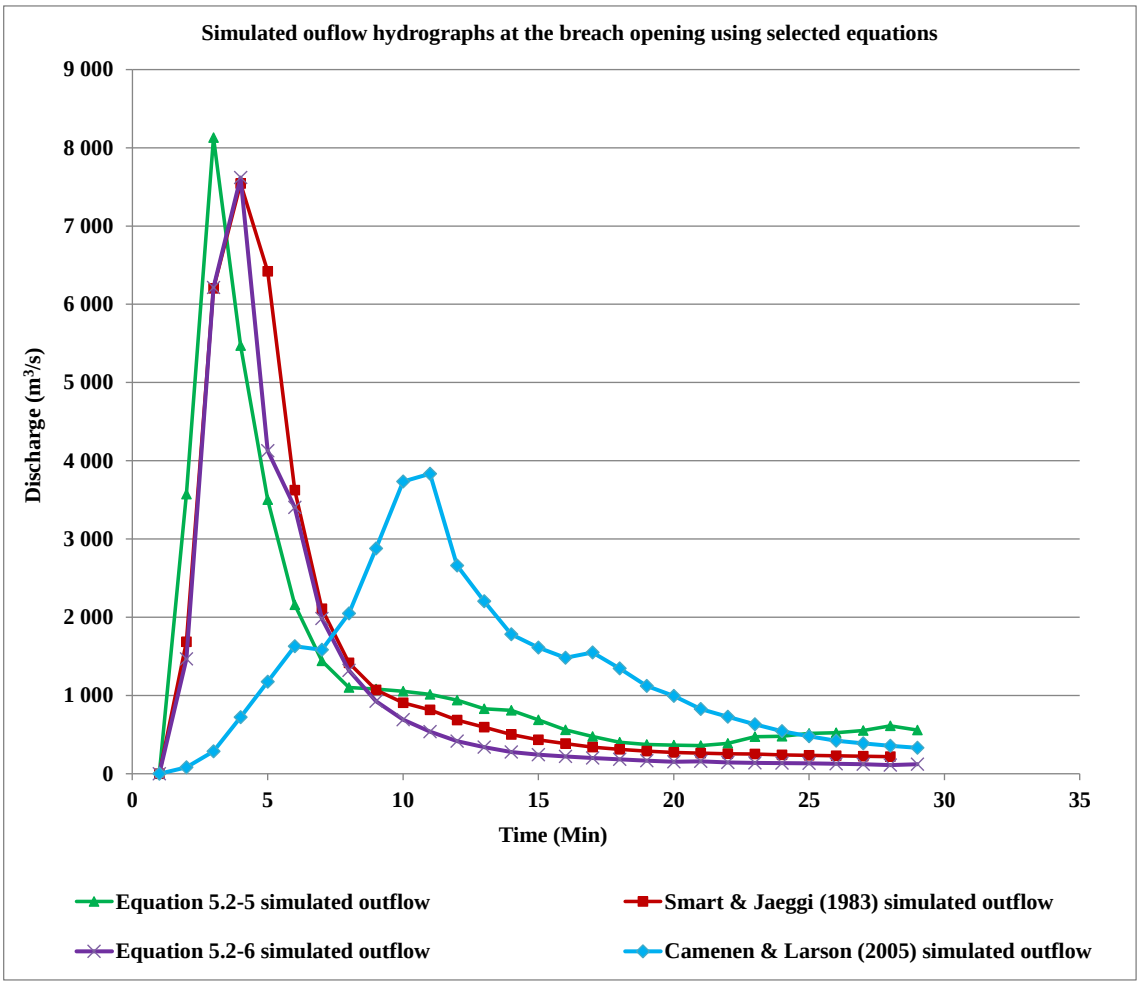


**Figure 6.10-3 Simulated outflow hydrograph at the breach opening for a constant inflow of 100 $m^3/s$ – Case Study 5**

In order to evaluate the realism of the results in Table 6.10-3, the results of the predicted peak discharge were compared with the estimated peak discharge using empirical equations from literature. Even though empirical equations are a conservative way of predicting dam-break characteristics, they are a better alternative in the absence of observed data. It could have been better to also compare the numerical model results with output results from other simpler methods of dam-break analysis such as the one-dimensional MIKE 11 numerical model, but this was not possible due to study time constraints. Empirical equations that provide envelope values were used instead. These empirical equations were: Hagen (1982) and Broich (1998). Hagen (1982) plotted the relationship between peak discharge ($Q_P$) and the product of reservoir storage volume (S) and dam height ($h_d$). Broich (1998) obtained a regression equation that gave the relationship between peak discharge ($Q_P$) to the depth of water ($h_w$) and volume of water ($V_w$) in the reservoir at the initial failure time. The two empirical equations were applied because they provide the upper limit envelope values for the peak discharge. The empirical equations are as follows:

$$Q_P = 0.54(h_d S)^{0.5} \qquad \text{Hagen (1982)} \qquad 6.10\text{-}1$$

$$Q_P = 72.611(V_w h_w^4)^{0.256} \qquad \text{Broich (1998)} \qquad 6.10\text{-}2$$

Where

$h_d$ Dam height

$h_w$ Water depth in the reservoir initiating failure

S Reservoir storage volume

$V_w$ Volume of water (in $10^6$ $m^3$)

The peak discharge predictions using the two empirical equations based on the dam characteristics for Case Study 5 are given in Table 6.10-4.

**Table 6.10-4 Peak discharge estimation using empirical equations**

| **Equation** | **Peak discharge ($m^3/s$)** |
|---|---|
| Hagen (1982) | 8752 |
| Broich (1998) | 6087 |

The peak discharges at the breach that were predicted by Equations 5.2-5 & 5.2-6 and Smart & Jäeggi (1983) sediment transport equation were found to be within the expected envelope values

from empirical predictor equations 6.10-1 and 6.10-2. Based on the given envelope values, Camenen & Larson (2005) underestimated the peak discharge.

Peak discharges and outflow hydrographs were also determined for a location 1.85 km downstream of the breach. Figure 6.10-4 shows the simulated peak discharges and outflow volumes 1.85 km downstream from the breach opening and Table 6.10-5 shows the simulated peak discharges and outflow volumes for each of the four sediment transport equations. Equation 5.2-5 (which predicted the highest peak at the breach opening) exhibited the highest peak at a location 1.85 km from the breach opening. The results show that although the predicted downstream flood peak were attenuated, the predicted peak discharges at the breach opening determined the probable peak discharges at the specific locations downstream of the embankment.

**Table 6.10-5 Predicted peak discharges by each of the four sediment transport equations at 1.85 km from the breach opening**

| **Sediment Transport Equation** | **Peak discharge ($m^3/s$)** | **Outflow volume ($10^6\ m^3$)** |
|---|---|---|
| Equation 5.2-5 | 5282 | 2.190 |
| Equation 5.2-6 | 3045 | 1.882 |
| Smart & Jäeggi (1983) | 3414 | 2.050 |
| Camenen & Larson (2005) | 2444 | 2.095 |

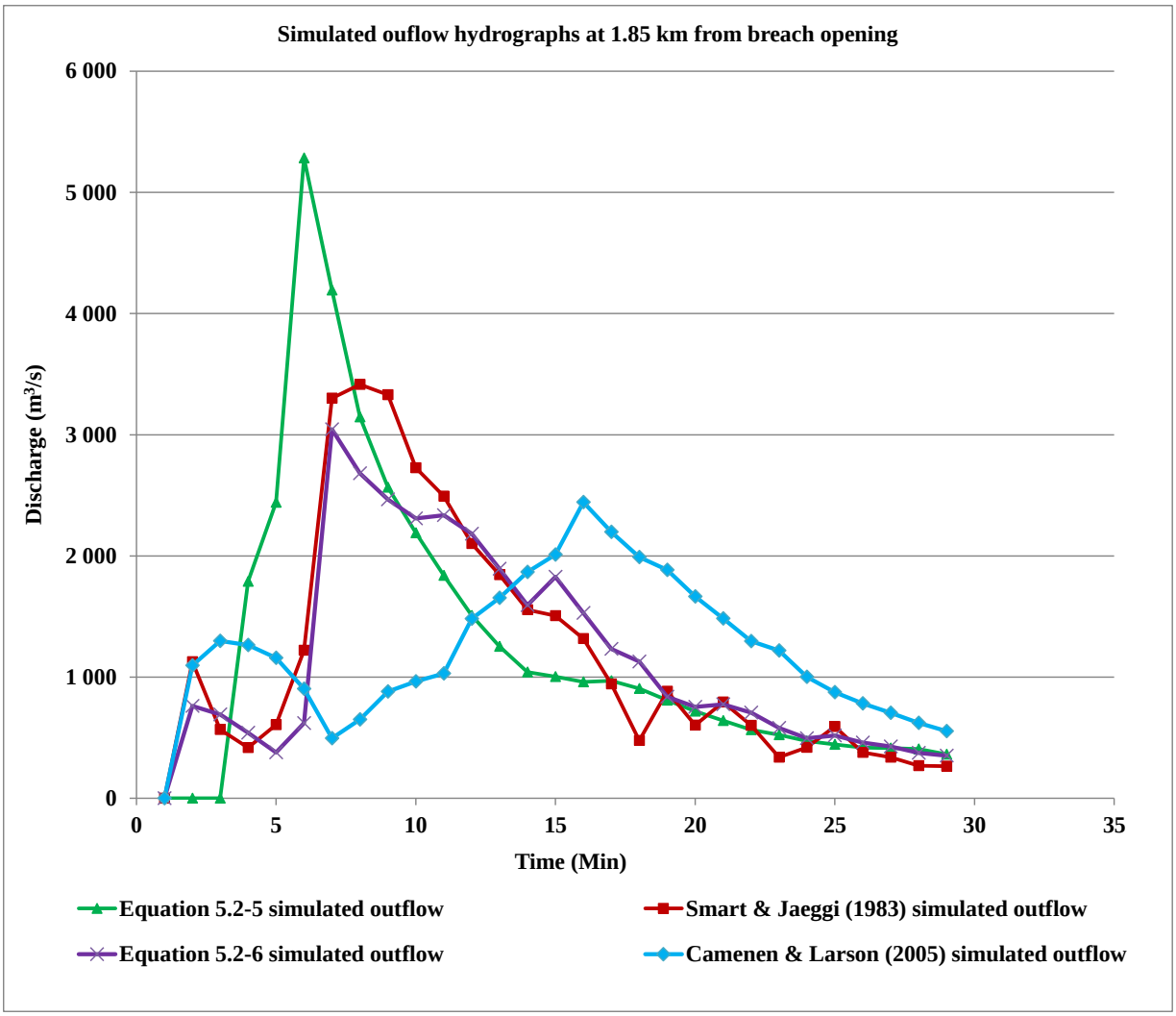


**Figure 6.10-4 Simulated outflow hydrographs at 1.85 km from the breach opening – Case Study 5**

The effect of the sediment transport equation on the final bed profile at the breach is shown in Figure 6.10-5. It was found that even though the Camenen & Larson (2005) predicted the lowest peak discharge, the final bed profile was similar to the bed profile simulated by Equation 5.2-5 which simulated the highest peak discharge. The deepest bed profile was predicted by the Smart & Jäeggi (1983) sediment transport equation while the lowest profile was predicted by Equation 5.2-6. It is evident that the predicted final bed profile is not directly related to the greatest peak discharge. For instance, Smart & Jäeggi (1983) scoured a deeper final bed profile than Equation 5.2-5 despite having a lower peak discharge. This is due to the fact that the peak discharge is related to the breach invert and water level at peak and not necessarily the final bed profile.

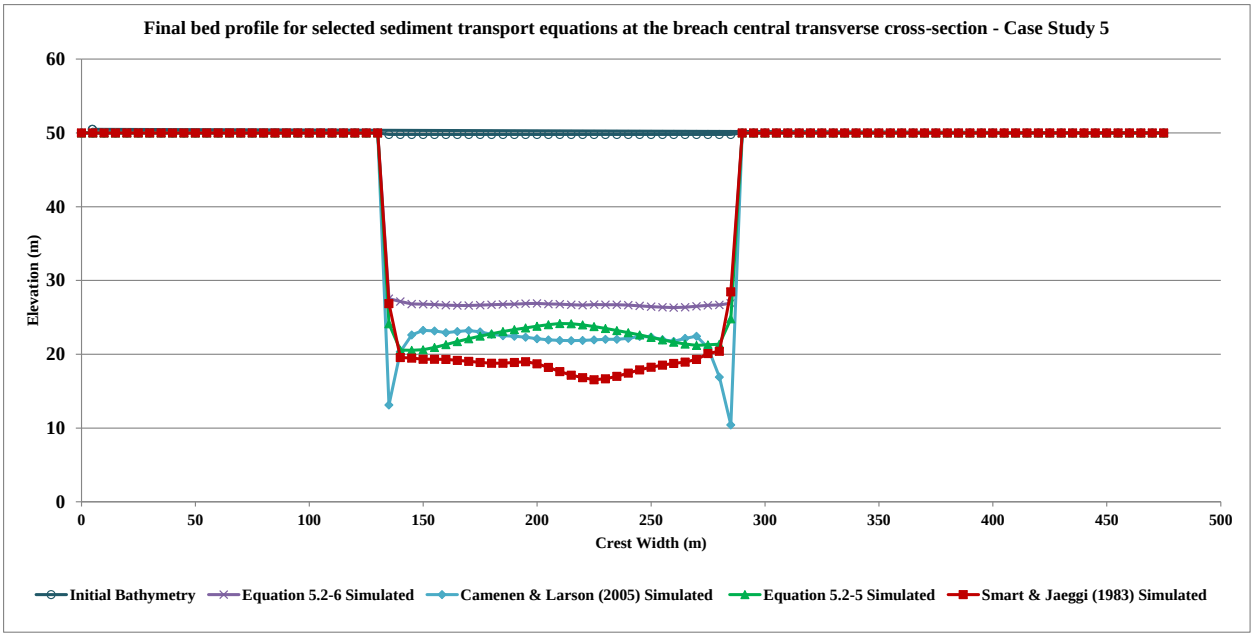


**Figure 6.10-5 Simulated final profiles using Equation 5.2-5, Equation 5.2-6, Smart & Jäeggi (1983) and Camenen & Larson (2005) sediment transport equations – Case Study 5**

## 6.11 Summary

The application of Equations 5.2-5 and 5.2-6 was demonstrated in dam-break modelling using five case studies. The performance of Equations 5.2-5 and 5.2-6 was assessed through a comparative analysis of the measured and predicted model output parameters for the two calibrated equations with two other sediment transport equations from literature, namely; Smart & Jäeggi (1983) and Camenen & Larson (2005). The application focused on the ability of the sediment transport equations to predict the following model output parameters: longitudinal and transverse bed profiles at the breach opening, peak discharge, time to peak and outflow volume.

The longitudinal bed profiles predicted by the four sediment transport equations for Case Study 1 showed different simulated temporal bed profiles for each equation. The measured temporal bed profiles in Case Study 1 were well reproduced by the newly calibrated sediment transport equations (Equations 5.2-5 and 5.2-6) and the Camenen & Larson (2005) sediment transport equation especially at the early breach depths of 0.05 m and 0.10 m.

In Case Study 2, the final breach dimension was well predicted by the newly calibrated sediment transport equations (Equations 5.2-5 and 5.2-6).

An assessment of the level of uncertainty due to the input of sediment transport equations showed that sediment transport equations have a particular range of best applicability with respect to slope data as evidenced by the failure by all four sediment transport equations to reproduce the peak discharge and times to peak in Case Studies 3 and 4.

The percentage slope of 60% in both Case Studies 3 and 4 was outside the calibration range for all the four sediment transport equations.

The agreement between simulated peak discharges in Case Study 5 and computed envelope peak discharge values using empirical formulations showed that the simulated model output results were generally reasonable.

It can be concluded that the newly calibrated equations (Equations 5.2-5 and 5.2-6) can be applied in the dam-break numerical simulation of peak discharge, flood volume and breach dimensions but could be limited in the prediction of time to peak or failure.

The Manning's resistance coefficient (n) had a marked effect on the peak discharge of the outflow hydrographs. Generally, the trend in the four case studies where sensitivity analysis of resistance was assessed showed that, for a higher Manning's resistance coefficient (n) in the numerical model, a lower peak discharge was observed while a high peak discharge was simulated for low Manning's resistance coefficients (n). The results showed that the numerical model output parameters were influenced by the combined effect of the sediment transport equations and the Manning's resistance coefficients (n).

Table 6.11-1 shows the final calibrated Manning's resistance coefficient (n) and the corresponding recommended sediment transport equation(s) for each case study.

**Table 6.11-1 Sensitivity analysis results**

| Case Study | Percentage slope on downstream embankment | Manning's resistance coefficient (n) | Recommended sediment transport equation (s) | Remarks |
|---|---|---|---|---|
| 1 | 33% (1V : 3H) | 0.040 | Equations 5.2-5 & 5.2-6 and Camenen & Larson (2005) | - |
| 2 | 33% (1V : 3H) | 0.040 | Equation 5.2-5 and 5.2-6 | - |
| 3 | 59% (1V : 1.7H) | 0.044 | None | Percentage slope outside calibration range – all sediment transport equations are not directly applicable |

| | | | | |
|---|---|---|---|---|
| 4 | 59% (1V : 1.7H) | 0.050 | None | Percentage slope outside calibration range – all sediment transport equations are not directly applicable |
| 5 | 33% (1V : 3H) | 0.045 | Equation 5.2-5, Equation 5.2-6 and Smart and Jäeggi (1983) | Smart and Jäeggi (1983) was derived on slope data up to 20% but performed better in this case study |

# CHAPTER 7 CONCLUSION AND DISCUSSION

High uncertainty in the prediction of output parameters in physically-based dam-break modelling is mainly due to the choice and formulation of the sediment transport equations. The application of different sediment transport equations can give model output parameters that differ by several orders of magnitude. Moreover, the uncertainty due to the choice of sediment transport equations is high in comparison to the uncertainty that is attributed to other input parameters such as bed roughness or resistance, eddy viscosity and angle of repose.

Dam-break floods are characterised by transport of sediment on very steep slopes up to 60%. Commonly used sediment transport equations in dam-break modelling were derived from data on mild and moderately steep slopes of up to 20%. The application of sediment transport equations that were calibrated on similar or comparative steep slopes has the potential to improve the prediction of sediment transport rates and reduce uncertainty in dam-break modelling.

The main focus of this dissertation was to develop empirical sediment transport equations for homogeneous earth dam-break analysis due to overtopping failure and to assess the levels of uncertainty that is associated with the sediment transport equations. The specific objectives were:

- To derive new empirical sediment transport equations for application in dam-break modelling on steep slopes
- To conduct an analytical comparison of the performance of the newly calibrated sediment transport equation against existing sediment transport equations from literature
- To evaluate the performance of the newly calibrated sediment transport equation in a dam-break numerical model and to compare the model output results with predictions by selected sediment transport equations from literature as well as to analyse the sensitivity of model output results to the application of the sediment transport equations.

The specific objectives were achieved and the main contribution of the research work that is presented in this dissertation is the determination of new calibrated sediment transport equations from steep slope data and the successful application of the equations in a physically-based dam-break numerical model.

Experimental studies were conducted in a laboratory flume and sediment transport rates were measured. In order to determine whether a sediment transport rate calculated by a selected sediment transport equation was practical or not, it was necessary to consider the corresponding flow. By converting sediment transport rates into concentrations, it was found that the applicability of a sediment transport equation could be judged by the practicality of the predicted concentrations at the unit discharges under consideration. The judgment of the applicability and sensitivity of the sediment transport equation should be done on a case by case basis with regard to the predicted concentration ranges in comparison to the amount of sediment that a particular

unit discharge can reasonably transport. This approach was applied in the assessment of the reasonableness of the predicted sediment transport concentrations.

The data from the experimental study was used to derive sediment transport equations. Four sediment transport formulations were investigated. The proposed sediment transport equations predict sediment transport rates as a function of particle sizes of the sample for which 30 and 90% were finer ($d_{30}$ and $d_{90}$); shear velocity, average flow velocity, friction slope, dimensionless shear stress and critical dimensionless shear stress. The validity and statistical significance of the newly calibrated sediment transport equations was confirmed using statistical test methods and the degree of correlation between measured and predicted sediment transport rates.

The proposed sediment transport equations provided satisfactorily predictions with a deviation of less than 22% between the measured and predicted sediment transport rates. Two newly calibrated sediment transport equations (Equations 5.2-5 and 5.2-6) were found to have better predictive capabilities out of the four formulations that were investigated. The analytical comparison showed that the sediment transport predictions by the newly calibrated sediment transport equations (Equation 5.2-6) were within the same order of magnitude as those of Meyer-Peter Müller (1948) and Camenen & Larson (2005) sediment transport equations even though the Meyer-Peter Müller (1948) equation overestimated sediment transport rates for higher unit discharges. The Smart and Jäeggi (1983) sediment transport equation predicted higher sediment transport rates in comparison to the measured sediment transport rates and those predicted by Equation 5.2-6.

The MIKE 21C numerical model was appplied to evaluate and compare the performance of the newly calibrated sediment transport equations in dam-break modelling using five dam-break case studies. The simulated results using the newly calibrated sediment transport equations (Equations 5.2-5 and 5.2-6) were compared with those predicted by two selected sediment transport equations from literature, namely Camenen & Larson (2005) and Smart & Jäeggi (1983). The embankment slopes for three case studies (Case Studies 1, 2 and 5) were within the slope data calibration range of the newly calibrated sediment transport equations but outside the calibration data range of the selected sediment transport equations from literature, namely Camenen & Larson (2005) and Smart and Jäeggi (1983). Embankment slopes for two case studies (Case Studies 3 & 4) were outside the calibration range of all the four sediment transport equations (Equations 5.2-5 and 5.2-6, Camenen & Larson (2005) and Smart and Jäeggi (1983)). Case Study 1 was applied to analyse the performance of the sediment transport equations by analysing temporal bed level changes. Case Study 2 investigated the effect of the sediment transport equation on the breach shape. Case Studies 3 & 4 investigated the numerical modelling of dam-break outflow hydrographs for very steep slopes. Case Study 5 analysed the effect of the sediment transport on the simulated peak discharge and outflow volume. The newly calibrated sediment transport equations appeared to perform better in all the applicable case studies (Case Studies 1, 2 and 5). To some extent, Camenen & Larson (2005) and Smart & Jäeggi (1983) sediment transport equations performed better in Case Studies 1 and 5 respectively. Consistent

and realistic predictions of numerical model output parameters were not possible when the sediment transport equations were applied to the two case studies with embankment slopes outside the recommended applicability range.

Model uncertainty to the input of sediment transport equations was assessed through sensitivity analysis by comparing model output results for the four sediment transport equations (Equation 5.2-5, Equation 5.2-6, Camenen & Larson (2005) and Smart and Jäeggi (1983)). The results from the numerical simulations can assist in understanding the level of variability of the model output results due to the application of different sediment transport equations. The results can be used to determine probable scenarios for output parameters such as peak discharge and flood water volumes.

Equations 5.2-5 and 5.1-6 are alternatives to the existing sediment transport equations in dam-break modelling considering that these two newly calibrated sediment transport equations were calibrated from steep slope data that are typical for on earth embankment dams. Nevertheless, any sediment transport equation that is to be applied to dam-break numerical modelling requires sensitivity analyses with the model output parameters in order to determine other possible scenarios. Professional judgment in the analysis of sensitivity, in particular with respect to the application of sediment transport equations, should always prevail. For instance, the predicted peak discharge by Equation 5.2-6 was in close agreement with the predicted peak discharge by Smart and Jäeggi (1983) for the same case study even though the two equations were derived from different slope range data. In that scenario, each sediment transport equation could have different predictive capabilities and limitations depending on the given input parameters and model configurations.

The study findings do not intend to invalidate the existing sediment transport equations but to highlight the importance of applying equations within their recommended applicability range and of comparing the results of two or three sediment transport equations. The comparison of the results can provide medium or worst case scenarios in the model output parameters such as outflow hydrograph peak, time to peak and outflow volumes. This information is crucial in dam safety planning, and for the development of early warning systems and disaster preparedness plans.

# CHAPTER 8 RECOMMENDATIONS

The sensitivity of sediment transport predictions to the equations and resistance coefficients that are applied in dam-break modelling were investigated for homogeneous earth dams only. Further studies are needed to analyse the effects of sediment transport dynamics on zoned embankments and complex embankment structures. Future sensitivity analyses need to investigate the effect of other sediment transport parameters such as soil mechanics and erodibility on the breaching processes and the effects of including or not including sediment shape parameter in the formulation of sediment transport equations. Earth dams are typically not homogeneous, but consists of a clay/non permeable core, as well as non-cohesive sediment. The application of sediment transport equations for non-cohesive sediment gives conservative estimates of sediment transport rates. The sediment transport equations were derived for non-cohesive soils and their applicability in cohesive construction material in non-homogeneous dams needs further evaluation.

The case studies for this study were limited to overtopping dam-break analysis of the whole or part of the embankment of earth dams. Future studies could investigate the application of the newly developed sediment transport equations for steep slopes in the numerical modelling of laboratory and field scale fuse plug spillway breaching.

Only a single numerical model was used for the simulations during the study, and some of the observed phenomenon could be due to the specific intrinsic properties of the modelling tool (MIKE 21C) that was applied. Another numerical model, preferably a three dimensional model could be used in the future to determine whether the observed phenomenon could be more accurately replicated.

# REFERENCES


1. Abderrezzak, KEK and Paquier, A. 2011. A*pplicability of sediment transport capacity formulas to dam-break flows over movable bed,* Journal of Hydraulic Engineering, ASCE / February 2011 / 209.
2. Abrahams, A. 2003. *Bed-load transport equation for sheet flow*, J. Hydraulic. Eng., 129(2), 159–163.
3. Ackers, P and White, WR. 1973. S*ediment transport: new approach and analysis*, Journal of the Hydraulic Division, ASCE, 99(HY11), 2041-2060.
4. Bagnold, RA. 1966. *An approach to the sediment transport problem from general physics*, USGS Professional Paper, 442-I, U.S. Gov. Print. Office, Washington, DC.
5. Bai, YC Xu, D Wang, YG and Zhang, MT. 2005. *2-D numerical simulation for water flow and sediment transport of dam-break wave*, ShuiLi XueBao 2005; 36(5):1–9 (In Chinese).
6. Basson, GR. 1999. *Development of a new sediment transport equation based on applied stream power,* River Sedimentation: Theory and Applications, Balkema, Rotterdam, Netherlands.
7. Beck, J. 2005. *Sediment transport dynamics in South African estuaries*, PhD Thesis, Sunscholar, University of Stellenbosch
8. Biscarini, C Di Francesco, S and Manciola, P. 2010. *CFD modelling approach for dam-break flow studies*, Hydrol. And Earth Syst. Sci., 14, 705–718, 2010, Online, viewed 14 September 2012, www.hydrol-earth-syst-sci.net/14/705/2010
9. Broere, D. 1999. *Breach erosion of earth dams*, Ms Dissertation, TU Delft
10. Broich, K. 1998. *Mathematical modelling of dam-break erosion caused by overtopping*, Proceedings of the 2nd CADAM workshop, Munich, 1998.
11. Brown, C. 1950. *Sediment transportation*, Engineering Hydraulics pp. 769–857.
12. Brown, RJ and Rogers, DC. 1981. *User's manual for program BRDAM*, US Bureau of Reclamation, Denver, Colorado.
13. Camenen, B and Larson, M. 2005. *A general equation for non-cohesive bed load sediment transport*, Estuarine Coastal Shelf *Sci.*, 63(1–2), 249–260.

14. Chen, YH and Anderson, BA. 1987. *Development of a methodology for estimating embankment damage due to flood overtopping*, Report No. FHWA RD-86/126, Federal Highway Administration, US Department of Transportation.
15. Cheng, NS. 1997. *Simplified settling velocity equation for sediment particle*, Journal of Hydraulic Engineering, ASCE, Vol. 123, No. 2, pp 149 - 1?2.
16. Cheng, NS. 2002. *Exponential formula for bed load transport*, J. Hydraul. Eng., 128(10), 942–946.
17. Costa, JE. 1985. *Floods from dam failures*, Open-file report, U.S. Department of the Interior Geological Survey, Denver, USA.
18. Cristofano, EA. 1965. *Method of computing rate of failure of earth-fill dams*, Bureau of Reclamation, Denver, Colorado.
19. DH1. 2011. *User Manual*, MIKE 21C and MIKE 11.
20. Dou, XP Li, TL and Dou, GR. 1999. *Numerical model of total sediment transport in the Yangtze Estuary*, Chin Ocean Eng., 1999; 13(3):277–86.
21. Du Boys, MP. 1879. *Etudes du r´egime du Rh^one et de laction exerc´ee par le eaux sur un lit `a fond de graviers ind´efiniment affouillable*, Annales des Ponts et Chauss´ees 5(18), 141–195.
22. Einstein, HA. 1942. *Formulas for the transportation of bed load*, ASCE Transactions 107, pp. 561-573.
23. Engelund, F and Hansen, E. 1967. *A monograph on sediment transport in alluvial streams*, Teknisk Forlag, Copenhagen, Denmark.
24. Engelund, F. and Hansen, E. 1972. *A Monograph on sediment transport in Alluvial Streams*, Teknish Forlag, Copenhagen.
25. Evans, SG. 1986. *The maximum discharge of outburst floods caused by the breaching of man-made and natural dams*, Can. Geotech. Journal, 23(3), 385–387.
26. Exner, FM. 1925. *On the interaction between water and sediment in rivers*, Acad. Wissenscaften Wien Math. Naturwiss.
27. Faeh, R. 2007. *Numerical modelling of breach erosion of river embankments*, Journal of Hydraulic Engineering (1002) ASCE / September 2007.
28. Floodsite. 2011. *Workshop on International Progress in Dam Breach Evaluation*, held at the Annual Conference of the Association of State Dam Safety Officials 2004 Dam Safety,

Phoenix, http://www.floodsite.net/html/search_results.asp?documentType (online accessed on 10 September 2011).

29. Fread, DL. 1984. *DAMBRK: The NWS dam-break flood forecasting Model*, National Oceanic and Atmospheric Administration, National Weather Service, Silver Spring, MD.
30. Fread, DL. 1988. *BREACH: an erosion model for earthen dam failures*, Hydrologic Research Laboratory, National Weather Service, NOAA.
31. Fread, DL. 1991. *BREACH, An erosion model for earthen dam failures*, Revision 1, August 1991, Online, viewed 1 November 2012 http://www.nws.noaa.gov/oh/hrl/rvrmech/documentation/breach.pdf.
32. Froehlich, DC. 1995a. *Peak outflow from breached embankment dam*, Journal of Water Resources Planning and Management, Vol. 121, no. 1, p. 90-97.
33. Froehlich, DC. 1995b. *Embankment dam breach parameters revisited*, In Water Resources Engineering, Proceedings of the 1995 ASCE Conference on Water Resources Engineering, San Antonio, Texas, August 14-18, 1995, p. 887-891.
34. Gee, DM. 2010. *Use of breach process models to estimate, HEC-RAS dam breach parameters*, Corps of Engineers Hydrologic Engineering Centre, 609 2nd St., Davis, CA.
35. Gomez, B and Church, M. 1989. *An assessment of bed load sediment transport formulae for gravel bed rivers*, Water Resources Research, 25-6, 1161–1186.
36. Guo, J. 1997. *The Albert Shields story*, *J. Hydraul. Eng.*, 123(7), 666.
37. Hagen, VK. 1982. *Re-evaluation of design floods and dam safety*, Proc., 14th Congress of Int. Comm. on Large Dams, Int. Comm. on Large Dams, Paris.
38. Hair, JF Anderson, RE Tathan, RL Black, W. 1995. *In: Multivariate data analysis with reading*, Fourth ed. Prentice Hall Inc, New Jersey.
39. Hanson, GJ Cook, KR and Hunt, SL. 2005. *Physical modelling of overtopping erosion and breach formation of cohesive embankments*, Trans. ASABE, 48(5), 1783–1794.
40. Harris, GW and Wagner, DA. 1967. *Outflow from breached earth dams*, Dissertation, presented to the Univ. of Utah, at Salt Lake City, Utah, in partial fulfilment of the requirements for the degree of Bachelor of Science.
41. Hassan, MAAM and Morris, MW. 2008. *IMPACT Project field tests data analysis*,

42. Hassan, M Morris, M Hanson, G and Lakham, K. 2010. *Breach Formation: Laboratory and Numerical Modelling of Breach Formation*, Available at www.floodsite.net/.../59_LaboratoryandNumericalModellingofBreachFormation.pdf.
43. Hazen, A. 1914. *Discussion on "Flood flows" by W.E Fuller*, Trans. American Society of Civil Eng., 77, 626-632.
44. Hassanzadeh, H Faiznia, S Shafai Bajestan M and Motamed, A. 2011. *Estimate of Sediment Transport Rate at Karkheh River in Iran Using Selected Transport Formulas*, World Applied Sciences Journal 13 (2): 376-384, 2011 ISSN 1818-4952., IDOSI Publications.
45. Hungr, O. 1987. *An extension of Bishop's simplified method of slope stability analysis to three dimensions*, Géotechnique 37
46. Hunziker, RP and Jäeggi MNR. 2002. *Grain sorting processes*, Journal Hydraul. Eng., 128, 1060–1068
47. Hydropower and Dams, 2014, Issue 1
48. IDRSM. 2001. Available at www.fema.gov
49. Ikeda, S. 1988. *Lateral bed load transport on side slopes*, Civil engineering practice, Vol. 2, Technomic, Lancaster, Pa., 299–307.
50. Kahawita, R. 2007. *Dam breach modelling – a literature review of numerical models*, Report T032700, CEA Technologies, Inc.
51. Khorram, S and Ergil, M. 2010. *A sensitivity analysis of total load prediction parameters in standard sediment transport equations*, Journal of the American Water Resources Association.
52. Kirkpatrick, GW. 1977. *Evaluation guidelines for spillway adequacy*, The evaluation of dam safety: Engineering Foundation Conf. Proc., ASCE, New York, 395–414.
53. Lou, WC. 1981. *Mathematical modelling of earth dam breaches*, Dissertation, presented to Colorado State Univ., at Fort Collins, Colo., in partial fulfillment of the requirements for the degree of Doctor of Philosophy.
54. Loukola, E and Houkuna, M. 1998. *A numerical erosion model for embankment dams failure and its use for risk assessment*, Proc. of the 2nd CADAM Meeting, Universiteit der Bundeswehr, Munchen, Germany.

55. Macchione, F. 2008. *Model for predicting floods due to earthen dam breaching. I: Formulation and evaluation*, J. Hydraul. Eng., 134(12), 1688–1696.

56. MacDonald, TC and Langridge-Monopolis, J. 1984. *Breaching characteristics of dam failures*, Journal of Hydraulic Engineering, ASCE vol. 110, no. 5, p. 567-586.

57. Meyer-Peter, E and Müller, R. 1948. *Formulas for bed load transport*, Proc., 2nd Meeting, IAHR, Stockholm, Sweden, 39–64.

58. MIT. 2010. Available on www.ocw.mit.edu/courses

59. Moges, EM. 2010, *Evaluation of sediment transport equations and parameter sensitivity analysis using SRH-2D Model*, MSc Thesis, University of Stuttgart

60. Mohamed, MAA. 2002. *Embankment breach formation and modelling methods*, Ph. D. dissertation. Open University, UK.

61. Mohamed, MAA Samuels, PG Morris, MW and Ghataora, GS. 2002. *Improving the Accuracy of Prediction of Breach Formation through Embankment Dams and Flood Embankment, Available at www.impact-project.net.*

62. Molinas, A and Wu, B. 2001. *Transport of sediment in large sand-bed river*, Journal of Hydraulic Research, VOL. 39, 2001, NO. 2, Fort Collins, CO 80526.

63. Morris, MW. 2000. *CADAM: Concerted action on dam-break modelling—final report*, Rep. No. SR 571, HR Wallingford.

64. Morris, MW and Hassan, MAAM. 2002. *IMPACT: Breach formation technical report WP2*, IMPACT Project. www.impact-project.net

65. Morris, MW Mohamed, MAAM and Vaskinn, KA. 2007. *Breach formation: field test and laboratory experiments*, J Hydraulic Res, 45(Extra Issue): 9–17

66. Morris MW. 2011. *Predicting Breach using AREBA*, Birmingham - 20th Sept 2011 FRMRC Flood Risk Research www.floodrisk.org.uk.

67. Nitsche, M Rickenmann, D Turowski, JM Badoux, A and Kirchner JW. 2011. *Evaluation of bed load transport predictions using flow resistance equations to account for macro-roughness in steep mountain streams***,** Water Resources Research, Vol. 47, W08513,

68. Oosthuizen, L. 2009. *Risk assessment of dams; a semi-critical review*, Presentation at SANCOLD Conference, Sustainable Development of Dams, 4-6 November 2009, Drakensberg, South Africa.

69. Pierce, MW Thornton, CI and Abt, SR. 2010. *Predicting peak outflow from breached embankment dams*, J. Hydrol. Eng., 15(5), 338–349.

70. Powledge, GR Ralston, DC Miller, P Chen, YH Clopper, PE and Temple, DM. 1989. *Mechanics of overflow erosion on embankments*, Part II. Hydraulic and design considerations, Journal of Hydraulic Engineering 115(8), 1056–1075.

71. Radyn, P. 2010. *Dambreekvloed Ontleding Van Grond- En Rotsvuldamme*, BSc Thesis, (in Afrikaans)

72. Rickenmann, D. 1991. *Hyperconcentrated flow and sediment transport at steep slopes*, J. Hydraul. Eng., 117(11), 1419–1439.

73. Rickenmann, D. 2001. *Comparison of bed load transport in torrents and gravel bed streams*, Water Resource. Res., 37(12), 3295–3305.

74. Rooseboom, A. 1992. *Sediment transport in rivers and reservoirs, A Southern African Perspective*, SA Water Research Commission Report 297/1/92.

75. SANCOLD. 1991. *Safety evaluation of dams, interim guidelines on dam-break floods*, South African Commission on Large Dams, Report No 2.

76. SCS. 1981. Soil Conservation Service *Simplified dam-breach routing procedure*, Technical Release No. 66 (Rev. 1), USDA, Washington, DC, 39.

77. Singh, VP and Quiroga, CA. 1987. *A dam-breach erosion model: I. Formulation*, Water Resources Management, 1 (3) 177-197.

78. Singh, KP and Snorrason, A. 1984. *Sensitivity of outflow peaks and flood stages to the selection of dam breach parameters and simulation models*, Journal of Hydrology 68, 295–310.

79. Sinnakaudan, SK Sulaiman, MS and Teoh, SH. 2010. *Total bed material load equation for high gradient rivers*, Journal of Hydro-environment Research 4 (2010), Available online at www.sciencedirect.com

80. Smart, GM. 1984. *Predicting the sediment capacity of a channel*, Challenges in African Hydrology and Water Resources, Proceedings of the Harare Symposium, July 1984. IAHS Publ. no. 144.

81. Smart, GM and Jäeggi, MNR. 1983. *Sediment transport on steep slopes*, Mitteilungen der Versuchsanstalt für Wasserbau, Hydrologie und Glaziologie, Vol. 64, Eidgenössische Technische Hochschule (ETH), Zürich, Switzerland.

82. Song, T Graf, WH and Lemmin, U. 1995. *Uniform flow in open channels with movable gravel bed*, J. Hydraul. Res., 32(6), 861–875.

83. Temple, DM Hanson, GJ Neilsen, ML and Cook, KR. 2005. *Simplified breach analysis model for homogeneous embankments: Part 1, Background and model components*, Proc., 25th Annual USSD Conference, U.S. Society on Dams, Denver.

84. Tingsanchali, T and Chinnarasri, C. 2001. *Numerical modelling of dam failure due to flow overtopping*, Hydrological Sciences Journal, 46(1): 113–130.

85. USBR. 2014. *Erosion and Sedimentation Manual*, www.usbr.gov, accessed January 2014.

86. USDA. 2013. *Soil Survey Manual*, www.nrcs.usda.gov/wps accessed March 2013

87. Van Damme, M. 2012. *AREBA - A Rapid Embankment Breach Assessment*, Part of PhD Thesis, Flood risk management research consortium, Oxford University/ HR Wallingford, UK.

88. Van Rijn, LC. 1984a. *Sediment transport. I: Bed load transport*, J. Hydraul. Eng., 110(10), 1431–1456.

89. Van Rijn, LC. 1984b. *Sediment transport. II: Suspended load transport*, J. Hydraul. Eng., 110(11), 1613–1641.

90. Van Rijn, LC. 1989. *Handbook: Sediment transport by currents and waves*, Report H461, Delft Hydraulics, Netherlands.

91. Velikanov, MA. 1954. *Gravitational Theory of Sediment Transport*, Journal of Science of the Soviet Union Geoplzysics, Vol. 4 (in Russian).

92. Von Thun, JL and Gillette, DR. 1990. *Guidance on Breach Parameters, Internal Memorandum*, U.S. Dept. of the Interior, Bureau of Reclamation, Denver, CO

93. Wahl, TL. 2009, *Evaluation of new models for simulating embankment dam breach*, Presented at ASDSO Dam Safety, Sept 27 – Oct 1, Hollywood, Florida.

94. Wahl, TL. 2010, *Dam breach modelling – an overview of analysis methods*, 2nd Joint Federal Interagency Conference, Las Vegas, NV, June 27 - July 1, 2010.

95. Walder, JS and O'Connor, JE. 1997. *Methods for predicting peak discharge of floods caused by failure of natural and constructed earth dams*, Water Resources Research, vol. 33, no. 10 October 1997, 12 p.

96. Wang, P. and Kahawita, R. 2002. *Modelling the hydraulics and erosion process in breach formation to overtopping*, Proceedings of the symposium held in Monte Verita,

Switzerland. Sedimentation and sediment transport. Edited by A. Gyr and W Kinzelbach. September 2002.

97. Wang, P Kahawita, R Mokhtari, A Phat, TM and Quach, TT. 2006. *Modelling breach formation in embankments due to overtopping*, ICOLD Conference, Barcelona, Spain, June 2006.
98. Wang, Z and Bowles, DS. 2006a. *Three dimensional non-cohesive earthen dam breach model - Part 1, Theory and methodology*, Advances in Water Resources.
99. Wang, Z and Bowles, DS. 2006b. *Three dimensional non-cohesive earthen dam breach model - Part 2, Validation and applications*, Advances in Water Resources.
100. Wu, BS and Long, YQ. 1993. *Corrections for the formula of sediment transport capacity in the Yellow River*, Yellow River 1993 (7):1–4 (in Chinese).
101. Wu, W Wang, SSY and Jia, Y. 2000. *Nonuniform sediment transport in alluvial rivers*, Journal of Hydraulic Research, 38:6, 427-434.
102. Wu, W. 2007. *Computational river dynamics*, Taylor and Francis, London.
103. Wu, W. 2008. *ASCE/EWRI Task Committee on Dam/Levee Breaching*, Journal of Hydraulic Engineering, ASCE.
104. Wu, W. 2011. *Earthen embankment breaching*, ASCE/EWRI Task Committee on Dam/Levee Breaching, Journal of Hydraulic Engineering, ASCE / DECEMBER 2011 / 1549.
105. Wu, W Marsooli, R and He, Z. 2011. *A depth-averaged two dimensional model of unsteady flow and sediment transport due to non-cohesive embankment break/breaching*, Journal of Hydraulic Engineering. Copyright 2011 by the American Society of Civil Engineers.
106. Xia, JQ Lin, BL Falconer, RA and Wang GQ. 2010. *Modelling dam-break flows over mobile beds using a 2D coupled approach*, Advances Water Resources 2010;33:171–83.
107. Xu, Y and Zhang, LM. 2009. *Breaching parameters for earth and rockfill dams*, Journal of Geotechnical and Geoenvironmental Engineering, ASCE, pp. 1957-1970.
108. Yang, CT. 1972. *Unit stream power and sediment transport*, J. Hydraul, Div. Am. Soc. Civ. Eng. 98:1805–1825.
109. Yang, CT. 1973. *Incipient motion and sediment transport*, ASCE Journal of the Hydraulics Division, V. 99(HY 10): 1679-1704.

110. Yang, CT and Stall, JB. 1974. *Unit stream power for sediment transport in natural rivers*, WRC Research Report NO. 88, Illinois State Water Survey, Urbana, Illinois Final Report Project No. B-075-1 LL.
111. Yang, CT. 1979. *Unit stream power equations for total load*, Journal of Hydrology, Vol. 40, 123-138.
112. Yang, CT. 1996. *Sediment Transport Theory and Practice*, The McGraw-Hill Companies, Inc.
113. Yang, SQ and Lim, SY. 2003. *Total load transport formula for flow in alluvial channels*, Journal of Hydraulic Engineering, ASCE 129(1):68-72.
114. Yang, SQ. 2005. *Interactions of boundary shear stress, secondary currents and velocity*, Journal Fluid Dynamics Research, Volume 36, Pages 121-136
115. Ying, A. 1996. *Sediment transport at very high concentrations and its movement behaviour*, Journal of Environmental Hydrology, The Electronic Journal of the International Association for Environmental Hydrology, On the World Wide Web at http://www.hydroweb.com.
116. Zagonjolli, M. 2007. *Dam-break modelling, risk assessment and uncertainty analysis for flood mitigation*, PhD Dissertation, UNESCO-IHE, Netherlands.
117. Zhang, G Liu, Y Han, Y and Xuan, XC. 2009. S*ediment transport and soil detachment on steep slopes: I. transport capacity estimation*, Soil Science Society of America, Volume 73, Number 4, July-August 2009.
118. Zhang, M and Wu, WM. 2011. *A two dimensional hydrodynamic and sediment transport model for dam-break based on finite volume method with quadtree grid*, Applied Ocean Research, doi:10.1016/j.apor.2011.07.004.
119. Zolghadr, M Hashemi, MR and Zomorodian, SMA. 2011. *Assessment of MIKE 21 Model in dam and dike simulation*, IJST, Transactions of Civil Engineering, Vol 35, No C2, pp 247-262, Iran

# APPENDICES

## APPENDIX A1: Measured sediment transport rates at $d_{50}$ = 0.2 mm, 1 mm and 2.4 mm

| Bed Slope (%) | Sediment Size (mm) | Flow Rate ($m^3/s$) | Unit Flow Rate ($m^2/s$) | Unit Sediment Discharge (kg/m/s) |
|---|---|---|---|---|
| 25 | 0.208 | 0.0185 | 0.0741 | 10.742 |
| 25 | 0.208 | 0.0201 | 0.0805 | 11.093 |
| 25 | 0.208 | 0.0224 | 0.0894 | 16.061 |
| 25 | 0.208 | 0.0256 | 0.1022 | 15.844 |
| 25 | 0.208 | 0.0278 | 0.1112 | 20.469 |
| 25 | 0.208 | 0.0303 | 0.1214 | 14.986 |
| 25 | 0.208 | 0.0329 | 0.1316 | 14.333 |
| 25 | 0.208 | 0.0351 | 0.1406 | 16.880 |
| 25 | 0.208 | 0.0380 | 0.1521 | 21.775 |
| 25 | 0.208 | 0.0399 | 0.1597 | 27.678 |
| 25 | 0.208 | 0.0428 | 0.1712 | 26.916 |
| 25 | 0.208 | 0.0450 | 0.1802 | 24.233 |
| 33 | 0.208 | 0.0182 | 0.0728 | 8.045 |
| 33 | 0.208 | 0.0201 | 0.0805 | 7.102 |
| 33 | 0.208 | 0.0227 | 0.0907 | 9.103 |
| 33 | 0.208 | 0.0259 | 0.1035 | 11.330 |
| 33 | 0.208 | 0.0284 | 0.1137 | 12.853 |
| 33 | 0.208 | 0.0307 | 0.1226 | 12.552 |
| 33 | 0.208 | 0.0329 | 0.1316 | 17.444 |
| 33 | 0.208 | 0.0351 | 0.1406 | 17.960 |
| 33 | 0.208 | 0.0380 | 0.1521 | 19.395 |
| 33 | 0.208 | 0.0401 | 0.1604 | 22.059 |
| 33 | 0.208 | 0.0426 | 0.1706 | 20.046 |
| 33 | 0.208 | 0.0455 | 0.1821 | 24.010 |
| 40 | 0.208 | 0.0169 | 0.0677 | 5.296 |
| 40 | 0.208 | 0.0201 | 0.0805 | 6.684 |
| 40 | 0.208 | 0.0220 | 0.0882 | 8.004 |
| 40 | 0.208 | 0.0256 | 0.1022 | 9.998 |
| 40 | 0.208 | 0.0351 | 0.1406 | 11.996 |
| 40 | 0.208 | 0.0380 | 0.1521 | 12.935 |
| 40 | 0.208 | 0.0399 | 0.1597 | 15.087 |
| 40 | 0.208 | 0.0428 | 0.1712 | 15.329 |
| 40 | 0.208 | 0.0457 | 0.1827 | 14.438 |

| Experiment ID No | Bed Slope (%) | Friction Slope (%) | Flow Rate ($m^3/s$) | Unit Discharge ($m^2/s$) | Average Depth (mm) | Average Velocity (m/s) | Sediment Size, $d_{50}$ (mm) | Dry Weight (kg) | Sediment Concentration ($kg/m^3$) | Unit Sediment Discharge (kg/m/s) |
|---|---|---|---|---|---|---|---|---|---|---|
| 251 | 25 | 24.200 | 0.020 | 0.082 | 21.0 | 3.893 | 2.4 | 6.18 | 241.926 | 21.760 |
| 252 | 25 | 24.484 | 0.023 | 0.091 | 23.0 | 3.944 | 2.4 | 6.35 | 215.504 | 21.508 |
| 253 | 25 | 24.484 | 0.025 | 0.101 | 26.0 | 3.882 | 2.4 | 7.13 | 222.360 | 24.693 |
| 254 | 25 | 24.476 | 0.026 | 0.102 | 27.0 | 3.785 | 2.4 | 9.65 | 236.144 | 26.550 |
| 255 | 25 | 24.727 | 0.027 | 0.110 | 27.5 | 3.996 | 2.4 | 9.14 | 214.753 | 25.961 |
| 256 | 25 | 24.854 | 0.030 | 0.120 | 28.5 | 4.214 | 2.4 | 9.35 | 219.364 | 28.986 |
| 257 | 25 | 24.296 | 0.033 | 0.133 | 29.5 | 4.505 | 2.4 | 7.73 | 213.494 | 31.211 |
| 258 | 25 | 24.735 | 0.035 | 0.141 | 35.0 | 4.016 | 2.4 | 7.02 | 195.790 | 30.275 |
| 259 | 25 | 24.906 | 0.038 | 0.152 | 37.0 | 4.110 | 2.4 | 8.32 | 221.128 | 36.990 |
| 260 | 25 | 24.544 | 0.041 | 0.164 | 38.5 | 4.248 | 2.4 | 11.38 | 206.089 | 37.081 |
| 261 | 25 | 24.297 | 0.042 | 0.170 | 41.0 | 4.145 | 2.4 | 8.43 | 175.612 | 32.832 |
| 262 | 25 | 24.307 | 0.046 | 0.183 | 42.0 | 4.350 | 2.4 | 9.34 | 160.918 | 32.346 |
| 263 | 25 | 24.143 | 0.008 | 0.032 | 7.0 | 4.625 | 1.0 | 17.22 | 558.285 | 19.885 |
| 264 | 25 | 23.829 | 0.009 | 0.036 | 7.0 | 5.195 | 1.0 | 13.20 | 585.476 | 23.424 |
| 265 | 25 | 22.978 | 0.010 | 0.041 | 6.5 | 6.252 | 1.0 | 13.34 | 583.732 | 26.098 |
| 266 | 25 | 23.444 | 0.011 | 0.045 | 7.5 | 6.027 | 1.0 | 18.78 | 550.312 | 27.364 |
| 267 | 25 | 23.610 | 0.012 | 0.048 | 8.0 | 5.950 | 1.0 | 18.82 | 568.915 | 29.791 |
| 268 | 25 | 23.206 | 0.014 | 0.058 | 8.5 | 6.814 | 1.0 | 21.27 | 542.053 | 34.539 |
| 331 | 33 | 30.577 | 0.020 | 0.081 | 18.0 | 4.472 | 2.4 | 12.40 | 286.552 | 25.377 |
| 332 | 33 | 32.764 | 0.022 | 0.087 | 19.0 | 4.573 | 2.4 | 7.26 | 267.318 | 25.552 |
| 333 | 33 | 31.587 | 0.025 | 0.101 | 22.5 | 4.486 | 2.4 | 11.64 | 256.142 | 28.444 |
| 334 | 33 | 32.902 | 0.028 | 0.114 | 26.0 | 4.374 | 2.4 | 6.39 | 261.177 | 32.674 |
| 335 | 33 | 32.512 | 0.030 | 0.121 | 27.5 | 4.414 | 2.4 | 6.65 | 257.777 | 34.424 |
| 336 | 33 | 32.583 | 0.033 | 0.133 | 29.0 | 4.582 | 2.4 | 6.39 | 229.152 | 33.500 |
| 337 | 33 | 31.862 | 0.035 | 0.141 | 31.0 | 4.534 | 2.4 | 13.31 | 247.528 | 38.275 |
| 338 | 33 | 31.465 | 0.036 | 0.143 | 31.0 | 4.617 | 2.4 | 7.13 | 231.614 | 36.465 |
| 339 | 33 | 31.452 | 0.039 | 0.156 | 34.0 | 4.585 | 2.4 | 9.53 | 237.320 | 40.699 |
| 340 | 33 | 32.478 | 0.040 | 0.161 | 35.0 | 4.600 | 2.4 | 17.47 | 227.257 | 40.251 |
| 341 | 33 | 31.052 | 0.046 | 0.183 | 36.5 | 5.006 | 2.4 | 17.64 | 234.088 | 47.055 |
| 342 | 33 | 30.015 | 0.046 | 0.183 | 36.5 | 5.006 | 2.4 | 17.11 | 225.605 | 45.349 |
| 343 | 33 | 30.795 | 0.008 | 0.032 | 6.5 | 4.981 | 1.0 | 17.45 | 713.050 | 25.397 |
| 344 | 33 | 30.093 | 0.009 | 0.036 | 6.5 | 5.595 | 1.0 | 13.95 | 648.400 | 25.942 |
| 345 | 33 | 30.099 | 0.010 | 0.041 | 7.0 | 5.806 | 1.0 | 13.95 | 627.998 | 28.077 |
| 346 | 33 | 29.299 | 0.011 | 0.045 | 7.0 | 6.457 | 1.0 | 17.45 | 621.778 | 30.918 |

| | | | | | | | | | | |
|---|---|---|---|---|---|---|---|---|---|---|
| 347 | 33 | 30.380 | 0.012 | 0.048 | 8.0 | 5.950 | 1.0 | 16.26 | 657.314 | 34.420 |
| 348 | 33 | 28.893 | 0.014 | 0.058 | 8.0 | 7.240 | 1.0 | 17.73 | 650.790 | 41.467 |
| 401 | 40 | 38.195 | 0.020 | 0.081 | 17.0 | 4.735 | 2.4 | 10.58 | 386.582 | 34.235 |
| 402 | 40 | 38.195 | 0.020 | 0.082 | 17.0 | 4.810 | 2.4 | 9.09 | 355.526 | 31.984 |
| 403 | 40 | 38.412 | 0.023 | 0.091 | 19.0 | 4.808 | 2.4 | 10.18 | 353.765 | 35.556 |
| 404 | 40 | 36.707 | 0.026 | 0.102 | 20.5 | 4.986 | 2.4 | 11.45 | 352.763 | 39.669 |
| 405 | 40 | 35.752 | 0.028 | 0.111 | 21.5 | 5.170 | 2.4 | 12.36 | 313.080 | 38.287 |
| 406 | 40 | 35.807 | 0.030 | 0.120 | 23.5 | 5.111 | 2.4 | 13.96 | 336.938 | 44.522 |
| 407 | 40 | 35.500 | 0.033 | 0.132 | 25.0 | 5.265 | 2.4 | 13.73 | 289.671 | 41.947 |
| 408 | 40 | 35.407 | 0.035 | 0.139 | 26.0 | 5.357 | 2.4 | 12.58 | 301.094 | 46.133 |
| 409 | 40 | 36.360 | 0.038 | 0.151 | 27.0 | 5.595 | 2.4 | 13.27 | 300.336 | 49.915 |
| 410 | 40 | 35.684 | 0.040 | 0.160 | 27.5 | 5.808 | 2.4 | 13.62 | 304.602 | 53.521 |
| 411 | 40 | 35.923 | 0.044 | 0.175 | 28.5 | 6.143 | 2.4 | 13.19 | 276.375 | 53.229 |
| 412 | 40 | 35.026 | 0.045 | 0.180 | 29.5 | 6.107 | 2.4 | 15.70 | 341.754 | 67.737 |
| 413 | 40 | 35.065 | 0.008 | 0.032 | 6.0 | 5.396 | 1.0 | 18.36 | 774.256 | 27.577 |
| 414 | 40 | 36.106 | 0.009 | 0.036 | 7.0 | 5.195 | 1.0 | 17.83 | 837.850 | 33.521 |
| 415 | 40 | 36.761 | 0.010 | 0.041 | 8.0 | 5.080 | 1.0 | 18.38 | 826.052 | 36.932 |
| 416 | 40 | 35.978 | 0.011 | 0.045 | 8.0 | 5.650 | 1.0 | 24.39 | 814.594 | 40.506 |
| 417 | 40 | 36.289 | 0.012 | 0.048 | 8.5 | 5.600 | 1.0 | 21.53 | 783.210 | 41.013 |
| 418 | 40 | 34.476 | 0.014 | 0.058 | 8.5 | 6.814 | 1.0 | 24.39 | 693.251 | 44.173 |

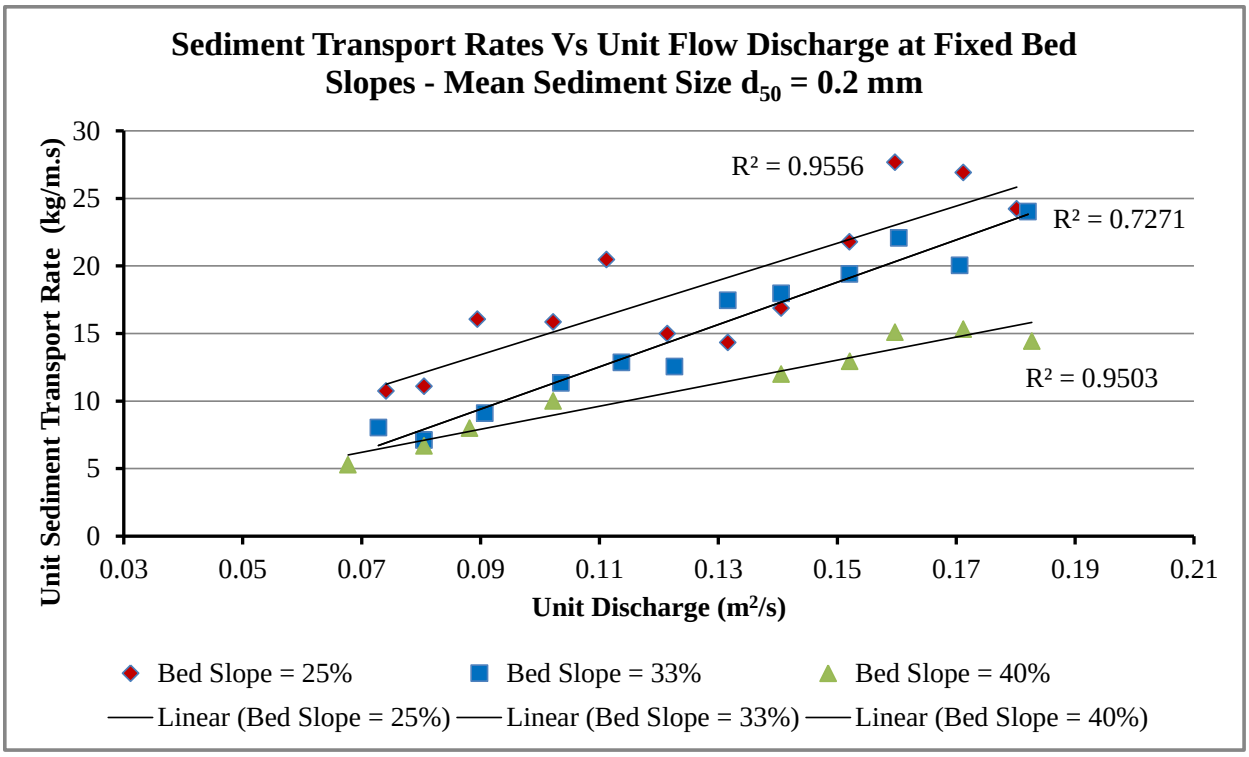


**Measured Unit Sediment Transport Rates against Unit Discharge for Median ($d_{50}$) Sediment Size = 0.2 mm**

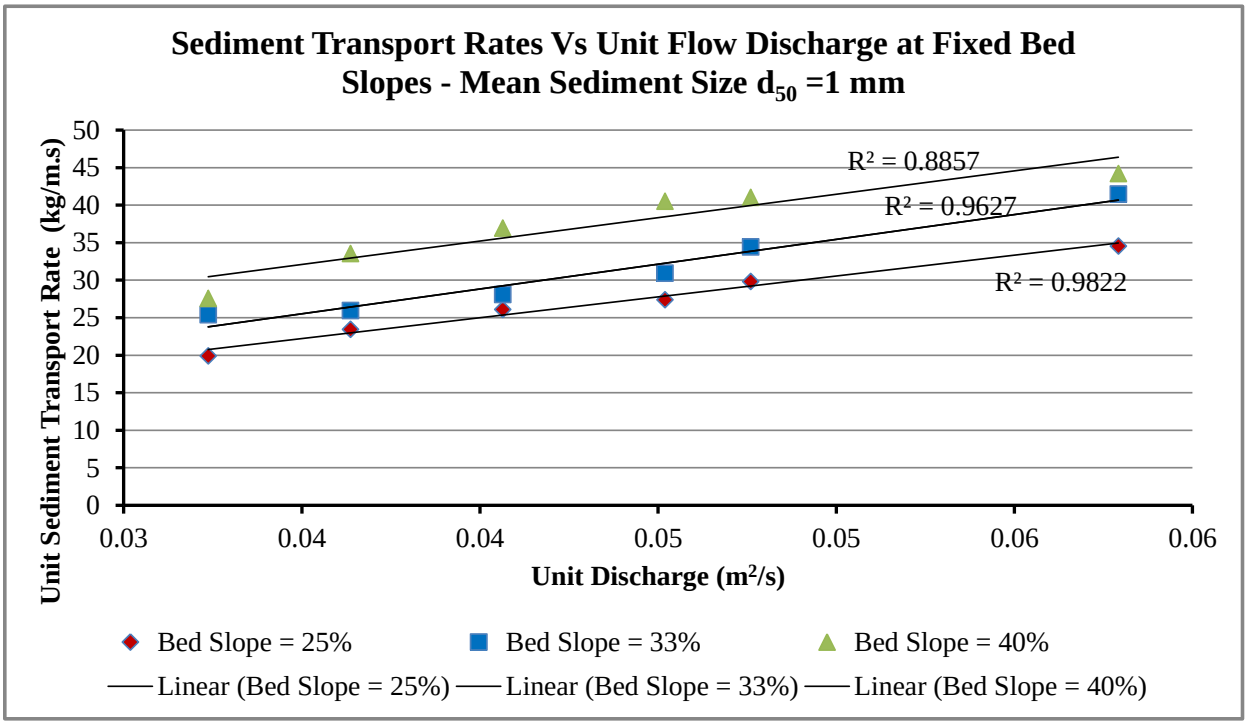


**Measured Unit Sediment Transport Rates against Unit Discharge for Median Sediment Size $d_{50}$ =1 mm**

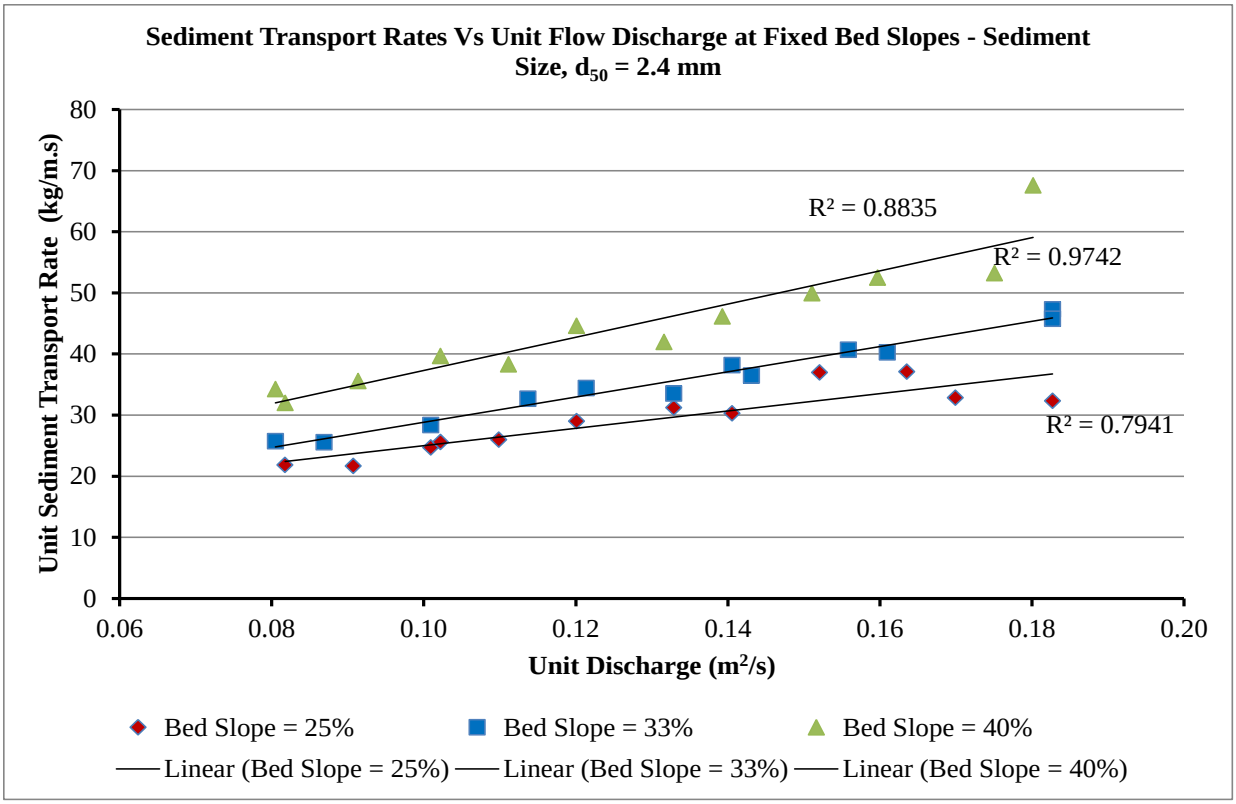


**Measured Unit Sediment Transport Rates against Unit Discharge for Median ($d_{50}$) Sediment Size = 2.4 mm**

**APPENDIX A2**

| 1D | Dimensionless sediment transport rate, $\emptyset$ | $\frac{d_{90}}{d_{30}}$ | Water surface or energy slope, $S_f$ | $\theta - \theta_{cr}$ | Resistance factor, $C$ | Log $\emptyset$ | Log $\frac{d_{90}}{d_{30}}$ | Log $S_f$ | Log $\theta - \theta_{cr}$ | Log $C$ |
|---|---|---|---|---|---|---|---|---|---|---|
| 1 | 18.612 | 1.1 | 24.2 | 1.277 | 17.437 | 1.270 | 0.053 | 1.384 | 0.106 | 1.241 |
| 2 | 18.397 | 1.1 | 24.5 | 1.420 | 16.782 | 1.265 | 0.053 | 1.389 | 0.152 | 1.225 |
| 3 | 21.121 | 1.1 | 24.5 | 1.611 | 15.536 | 1.325 | 0.053 | 1.389 | 0.207 | 1.191 |
| 4 | 22.709 | 1.1 | 24.5 | 1.675 | 14.866 | 1.356 | 0.053 | 1.389 | 0.224 | 1.172 |
| 5 | 22.206 | 1.1 | 24.7 | 1.724 | 15.472 | 1.346 | 0.053 | 1.393 | 0.237 | 1.190 |
| 6 | 24.793 | 1.1 | 24.9 | 1.798 | 15.988 | 1.394 | 0.053 | 1.395 | 0.255 | 1.204 |
| 7 | 26.696 | 1.1 | 24.3 | 1.820 | 16.988 | 1.426 | 0.053 | 1.386 | 0.260 | 1.230 |
| 8 | 25.895 | 1.1 | 24.7 | 2.208 | 13.780 | 1.413 | 0.053 | 1.393 | 0.344 | 1.139 |
| 9 | 31.639 | 1.1 | 24.9 | 2.354 | 13.668 | 1.500 | 0.053 | 1.396 | 0.372 | 1.136 |
| 10 | 31.718 | 1.1 | 24.5 | 2.415 | 13.953 | 1.501 | 0.053 | 1.390 | 0.383 | 1.145 |
| 11 | 28.083 | 1.1 | 24.3 | 2.548 | 13.259 | 1.448 | 0.053 | 1.386 | 0.406 | 1.123 |
| 12 | 27.667 | 1.1 | 24.3 | 2.613 | 13.747 | 1.442 | 0.053 | 1.386 | 0.417 | 1.138 |
| 13 | 61.750 | 1.9 | 24.1 | 0.993 | 35.921 | 1.791 | 0.272 | 1.383 | -0.003 | 1.555 |
| 14 | 72.742 | 1.9 | 23.8 | 0.979 | 40.615 | 1.862 | 0.272 | 1.377 | -0.009 | 1.609 |
| 15 | 81.044 | 1.9 | 23.0 | 1.014 | 48.086 | 1.909 | 0.272 | 1.361 | 0.006 | 1.682 |
| 16 | 84.977 | 1.9 | 23.4 | 1.035 | 45.887 | 1.929 | 0.272 | 1.370 | 0.015 | 1.662 |
| 17 | 92.514 | 1.9 | 23.6 | 1.115 | 43.711 | 1.966 | 0.272 | 1.373 | 0.047 | 1.641 |
| 18 | 107.257 | 1.9 | 23.2 | 1.167 | 48.986 | 2.030 | 0.272 | 1.366 | 0.067 | 1.690 |
| 19 | 21.706 | 1.1 | 30.6 | 1.387 | 19.247 | 1.337 | 0.053 | 1.485 | 0.142 | 1.284 |
| 20 | 21.856 | 1.1 | 32.8 | 1.575 | 18.505 | 1.340 | 0.053 | 1.515 | 0.197 | 1.267 |
| 21 | 24.330 | 1.1 | 31.6 | 1.805 | 16.991 | 1.386 | 0.053 | 1.500 | 0.256 | 1.230 |
| 22 | 27.948 | 1.1 | 32.9 | 2.182 | 15.098 | 1.446 | 0.053 | 1.517 | 0.339 | 1.179 |
| 23 | 29.444 | 1.1 | 32.5 | 2.282 | 14.905 | 1.469 | 0.053 | 1.512 | 0.358 | 1.173 |
| 24 | 28.654 | 1.1 | 32.6 | 2.415 | 15.051 | 1.457 | 0.053 | 1.513 | 0.383 | 1.178 |
| 25 | 32.738 | 1.1 | 31.9 | 2.526 | 14.566 | 1.515 | 0.053 | 1.503 | 0.402 | 1.163 |
| 26 | 31.190 | 1.1 | 31.5 | 2.494 | 14.924 | 1.494 | 0.053 | 1.498 | 0.397 | 1.174 |
| 27 | 34.812 | 1.1 | 31.5 | 2.739 | 14.156 | 1.542 | 0.053 | 1.498 | 0.438 | 1.151 |
| 28 | 34.429 | 1.1 | 32.2 | 2.887 | 13.839 | 1.537 | 0.053 | 1.508 | 0.460 | 1.141 |
| 29 | 40.248 | 1.1 | 31.1 | 2.906 | 15.013 | 1.605 | 0.053 | 1.492 | 0.463 | 1.176 |
| 30 | 38.789 | 1.1 | 30.0 | 2.807 | 15.270 | 1.589 | 0.053 | 1.477 | 0.448 | 1.184 |

| | | | | | | | | | | |
|---|---|---|---|---|---|---|---|---|---|---|
| 31 | 78.868 | 1.9 | 30.8 | 1.185 | 35.545 | 1.897 | 0.272 | 1.488 | 0.074 | 1.551 |
| 32 | 80.560 | 1.9 | 30.1 | 1.157 | 40.391 | 1.906 | 0.272 | 1.478 | 0.063 | 1.606 |
| 33 | 87.190 | 1.9 | 30.1 | 1.250 | 40.382 | 1.940 | 0.272 | 1.479 | 0.097 | 1.606 |
| 34 | 96.013 | 1.9 | 29.3 | 1.215 | 45.523 | 1.982 | 0.272 | 1.467 | 0.085 | 1.658 |
| 35 | 106.889 | 1.9 | 30.4 | 1.449 | 38.534 | 2.029 | 0.272 | 1.483 | 0.161 | 1.586 |
| 36 | 128.773 | 1.9 | 28.9 | 1.375 | 48.080 | 2.110 | 0.272 | 1.461 | 0.138 | 1.682 |
| 37 | 29.283 | 1.1 | 38.2 | 1.645 | 18.762 | 1.467 | 0.053 | 1.582 | 0.216 | 1.273 |
| 38 | 27.357 | 1.1 | 38.2 | 1.645 | 19.060 | 1.437 | 0.053 | 1.582 | 0.216 | 1.280 |
| 39 | 30.412 | 1.1 | 38.4 | 1.854 | 17.970 | 1.483 | 0.053 | 1.584 | 0.268 | 1.255 |
| 40 | 33.931 | 1.1 | 36.7 | 1.913 | 18.353 | 1.531 | 0.053 | 1.565 | 0.282 | 1.264 |
| 41 | 32.749 | 1.1 | 35.8 | 1.955 | 18.829 | 1.515 | 0.053 | 1.553 | 0.291 | 1.275 |
| 42 | 38.082 | 1.1 | 35.8 | 2.145 | 17.790 | 1.581 | 0.053 | 1.554 | 0.331 | 1.250 |
| 43 | 35.879 | 1.1 | 35.5 | 2.265 | 17.845 | 1.555 | 0.053 | 1.550 | 0.355 | 1.252 |
| 44 | 39.460 | 1.1 | 35.4 | 2.351 | 17.825 | 1.596 | 0.053 | 1.549 | 0.371 | 1.251 |
| 45 | 42.694 | 1.1 | 36.4 | 2.511 | 18.030 | 1.630 | 0.053 | 1.561 | 0.400 | 1.256 |
| 46 | 45.779 | 1.1 | 35.7 | 2.509 | 18.719 | 1.661 | 0.053 | 1.552 | 0.400 | 1.272 |
| 47 | 45.530 | 1.1 | 35.9 | 2.620 | 19.383 | 1.658 | 0.053 | 1.555 | 0.418 | 1.287 |
| 48 | 57.939 | 1.1 | 35.0 | 2.645 | 19.183 | 1.763 | 0.053 | 1.544 | 0.422 | 1.283 |
| 49 | 85.637 | 1.9 | 35.1 | 1.248 | 37.560 | 1.933 | 0.272 | 1.545 | 0.096 | 1.575 |
| 50 | 104.098 | 1.9 | 36.1 | 1.508 | 32.995 | 2.017 | 0.272 | 1.558 | 0.179 | 1.518 |
| 51 | 114.687 | 1.9 | 36.8 | 1.763 | 29.908 | 2.060 | 0.272 | 1.565 | 0.246 | 1.476 |
| 52 | 125.787 | 1.9 | 36.0 | 1.724 | 33.624 | 2.100 | 0.272 | 1.556 | 0.237 | 1.527 |
| 53 | 127.362 | 1.9 | 36.3 | 1.851 | 32.192 | 2.105 | 0.272 | 1.560 | 0.267 | 1.508 |
| 54 | 137.175 | 1.9 | 34.5 | 1.756 | 40.189 | 2.137 | 0.272 | 1.538 | 0.245 | 1.604 |

# APPENDIX A3: F DISTRIBUTION TABLE

| / | **$df_1$=1** | **2** | **3** | **4** | **5** | **6** | **7** | **8** | **9** | **10** | **12** | **15** | **20** | **24** | **30** | **40** | **60** | **120** | ∞ |
|---|---|---|---|---|---|---|---|---|---|---|---|---|---|---|---|---|---|---|---|
| **$df_2$=1** | 161.4476 | 199.5000 | 215.7073 | 224.5832 | 230.1619 | 233.9860 | 236.7684 | 238.8827 | 240.5433 | 241.8817 | 243.9060 | 245.9499 | 248.0131 | 249.0518 | 250.0951 | 251.1432 | 252.1957 | 253.2529 | 254.3144 |
| **2** | 18.5128 | 19.0000 | 19.1643 | 19.2468 | 19.2964 | 19.3295 | 19.3532 | 19.3710 | 19.3848 | 19.3959 | 19.4125 | 19.4291 | 19.4458 | 19.4541 | 19.4624 | 19.4707 | 19.4791 | 19.4874 | 19.4957 |
| **3** | 10.1280 | 9.5521 | 9.2766 | 9.1172 | 9.0135 | 8.9406 | 8.8867 | 8.8452 | 8.8123 | 8.7855 | 8.7446 | 8.7029 | 8.6602 | 8.6385 | 8.6166 | 8.5944 | 8.5720 | 8.5494 | 8.5264 |
| **4** | 7.7086 | 6.9443 | 6.5914 | 6.3882 | 6.2561 | 6.1631 | 6.0942 | 6.0410 | 5.9988 | 5.9644 | 5.9117 | 5.8578 | 5.8025 | 5.7744 | 5.7459 | 5.7170 | 5.6877 | 5.6581 | 5.6281 |
| **5** | 6.6079 | 5.7861 | 5.4095 | 5.1922 | 5.0503 | 4.9503 | 4.8759 | 4.8183 | 4.7725 | 4.7351 | 4.6777 | 4.6188 | 4.5581 | 4.5272 | 4.4957 | 4.4638 | 4.4314 | 4.3985 | 4.3650 |
| | | | | | | | | | | | | | | | | | | | |
| **6** | 5.9874 | 5.1433 | 4.7571 | 4.5337 | 4.3874 | 4.2839 | 4.2067 | 4.1468 | 4.0990 | 4.0600 | 3.9999 | 3.9381 | 3.8742 | 3.8415 | 3.8082 | 3.7743 | 3.7398 | 3.7047 | 3.6689 |
| **7** | 5.5914 | 4.7374 | 4.3468 | 4.1203 | 3.9715 | 3.8660 | 3.7870 | 3.7257 | 3.6767 | 3.6365 | 3.5747 | 3.5107 | 3.4445 | 3.4105 | 3.3758 | 3.3404 | 3.3043 | 3.2674 | 3.2298 |
| **8** | 5.3177 | 4.4590 | 4.0662 | 3.8379 | 3.6875 | 3.5806 | 3.5005 | 3.4381 | 3.3881 | 3.3472 | 3.2839 | 3.2184 | 3.1503 | 3.1152 | 3.0794 | 3.0428 | 3.0053 | 2.9669 | 2.9276 |
| **9** | 5.1174 | 4.2565 | 3.8625 | 3.6331 | 3.4817 | 3.3738 | 3.2927 | 3.2296 | 3.1789 | 3.1373 | 3.0729 | 3.0061 | 2.9365 | 2.9005 | 2.8637 | 2.8259 | 2.7872 | 2.7475 | 2.7067 |
| **10** | 4.9646 | 4.1028 | 3.7083 | 3.4780 | 3.3258 | 3.2172 | 3.1355 | 3.0717 | 3.0204 | 2.9782 | 2.9130 | 2.8450 | 2.7740 | 2.7372 | 2.6996 | 2.6609 | 2.6211 | 2.5801 | 2.5379 |
| | | | | | | | | | | | | | | | | | | | |
| **11** | 4.8443 | 3.9823 | 3.5874 | 3.3567 | 3.2039 | 3.0946 | 3.0123 | 2.9480 | 2.8962 | 2.8536 | 2.7876 | 2.7186 | 2.6464 | 2.6090 | 2.5705 | 2.5309 | 2.4901 | 2.4480 | 2.4045 |
| **12** | 4.7472 | 3.8853 | 3.4903 | 3.2592 | 3.1059 | 2.9961 | 2.9134 | 2.8486 | 2.7964 | 2.7534 | 2.6866 | 2.6169 | 2.5436 | 2.5055 | 2.4663 | 2.4259 | 2.3842 | 2.3410 | 2.2962 |
| **13** | 4.6672 | 3.8056 | 3.4105 | 3.1791 | 3.0254 | 2.9153 | 2.8321 | 2.7669 | 2.7144 | 2.6710 | 2.6037 | 2.5331 | 2.4589 | 2.4202 | 2.3803 | 2.3392 | 2.2966 | 2.2524 | 2.2064 |
| **14** | 4.6001 | 3.7389 | 3.3439 | 3.1122 | 2.9582 | 2.8477 | 2.7642 | 2.6987 | 2.6458 | 2.6022 | 2.5342 | 2.4630 | 2.3879 | 2.3487 | 2.3082 | 2.2664 | 2.2229 | 2.1778 | 2.1307 |
| **15** | 4.5431 | 3.6823 | 3.2874 | 3.0556 | 2.9013 | 2.7905 | 2.7066 | 2.6408 | 2.5876 | 2.5437 | 2.4753 | 2.4034 | 2.3275 | 2.2878 | 2.2468 | 2.2043 | 2.1601 | 2.1141 | 2.0658 |
| | | | | | | | | | | | | | | | | | | | |
| **16** | 4.4940 | 3.6337 | 3.2389 | 3.0069 | 2.8524 | 2.7413 | 2.6572 | 2.5911 | 2.5377 | 2.4935 | 2.4247 | 2.3522 | 2.2756 | 2.2354 | 2.1938 | 2.1507 | 2.1058 | 2.0589 | 2.0096 |
| **17** | 4.4513 | 3.5915 | 3.1968 | 2.9647 | 2.8100 | 2.6987 | 2.6143 | 2.5480 | 2.4943 | 2.4499 | 2.3807 | 2.3077 | 2.2304 | 2.1898 | 2.1477 | 2.1040 | 2.0584 | 2.0107 | 1.9604 |
| **18** | 4.4139 | 3.5546 | 3.1599 | 2.9277 | 2.7729 | 2.6613 | 2.5767 | 2.5102 | 2.4563 | 2.4117 | 2.3421 | 2.2686 | 2.1906 | 2.1497 | 2.1071 | 2.0629 | 2.0166 | 1.9681 | 1.9168 |
| **19** | 4.3807 | 3.5219 | 3.1274 | 2.8951 | 2.7401 | 2.6283 | 2.5435 | 2.4768 | 2.4227 | 2.3779 | 2.3080 | 2.2341 | 2.1555 | 2.1141 | 2.0712 | 2.0264 | 1.9795 | 1.9302 | 1.8780 |
| **20** | 4.3512 | 3.4928 | 3.0984 | 2.8661 | 2.7109 | 2.5990 | 2.5140 | 2.4471 | 2.3928 | 2.3479 | 2.2776 | 2.2033 | 2.1242 | 2.0825 | 2.0391 | 1.9938 | 1.9464 | 1.8963 | 1.8432 |
| | | | | | | | | | | | | | | | | | | | |
| **21** | 4.3248 | 3.4668 | 3.0725 | 2.8401 | 2.6848 | 2.5727 | 2.4876 | 2.4205 | 2.3660 | 2.3210 | 2.2504 | 2.1757 | 2.0960 | 2.0540 | 2.0102 | 1.9645 | 1.9165 | 1.8657 | 1.8117 |
| **22** | 4.3009 | 3.4434 | 3.0491 | 2.8167 | 2.6613 | 2.5491 | 2.4638 | 2.3965 | 2.3419 | 2.2967 | 2.2258 | 2.1508 | 2.0707 | 2.0283 | 1.9842 | 1.9380 | 1.8894 | 1.8380 | 1.7831 |
| **23** | 4.2793 | 3.4221 | 3.0280 | 2.7955 | 2.6400 | 2.5277 | 2.4422 | 2.3748 | 2.3201 | 2.2747 | 2.2036 | 2.1282 | 2.0476 | 2.0050 | 1.9605 | 1.9139 | 1.8648 | 1.8128 | 1.7570 |
| **24** | 4.2597 | 3.4028 | 3.0088 | 2.7763 | 2.6207 | 2.5082 | 2.4226 | 2.3551 | 2.3002 | 2.2547 | 2.1834 | 2.1077 | 2.0267 | 1.9838 | 1.9390 | 1.8920 | 1.8424 | 1.7896 | 1.7330 |
| **25** | 4.2417 | 3.3852 | 2.9912 | 2.7587 | 2.6030 | 2.4904 | 2.4047 | 2.3371 | 2.2821 | 2.2365 | 2.1649 | 2.0889 | 2.0075 | 1.9643 | 1.9192 | 1.8718 | 1.8217 | 1.7684 | 1.7110 |
| | | | | | | | | | | | | | | | | | | | |
| **26** | 4.2252 | 3.3690 | 2.9752 | 2.7426 | 2.5868 | 2.4741 | 2.3883 | 2.3205 | 2.2655 | 2.2197 | 2.1479 | 2.0716 | 1.9898 | 1.9464 | 1.9010 | 1.8533 | 1.8027 | 1.7488 | 1.6906 |
| **27** | 4.2100 | 3.3541 | 2.9604 | 2.7278 | 2.5719 | 2.4591 | 2.3732 | 2.3053 | 2.2501 | 2.2043 | 2.1323 | 2.0558 | 1.9736 | 1.9299 | 1.8842 | 1.8361 | 1.7851 | 1.7306 | 1.6717 |
| **28** | 4.1960 | 3.3404 | 2.9467 | 2.7141 | 2.5581 | 2.4453 | 2.3593 | 2.2913 | 2.2360 | 2.1900 | 2.1179 | 2.0411 | 1.9586 | 1.9147 | 1.8687 | 1.8203 | 1.7689 | 1.7138 | 1.6541 |
| **29** | 4.1830 | 3.3277 | 2.9340 | 2.7014 | 2.5454 | 2.4324 | 2.3463 | 2.2783 | 2.2229 | 2.1768 | 2.1045 | 2.0275 | 1.9446 | 1.9005 | 1.8543 | 1.8055 | 1.7537 | 1.6981 | 1.6376 |
| **30** | 4.1709 | 3.3158 | 2.9223 | 2.6896 | 2.5336 | 2.4205 | 2.3343 | 2.2662 | 2.2107 | 2.1646 | 2.0921 | 2.0148 | 1.9317 | 1.8874 | 1.8409 | 1.7918 | 1.7396 | 1.6835 | 1.6223 |
| | | | | | | | | | | | | | | | | | | | |
| **40** | 4.0847 | 3.2317 | 2.8387 | 2.6060 | 2.4495 | 2.3359 | 2.2490 | 2.1802 | 2.1240 | 2.0772 | 2.0035 | 1.9245 | 1.8389 | 1.7929 | 1.7444 | 1.6928 | 1.6373 | 1.5766 | 1.5089 |
| **60** | 4.0012 | 3.1504 | 2.7581 | 2.5252 | 2.3683 | 2.2541 | 2.1665 | 2.0970 | 2.0401 | 1.9926 | 1.9174 | 1.8364 | 1.7480 | 1.7001 | 1.6491 | 1.5943 | 1.5343 | 1.4673 | 1.3893 |
| **120** | 3.9201 | 3.0718 | 2.6802 | 2.4472 | 2.2899 | 2.1750 | 2.0868 | 2.0164 | 1.9588 | 1.9105 | 1.8337 | 1.7505 | 1.6587 | 1.6084 | 1.5543 | 1.4952 | 1.4290 | 1.3519 | 1.2539 |
| ∞ | 3.8415 | 2.9957 | 2.6049 | 2.3719 | 2.2141 | 2.0986 | 2.0096 | 1.9384 | 1.8799 | 1.8307 | 1.7522 | 1.6664 | 1.5705 | 1.5173 | 1.4591 | 1.3940 | 1.3180 | 1.2214 | 1.0000 |

APPENDIX A4

Equation 5.2-5 Discrepancy Errors

| ID | Bed Slope (%) | Flow Rate ($m^3/s$) | Unit Discharge ($m^2/s$) | Friction Slope (%) | Water Surface Slope (%) | Measured Unit Sediment Transport Rate (kg/m/s) | Calculated Unit Sediment Transport Rate (kg/m/s) | Discrepancy Error (%) |
|---|---|---|---|---|---|---|---|---|
| 1 | 25 | 0.020 | 0.082 | 24.2 | 25.6 | 21.760 | 21.365 | 1.815 |
| 2 | 25 | 0.023 | 0.091 | 24.5 | 25.6 | 21.508 | 23.313 | -8.393 |
| 3 | 25 | 0.025 | 0.101 | 24.5 | 25.5 | 24.693 | 25.021 | -1.330 |
| 4 | 25 | 0.026 | 0.102 | 24.5 | 25.6 | 26.550 | 25.018 | 5.769 |
| 5 | 25 | 0.027 | 0.110 | 24.7 | 25.5 | 25.961 | 27.024 | -4.093 |
| 6 | 25 | 0.030 | 0.120 | 24.9 | 25.5 | 28.986 | 29.415 | -1.481 |
| 7 | 25 | 0.033 | 0.133 | 24.3 | 25.7 | 31.211 | 31.809 | -1.917 |
| 8 | 25 | 0.035 | 0.141 | 24.7 | 25.5 | 30.275 | 32.200 | -6.360 |
| 9 | 25 | 0.038 | 0.152 | 24.9 | 25.5 | 36.990 | 34.463 | 6.830 |
| 10 | 25 | 0.041 | 0.164 | 24.5 | 25.6 | 37.081 | 36.315 | 2.066 |
| 11 | 25 | 0.042 | 0.170 | 24.3 | 25.9 | 32.832 | 36.718 | -11.838 |
| 12 | 25 | 0.046 | 0.183 | 24.3 | 25.8 | 32.346 | 39.298 | -21.490 |
| 13 | 33 | 0.020 | 0.081 | 30.6 | 32.9 | 25.377 | 20.810 | -4.652 |
| 14 | 33 | 0.022 | 0.087 | 32.8 | 32.7 | 25.552 | 23.287 | 0.584 |
| 15 | 33 | 0.025 | 0.101 | 31.6 | 32.9 | 28.444 | 28.969 | -11.000 |
| 16 | 33 | 0.028 | 0.114 | 32.9 | 32.7 | 32.674 | 28.284 | -3.360 |
| 17 | 33 | 0.030 | 0.121 | 32.5 | 32.8 | 34.424 | 29.397 | 1.322 |
| 18 | 33 | 0.033 | 0.133 | 32.6 | 32.8 | 33.500 | 34.977 | -1.270 |
| 19 | 33 | 0.035 | 0.141 | 31.9 | 32.9 | 38.275 | 26.167 | -3.114 |
| 20 | 33 | 0.036 | 0.143 | 31.5 | 33.0 | 36.465 | 29.246 | -14.458 |
| 21 | 33 | 0.039 | 0.156 | 31.5 | 33.0 | 40.699 | 31.486 | -10.692 |
| 22 | 33 | 0.040 | 0.161 | 32.2 | 32.9 | 40.251 | 34.927 | -6.894 |
| 23 | 33 | 0.046 | 0.183 | 31.1 | 33.1 | 47.055 | 36.372 | -5.661 |
| 24 | 33 | 0.046 | 0.183 | 30.0 | 33.3 | 45.349 | 39.320 | -17.372 |
| 25 | 40 | 0.020 | 0.081 | 38.2 | 40.1 | 34.235 | 40.106 | -4.785 |
| 26 | 40 | 0.020 | 0.082 | 38.2 | 40.1 | 31.984 | 40.517 | -11.111 |
| 27 | 40 | 0.023 | 0.091 | 38.4 | 40.1 | 35.556 | 42.886 | -5.374 |
| 28 | 40 | 0.026 | 0.102 | 36.7 | 40.2 | 39.669 | 44.612 | -10.834 |
| 29 | 40 | 0.028 | 0.111 | 35.8 | 40.3 | 38.287 | 48.971 | -4.073 |

| | | | | | | | | |
|---|---|---|---|---|---|---|---|---|
| 30 | 40 | 0.030 | 0.120 | 35.8 | 40.3 | 44.522 | 47.829 | -5.468 |
| 31 | 40 | 0.033 | 0.132 | 35.5 | 40.3 | 41.947 | 25.439 | -0.165 |
| 32 | 40 | 0.035 | 0.139 | 35.4 | 40.1 | 46.133 | 28.267 | -8.963 |
| 33 | 40 | 0.038 | 0.151 | 36.4 | 40.1 | 49.915 | 31.005 | -10.429 |
| 34 | 40 | 0.040 | 0.160 | 35.7 | 40.1 | 53.521 | 34.001 | -9.971 |
| 35 | 40 | 0.044 | 0.175 | 35.9 | 40.1 | 53.229 | 35.245 | -2.395 |
| 36 | 40 | 0.045 | 0.180 | 35.0 | 40.1 | 67.737 | 41.782 | -0.758 |
| 37 | 25 | 0.008 | 0.032 | 24.1 | 25.3 | 19.885 | 31.258 | 8.696 |
| 38 | 25 | 0.009 | 0.036 | 23.8 | 25.3 | 23.424 | 31.779 | 0.642 |
| 39 | 25 | 0.010 | 0.041 | 23.0 | 25.3 | 26.098 | 34.503 | 2.960 |
| 40 | 25 | 0.011 | 0.045 | 23.4 | 25.3 | 27.364 | 36.626 | 7.671 |
| 41 | 25 | 0.012 | 0.048 | 23.6 | 25.3 | 29.791 | 38.621 | -0.871 |
| 42 | 25 | 0.014 | 0.058 | 23.2 | 25.3 | 34.539 | 40.661 | 8.672 |
| 43 | 33 | 0.008 | 0.032 | 30.8 | 32.7 | 25.397 | 43.544 | -3.807 |
| 44 | 33 | 0.009 | 0.036 | 30.1 | 32.7 | 25.942 | 45.489 | 1.397 |
| 45 | 33 | 0.010 | 0.041 | 30.1 | 32.7 | 28.077 | 49.804 | 0.221 |
| 46 | 33 | 0.011 | 0.045 | 29.3 | 32.7 | 30.918 | 51.779 | 3.256 |
| 47 | 33 | 0.012 | 0.048 | 30.4 | 32.7 | 34.420 | 56.565 | -6.267 |
| 48 | 33 | 0.014 | 0.058 | 28.9 | 32.7 | 41.467 | 28.681 | -4.005 |
| 49 | 40 | 0.008 | 0.032 | 35.1 | 40.1 | 27.577 | 31.432 | 6.233 |
| 50 | 40 | 0.009 | 0.036 | 36.1 | 40.1 | 33.521 | 34.183 | 7.441 |
| 51 | 40 | 0.010 | 0.041 | 36.8 | 40.1 | 36.932 | 37.644 | 7.064 |
| 52 | 40 | 0.011 | 0.045 | 36.0 | 40.1 | 40.506 | 39.165 | 4.507 |
| 53 | 40 | 0.012 | 0.048 | 36.3 | 40.1 | 41.013 | 46.415 | -5.075 |
| 54 | 40 | 0.014 | 0.058 | 34.5 | 40.1 | 44.173 | 21.365 | 1.815 |

Equation 5.2-6 Discrepancy Errors

| **ID** | **Bed Slope (%)** | **Flow Rate ($m^3/s$)** | **Unit Discharge ($m^2/s$)** | **Friction Slope (%)** | **Water Surface Slope (%)** | **Measured Unit Sediment Transport Rate (kg/m/s)** | **Calculated Unit Sediment Transport Rate (kg/m/s)** | **Discrepancy Error (%)** |
|---|---|---|---|---|---|---|---|---|
| 1 | 25 | 0.020 | 0.082 | 24.2 | 25.6 | 21.760 | 20.096 | 7.65 |
| 2 | 25 | 0.023 | 0.091 | 24.5 | 25.6 | 21.508 | 21.871 | -1.69 |
| 3 | 25 | 0.025 | 0.101 | 24.5 | 25.5 | 24.693 | 23.355 | 5.42 |
| 4 | 25 | 0.026 | 0.102 | 24.5 | 25.6 | 26.550 | 23.315 | 12.18 |
| 5 | 25 | 0.027 | 0.110 | 24.7 | 25.5 | 25.961 | 25.191 | 2.97 |
| 6 | 25 | 0.030 | 0.120 | 24.9 | 25.5 | 28.986 | 27.394 | 5.49 |

| | | | | | | | | |
|---|---|---|---|---|---|---|---|---|
| 7 | 25 | 0.033 | 0.133 | 24.3 | 25.7 | 31.211 | 29.515 | 5.43 |
| 8 | 25 | 0.035 | 0.141 | 24.7 | 25.5 | 30.275 | 29.722 | 1.83 |
| 9 | 25 | 0.038 | 0.152 | 24.9 | 25.5 | 36.990 | 31.760 | 14.14 |
| 10 | 25 | 0.041 | 0.164 | 24.5 | 25.6 | 37.081 | 33.364 | 10.02 |
| 11 | 25 | 0.042 | 0.170 | 24.3 | 25.9 | 32.832 | 33.615 | -2.38 |
| 12 | 25 | 0.046 | 0.183 | 24.3 | 25.8 | 32.346 | 35.942 | -11.12 |
| 13 | 33 | 0.020 | 0.081 | 30.6 | 32.9 | 25.377 | 25.348 | 0.11 |
| 14 | 33 | 0.022 | 0.087 | 32.8 | 32.7 | 25.552 | 28.461 | -11.38 |
| 15 | 33 | 0.025 | 0.101 | 31.6 | 32.9 | 28.444 | 30.318 | -6.59 |
| 16 | 33 | 0.028 | 0.114 | 32.9 | 32.7 | 32.674 | 33.569 | -2.74 |
| 17 | 33 | 0.030 | 0.121 | 32.5 | 32.8 | 34.424 | 34.837 | -1.20 |
| 18 | 33 | 0.033 | 0.133 | 32.6 | 32.8 | 33.500 | 37.586 | -12.20 |
| 19 | 33 | 0.035 | 0.141 | 31.9 | 32.9 | 38.275 | 38.149 | 0.33 |
| 20 | 33 | 0.036 | 0.143 | 31.5 | 33.0 | 36.465 | 38.492 | -5.56 |
| 21 | 33 | 0.039 | 0.156 | 31.5 | 33.0 | 40.699 | 40.588 | 0.27 |
| 22 | 33 | 0.040 | 0.161 | 32.2 | 32.9 | 40.251 | 42.268 | -5.01 |
| 23 | 33 | 0.046 | 0.183 | 31.1 | 33.1 | 47.055 | 46.155 | 1.91 |
| 24 | 33 | 0.046 | 0.183 | 30.0 | 33.3 | 45.349 | 44.927 | 0.93 |
| 25 | 40 | 0.020 | 0.081 | 38.2 | 40.1 | 34.235 | 31.026 | 9.37 |
| 26 | 40 | 0.020 | 0.082 | 38.2 | 40.1 | 31.984 | 31.542 | 1.38 |
| 27 | 40 | 0.023 | 0.091 | 38.4 | 40.1 | 35.556 | 34.109 | 4.07 |
| 28 | 40 | 0.026 | 0.102 | 36.7 | 40.2 | 39.669 | 35.934 | 9.42 |
| 29 | 40 | 0.028 | 0.111 | 35.8 | 40.3 | 38.287 | 37.718 | 1.49 |
| 30 | 40 | 0.030 | 0.120 | 35.8 | 40.3 | 44.522 | 39.572 | 11.12 |
| 31 | 40 | 0.033 | 0.132 | 35.5 | 40.3 | 41.947 | 42.235 | -0.69 |
| 32 | 40 | 0.035 | 0.139 | 35.4 | 40.1 | 46.133 | 44.039 | 4.54 |
| 33 | 40 | 0.038 | 0.151 | 36.4 | 40.1 | 49.915 | 48.270 | 3.30 |
| 34 | 40 | 0.040 | 0.160 | 35.7 | 40.1 | 53.521 | 50.053 | 6.48 |
| 35 | 40 | 0.044 | 0.175 | 35.9 | 40.1 | 53.229 | 54.637 | -2.65 |
| 36 | 40 | 0.045 | 0.180 | 35.0 | 40.1 | 67.737 | 54.441 | 19.63 |
| 37 | 25 | 0.008 | 0.032 | 24.1 | 25.3 | 19.885 | 19.468 | 2.10 |
| 38 | 25 | 0.009 | 0.036 | 23.8 | 25.3 | 23.424 | 21.759 | 7.11 |
| 39 | 25 | 0.010 | 0.041 | 23.0 | 25.3 | 26.098 | 26.892 | -3.04 |
| 40 | 25 | 0.011 | 0.045 | 23.4 | 25.3 | 27.364 | 26.308 | 3.86 |
| 41 | 25 | 0.012 | 0.048 | 23.6 | 25.3 | 29.791 | 27.290 | 8.40 |
| 42 | 25 | 0.014 | 0.058 | 23.2 | 25.3 | 34.539 | 32.333 | 6.39 |
| 43 | 33 | 0.008 | 0.032 | 30.8 | 32.7 | 25.397 | 24.451 | 3.72 |
| 44 | 33 | 0.009 | 0.036 | 30.1 | 32.7 | 25.942 | 27.107 | -4.49 |
| 45 | 33 | 0.010 | 0.041 | 30.1 | 32.7 | 28.077 | 29.642 | -5.57 |

| | | | | | | | | |
|---|---|---|---|---|---|---|---|---|
| 46 | 33 | 0.011 | 0.045 | 29.3 | 32.7 | 30.918 | 32.420 | -4.86 |
| 47 | 33 | 0.012 | 0.048 | 30.4 | 32.7 | 34.420 | 33.541 | 2.55 |
| 48 | 33 | 0.014 | 0.058 | 28.9 | 32.7 | 41.467 | 39.565 | 4.59 |
| 49 | 40 | 0.008 | 0.032 | 35.1 | 40.1 | 27.577 | 28.015 | -1.59 |
| 50 | 40 | 0.009 | 0.036 | 36.1 | 40.1 | 33.521 | 30.595 | 8.73 |
| 51 | 40 | 0.010 | 0.041 | 36.8 | 40.1 | 36.932 | 33.149 | 10.24 |
| 52 | 40 | 0.011 | 0.045 | 36.0 | 40.1 | 40.506 | 36.428 | 10.07 |
| 53 | 40 | 0.012 | 0.048 | 36.3 | 40.1 | 41.013 | 37.837 | 7.74 |
| 54 | 40 | 0.014 | 0.058 | 34.5 | 40.1 | 44.173 | 44.614 | -1.00 |